The Dissertation Committee for Harold Edward Gaubert III Certifies that this is the approved version of the following dissertation:

Nanoscale Orthogonal Biofunctionalization Imprint Lithography and its Applications for Studying Nanoscale Cell Surface Interactions

Committee:

Wolfgang Frey, Supervisor

Krishnendu Roy

Grady Rylander

Li Shi

Laura Suggs

Nanoscale Orthogonal Biofunctionalization Imprint Lithography and its Applications for Studying Nanoscale Cell Surface Interactions

by

Harold Edward Gaubert III, B.S.; M.S.; M.B.A.

Dissertation

Presented to the Faculty of the Graduate School of

The University of Texas at Austin

in Partial Fulfillment

of the Requirements

for the Degree of

Doctor of Philosophy

The University of Texas at Austin

December 2007

Dedication

To my wonderful and loving wife

Acknowledgements

I am very grateful to my supervisor Dr. Wolfgang Frey who made this research possible. I would like to thank John Slater for all of his knowledgeable help. I would like to sincerely thank the Center for Nano and Molecular Science and Technology at UT Austin for their facilities and Welch foundation for financial support. I also would like to thank the Microelectronics Research Center at UT Austin for use of their facilities. I also give thanks to my the supportive group members of the Frey Lab: John Slater, Alex Chang, Bongsu Jung, Ruben Morones, Soyeun Park, Pamela Basto, Patrick Boyce, Dave Kahn and Adnaan Wasey.

Nanoscale Orthogonal Biofunctionalization Imprint Lithography and its Applications for Studying Nanoscale Cell Surface Interactions

Publication No._____

Harold Edward Gaubert III, Ph.D.

The University of Texas at Austin, 2007

Supervisor: Wolfgang Frey

Surfaces with nanopatterned biological functionality are important prerequisites for many applications including developing biosensors, tissue engineering scaffolds and Bio-MEMS devices. This work presents a versatile technique, termed nanoscale orthogonal biofunctionalization imprint lithography, which allows "top-down" high-precision nanopatterning of proteins that can meet the demands of various applications. To show applicability of this technique, it was used to create disposable large scale arrays of nanopatterned cell adhesion proteins for cell culture for the purpose of investigating the influence of nanoscale geometrical parameters on cell-surface interactions. These cell culture arrays were used to systematically vary the size, spacing and density of fibronectin adhesion clusters, which are expected to modulate the signaling induced by the cell adhesion, the clustering of adhesion molecules and the force generated in the cytoskeleton. As a result, it was first determined that the nanopatterned adhesion sites

provided an upper limit to the size of a corresponding cell focal adhesion. Cell morphology, actin stress fibers, vinculin distribution, proliferation and motility were all influenced by nanoscale fibronectin island size, and in some cases, the distance between patterns. Several parameters depended biphasically on the pattern size, indicating a very fine regulation of the associated cell signaling. Adhesion area and local stress on the adhesion are modulated by the adhesion size, and the cell response on the nanopattern shows strong parallels to the response on elastic adhesion substrates. In addition, chemical signaling may be influenced directly by changing the activity of associated enzymes. The results of this work build a basis for an understanding of adhesion on the nanoscale level and offer design criteria for the engineering of biomaterials and tissue scaffolds.

TABLE OF CONTENTS

LIST OF TABLES

LIST OF FIGURES

CHAPTER 1: INTRODUCTION

1.1 INTRODUCTION AND MOTIVATION

As the electronics industry has gradually transitioned into the nanoscale regime, similar advances have been made in bionanotechnology. The ability to combine nanoscale interactions with biotechnology has opened up numerous opportunities for biotechnology and medical applications. Nanopatterning offers the ability to increase the density of chip arrays and sensitivity for some applications while lowering the cost, being amenable to multicomponent detection and increasing the efficiency of biochemical assays. The usefulness of these advancements depends on the ability to efficiently and to cost effectively fabricate devices that incorporate these technologies.

Surfaces with nanopatterned biological functionality are important prerequisites for many applications including developing biosensors, tissue engineering scaffolds and Bio-MEMS devices. One goal of this work was to develop a versatile technique that allows "top-down" high-precision nanopatterning of proteins that can meet the demands of various applications. In many instances, it is important that these nanopatterned surfaces be large, on the order of cm^2, that they can be produced quickly and inexpensively, and that the nanofeatures and the background can be independently functionalized in order to have a well-defined pattern of dual biological functionality.

To show the applicability of the technique, it was used to create disposable large scale nanopatterned protein cell culture arrays for the investigation of cell-surface interactions. It is well known that endothelial cells can be influenced by soluble factors, shear stress and mechanical stress applied from a substrate. However, knowledge of how low-level nanoscale surface properties influence cellular behavior is not well understood. Cellular adhesions to the extracellular matrix (ECM) play an important role in cellular

proliferation, motility, differentiation, gene expression and overall cell survival. It has been shown that cellular behavior is dependent on average densities of ECM protein. Results from this work suggest a qualitative agreement with average density but that clustering the ECM protein on nanopatterned surfaces drives similar behavior at a much lower average density of ECM protein. This highlights an important distinction between clustered and homogenously distributed ECM proteins. By utilizing the nanopatterned protein cell culture array, a systematic approach to limiting integrin cluster size and spacing for investigating cell behavior was employed for the first time and could provide insight into the process of mechano-phenotype control.

CHAPTER 2: BACKGROUND

2.1 INTRODUCTION

There is a continuing need for advanced biomaterials in tissue engineering applications. Although the focus of this work is on the development of large scale nanopatterned cell culture protein arrays, it fits within the larger scope that advanced materials must be designed to interact with living components and express the correct environmental parameters. Gaining a greater understanding of the complex interactions between endothelial cells and their environment through the use of a nanopatterned cell culture array will aid in the development of next generation biomaterials for artificial vascular grafts and will also provide insight into advanced biomaterials in general.

2.2 ADVANCED BIOMATERIALS

Biomaterials are defined as any synthetic or natural material that is placed in contact with a living tissue. As with most foreign objects placed inside the body, biomaterials elicit several native responses. The traditional short-term dominant responses to biomaterials are protein adsorption, platelet adsorption and local inflammatory responses. When left in permanent contact, biomaterials can induce a foreign body response including chronic inflammation and eventual fibrous encapsulation (Babensee, Anderson et al. 1998; Anderson and Langone 1999). Traditionally, biomaterials were designed with the goal of minimizing these negative effects. However, newer classes of biomaterials are being designed to be bioactive in a way that enables them to induce specific local cellular behavior while still minimizing negative effects

(Healy 1999; Hubbell 1999; Griffith 2002; Boontheekul and Mooney 2003; Chen, Jiang et al. 2005; Lutolf and Hubbell 2005).

The development of next generation active biomaterials has resulted in a paradigm shift from designing materials around how cells react to them to understanding how surface cues induce specific phenotype expressions in cells. The knowledge and understanding of this biology has led to the incorporation of these cues into biomaterials. Some of the current methods being developed for creating bioactive biomaterials are surface modifications, immobilization of bioactive peptides on surfaces and synthetic materials that incorporate signaling molecules (Ratner and Bryant 2004). Biomaterials that display biological functionality on their surfaces are thought to induce cellular responses by allowing specific integrins to bind. Cells attached to these surfaces receive surface mediated cues that cause a cascade of intracellular events. By modifying the bioactive nature of the surface, it is thought that biomaterial surfaces can initiate intracellular signals, which are then used to direct specific cell responses.

Adhesion of cells, in particular endothelial cells (EC), to biomaterial surfaces can be controlled by adsorption of short oligopeptide sequences that form receptor-binding domains. There are a number of sequences that have been found to be successful (Shin, Jo et al. 2003). One of the most common sequences used is arginine-glycine-aspartic acid (RGD). RGD is found on a number of extracellular matrix (ECM) proteins including fibronectin (Pierschbacher and Ruoslahti 1984), collagen (Staatz, Fok et al. 1991), vitronectin (Smith and Cheresh 1988) and laminin (Aumailley, Gerl et al. 1990) and is relatively easy to synthesize. As an alternative to short oligopeptide sequences, the full ECM protein such as fibronectin (FN) can also be adsorbed to the surface. The full FN protein has been found to provide several synergistic binding effects over the short

oligopeptide sequences that enhance cell surface adhesion (Hersel, Dahmen et al. 2003; Vogel and Baneyx 2003).

Additionally, the creation of non-biofouling surfaces, those that resist protein adsorption due to a wound healing response and prevent encapsulation, is important for active biomaterials. An active area of research in creating non-biofouling surfaces has been using surfaces coated with Poly(ethylene glycol) (PEG), which is known to resist cell and non-specific protein adhesion (Kingshott and Griesser 1999). Surfaces can be functionalized by attaching a PEG layer by covalent immobilization or adsorption to the surface. Additionally, other materials such as fluorinated ethylene propylene copolymer (FEP) (Shen, Martinson et al. 2002), phospholipids (Ishihara, Ziats et al. 1991) and saccharide surfaces (Holland, Qiu et al. 1998) have shown to create successful non-biofouling surfaces.

2.2 CLINICAL SIGNIFICANCE

Over 600,000 peripheral and coronary bypass grafts are conducted annually in the United States and Europe (Angelini 1992; Caes and Vannooten 1994; Motwani and Topol 1998; Pomposelli, Arora et al. 1998; Tarry, Walsh et al. 1998; Byrne, Darling et al. 1999). Autologous transplants of an artery or vein are the preferred method for cardiac or peripheral bypass. However, there are a limited number of arterial vessels and diameters available. Venous vessels are more abundant but they lack vasomotor tone and are prone to thrombosis and hyperpastic occlusion, with only 40% remaining open after 10 years (Edelman 1999; Parikh and Edelman 2000). Autologous transplants must be harvested from healthy sites, which cause damage and introduce the possibility of wound failure and infection of the site. In approximately thirty percent of patients requiring a bypass

procedure, an autologous transplant is not appropriate (Tiwari, Salacinski et al. 2001). In these cases, patients may undergo the procedure using prosthetic grafts.

Prosthetic grafts have been successful in cases of large diameter vessel replacements that are used in high flow settings. However, for small diameter vessels under 6 mm, synthetic replacements have been less successful and are prone to thrombosis and intimal hyperplasia around the anastomoses (Abbott, Megerman et al. 1987; Ip, Fuster et al. 1991; Ao, Hawthorne et al. 2000). The reason for failure of the smaller vessels can be attributed to lower flow rates and compliance mismatch between the prosthetic vessel and the native vessel. This is a particular problem for small vessel replacement in coronary bypass and below-knee reconstruction.

It has been demonstrated that by lining smaller diameter artificial vascular grafts with a layer of endothelial cells, thrombosis of the prosthesis can be reduced (Herring, Gardner et al. 1978). The rational behind using autologous endothelial cells (EC) to line the lumen of the graft is that they will perform similar functions to that of a healthy blood vessel such as forming an antithrombogenic surface. In studies using expanded polytetrafluoroethylene (EPTFE) lined with endothelial cells, these prosthesis showed an increased patency rate of 70% in comparison to unlined grafts that had a patency of 20% over a nine year period (Magometschnigg, Kadletz et al. 1992; Tassiopoulos and Greisler 2000).

Endothelial cells play an important role as a bioregulator of cardiovascular physiology in addition to providing an antithrombogenic surface for blood flow. They are key mediator in platelet activation, adhesion and aggregation (Autio, Maloranta et al. 1989). They also have a role in controlling blood flow (Furchgott and Zawadzki 1980), vessel tone (Furchgott and Zawadzki 1980) and leukocyte adhesion (Cybulsky and Gimbrone 1991). A large body of research has been conducted on ways to introduce

endothelial cells on prosthetic materials while preserving their phenotype and, more importantly, strongly adhering them to the surface (Parikh and Edelman 2000; Salacinski, Tiwari et al. 2001). Endothelial cell adhesion strength and phenotype is influenced by cell-surface interactions (Canfield, Boothandford et al. 1990), biochemical signaling (Risau 1995), mechanical strain due to blood shear stress (Davies and Tripathi 1993; Davies, Robotewskyj et al. 1994; Topper and Gimbrone 1999; Stamatas and McIntire 2001) and cell-to-cell contacts. However, the interplay between the signals and how one parameter can be used to influence the others is not clear (Olivier, Yen et al. 1999; Topper and Gimbrone 1999).

2.3 ENGINEERING CELL-SURFACE INTERACTIONS

Cellular adhesions to the ECM play an important role in cellular proliferation, motility, differentiation, gene expression and overall cell survival (Petit and Thiery 2000; Lauffenburger and Wells 2001; Ruegg and Mariotti 2003; Vogel and Baneyx 2003). Adhesions are formed by protein clusters that are classified as either focal complexes or focal adhesions. Focal complexes are defined as large protein anchorages that are generally found at the ends of actin stress fibers. Focal adhesions are defined as smaller protein anchorages that are found at the outer edge of the cell, usually associated with the end of a filopodia or lamellipodia. Adhesions are mediated by integrins, large transmembrane proteins that comprise a large family of alpha-beta heterodimeric transmembrane glycoprotein receptors. There are 24 known integrin receptors made from a combination of 8 beta and 18 alpha subunits (Miranti and Brugge 2002). Extracellularly, integrins have large domains involved in both acting as a structural link and as a signaling receptor. Intracellularly, they have short cytoplasmic tails that interact with the cytoskeleton signaling network.

The natural surface environment of cells consists of a complex set of topographical and chemical cues that influence a wide range of cellular functions including proliferation, differentiation, morphology, motility, apoptosis and gene expression (Blau and Baltimore 1991; Zamir and Geiger 2001). It is well documented that cells react to micron-scale surface cues which can greatly affect the cellular functions described above. More recently, the importance of nanoscale interactions is emerging. A greater knowledge of how the cell interacts at the nanoscale will help provide a molecular picture of what actually drives these surface initiated responses.

In order to study nanoscale cell-surface interactions at the molecular level, it is necessary to create an experimental system of well-defined adhesion points and topography. To date, expansion into the nanoscale regime has been limited by the technical challenge and expense. Techniques such as electron beam lithography and ion beam milling yield high resolution samples but their serial nature and expense make them infeasible for the quantity of samples needed for biological experiments. A number of self-assembly techniques have also emerged, but all have several inherent limitations that prevent them from producing a clear molecular picture of cell-surface interactions.

The work in this dissertation presents a "top-down" nanofabrication technique, termed nanoscale orthogonal biofunctionalization imprint lithography (NOBIL), which allows the rapid fabrication of biologically functionalized nanopatterns based on a parallel imprinting technique. It allows complete control of nanotopography and biochemical functionality with nanoscale precision. Incorporating orthogonal chemistry, two different surface chemical functionalities can be expressed in highly defined areas enabling complete control of integrin attachment points. The technique overcomes limitations associated with self-assembly techniques while offering the precision of electron beam lithography or ion beam milling at a fraction of the cost and time. It is an

extremely powerful technique for studying nanoscale cell-surface interactions which, in turn, will provide valuable information for the creation of next generation biomaterials.

2.4 MICRO-PATTERNED SURFACES

Many advances in investigating cell-surfaces interactions were brought about by the advent of soft lithography. The term "soft lithography" (Whitesides, Ostuni et al. 2001) encompasses a variety of techniques including microcontact printing (Abbott, Folkers et al. 1992; Kumar, Biebuyck et al. 1992; Kumar and Whitesides 1993; Abbott, Kumar et al. 1994), elastomeric membranes for use in dry liftoff (Duffy, Jackman et al. 1999; Jackman, Duffy et al. 1999; Folch, Jo et al. 2000; Ostuni, Kane et al. 2000) and patterning using microfluidic systems (Kenis, Ismagilov et al. 1999; Takayama, Ostuni et al. 2001). The discussion of micro-patterned surfaces will be limited to microcontact printing and elastomeric membranes for dry liftoff. Both of these techniques enable reproducible bench-top patterning of spatially and chemically well-defined proteins onto surfaces with micron scale resolution without the use of traditional cleanroom equipment. The advent of this technique opened up a new realm of cell-surface studies that could inexpensively be conducted with high precision.

Microcontact printing is a method that allows the biological patterning of surfaces by printing with an elastomeric stamp. Although there are a variety of materials for creating stamps (Schmid and Michel 2000), the most common material used is Poly(dimethylsiloxane) (PDMS). Microcontact printing works very similarly to traditional ink rubberstamping. The surface of the stamp has a three-dimensional topography that represents the pattern to be printed. The stamp is formed by solid surface replica molding (Xia, Kim et al. 1996; Zhao, Xia et al. 1996; Xia, McClelland et al. 1997). The molding is usually performed on a silicon wafer with the topography defined

by photolithography, as shown in Figure 2.3.1. To print with the elastomeric stamp, it is first inked in an alkanethiolate solution and brought into contact with a silicon or a glass gold coated substrate. The alkanethiolate solution reacts with the gold to form a self-assembled monolayer (SAM) in the areas where the stamp comes into contact with the substrate. After removing the stamp, the unpatterned areas can then be backfilled with a different alkanethiolate solution. Thus, this creates two surface chemical functionalities at a micron scale resolution.

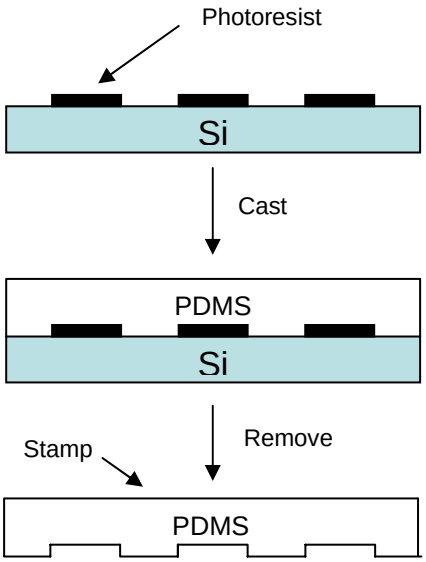

Figure 2.3.1: A schematic outline of fabricating a PDMS stamp from a Si photoresist master.

PDMS can also be used to create elastomeric membranes for dry liftoff that works similarly to traditional photolithography resist in microelectronics processing. Both materials serve as a mask to the underlying substrate and are then lifted off. Traditionally, microelectronic photoresist requires treatment with an organic solvent to dissolve the resist which is incompatible with biological patterning. Elastomeric membranes provide the advantage that they are biologically compatible and can simply be peeled off after patterning the substrate.

These patterning techniques have been used to investigate cell-surface interactions on the micron scale and their importance in proliferation, differentiation, migration and apoptosis (Chen, Mrksich et al. 1997; Huang, Chen et al. 1998; Dertinger, Jiang et al. 2002; McBeath, Pirone et al. 2004). For instance, Chen *et al.* found that human capillary endothelial cells attached to ECM coated islands created by microcontact printing could induce apoptosis or proliferation depending on the size of the coated island (Chen, Mrksich et al. 1997). This was related to the allowable spreading area of the cell, as cells with a smaller spreading area had a greater probability of undergoing apoptosis. However, in these experiments, as allowable spreading area increased so did the available total area of allowable integrin binding. To separate these two effects, a substrate was created with FN posts varying from 3 μm to 5 μm that allowed cell spreading to increase without a large increase in ECM binding area. The results of the experiment found that cell shape was important in determining whether cells undergo apoptosis, independent of the contact area of the ECM protein used for adhesion.

The well-defined nature of microcontact printing made it amenable to experiments that were previously difficult or impossible. For instance, it was suspected that cell-to-cell contacts played a role in proliferation of cells. However, in using traditional methods, cell-to-cell contacts could not be controlled as cells were randomly dispersed across a sample. In using microcontact printing, Chen *et al.* defined sites for cell adhesion in order to study the influence of cell-to-cell contacts on proliferation (Nelson and Chen 2002). G_0 synchronized cells were seeded on these patterns and the entry into S phase was quantified according to the number of cell-to-cell contacts. It was found that the number of cell-to-cell contacts correlates positively with entry into S phase. To differentiate proliferation increases from cell-to-cell contacts versus diffusible

paracrine signals, cells were seeded on bowtie shaped patterns with 2 to 5 μm gaps. It was concluded that direct contact between the cells and not diffusible paracrine signals induced cell proliferation.

2.5 NANOSTRUCTURED SURFACES

The majority of work on cell-surface interactions has been conducted on the micron scale, and it is poorly understood how the chemical and physical properties of biomaterial surfaces influence cell phenotype on the nanometer scale. This is partly due to the fact that top-down patterning of biomaterials on the nanoscale has been restricted by the difficulty and expense of the currently available techniques (Xia, Rogers et al. 1999) such as electron beam lithography (Thompson, Willson et al. 1994), focused ion beam milling (Madou 2002) and scanning probe lithography (Mirkin 2001; Zhang, Chung et al. 2003). Although these serial techniques result in high-resolution patterns, they are limited by their particularly slow writing speed and high cost per sample. Furthermore, the development of "soft lithography" into the nanometer range has been limited (Xia, Rogers et al. 1999; Schmid and Michel 2000; Gates, Xu et al. 2005) and has not reached the resolution scale or pattern fidelity of the above techniques. Overall, it has been difficult to fabricate large scale patterns (25 mm x 25 mm) in the quantity necessary for repeated biological experiments.

To further elucidate the relationship between integrin binding, focal adhesion formation, and the signaling induced by these processes, it is necessary to control both the topography and the specific lateral protein arrangement on the nanoscale. So far there are very few nanolithography techniques that are able to immobilize proteins in a controlled distribution of both pattern dimensions and nanotopography. Even fewer of these techniques allow for orthogonal surface chemistry, the separation of protein adsorption and cell adhesion rejecting areas, and sites of controlled cell adhesion to

specific proteins. The most promising way to achieve this is by creating a composite of two materials that allows for the use of two different immobilization strategies.

Before arriving in the Frey lab, previous members had designed a self-assembly technique for creating nanostructured surfaces based on nanosphere lithography (Figure 2.4.1) (Hulteen and Vanduyne 1995; Frey, Woods et al. 2000). This technique uses mono-disperse polystyrene spheres that are deposited by a capillary deposition machine (Matsushita, Yagi et al. 2000; Matsushita, Miwa et al. 2001) to create a densely packed monolayer or bilayer of spheres. Gold nanostructures are formed by thermally evaporating a thin adhesion layer of chromium followed by a thicker layer of gold across the substrate. The spheres are then lifted off the surface, leaving nanosized structures on the surface that formed in between the gaps in the spheres. The relative width of the nanostructures can be varied by changing the diameter of the spheres. The height can be controlled by the quantity of metal deposited in the evaporation.

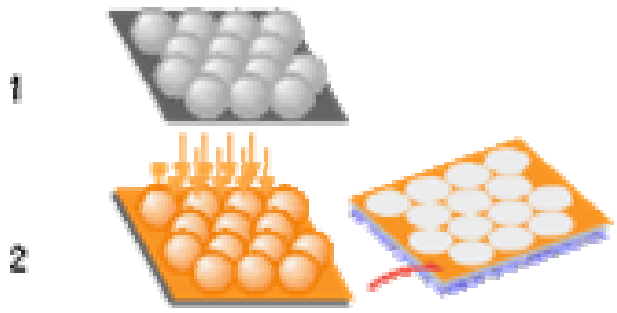

Figure 2.4.1: Schematic representation of the main fabrication steps for nanosphere lithography. (1) Polystyrene nanospheres are deposited onto the surface of the substrate. (2) Gold is evaporated onto the substrate followed by washing spheres off the substrate leaving gold nanotriangles.

Although this technique has yielded valuable data about cells and the interactions on the nanoscale, it has several drawbacks. First, the feature size and spacing ratio cannot be varied independently. The feature size for monolayers is a function S_{pacing} =

0.577 $D_{iameter}$, and for bilayers, a function of S_{pacing} = 0.155 $D_{iameter}$. This narrows the amount of pattern variations that are possible. Secondly, the technique is defect prone due to the nature of the self-assembly process and a certain amount of poly dispersity in the polystyrene sphere layers. Lastly, it is not possible to create more than two pattern sizes on a single substrate. This significantly increases the number of experiments that need to be conducted.

As a solution to these limitations, I developed a nanofabrication technique based on "step-and-flash imprint lithography" (SFIL) (Colburn, Johnson et al. 1999; Bailey, Choi et al. 2000; Colburn, Grot et al. 2000; Bailey, Smith et al. 2001; Choi, Meissl et al. 2001; Colburn, Bailey et al. 2001; Colburn, Grot et al. 2001; Colburn, Suez et al. 2001; Bailey, Johnson et al. 2002; Dauksher, Nordquist et al. 2002; Johnson, Resnick et al. 2003; Resnick, Dauksher et al. 2003; Resnick, Mancini et al. 2003; Stewart, Johnson et al. 2005; Wang, Rafferty et al. 2005). SFIL has been developed for semiconductor applications but so far has not been used in biological applications. The SFIL process allows the imprinting of patterns as large as 25 mm x 25 mm at resolutions below 30 nm in minutes, compared to a serial technique, such as electron beam lithography, where several days are needed to create an identical pattern. Being a top-down approach, it allows the printing of multiple sized patterns on a single substrate with little to no defects. Thus, in a single experiment, multiple diameter-to-pitch ratios can be explored while keeping the experimental variables the same for all cells on different patterns. Additionally, it allows the precise control of nanotopography and creation of nanostructured surfaces consisting of two materials allowing biofunctionalization using orthogonal chemistry.

2.7 CONCLUSIONS

The development of a disposable large scale array of nanopatterned proteins has broad applications including biosensors, tissue engineering scaffolds and Bio-MEMS devices. It also allows sophisticated biological experiments to be conducted that investigate cell surface interactions. These types of experiments are important for the development of advanced biomaterials by providing knowledge about how specific signaling events and therefore cellular phenotype can be induced by engineering the nanoscale surface parameters.

REFERENCES

Abbott, N. L., J. P. Folkers, et al. (1992). "Manipulation of the Wettability of Surfaces on the 0.1-Micrometer to 1-Micrometer Scale through Micromachining and Molecular Self-Assembly." Science **257**(5075): 1380-1382.

Abbott, N. L., A. Kumar, et al. (1994). "Using Micromachining, Molecular Self-Assembly, and Wet Etching to Fabricate 0.1-1-Mu-M-Scale Structures of Gold and Silicon." Chemistry of Materials **6**(5): 596-602.

Abbott, W. M., J. Megerman, et al. (1987). "Effect of Compliance Mismatch on Vascular Graft Patency." Journal of Vascular Surgery **5**(2): 376-382.

Anderson, J. M. and J. J. Langone (1999). "Issues and perspectives on the biocompatibility and immunotoxicity evaluation of implanted controlled release systems." Journal of Controlled Release **57**(2): 107-113.

Angelini, G. D. (1992). "Saphenous-Vein Graft Failure - Etiologic Considerations and Strategies for Prevention." Current Opinion in Cardiology **7**(6): 939-944.

Ao, P. Y., W. J. Hawthorne, et al. (2000). "Development of intimal hyperplasia in six different vascular prostheses." European Journal of Vascular and Endovascular Surgery **20**(3): 241-249.

Aumailley, M., M. Gerl, et al. (1990). "Identification of the Arg-Gly-Asp Sequence in Laminin-a Chain as a Latent Cell-Binding Site Being Exposed in Fragment P1." Febs Letters **262**(1): 82-86.

Autio, I., U. Maloranta, et al. (1989). "Cultured Bovine Aortic Endothelial-Cells Secrete Factor(S) Chemotactic for Aortic Smooth-Muscle Cells." Artery **16**(2): 72-83.

Babensee, J. E., J. M. Anderson, et al. (1998). "Host response to tissue engineered devices." Advanced Drug Delivery Reviews **33**(1-2): 111-139.

Bailey, T., B. J. Choi, et al. (2000). "Step and flash imprint lithography: Template surface treatment and defect analysis." Journal of Vacuum Science & Technology B **18**(6): 3572-3577.

Bailey, T., B. Smith, et al. (2001). "Step and flash imprint lithography: Defect analysis." Journal of Vacuum Science & Technology B **19**(6): 2806-2810.

Bailey, T. C., S. C. Johnson, et al. (2002). "Step and flash imprint lithography: An efficient nanoscale printing technology." Journal of Photopolymer Science and Technology **15**(3): 481-486.

Blau, H. M. and D. Baltimore (1991). "Differentiation Requires Continuous Regulation." Journal of Cell Biology **112**(5): 781-783.

Boontheekul, T. and D. J. Mooney (2003). "Protein-based signaling systems in tissue engineering." Current Opinion in Biotechnology **14**(5): 559-565.

Byrne, J., R. C. Darling, et al. (1999). "Infrainguinal arterial reconstruction for claudication: Is it worth the risk? An analysis of 409 procedures." Journal of Vascular Surgery **29**(2): 259-267.

Caes, F. L. and G. J. Vannooten (1994). "Use of Internal Mammary Artery for Emergency Grafting after Failed Coronary Angioplasty." Annals of Thoracic Surgery **57**(5): 1295-1299.

Canfield, A. E., R. P. Boothandford, et al. (1990). "Thrombospondin Gene-Expression by Endothelial-Cells in Culture Is Modulated by Cell-Proliferation, Cell-Shape and the Substratum." Biochemical Journal **268**(1): 225-230.

Chen, C. S., X. Y. Jiang, et al. (2005). "Microengineering the environment of mammalian cells in culture." Mrs Bulletin **30**(3): 194-201.

Chen, C. S., M. Mrksich, et al. (1997). "Geometric control of cell life and death." Science **276**(5317): 1425-1428.

Choi, B. J., M. Meissl, et al. (2001). Layer-to-layer alignment for step and flash imprint lithography, USA, SPIE-Int. Soc. Opt. Eng

SPIE.

Colburn, M., T. Bailey, et al. (2001). "Development and advantages of step-and-flash lithography." Solid State Technology **44**(7): 67-+.

Colburn, M., A. Grot, et al. (2000). Step and flash imprint lithography for sub-100 nm patterning, USA, SPIE-Int. Soc. Opt. Eng

SPIE.

Colburn, M., A. Grot, et al. (2001). "Patterning nonflat substrates with a low pressure, room temperature, imprint lithography process." Journal of Vacuum Science & Technology B **19**(6): 2162-2172.

Colburn, M., S. Johnson, et al. (1999). "Step and flash imprint lithography: a new approach to high-resolution patterning." Proc. SPIE, Emerging Lithographic Technologies III, Yuli Vladimirsky; Ed **3676**: 379-389.

Colburn, M., I. Suez, et al. (2001). "Characterization and modeling of volumetric and mechanical properties for step and flash imprint lithography photopolymers." Journal of Vacuum Science & Technology B **19**(6): 2685-2689.

Cybulsky, M. I. and M. A. Gimbrone (1991). "Endothelial Expression of a Mononuclear Leukocyte Adhesion Molecule During Atherogenesis." Science **251**(4995): 788-791.

Dauksher, W. J., K. J. Nordquist, et al. (2002). "Characterization of and imprint results using indium tin oxide-based step and flash imprint lithography templates." Journal of Vacuum Science & Technology B **20**(6): 2857-2861.

Davies, P. F., A. Robotewskyj, et al. (1994). "Quantitative Studies of Endothelial-Cell Adhesion - Directional Remodeling of Focal Adhesion Sites in Response to Flow Forces." Journal of Clinical Investigation **93**(5): 2031-2038.

Davies, P. F. and S. C. Tripathi (1993). "Mechanical-Stress Mechanisms and the Cell - an Endothelial Paradigm." Circulation Research **72**(2): 239-245.

Dertinger, S. K. W., X. Y. Jiang, et al. (2002). "Gradients of substrate-bound laminin orient axonal specification of neurons." Proceedings of the National Academy of Sciences of the United States of America **99**(20): 12542-12547.

Duffy, D. C., R. J. Jackman, et al. (1999). "Patterning electroluminescent materials with feature sizes as small as 5 mu m using elastomeric membranes as masks for dry lift-off." Advanced Materials **11**(7): 546-+.

Edelman, E. R. (1999). "Vascular tissue engineering - Designer arteries." Circulation Research **85**(12): 1115-1117.
Folch, A., B. H. Jo, et al. (2000). "Microfabricated elastomeric stencils for micropatterning cell cultures." Journal of Biomedical Materials Research **52**(2): 346-353.
Frey, W., C. K. Woods, et al. (2000). "Ultraflat nanosphere lithography: A new method to fabricate flat nanostructures." Advanced Materials **12**(20): 1515-1519.
Furchgott, R. F. and J. V. Zawadzki (1980). "The Obligatory Role of Endothelial-Cells in the Relaxation of Arterial Smooth-Muscle by Acetylcholine." Nature **288**(5789): 373-376.
Gates, B. D., Q. B. Xu, et al. (2005). "New approaches to nanofabrication: Molding, printing, and other techniques." Chemical Reviews **105**(4): 1171-1196.
Griffith, L. G. (2002). Emerging design principles in Biomaterials and scaffolds for tissue engineering. Reparative Medicine: Growing Tissues and Organs. **961:** 83-95.
Healy, K. E. (1999). "Molecular engineering of materials for bioreactivity." Current Opinion in Solid State & Materials Science **4**(4): 381-387.
Herring, M., A. Gardner, et al. (1978). "Single-Staged Technique for Seeding Vascular Grafts with Autogenous Endothelium." Surgery **84**(4): 498-504.
Hersel, U., C. Dahmen, et al. (2003). "RGD modified polymers: biomaterials for stimulated cell adhesion and beyond." Biomaterials **24**(24): 4385-4415.
Holland, N. B., Y. X. Qiu, et al. (1998). "Biomimetic engineering of non-adhesive glycocalyx-like surfaces using oligosaccharide surfactant polymers." Nature **392**(6678): 799-801.
Huang, S., C. S. Chen, et al. (1998). "Control of cyclin D1, p27(Kip1), and cell cycle progression in human capillary endothelial cells by cell shape and cytoskeletal tension." Molecular Biology of the Cell **9**(11): 3179-3193.
Hubbell, J. A. (1999). "Bioactive biomaterials." Current Opinion in Biotechnology **10**(2): 123-129.
Hulteen, J. C. and R. P. Vanduyne (1995). "Nanosphere Lithography - a Materials General Fabrication Process for Periodic Particle Array Surfaces." Journal of Vacuum Science & Technology a-Vacuum Surfaces and Films **13**(3): 1553-1558.
Ip, J. H., V. Fuster, et al. (1991). "The Role of Platelets, Thrombin and Hyperplasia in Restenosis after Coronary Angioplasty." Journal of the American College of Cardiology **17**(6): B77-B88.
Ishihara, K., N. P. Ziats, et al. (1991). "Protein Adsorption from Human Plasma Is Reduced on Phospholipid Polymers." Journal of Biomedical Materials Research **25**(11): 1397-1407.
Jackman, R. J., D. C. Duffy, et al. (1999). "Using elastomeric membranes as dry resists and for dry lift-off." Langmuir **15**(8): 2973-2984.
Johnson, S., D. J. Resnick, et al. (2003). "Fabrication of multi-tiered structures on step and flash imprint lithography templates." Microelectronic Engineering **67-8**: 221-228.
Kenis, P. J. A., R. F. Ismagilov, et al. (1999). "Microfabrication inside capillaries using multiphase laminar flow patterning." Science **285**(5424): 83-85.

Kingshott, P. and H. J. Griesser (1999). "Surfaces that resist bioadhesion." Current Opinion in Solid State & Materials Science **4**(4): 403-412.
Kumar, A., H. A. Biebuyck, et al. (1992). "The Use of Self-Assembled Monolayers and a Selective Etch to Generate Patterned Gold Features." Journal of the American Chemical Society **114**(23): 9188-9189.
Kumar, A. and G. M. Whitesides (1993). "Features of Gold Having Micrometer to Centimeter Dimensions Can Be Formed through a Combination of Stamping with an Elastomeric Stamp and an Alkanethiol Ink Followed by Chemical Etching." Applied Physics Letters **63**(14): 2002-2004.
Lauffenburger, D. A. and A. Wells (2001). "Getting a grip: new insights for cell adhesion and traction." Nature Cell Biology **3**(5): E110-E112.
Lutolf, M. P. and J. A. Hubbell (2005). "Synthetic biomaterials as instructive extracellular microenvironments for morphogenesis in tissue engineering." Nature Biotechnology **23**(1): 47-55.
Madou, M. J. (2002). Fundamentals of microfabrication : the science of miniaturization. Boca Raton, CRC Press.
Magometschnigg, H., M. Kadletz, et al. (1992). "Prospective Clinical-Study with Invitro Endothelial-Cell Lining of Expanded Polytetrafluoroethylene Grafts in Crural Repeat Reconstruction." Journal of Vascular Surgery **15**(3): 527-535.
Matsushita, S. I., T. Miwa, et al. (2001). "Stable two-dimensional fine-particle arrays in solution." Langmuir **17**(4): 988-992.
Matsushita, S. I., Y. Yagi, et al. (2000). "Light propagation in composite two-dimensional arrays of polystyrene spherical particles." Langmuir **16**(2): 636-642.
McBeath, R., D. M. Pirone, et al. (2004). "Cell shape, cytoskeletal tension, and RhoA regulate stem cell lineage commitment." Developmental Cell **6**(4): 483-495.
Miranti, C. K. and J. S. Brugge (2002). "Sensing the environment: a historical perspective on integrin signal transduction." Nature Cell Biology **4**(4): E83-E90.
Mirkin, C. A. (2001). "Dip-pen nanolithography: Automated fabrication of custom multicomponent, sub-100-nanometer surface architectures." Mrs Bulletin **26**(7): 535-538.
Motwani, J. G. and E. J. Topol (1998). "Aortocoronary saphenous vein graft disease - Pathogenesis, predisposition, and prevention." Circulation **97**(9): 916-931.
Nelson, C. M. and C. S. Chen (2002). "Cell-cell signaling by direct contact increases cell proliferation via a PI3K-dependent signal." Febs Letters **514**(2-3): 238-242.
Olivier, L. A., J. Yen, et al. (1999). "Short-term cell/substrate contact dynamics of subconfluent endothelial cells following exposure to laminar flow." Biotechnology Progress **15**(1): 33-42.
Ostuni, E., R. Kane, et al. (2000). "Patterning mammalian cells using elastomeric membranes." Langmuir **16**(20): 7811-7819.
Parikh, S. A. and E. R. Edelman (2000). "Endothelial cell delivery for cardiovascular therapy." Advanced Drug Delivery Reviews **42**(1-2): 139-161.
Petit, V. and J. P. Thiery (2000). "Focal adhesions: structure and dynamics." Biology of the Cell **92**(7): 477-494.

Pierschbacher, M. D. and E. Ruoslahti (1984). "Cell Attachment Activity of Fibronectin Can Be Duplicated by Small Synthetic Fragments of the Molecule." Nature **309**(5963): 30-33.
Pomposelli, F. B., S. Arora, et al. (1998). "Lower extremity arterial reconstruction in the very elderly: Successful outcome preserves not only the limb but also residential status and ambulatory function." Journal of Vascular Surgery **28**(2): 215-223.
Ratner, B. D. and S. J. Bryant (2004). "Biomaterials: Where we have been and where we are going." Annual Review of Biomedical Engineering **6**: 41-75.
Resnick, D. J., W. J. Dauksher, et al. (2003). "Imprint lithography for integrated circuit fabrication." Journal of Vacuum Science & Technology B **21**(6): 2624-2631.
Resnick, D. J., D. Mancini, et al. (2003). "Improved step and flash imprint lithography templates for nanofabrication." Microelectronic Engineering **69**(2-4): 412-419.
Risau, W. (1995). "Differentiation of Endothelium." Faseb Journal **9**(10): 926-933.
Ruegg, C. and A. Mariotti (2003). "Vascular integrins: pleiotropic adhesion and signaling molecules in vascular homeostasis and angiogenesis." Cellular and Molecular Life Sciences **60**(6): 1135-1157.
Salacinski, H. J., A. Tiwari, et al. (2001). "Cellular engineering of vascular bypass grafts: role of chemical coatings for enhancing endothelial cell attachments." Medical & Biological Engineering & Computing **39**(6): 609-618.
Schmid, H. and B. Michel (2000). "Siloxane polymers for high-resolution, high-accuracy soft lithography." Macromolecules **33**(8): 3042-3049.
Shen, M. C., L. Martinson, et al. (2002). "PEO-like plasma polymerized tetraglyme surface interactions with leukocytes and proteins: in vitro and in vivo studies." Journal of Biomaterials Science-Polymer Edition **13**(4): 367-390.
Shin, H., S. Jo, et al. (2003). "Biomimetic materials for tissue engineering." Biomaterials **24**(24): 4353-4364.
Smith, J. W. and D. A. Cheresh (1988). "The Arg-Gly-Asp Binding Domain of the Vitronectin Receptor - Photoaffinity Cross-Linking Implicates Amino-Acid Residues-61-203 of the Beta-Subunit." Journal of Biological Chemistry **263**(35): 18726-18731.
Staatz, W. D., K. F. Fok, et al. (1991). "Identification of a Tetrapeptide Recognition Sequence for the Alpha-2-Beta-1-Integrin in Collagen." Journal of Biological Chemistry **266**(12): 7363-7367.
Stamatas, G. N. and L. V. McIntire (2001). "Rapid flow-induced responses in endothelial cells." Biotechnology Progress **17**(3): 383-402.
Stewart, M. D., S. C. Johnson, et al. (2005). "Nanofabrication with step and flash imprint lithography." Journal of Microlithography Microfabrication and Microsystems **4**(1).
Takayama, S., E. Ostuni, et al. (2001). "Topographical micropatterning of poly(dimethylsiloxane) using laminar flows of liquids in capillaries." Advanced Materials **13**(8): 570-+.
Tarry, W. C., D. B. Walsh, et al. (1998). "Fate of the contralateral leg after infrainguinal bypass." Journal of Vascular Surgery **27**(6): 1039-1047.

Tassiopoulos, A. K. and H. P. Greisler (2000). "Angiogenic mechanisms of endothelialization of cardiovascular implants: a review of recent investigative strategies." Journal of Biomaterials Science-Polymer Edition **11**(11): 1275-1284.
Thompson, L. F., C. G. Willson, et al. (1994). Introduction to microlithography. Washington, DC, American Chemical Society.
Tiwari, A., H. J. Salacinski, et al. (2001). "Tissue engineering of vascular bypass grafts: Role of endothelial cell extraction." European Journal of Vascular and Endovascular Surgery **21**(3): 193-201.
Topper, J. N. and M. A. Gimbrone (1999). "Blood flow and vascular gene expression: fluid shear stress as a modulator of endothelial phenotype." Molecular Medicine Today **5**(1): 40-46.
Vogel, V. and G. Baneyx (2003). "The tissue engineering puzzle: A molecular perspective." Annual Review of Biomedical Engineering **5**: 441-463.
Wang, D., T. Rafferty, et al. (2005). "Advanced prototyping using step-and-flash imprint." Solid State Technology **48**(12): 60-62.
Whitesides, G. M., E. Ostuni, et al. (2001). "Soft lithography in biology and biochemistry." Annual Review of Biomedical Engineering **3**: 335-373.
Xia, Y. N., E. Kim, et al. (1996). "Complex optical surfaces formed by replica molding against elastomeric masters." Science **273**(5273): 347-349.
Xia, Y. N., J. J. McClelland, et al. (1997). "Replica molding using polymeric materials: A practical step toward nanomanufacturing." Advanced Materials **9**(2): 147-149.
Xia, Y. N., J. A. Rogers, et al. (1999). "Unconventional methods for fabricating and patterning nanostructures." Chemical Reviews **99**(7): 1823-1848.
Zamir, E. and B. Geiger (2001). "Components of cell-matrix adhesions." Journal of Cell Science **114**(20): 3577-3579.
Zhang, H., S. W. Chung, et al. (2003). "Fabrication of sub-50-nm solid-state nanostructures on the basis of dip-pen nanolithography." Nano Letters **3**(1): 43-45.
Zhao, X. M., Y. N. Xia, et al. (1996). "Fabrication of three-dimensional micro-structures: Microtransfer molding." Advanced Materials **8**(10): 837-&.

CHAPTER 3: SFIL PROCESS DEVELOPMENT

3.1 INTRODUCTION

The goal of this chapter is to demonstrate a versatile technique that allows "top-down" high-precision nanopatterning of proteins that can meet the demands of various applications. The initial steps of the technique harness the benefits of Step and Flash Imprint Lithography (SFIL) and build upon them to create a robust process to create nanostructured bio-active surfaces. Chapter Three of this dissertation covers the experimental work in developing the conventional portion of the SFIL process. Chapter Four covers adaptations and extensions of the conventional SFIL process to create samples amenable to biological functionalization. This chapter will begin with a brief overview of the SFIL process followed by detailed experimental sections.

3.2 SFIL PROCESS OVERVIEW

SFIL is a technique that uses a high resolution quartz master template to imprint into an organosilicon monomer that can be photopolymerized to define nanotopography on the surface of a substrate. The quartz template can be reused after each imprint, enabling the subsequent "stepping" across a larger wafer so that 25 mm x 25 mm imprints can cover an entire 800 mm wafer. The pattern on the quartz master template is created using standard e-beam lithography, which enables the creation of extremely high resolution topographies on the order of 30 nm.

The processing steps of SFIL are detailed in Figure 3.1.1. First, an anti-reflective coating is spin coated onto the substrate, which serves as an etch transfer layer in the bilayer resist structure. Drops of organosilicon monomer are then dispensed onto the

substrate and the quartz template is placed in contact with the liquid resist. UV exposure through the backside of the template polymerizes the organosilicon resist. The quartz template is then released from the imprint, leaving a topographical replica of the quartz master in the resist. Reactive ion etching (RIE) is used to transfer the pattern of the polymerized organosilicon resist into the etch barrier. Subsequent RIE steps then further define the etch barrier, leaving a high aspect ratio structure on the substrate surface.

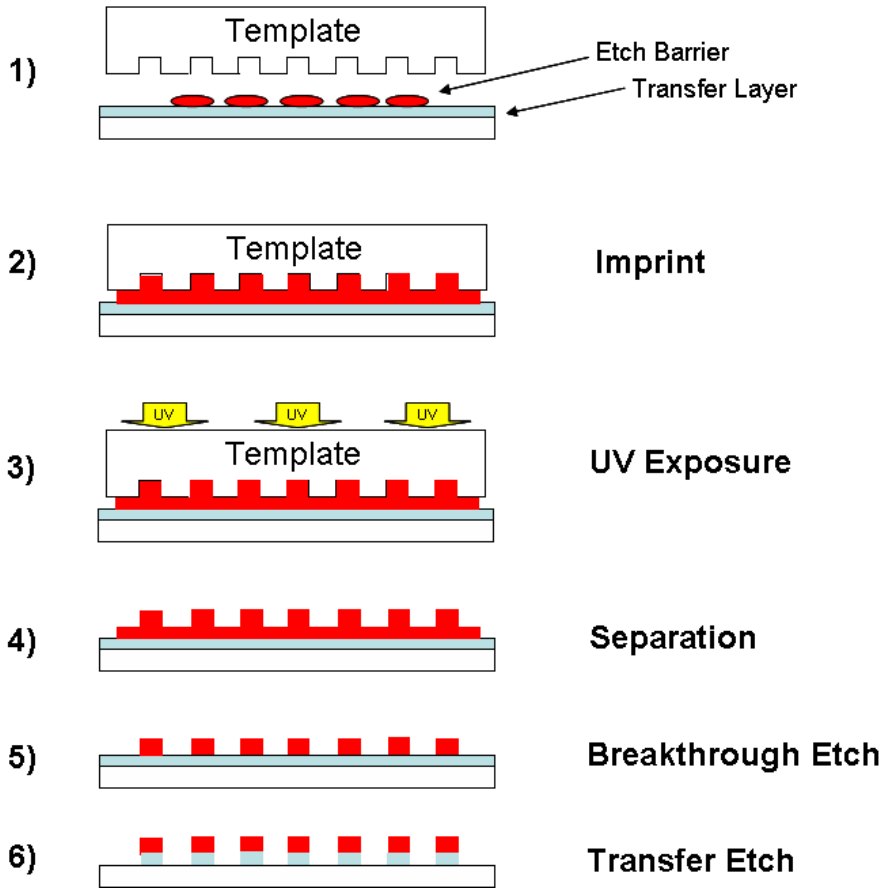

Figure 3.1.1: (1) Imprint etch barrier droplets are dispensed onto the substrate. (2) Template is placed in contact with liquid etch barrier which conforms to template topography. (3) UV exposure through the backside of the quartz template polymerizes the etch barrier. (4) The template is separated, leaving the template topography in the etch barrier. (5) A breakthrough etch removes excess etch barrier. (6) Further etching is used to transfer the topography into the transfer layer.

3.3 TEMPLATE FABRICATION

The SFIL template master is one of the most important aspects of the SFIL process, as it ultimately defines the maximum attainable quality of the imprint. All imprinting techniques are one-to-one processes where every feature, defect and unevenness in the template is directly replicated in the imprint. This section begins by providing an overview of the fabrication procedure to produce high quality templates for the SFIL process. This is followed by a detailed examination of each step including experimental details.

The goal of the template fabrication procedure is to create high resolution nano-topography on a very uniform and flat quartz plate. This requires the use of serial nanolithography techniques such as ion beam (Ruchhoeft, Colburn et al. 1999) or electron beam lithography (Thompson, Willson et al. 1994). As shown in Figure 3.2.1, electron beam lithography can be used to define high resolution nano-features in an electron sensitive polymer. The regions exposed to the electron beam can then be dissolved using an organic solvent. Using a dry etch, the exposed features are transferred into the chromium layer and subsequently transferred into quartz. Finally, the template is thoroughly cleaned removing any remaining material from the surface.

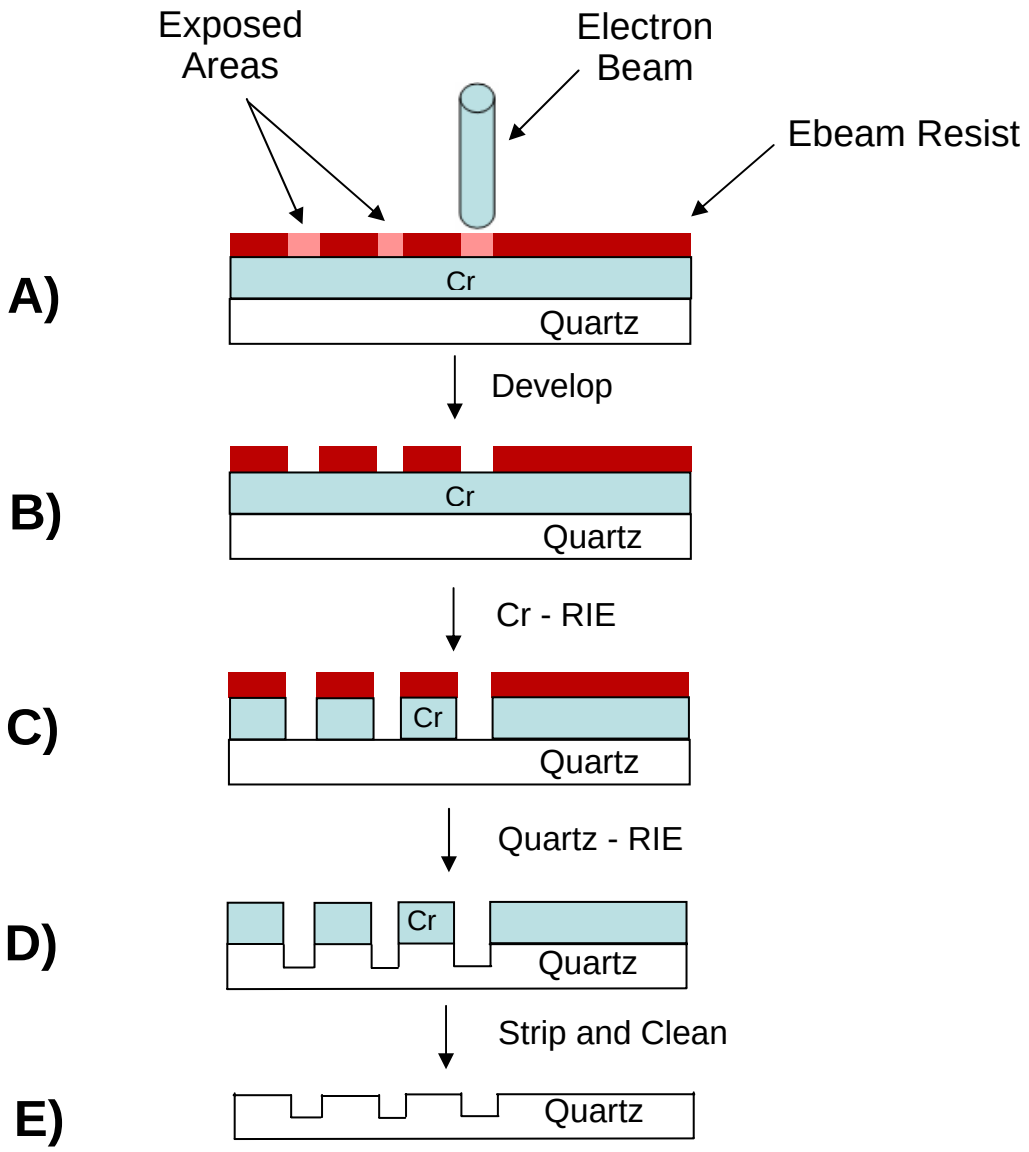

Figure 3.2.1: Schematic diagram of the template fabrication process. (A) High resolution features are written into an electron sensitive electron beam resist. (B) The resist is developed. (C) Features are transferred into a Cr layer that will serve as a hard mask. (D) Features are transferred into quartz. (E) Cr is stripped and any remaining organic material is removed.

The substrate of choice for SFIL templates is industry standard photomasks blanks (HOYA 6025, 6 x 6 x 0.25 inch). They offer extremely smooth surfaces ideal for high resolution electron beam imaging. Additionally, the 0.25 inch thickness reduces the

compliance of the template which minimizes imprint distortions. The Imprio 100, the imprinting machine used in this work, dictates a template size of 65 mm x 65 mm. Four individual template substrates were diced from a single photomask blank (Molecular Imprints) (Figure 3.2.2).

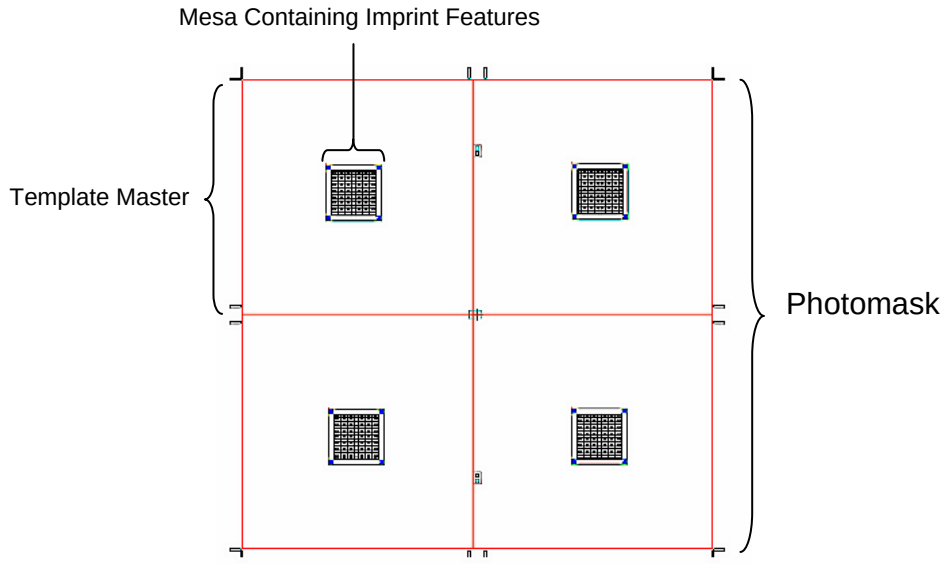

Figure 3.2.2: Dicing schematic showing template locations on photomask blank.

The feature topography of the template is created on a square pad in the center of the template known as the mesa. The mesa is a raised portion of the template that sits approximately 15 μm high. To create a mesa on the templates, traditional contact photolithography was used with a 1 μm thick NOVALAC (Shipley) photoresist. The patterned photoresist was then developed leaving resist only in the mesa region. The quartz mesa was defined by wet etching in buffered HF.

Before the template can be written with electron beam lithography, it is necessary to coat the template with a thin layer of chromium. The chromium serves two purposes.

First, it serves as a conductive layer so that excess charge can be dissipated during the electron beam lithography process. Secondly, it acts as a hard mask that provides etch resistant features that are later used in subsequent etching steps to transfer nanopatterns into the quartz mask. Traditional photomasks use a 100 nm chromium layer to meet opacity requirements. However, this is too thick for high resolution transfer quartz etching. A thin 15 nm chromium layer was found to be optimal and was deposited using an electron beam evaporator (CHA Industries).

An advantage of top-down approaches over self-assembly techniques is that the nanopatterns can be defined in a CAD environment. For this work, nanopatterns were designed in L-Edit and then converted to a machine readable format for the electron beam lithography tool. Imaging was performed using diluted 1:3 ZEP520A : ZEP A (Zeon Chemicals) positive photoresist that was spin coated onto the template at 3000 RPM for 60 seconds. After postbaking at 180ºC on a hot plate, the film thickness was measured with a Rudalph Ellipsometer to be 1500Å. The writing was performed using a JOEL-6000 electron beam lithography instrument with a beam current of 100 pA and area dose of 180 μC/cm. The exposed template was then developed in ZED-N50 (Zeon Chemicals) for 3 minutes and rinsed with IPA.

As mentioned above, the chromium layer acts as a hard mask for etching into the quartz substrate. The chromium layer can be defined by either using a wet etchant or a reactive ion etch (RIE). Wet etching is disadvantageous by being very isotropic in contrast to RIE and not particularly suited for reproducing high resolution features (Smith, Wasson et al. 2001). Therefore, an RIE etching process was selected to define the chromium hard mask. The RIE process was carried out in a Bachtop VII RIE etcher in a two step process. First, a short 5 second descum was used to remove any remaining electron beam photoresist residue in the exposed areas that was left from the wet

development process. The RIE parameters used were O_2 at 15 standard cubic centimeters per minute (SCCM) and a pressure of 5 mTorr and power of 100 watts. Secondly, the pattern was etched into the chromium layer by using a combination of O_2 at 2.25 SCCM and Cl_2 at 9.7 SCCM and a pressure of 80 mTorr and power of 75 watts. Next, the quartz was etched to a depth of 100 nm using a Plasma Therm 790 RIE etcher with CF_4 at 20 SCCM at a pressure of 5 mTorr and power of 200 watts. The final steps in the template fabrication process are removing the remaining photoresist and the chromium hard mask. The photoresist was stripped using a standard piranha bath 4:1 H_2SO_4:H_2O_2 at 105 °C for 10 minutes. The chromium was removed using Cyantek CR-7 perchloric based etchant for 3 minutes at room temperature.

The fabrication process was characterized using a resolution target that was written onto the template, shown in Figure 3.2.3 as a CAD image. The target consists of posts of varying diameter and pitch with the smallest being 25 nm in diameter. A FEI Strata DB235 field emission scanning electron microscope was used to characterize the transfer of the pattern into the chromium hard mask, as shown in Figure 3.2.4. At the present date, the smallest features that were successfully transferred into the chromium layer with our instrument were 45 nm in size. After a subsequent quartz etching process, the templates were imprinted into a photocurable resist as described in detail below. The replica remaining in the photocurable resist was then characterized using a Hitachi S-4500. The results are shown in Figure 3.2.5, where the original size of the electron beam written posts onto the template were 60 nm, the written features were transferred as 80 nm posts in monomer resist. The difference in resolution from the initial pattern is due to the combination effect of suboptimal parameters in the electron beam lithography process and RIE etching process. As these process steps are further optimized, the minimum successful feature size will approach the sub 30 nm range.

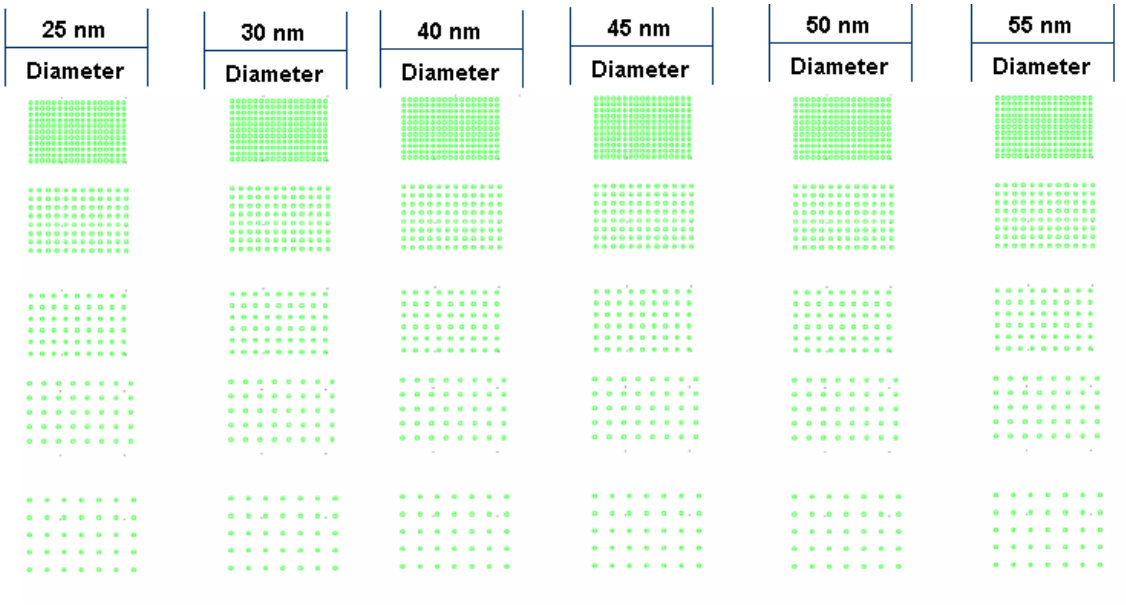

Figure 3.2.3: CAD image of template characterization resolution target.

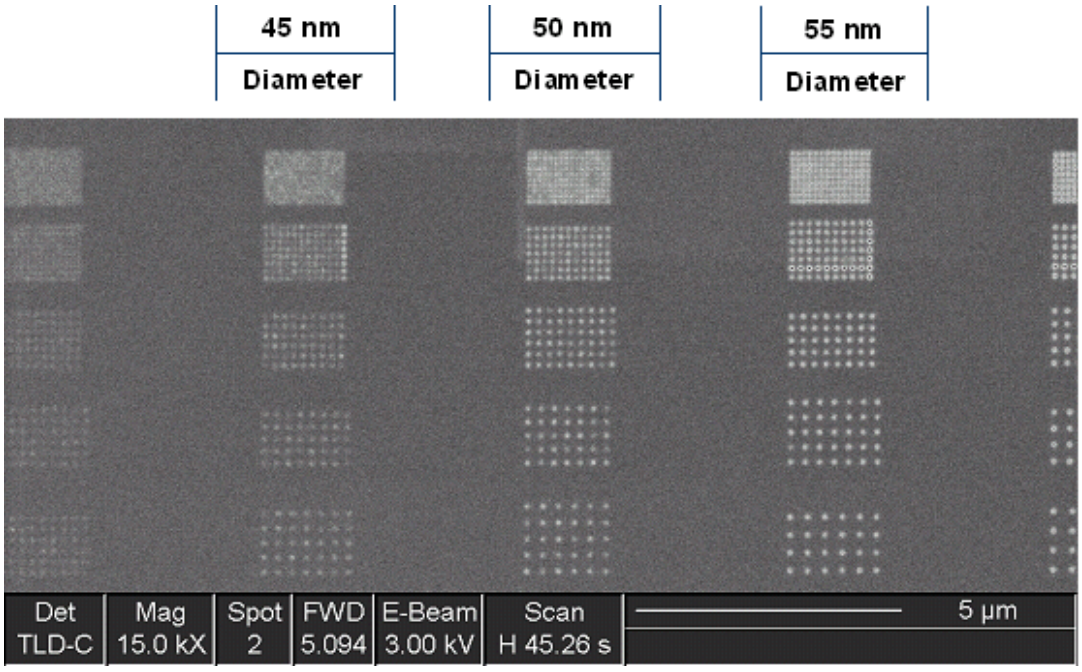

Figure 3.2.4: SEM image of chromium mask layer after RIE etching of chrome. Features in the 55 nm rage were clearly defined but the quality of the patterning quickly degraded for features smaller than 50 nm.

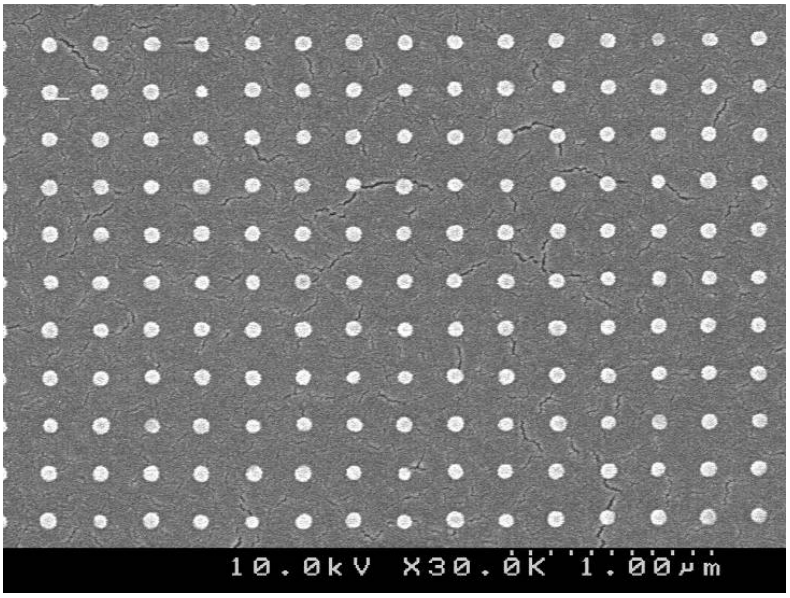

Figure 3.2.5: SEM image of SFIL resist with 80 nm diameter imprinted posts. The original written diameter using electron beam lithography on the template was 60 nm. The possessing steps used to fabricate the template resulted in the broadening of the features.

3.4.1 SFIL PROCESS

In the following sections, a detailed description of the SFIL process will be presented. This will cover both the experimental parameters concerning the imprinting process as well as modifications to the SFIL process to achieve samples that can be biologically functionalized. The template used in the SFIL development work was a generous gift from Molecular Imprints. It consists of a matrix of posts that are of varying diameter and pitch, as shown in Figure 3.3.1. Each sub square of posts is 1 mm x 1 mm and the total mesa size is 10 mm x 10 mm.

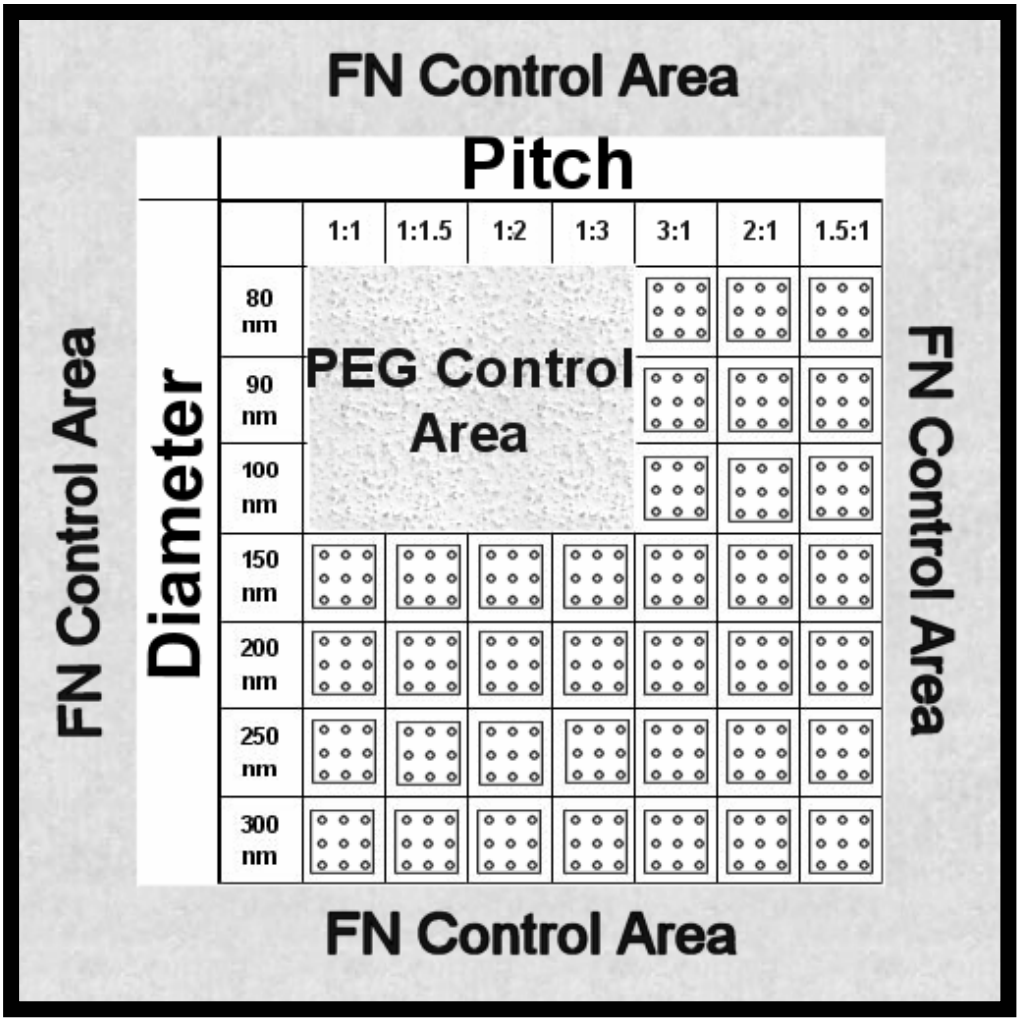

Figure 3.3.1 Schematic diagram of features on imprinting template.

3.4.2 SFIL TEMPLATE PREPARATION

A critical step in the imprinting process is being able to release the template from the cured monomer. Cured monomer that adheres to the template not only ruins that particular imprint but also subsequent imprints. The two most common scenarios of release failure are delamination or feature rupture, as shown in Figure 3.3.2. Successful release is governed by the surface energy of the template and substrate as well as the bulk properties of the imprint resist.

The SFIL template was cleaned before use using a standard piranha bath 4:1 H2SO4:H2O2 at 105 °C for 1 hour. It was thoroughly rinsed with deionized water and dried with nitrogen. To reduce the surface energy of the template, Relmat, an anti-adhesion coating (Molecular Imprints), was applied to the template. The template was then rinsed with IPA to remove any excess Relmat and dried with nitrogen.

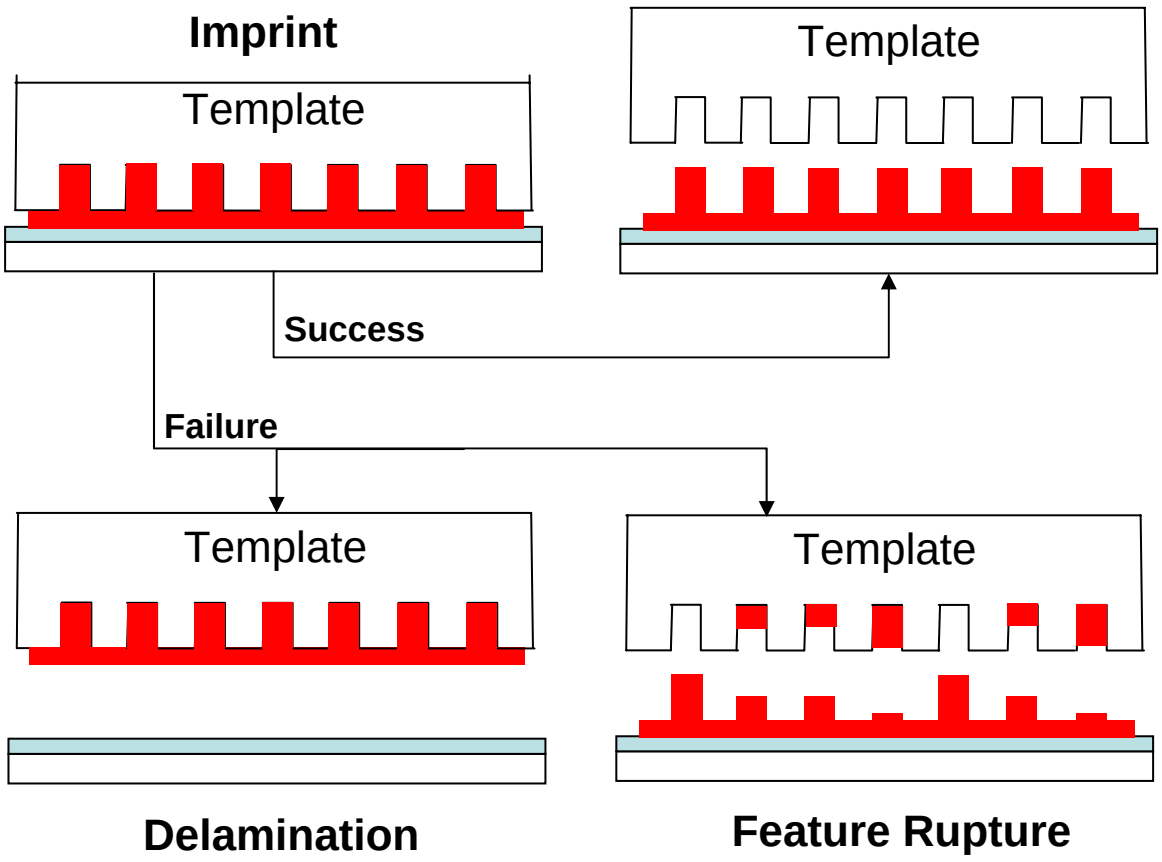

Figure 3.3.2: Depiction of the two most common forms of release failure: delamination and feature rupture.

3.5.1 SFIL SUBSTRATES

Substrate selection for SFIL is limited by the nature of the imprinting and liftoff processes. Substrate flatness and uniformity directly correlate with residual layer

thickness and quality. Therefore, extremely flat and uniform substrates are highly desired. Even slight undulations in the substrate cause unevenness in the imprint. This can render the imprints unusable because they become impossible to properly dry etch with RIE. Minor imprint thickness variations can be accommodated to some extent with certain RIE etching conditions, as will be discussed in Section 4.2. Although these compensations yield an imprint that is suitable for traditional semiconductor processing, they are usually not suitable for metal liftoff because the remaining residual material is too thin. Because the substrate requirements needed for later biological functionalization requires metal liftoff, it dictates tighter flatness and uniformity requirements over typical SFIL substrates.

A major concern with the SFIL process is the cleanliness of the substrate. Even small dirt particles measuring less than a micron on the surface of the wafer can cause major imprinting problems. As the template approaches the substrate surfaces, forces are measured to enable the imprinting tool to gauge when the template has come into contact with the surface. It is indistinguishable whether the template has come into contact with the substrate surface or with a dirt particle. If the template contacts a dirt particle instead of touching the surface, this will send a false message to the imprint controller that the surface has been reached. Major problems ensue if the template has come close enough to the surface to touch the monomer but not far enough to displace the liquid. Upon exposure with UV, the monomer is then cured onto the template but is weakly bonded to the substrate. Upon lifting the template from the surface, the entire cured monomer is ruptured and adheres to the template. This renders the template unusable, and it must be unloaded from the tool, thoroughly cleaned and recoated with an anti-adhesion agent before it may be used again.

3.5.2 SFIL ON TRANSPARENT SUBSTRATES

In developing this process, both optically transparent and non-transparent substrates were investigated. For further biological studies, it was desired to have a substrate that was optically transparent. This would allow the platform to be easily transitioned for use of several established biological analysis techniques in our lab such as total internal reflectance microscopy (TIRF) (Mathur, Truskey et al. 2000; Mathur, Truskey et al. 2000). Double side polished (DSP) pyrex, fused silica, quartz and borofloat wafers were investigated as possible substrate candidates.

Difficulty in detecting dirt on the substrate while in the imprinting tool proved to be the major obstacle to imprinting on transparent substrates. In contrast to reflective substrates, dirt particles could be identified and imprints could be made around the trouble areas. Additionally, several calibration steps to achieve optimal imprinting results require refinement of tool settings based on the uniformity of previous imprints. The transparent nature of the substrates made it impossible to optically quantify the necessary information in order to fine-tune the imprinting process. Also, the 8 inch glass substrates in general had logistical problems because they could not fit in a number of processing tools without being cut. Cutting mid-process introduced problems because the glass wafers could not be easily cleaved like silicon and required a wet dicing saw for accurate breaks. Moreover, wet dicing is an extremely dirty process that deposits a layer of cutting debris across the surface of the substrate, rendering it infeasible for mid-process use. As a result, the 8 inch glass wafers were scribed by hand resulting in low imprinting yields since most breaks erratically branched off and ruined good imprints. However, 4 inch substrates could be used without requiring cutting mid-process and ultimately resulted in higher yields. The devices on the 4 inch substrates were separated using a wet dicing saw at the end of the process, which minimized any contamination

issues. The tradeoff between the two sizes is decreased throughput and decreased leveling precision on the 4 inch substrates.

In addition to the processing challenges, we experienced major problems with the quality of the transparent materials used for this portion of the work. Although relatively high-quality DSP pyrex, fused silica, quartz and borofloat wafers were purchased, the surface quality specifications for glass substrates are far below what is expected for a prime Si DSP wafer. This caused major processing problems because all of the transparent materials used had long-range distortions over several millimeters which resulted in non-uniform imprints.

The solution to the long-range distortions was procurement of higher quality materials. From the work in this section, we did not observe a difference in imprint quality from one transparent material to another. Imprint quality appears to be only a function of surface quality. Future work may want to explore sapphire as a possible substrate material since it is commercially available with surface uniformity properties similar to prime DSP Si.

In conclusion, the current optimal substrate for achieving the highest resolution and yield was prime double side polished, 200 mm silicon wafers with an epitaxially grown layer of silicon on the front side. It provided the smoothest, most uniform surface for imprinting and very high yield rates. The reflective nature made it easy to identify dirt during the imprinting process. Furthermore, the settings of the imprinting tool could be fine-tuned during the stepping process so uniformity of the imprints could be analyzed optically.

3.5.3 SFIL SUBSTRATE PREPARATION

All wafer substrates used were cleaned using a standard piranha bath 2:1 H2SO4:H2O2 at 95 °C for 12 minutes. They were thoroughly rinsed with deionized water and dried with nitrogen. It was necessary to treat the substrate surfaces with an adhesion promoter to prevent delamination of the cured imprint resist. DUV-30J (Brewer Science), a bottom antireflective coating, was spin coated onto the substrates at 3500 RPM for 60 seconds. After postbaking at 205ºC for 60 seconds on a hot plate, the film thickness was measured with a Rudalph Ellipsometer to be 50 nm.

Another important role of the BARC coating is to act as an etching transfer layer in the bilayer resist scheme (Figure 3.1.1). Using a silicon containing resist as an etch barrier and a non-silicon containing BARC layer, significant etch selectivity between the layers can be achieved with RIE. This allows features to be created that have a higher aspect ratio than those on the template master. Etching of the bilayer structures will be considered further in Section 4.2.

3.6.1 DISPENSING SILICON CONTAINING MONOMER

After leveling both the wafer and template and ensuring that they are in the same plane, monomer was dispensed on the surface to begin the imprinting process. The volume of silicon containing monomer dispensed plays an important role in achieving a uniform imprint. Too large of a volume of monomer dispensed leads to monomer attaching and polymerizing to the outside edge of the template and thereby ruining subsequent imprints. Too little monomer dispensed results in non-uniform imprints and often feature ruptures which foul subsequent imprints. The ideal volume to be dispensed

can be calculated by finding the volume of material needed to fill in the voids in the template as well as a buffer layer of 30 nm. For the template used in this work, the volume was calculated to be approximately 30 nanoliters. The variables in dispensing monomer were controlled using a micropiezoelectric jet system and moving the substrate with an X-Y stage. To achieve a uniform distribution of the silicon containing monomer beneath the template, it was necessary to dispense the monomer in droplets. This allowed each droplet dispensed to have a unique volume dependent upon the amount needed to fill the voids in that particular quadrant of the template. The optimized drop pattern that was developed for the template in this work is shown in Figure 3.3.3. The size of the circles corresponds to the volume of drop dispensed. This pattern was then further optimized during imprinting to account for slight leveling mismatches between the template and the substrate.

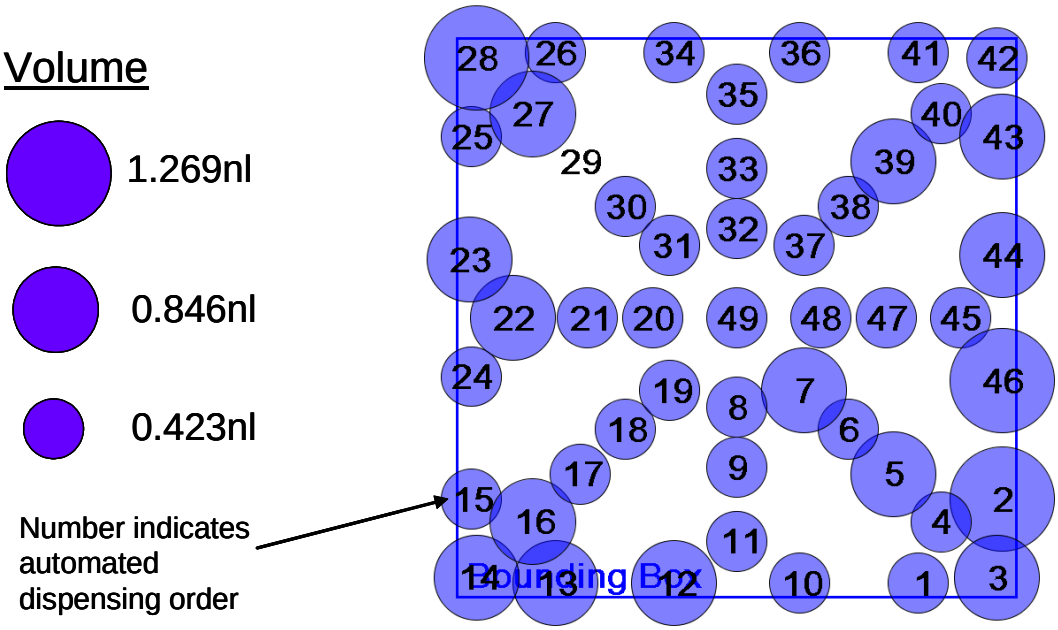

Figure 3.3.3: Depiction of optimized monomer droplet distribution for the template in this work. The identification numbers on the drops correspond to data rows in the automated dispense matrix. The size of the circle corresponds to the volume of drop dispensed.

3.6.2 TEMPLATE IMPRINTING

After dispensing the silicon containing monomer, the template was placed into intimate contact with the drop pattern. Helium was flushed continuously around the template to decrease the presence of oxygen, which inhibits the free radical polymerization of the monomer. Experimentally, it was found that the time needed for the liquid to fill the voids in the template and for the system to become stable was approximately 90 seconds. When in contact with the liquid, the levelness of the template was controlled by applying force on three locations on the template. Typical corner forces at these locations were approximately 0.7 N with a total force of 2.1 N. After 90 seconds, the monomer was polymerized by illuminating through the backside of the quartz template with UV light source. The template is then separated from the polymerized resist and the imprinting process is repeated across the surface of the substrate. A 200 mm wafer can hold up to 154 – 10 mm x 10 mm imprints and typical yields are greater than 95%. A completed wafer is shown in Figure 3.3.4.

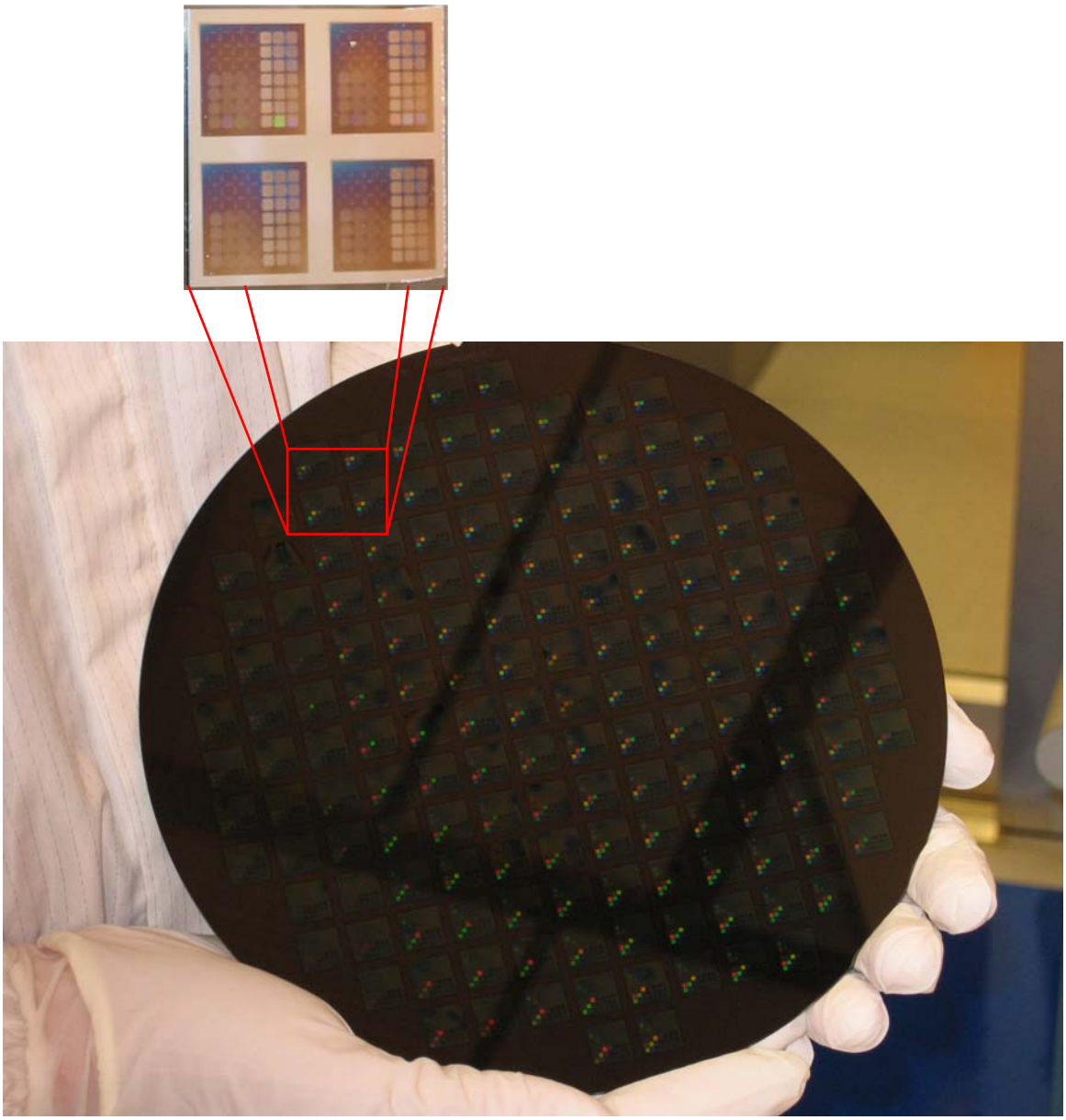

Figure 3.3.4: Completed 200 mm silicon wafer containing 154 imprints.

Ideally, the template should come within a few nanometers of the surface and be completely level with the proper volume of monomer dispensed as in Figure 3.3.5a. However, often the process has a combination of non-idealities. If too much of the monomer is dispensed, an excessive RIE breakthrough etch distance is required which

leads to broadening of the features (Figure 3.3.5b). If too little monomer is dispensed, this leads to non-uniform imprints and often feature rupture (Figure 3.3.5c). When the template is not in the same plane as the substrate, this causes the etch barrier to be non-uniform (Figure 3.3.5d). The thicker portion requires a longer breakthrough etch to reach the BARC layer and often the thinner regions are etched away before this point is reached. Thus, the etching process can be tuned to save the thick portion or the thin portion but not both. Lastly, slight undulations in the surface of the wafer causes unevenness in the imprint and identical etching problems as discussed above (Figure 3.3.5e).

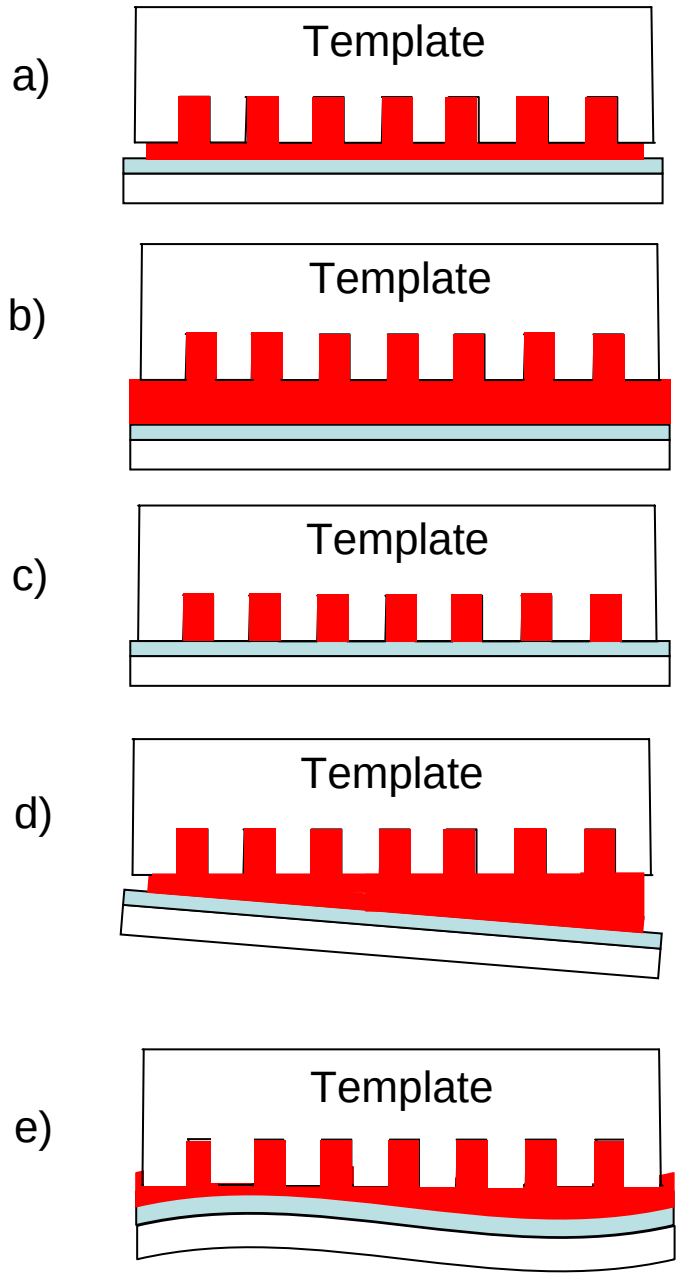

Figure 3.3.5: Depiction of common imprint problems. (a) The ideal thickness of the residual imprint monomer should be several nanometers thick and uniform. (b) Too large of a volume of monomer leads to pattern degradation during RIE etch steps. (c) Too little of a volume results in non-uniform imprints and often feature rupture. (d) The template and substrate are not in the same plane resulting in non-uniformity in the imprint. (e) Undulations in the substrate are a major cause of imprint non-uniformity.

REFERENCES

Mathur, A. B., G. A. Truskey, et al. (2000). "Atomic force and total internal reflection fluorescence microscopy for the study of force transmission in endothelial cells." Biophysical Journal **78**(4): 1725-1735.

Mathur, A. B., G. A. Truskey, et al. (2000). "Total internal reflection microscopy and atomic force microscopy (TIRFM-AFM) to study stress transduction mechanisms in endothelial cells." Critical Reviews in Biomedical Engineering **28**(1-2): 197-202.

Ruchhoeft, P., M. Colburn, et al. (1999). "Patterning curved surfaces: Template generation by ion beam proximity lithography and relief transfer by step and flash imprint lithography." Journal of Vacuum Science & Technology B **17**(6): 2965-2969.

Smith, K. H., J. R. Wasson, et al. (2001). "Cr absorber etch process for extreme ultraviolet lithography mask fabrication." Journal of Vacuum Science & Technology B **19**(6): 2906-2910.

Thompson, L. F., C. G. Willson, et al. (1994). Introduction to microlithography. Washington, DC, American Chemical Society.

CHAPTER 4: ETCH AND LIFTOFF PROCESS DEVELOPMENT

4.1 OVERVIEW OF ETCHING PROCESS

The etching process is used to convert the topography in the bilayer resist structure into a usable structure for further processing. The etching processes can be divided into two separate processes. First, the silicon containing upper resist layer is etched in what is termed a "breakthrough" etch. This short etch is used to expose the lower or transfer layer in the recessed portions of the upper layer, as shown in Figure 4.1.1b. Second, an anisotropic etch that is selective for the transfer layer is used to transfer the recessed regions from the upper layer into the lower layer (Figure 4.1.1c). The resultant is a resist structure that can have a higher aspect ratio than the original template depending on the transfer layer thickness.

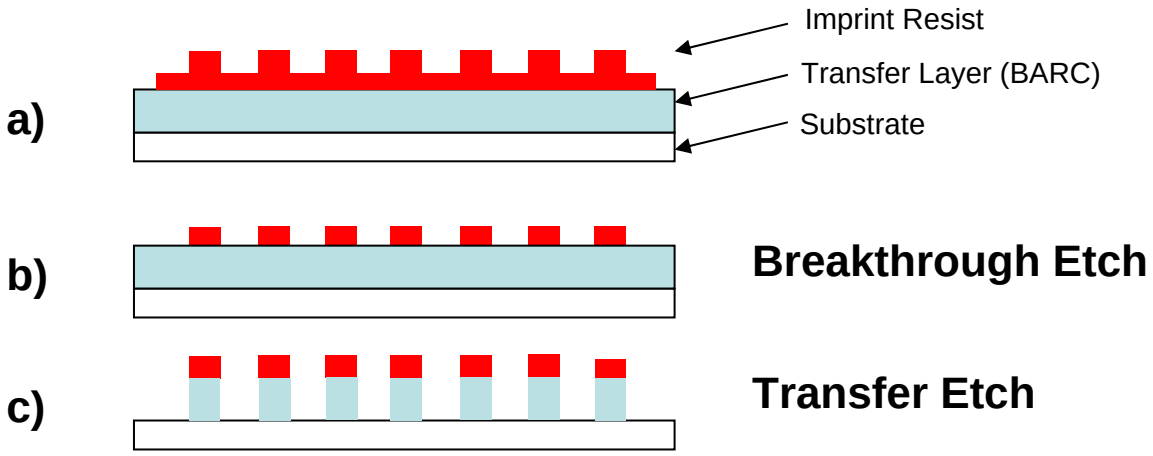

Figure 4.1.1: Depiction of the two step RIE process. (a) Bilayer resist structure immediately after imprinting. (b) A breakthrough etch is used to remove material from the upper layer exposing the underlying transfer layer. (c) A transfer etch is used to selectively etch the lower transfer layer and not the upper layer effectively using the upper layer as a mask.

4.2 REACTIVE ION ETCHING PROCESS DEVELOPMENT

Reactive ion etching uses high energy fields to rapidly dissociate a feed gas to form highly energetic ions, photons, electrons and reactive radicals. Under high electric fields, ionic species are bombarded onto the surface which causes both a physical and chemical removal of atoms from the surface. Four main factors control the etching rate and profile in reactive ion etching: feed gas chemistry, gas flow rate, power and reactor pressure. Feed gas chemistry plays an important role in determining the etch selectivity between two materials. Reacting gas in a chamber can either react with the material to form volatile or non-volatile components. Volatile components are removed by the continuous vacuum pumping of the reaction chamber whereas non-volatile components remain on the surface of the material. For instance, oxygen ions are highly reactive with organic compounds and results in the formation of volatile components such as CO and CO_2. However, silicon containing materials react with oxygen ions to form non-volatile silicon dioxide. An oxygen etch therefore provides etch selectivity between organic compounds and silicon containing compounds by reactant volatility. Another means of achieving selectivity is choosing a feed gas that is reactive with one material and not another. For instance, CHF_3 dissociates to form a fluorinated ion that is highly reactive with silicon containing compounds to form volatile component SiF_4. However, fluorinated ions are relatively uncreative with organic materials. Thus, the CHF_3 gas chemistry provides another selectivity between organic materials and silicon containing materials.

Ion and radical concentrations in the reactor chamber are controlled by the gas flow rates and the reactor power. The power controls both the ion density of the plasma and the acceleration of the ions onto the surface. A higher reactor bias power results in ions that are accelerated with more force into the surface and a more anisotropic and

faster rate of etch. The chamber pressure also plays an important role in controlling the anisotropy of the etch. Etching at low pressures reduces the mean free path of ions, (the distance before an atom collides with another atom) and changes trajectory. Lower pressure inherently increases the anisotropy of the etch but with the tradeoff of a lower etch rate.

The goal in designing the etching process was to have a surface structure that was amenable to metal liftoff, which still preserved the critical dimensions of the imprint resist. This dictated that the etch be both highly selective and highly anisotropic. The parameters that were adjusted to achieve this goal were the thickness of the residual layer, thickness of the imprint resist, reactor gas chemistry, feed gas flow rates, chamber pressure, chamber power and reaction times.

Gas chemistry was selected in order to achieve high selectivity between the silicon containing polymer upper layer and the organic lower layer. In the first etching step, the "breakthrough" etch was performed using a combination of CHF_3 and O_2. Chlorofluorocarbons by themselves will often produce polymer deposition onto the surface in parallel with an etching process. A low concentration of oxygen was added to the reactor to suppress polymerization (Mogab, Adams et al. 1978). Figure 4.2.1 shows SEM images of the unetched resist stack and Figure 4.2.2 shows the resist stack after the breakthrough etch step. The transfer etch was conducted using O_2. In this etch, radical oxygen reacted with the upper silicon containing polymer to form a hard SiO_2 mask while the lower organic BARC layer reacted to form volatile components.

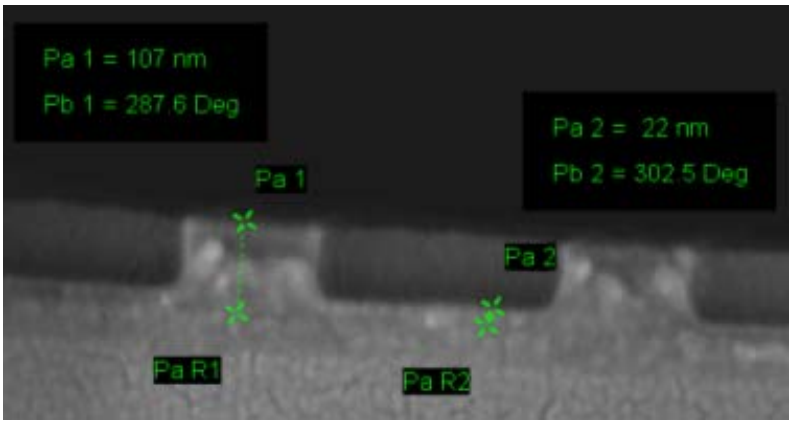

Figure 4.2.1: SEM image of the imprinted silicon containing monomer and the underlying BARC layer. The line 'Pa 1 – Pa R1' corresponds to the imprinted monomer and is 107 nm thick. The line 'Pa 2 – Pa R2' corresponds to the 22 nm of residual silicon containing monomer that needs to be removed to access the underlying BARC layer. Although somewhat difficult to see in this image, the BARC layer extends from the top of the 'Pa R1' labeled box to the 'Pa R1' cross marker. Both the 'Pa R1' box and the 'Pa R2' box align to the border between the bare silicon surface and the bottom of the BARC layer. The BARC layer is 40 nm thick and is not labeled in this image.

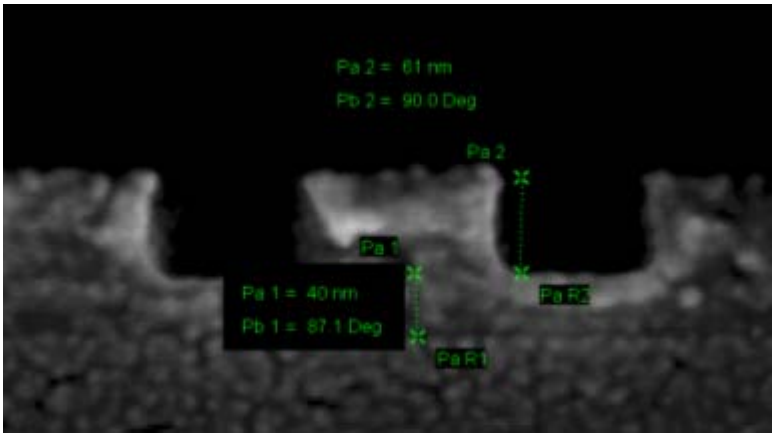

Figure 4.2.2: SEM image of the imprinted silicon containing monomer and the underlying BARC layer after the breakthrough etch. The line 'Pa 1 – Pa R1' corresponds to the underlying BARC layer. The line 'Pa 2 – Pa R2' corresponds to the remaining silicon containing monomer. During the etching process approximately 40 nm of silicon containing monomer has been removed in a CHF_3 plasma etch. Notice that minimal damage has been done to the underlying BARC layer as it is still 40 nm thick.

Etch rate data was collected for the underlying BARC layer by spin coating silicon wafers with DUV-30J (Brewer Science) as described above. The film thickness on the wafers was measured with an ellipsometer, was etched for a specified length of time and was measured with the ellipsometer. Etch rates for both the silicon-containing polymer and the bilayer structures were measured using a field emission scanning electron microscope (LEO 1530).

After establishing baseline etching rates, the reactor power, gas concentrations, gas flow rates and reactor pressure were optimized to achieve high selectivity and an anisotropic etch. Data concerning the etch profile of the bilayer structure was collected using a field emission scanning electron microscope (LEO 1530). Final parameters are shown in Tables 4.2.1 and 4.2.2.

Breakthrough Etch	
Parameter	**Value**
O2 Flow Rate	5 sccm
CHF3 Flow Rate	40 sccm
Chamber Pressure	25 mTorr
Time	30 sec
RF	450 V

Table 4.2.1: Optimized RIE parameters for the breakthrough etch.

Transfer Etch	
Parameter	**Value**
O2 Flow Rate	8 sccm
Chamber Pressure	5 mTorr
Time	150 sec
RF	300 V

Table 4.2.2: Optimized RIE parameters for the transfer etch.

4.3 METAL LIFTOFF PROCESS DEVELOPMENT

The goal of the metallization and liftoff procedure was to develop a successful process that could transform the imprinted features into gold nanostructures on the surface of the substrate. These gold nanostructures would later serve as protein immobilization points, as will be discussed in Section 5.2. Metal liftoff works by coating the entire substrate with a thin film of metal. The substrate is usually either placed in an organic solvent or oxidizing solution to remove all of the organic resist from the substrate. Metal that is attached to the resist will also be removed or "lifted off", whereas metal that is attached directly to the substrate will remain.

Metallization was performed by thermally evaporating (Denton) a 3 nm layer of chromium (Kurt Lesker) as an adhesion layer and then followed by 17 nm of gold (Kurt Lesker). Optimal lift off was performed in TL1 (NH_4OH:H_2O_2:H_2O - 1:1:6) at 80 °C for 270 seconds. Piranha (H_2SO_4:H_2O_2 - 2:1) at 80 °C for 60 seconds also worked for some resist structures but often was too aggressive and would remove gold nanostructures from the substrate surface.

Several obstacles had to be overcome in the development of the metallization and liftoff process. The first set of problems stemmed from the actual structure of the bilayer resist after etching. The most common structure-related failure was from metal bridging between nanostructures, which resulted in failed liftoff. The bridging was caused by a combination of the thinness of the residual layers and the level of anisotropy of the etch. Figure 4.3.3 shows that when the residual layer is too thin, the metal bond between the top of the resist and substrate is strong enough to withstand the liftoff process and form a metal bridge. Experimentally, it was determined that the residual layer needed to be larger than approximately 100 nm for successful liftoff. However, simply increasing the thickness of the structure posed some difficulty. Increasing the silicon containing upper

layer of the bilayer structure was not an option because it would always be the same height due to the breakthrough etch. There is also a maximum thickness for the BARC layer due to the fact that at some point during etching the upper resist layer will be etched off. At this point there would be no upper hard mask to define etch selectivity. The entire structure would etch at the same rate and, thus, negate any additional thickness of the BARC layer. Although increasing the BARC layer helped, it had the tradeoff of a thicker layer leading to less accurate reproduction of features, less stable structures and, most importantly, less vertical sidewalls. Figure 4.3.4 shows that if the sidewalls are sloped, even with a thick residual layer, bridging will result. The ideal structure for liftoff is one with significant undercut of the BARC layer. This will minimize bridging problems and require thinner residual layers for successful liftoff, as shown in Figure 4.3.5. The solution to obtaining the ideal structure was a careful balance of the etching parameters between the residual BARC layer and silicon containing monomer. Figure 4.3.6 shows a SEM image of a sample after etching with an 18 nm coat of Au. Notice the undercut of the BARC layer and the crack in the Au layer between the Au posts and the upper Au material.

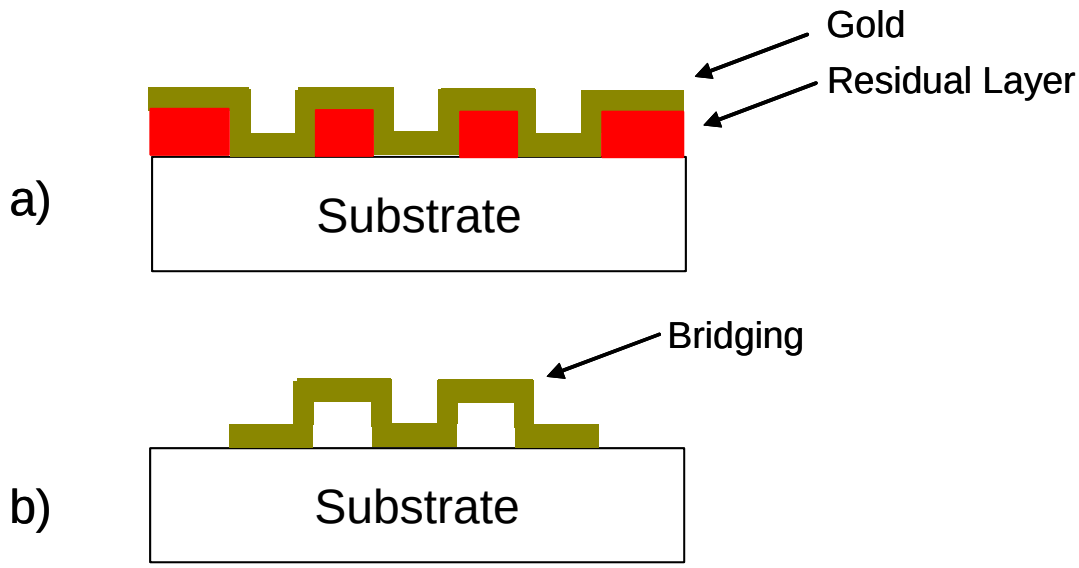

Figure 4.3.3: If the residual layer is to too thin, the bond between the metal on the top of the resist and metal on the bottom of the resist can become strong enough to withstand the liftoff process resulting in bridging. (a) Before liftoff. (b) After liftoff.

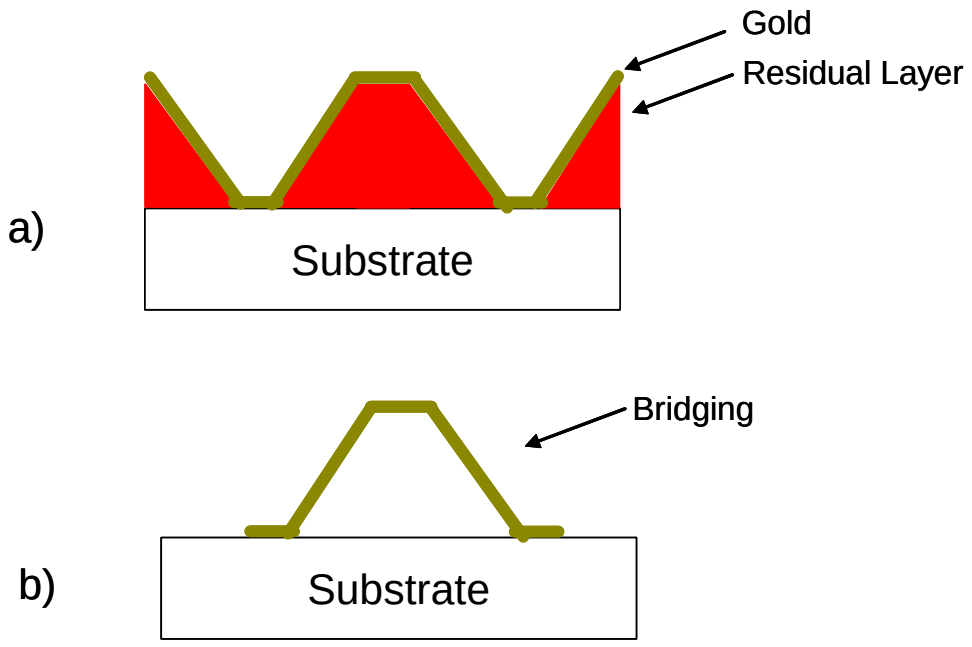

Figure 4.2.4: Even with a thick residual layer, if the walls have a significant slope this will also lead to bridging. The material ratios and dimensions in this Figure are exaggerated for clarity. (a) Before liftoff. (b) After liftoff.

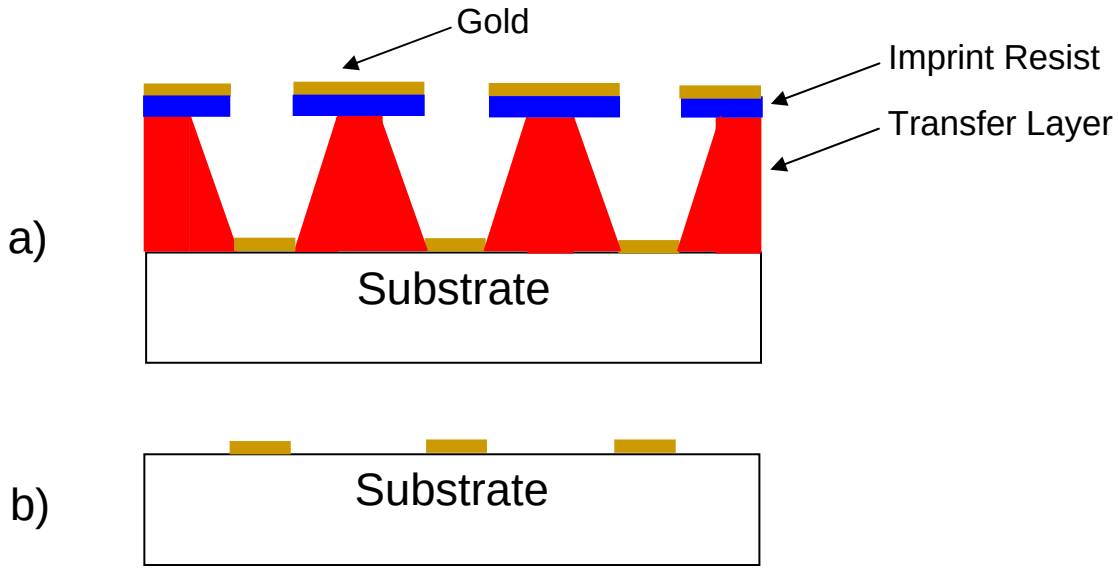

Figure 4.2.5: The ideal situation is to have some amount of undercut to prevent metal bridging. The height of the transfer layer has been exaggerated for clarity. (a) Before liftoff. (b) After liftoff.

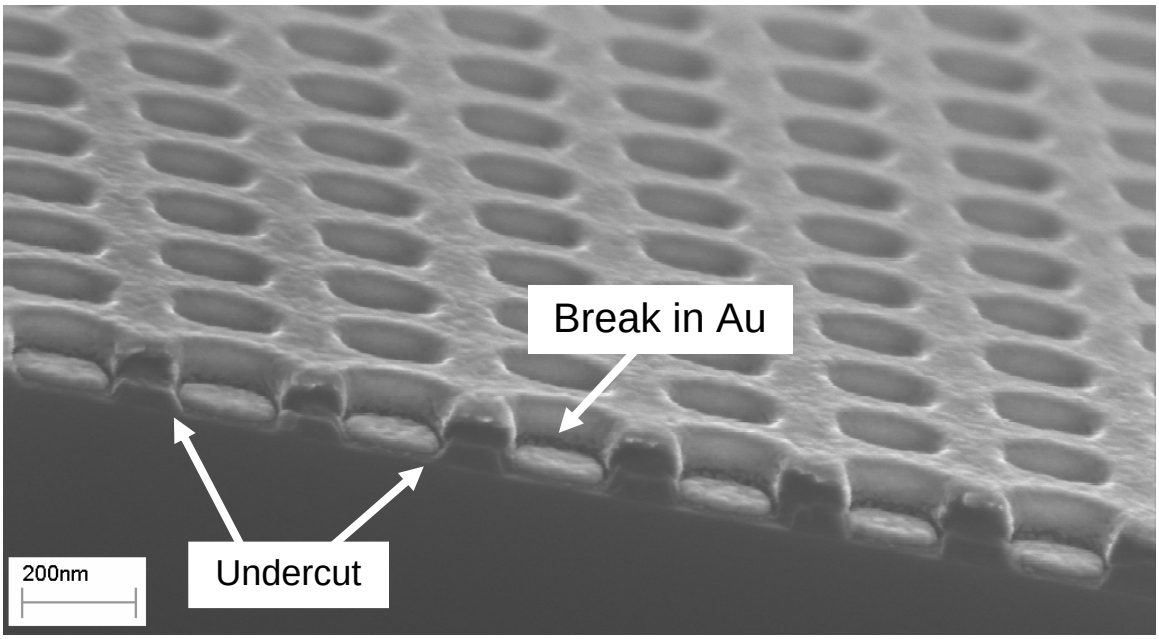

Figure 4.2.6: SEM image of a sample after etching and then coated with an 18 nm layer of Au. Notice that the BARC has an undercut similar to depicted in Figure 4.2.5. The undercut allows a clean break between the Au top layer and the deposited Au posts on the silicon wafer.

Although the BARC layer proved to be indispensable as an adhesion promoter and as an etching transfer layer, it was not easily removed. No organic solvent was found that could successfully remove the resist. The only options that worked were strong oxidizing solutions such as piranha and TL1. Although piranha produced successful liftoff, it was often difficult to control. Often areas would liftoff at significantly different time points depending on the ease of access of the solution into and around the nanostructures. This posed a problem because the now exposed nanostructures in the lifted off areas were exposed to the aggressive piranha solution for the duration of time it took for the rest of the sample to complete liftoff. Often during this period, the piranha would begin to remove the earliest exposed nanostructures. Although the ammonium hydroxide in the TL1 solution is known to etch Au to some extent, it showed a high degree of selectivity between Au and the BARC layer. Diluted TL1 also proved to be much less aggressive than Piranha. After the optimization of the RIE etching parameters above, uniform liftoff was achieved with diluted TL1 where the resist-supported Au layer would peel off as a single sheet.

4.4 CONSIDERATIONS FOR TRANSPARENT SUBSTRATES

As discussed in Section 3.5.2, transparent substrates were explored due to their optical compatibility with many conventional microscopy tools. A challenge that was encountered was due to the low quality standards of glass DSP wafers in comparison to the silicon DSP wafers. The glass DSP wafers we received had long range distortions, which prevented us from achieving uniform imprints across the wafer surface in most cases. Future work in this area could resolve these problems by procuring higher quality glass substrates with surface properties similar to prime grade silicon DSP wafers. Due

to research financial constraints, we developed a technique to compensate for the deviations in the materials we had available.

The difficulty with etching non-uniform substrates is that for a given etching recipe, part of the samples are overetched while other parts are underetched, as shown in Figure 4.4.1. After liftoff, this results in three different areas: (1) Underetched areas have no Au; (2) Overetched areas have only Au or bridging between transferred patterns; and (3) Areas etched properly have patterns that have been transferred successfully.

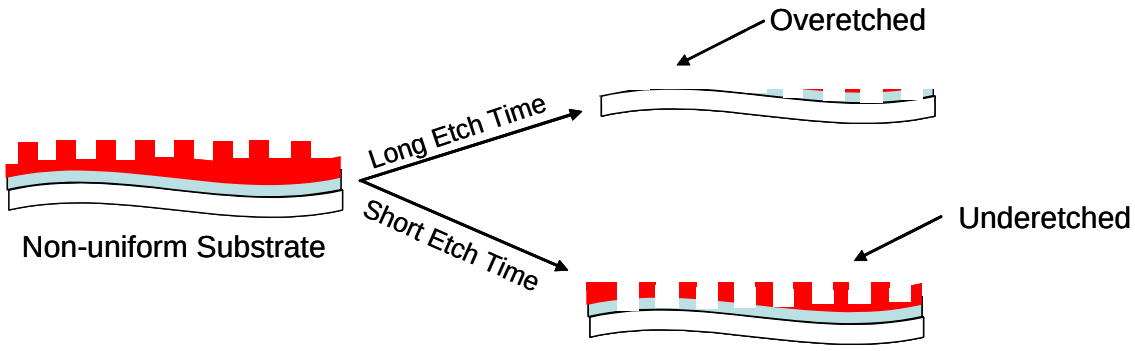

Figure 4.4.1: Cartoon depiction of a non-uniform substrate and the problems associated with etching a usable pattern. Long etching times result in overetching some portions of a sample, while short etching times result in underetching of other parts of a sample.

All NOBIL samples, whether on glass or on silicon, display visible color bands that correspond to film thickness. A metrology tool, such as an ellipsometer or nomarski microscope, can be used to determine film thickness, as discussed in Chapter 3. However, no metrology tools were available in our cleanroom for measuring film thickness on transparent substrates. The next best tool was the human eye, which worked very well in determining relative thicknesses based on color bands. A color band calibration chart was created by taking images with a digital camera before etching, after etching and after liftoff. The calibration chart was used as a reference to adjust the

etching times for each sample in order to achieve maximum usable area yield. This resulted in significantly higher yields by customizing the etching parameters for each sample at the cost of low throughput. Figure 4.4.2 shows the results of two different degrees of non-uniformity and the resulting usable etched areas.

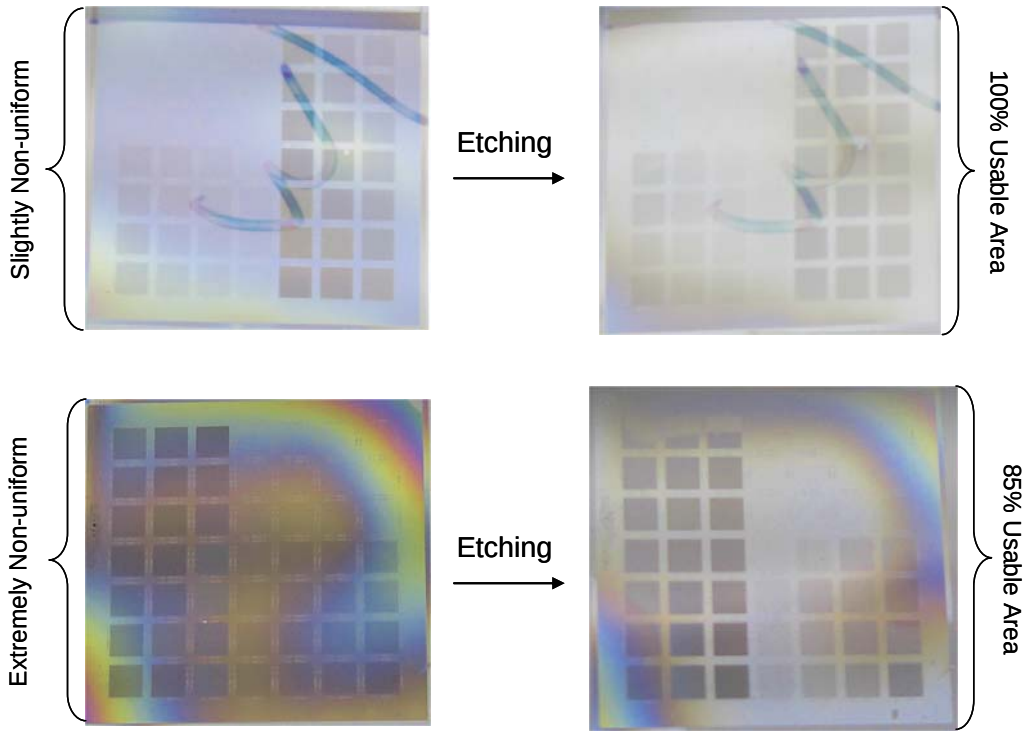

Figure 4.4.2: (Left) Digital photograph of an unetched slightly non-uniform substrate and extremely non-uniform substrate. (Right) Digital photograph showing the resulting samples after running a customized etching protocol to optimize sample yield.

REFERENCES

Mogab, C. J., A. C. Adams, et al. (1978). "Plasma Etching of Si and Sio2 - Effect of Oxygen Additions to Cf4 Plasmas." Journal of Applied Physics **49**(7): 3796-3803.

CHAPTER 5: SURFACE FUNCTIONALIZATION AND SAMPLE CHARACTERIZATION

5.1 OVERVIEW

This chapter reviews the methodology to biologically functionalize the patterned surfaces and several studies that were performed to characterize different properties of the bioactive surfaces. It begins by investigating pattern transfer fidelity immediately after liftoff in order to quantify pattern transfer resolution. Next, the methodology of orthogonal surface functionalization is presented and characterized using adhesion force mapping with AFM. Lastly, the methodology of adsorption of fibronectin is presented and then characterized using immunofluorescence and used to observe cellular behavior on the patterns.

5.2 PATTERN TRANSFER CHARACTERIZATION

Following liftoff, the samples were characterized using an AFM (Digital Instruments Dimension 3100) in contact mode with a silicon nitride tip (Veeco – DNP20) in air. The step height between the wafer surface and the nanofeatures was found to be homogeneously 20 ±0.5 nm over the entire 100 mm^2 sample, i.e. independent of pattern size or pitch down to our minimum size of 60 nm. The surface roughness of the gold islands was calculated to be 1.4 nm rms. The surface roughness of the silicon surfaces was below 1.5 nm rms. These very low roughnesses indicate that no residual resist was present and that the gold islands were not damaged during the liftoff process. Figure 5.2.1 shows a height cross section of 150 nm diameter posts spaced 150 nm apart.

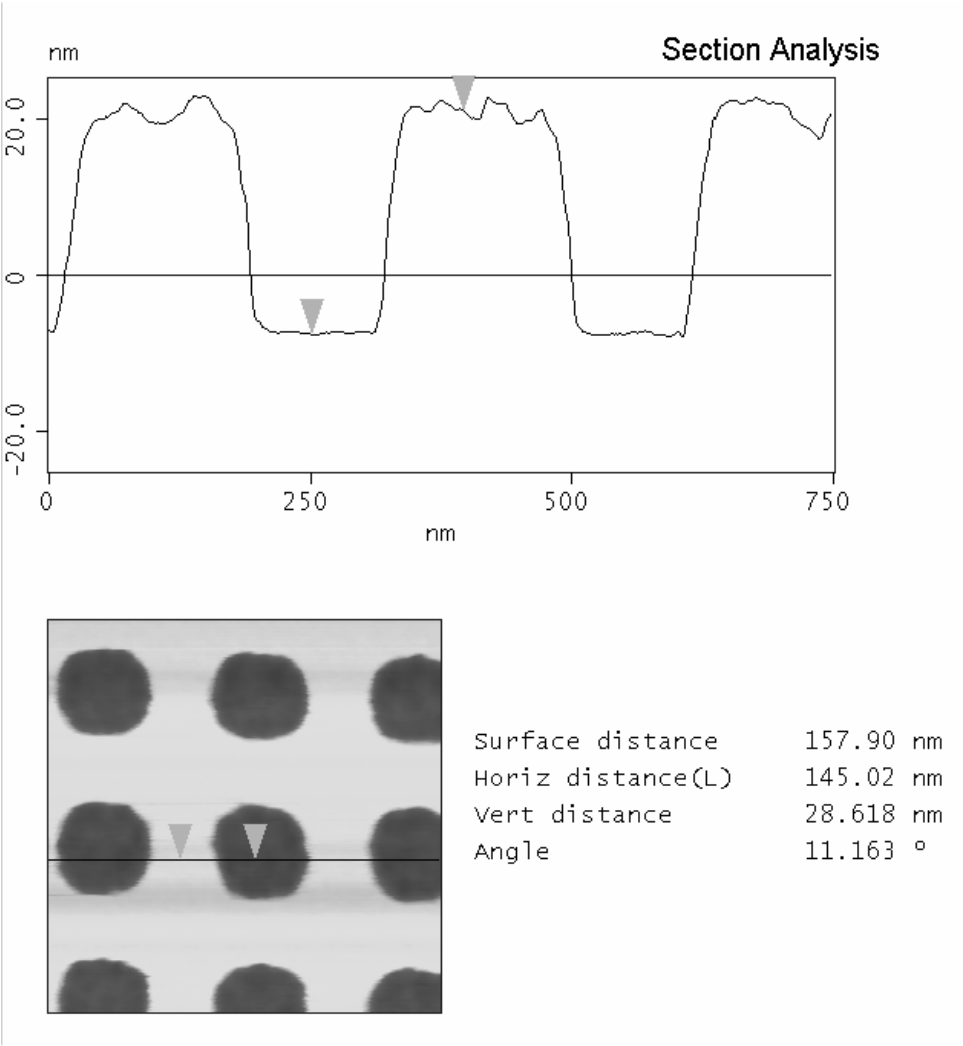

Figure 5.2.1: AFM height cross section of 150 nm gold posts spaced 150 nm apart.

The pattern transfer was analyzed taking 3 AFM scans at 512 points/line of 8 pattern-pitch pairs in each direction and averaging the length of the pattern, pitch, and pattern-pitch pairs. This was performed on the quartz master template and the resulting transferred sample with Au posts to quantify differences in transfer size. This process was performed for 8 different patterns with pattern-spacing of 100/100, 150/150, 150/300, 250/250, 300/600, 600/200, 900/300 and 120/80, representative of the entire spectrum of pattern resolutions. Figure 5.2.2 shows deviations from a perfect transfer

between the measured template features and the final transferred pattern size. Deviations were consistently less than 5% and no systematic deviations were found that depend on pattern size or pitch. This demonstrates a well-defined and reproducible pattern transfer, even for pattern sizes or pitch distances as large as 900 nm.

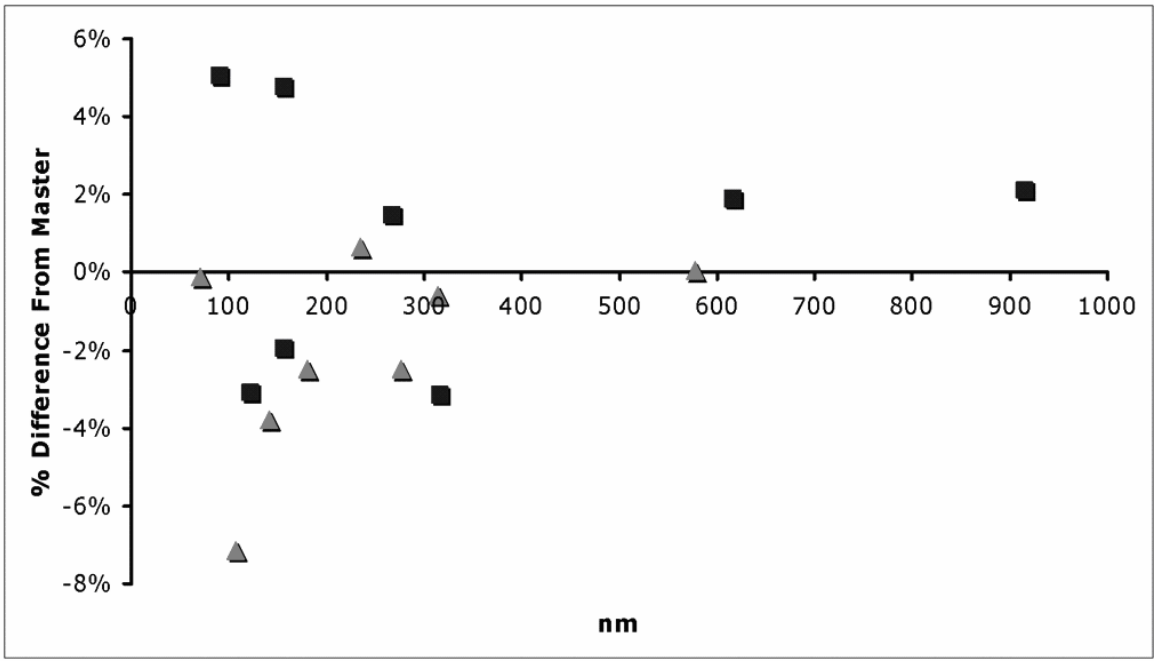

Figure 5.2.2: Plot showing the final post diameter and post spacing in relation to the imprint template. (Squares) Represent the average cross-section diameter deviation of a transferred Au post from the average cross-section diameter of a post on the quartz template. (Triangles) Represent the average distance between transferred Au posts to the average distance between posts on the quartz template.

5.3 ORTHOGONAL SURFACE FUNCTIONALIZATION

A key feature of the nanofabrication process developed in this work is the allowance for the highly precise nano-design of composite nanostructured surfaces that are amenable to orthogonal surface chemistry. In this modality, each of the two different

materials can be individually functionalized to yield different biological functionalities. As shown in Figure 5.3.1, PEG terminated silanes can be reacted with the silicon dioxide layer of the substrate surface to create a functionality that rejects protein adsorption and cell adhesion. The gold regions can be reacted with hexadecane thiols to form a hydrophobic SAM that adsorbs proteins. Proteins adsorbed in these regions, for instance fibronectin, can then promote cell adhesion in these areas. Although the motif presented in this section involves the use of hexadecane-thiol, PEG terminated silane and fibronectin, there are large number of surface functionalities that can be introduced with this platform.

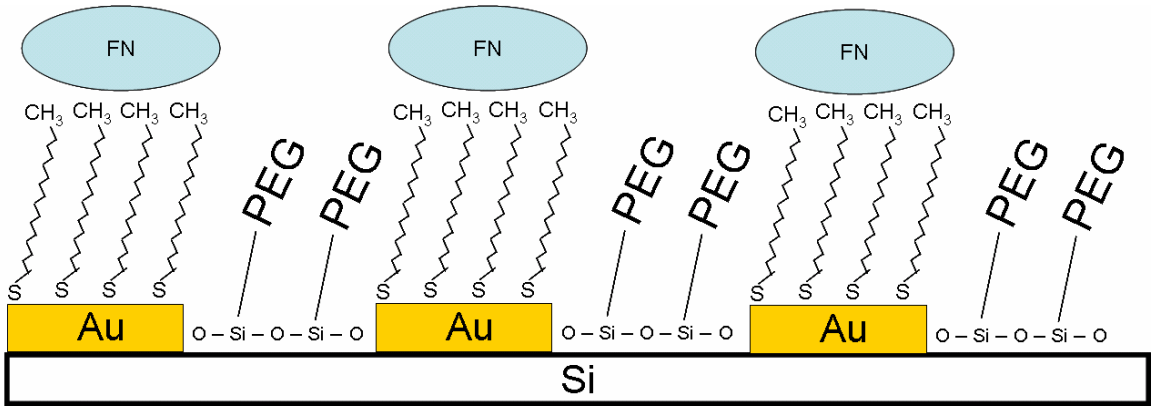

Figure 5.3.1: Cartoon detailing the orthogonal biofunctionalization of nanopatterned surfaces. The surface silicon dioxide is reacted with PEG terminated silanes, which reject protein adsorption. The gold regions are reacted with hexadecanethiol, which adsorb FN.

For the functionalization strategy to work, NOBIL relies on the complete removal of the silicon containing resist from the silicon surface. Additionally, in the absence of resist residues from the liftoff process, there must be a reasonable chemically reactive silicon dioxide layer surrounding the Au posts. To achieve these two requirements, the nanostructured surfaces were treated with a 10 min O_2 plasma (March CS17F) at 40 sccm

at 100W to produce a more reactive silicon dioxide layer and remove any residual organic debris. Immediately afterwards, the samples were cooled with N_2 and immersed in a solution containing 48.5 µl toluene (Fisher), 38.8 µl of HCL (Fischer), 16.0 µl of hexadecanethiol (Aldrich), and 1.0 ml of PEG-terminated silane (Gelest) for 48 hours while stirring. The nanopatterned samples were then rinsed in toluene, twice in ethanol, dried with nitrogen to remove any excess PEG. Finally, they were baked at 100°C for 1 hour to crosslink the PEG. The protocol for the chemical functionalization of the surfaces used in this work was adapted from a procedure developed by John Slater in the Frey lab.

5.4 ADHESION FORCE MAPPING WITH AFM

Since NOBIL samples have very well-defined features with low roughness, it was possible to perform physico-chemical force mapping with AFM to show selective functionalization on a sample in which the gold nanoislands were functionalized with hexadecane thiol (HDT) and the silicon background with a PEG-silane. Physico-chemical force mapping, used previously to image micro-contact printed thiols with different terminal functionality (Okabe, Furugori et al. 2000), allowed functionalization of the nanopatterns to be shown on a nanometer scale. The forces measured correspond to a local wetting mapping, as the atmospherically created thin water layer appeared to vary slightly in thickness for hydrophobic versus hydrophilic regions. While a thin water layer released the tip early and registered as zero force, a thick water layer will trap the tip longer and register as a large adhesive force. Maximum adhesive forces upon retraction were used to create an adhesion map of the nanopatterned surface. The adhesion forces are not dependent on the topography although topographical information

can be extracted from the force return position of the AFM tip, thus, allowing one to correlate the liftoff forces with the nanopattern.

Physico-chemical force mapping was performed using an atomic force microscope (AFM) (Digital Instruments Dimension 3100) with an unmodified silicon nitride tip (DNP-20, Vecco). Data was analyzed using both Nanoscope (Digital Instruments) software and a custom written program for IGOR 5 (Wavemetrics). As a baseline, AFM experiments were performed on a non-functionalized freshly RCA1-treated sample, which left the gold and SiO_2 surfaces with a near-zero contact angle. The adhesion mapping showed little contrast with strong adhesion forces, except at the rims of the features (Figure 5.4.1a). The experiment was repeated for surfaces treated with HDT only (Figure 5.4.1b), and with both HDT and PEG-silane (Figure 5.4.1c). The data from the samples functionalized with only HDT show a much stronger contrast between pattern and background as the nanofeatures have become hydrophobic, which is reflected in a pronounced double peak at 0 and 0.9 nN in the force histogram (Figure 5.4.2). Simultaneous functionalization with both HDT and PEG-silane led to a reduced contrast as the PEG layer is less hydrophilic than a freshly cleaned wafer, so in comparison to both the untreated and the HDT surface, adhesion forces are reduced to about 0.6 nN (Figure 5.4.1c). Some samples show small dots on the nanopattern in the force mapping, which are barely visible in the height image (not shown), possibly stemming from small PEG-silane clusters that have adhered to the HDT surface. We have found earlier that orthogonal functionalization should be done simultaneously to minimize cross-contamination of the different areas (Slater and Frey). The clear contrast between the different surface functionalizations shows that the technique of force mapping can be used to easily image physico-chemical differences with nanometer resolution.

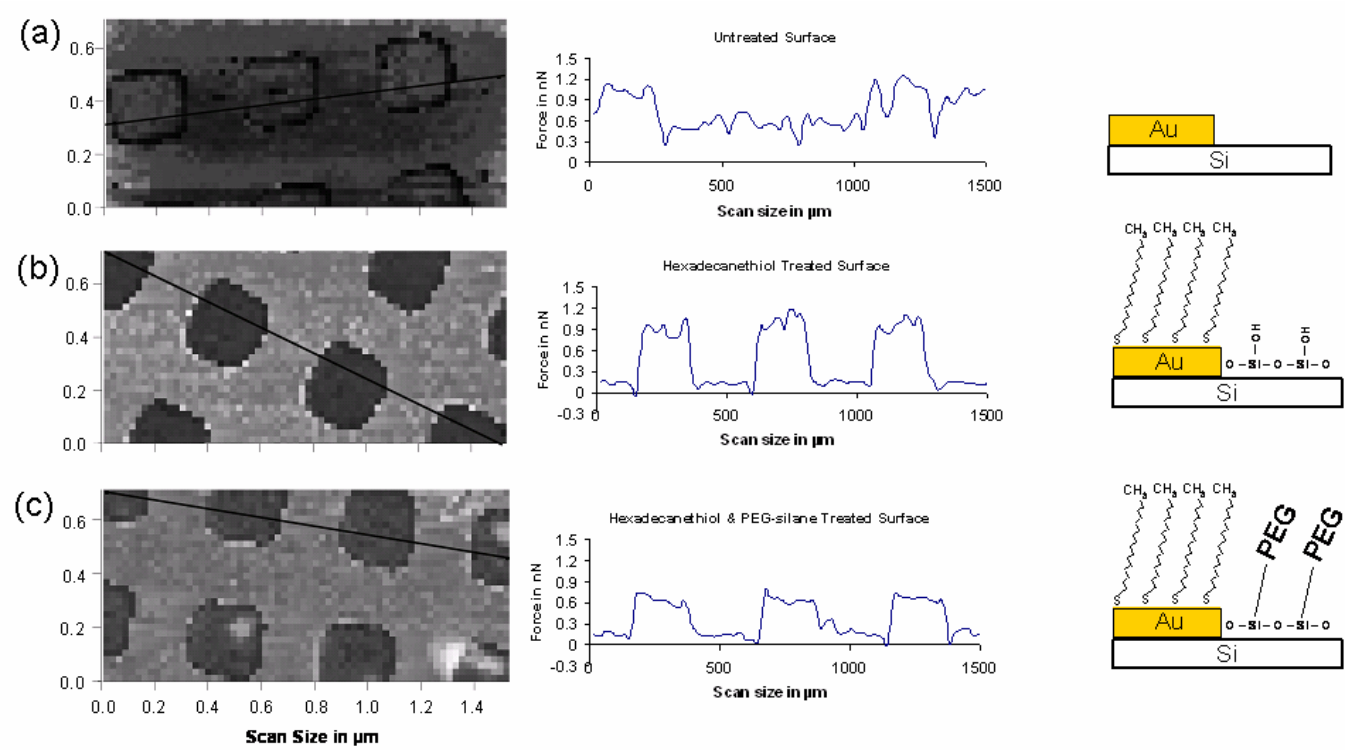

Figure 5.4.1: (a) Left - Graphical view of the surface forces of an untreated surface. Middle – Cross sectional force map of the untreated surface. Right - Cartoon depicting the surface chemistry of untreated surface. (b) Left - Graphical view of the surface forces of a surface treated with only HDT. Middle – Cross sectional force map of a surface treated with only HDT. Right- Cartoon depicting surface chemistry of a surface treated with only HDT. (c) Left - Graphical view of the surface forces of a surface treated with both HDT and PEG-silane. Middle – Cross sectional force map of a surface treated with both HDT and PEG-silane. Right- Cartoon depicting the surface chemistry of a surface treated with both HDT and PEG-silane.

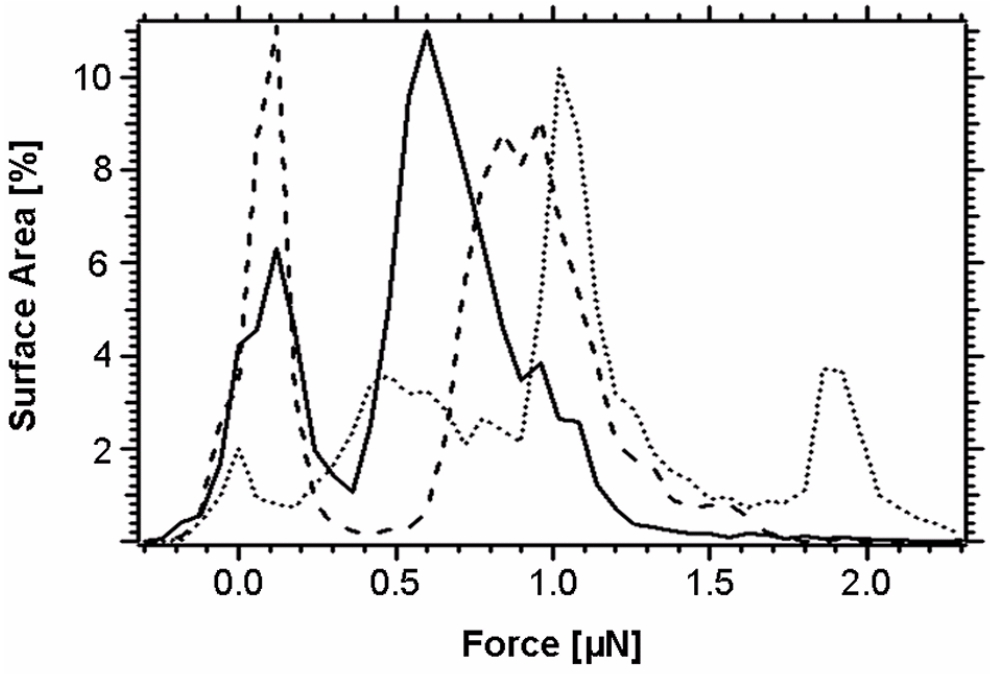

Figure 5.4.2: Histogram of the adhesion forces that were collected from cross sectional scans. (Dotted Line) – Corresponds to the bare silicon surface and does not show any hydrophobicity peak. (Dashed line) – HDT-only treated surface. (Solid line) HDT and PEG-silane treated surface.

5.5 PATTERN FUNCTIONALIZATION WITH FIBRONECTIN

Fibronectin is a highly elastic ECM protein, which cells can stretch up to four-times its relaxed length. Endothelial cells bind to fibronectin via the α5β1 integrin as a means to attach and exert force on the ECM. The main cellular binding site on fibronectin is located on the FN-III-10 subunit and consists of the well known RGD attachment sequence. Some studies have used purely the RGD sequence immobilized onto surfaces to investigate cellular adhesion and integrin clustering behavior (Roberts, Chen et al. 1998; Koo, Irvine et al. 2002; Hersel, Dahmen et al. 2003; Arnold, Cavalcanti-Adam et al. 2004). Although just the RGD sequence could be easily bound to the surface, it was deemed advantageous to use the entire protein because it is known to promote stronger adhesion due to synergistic effects (Hersel, Dahmen et al. 2003; Vogel and Baneyx 2003).

Fibronectin selectively adsorbs to hydrophobic surfaces while not attaching to a passivated layer such as PEG. The orthogonal surface chemistry described in Section 5.3 allows the selectivity between the thiolated-Au and background PEG so that fibronectin only adsorbs to the thiolated-Au posts. Following the surface chemistry protocol outlined in Section 5.3, the samples were immersed in ETOH(AAPER) for 5 minutes as a sterilization procedure. Once moved to a sterile hood, they were then thoroughly rinsed in 50 ml of HEPES-buffered saline solution for 60 seconds, two times to remove any remaining EtOH. 125 μL of a 10μg/ml of either a bovine or human plasma fibronectin (Sigma, Saint Louis, MO) solution was placed on the sample surface for 20 minutes at 37°C and 5% CO_2. The samples were then thoroughly rinsed in 50 ml of HEPES-buffered saline solution for 60 seconds thrice to remove any excess fibronectin. The

samples were then ready for either cell seeding or immunofluorescence studies of the adsorbed fibronectin.

5.6 IMMUNOFLUORESCENCE INVESTIGATION OF ADSORBED FIBRONECTIN

To validate the presence of fibronectin adhering only to the chemically modified Au posts, the samples were immunofluorescently labeled for fibronectin. Following the fibronectin adsorption procedure described in Section 5.5, the samples were covered with 10% goat serum (Sigma) in PBS (Lonza) for 30 minutes at room temperature to block unspecific binding of antibodies. The samples were then exposed to 125 µL of a 6 µg/ml fibronectin antibody (Abcam) for 12 hours at 4ºC. Afterwards, the samples were washed with rocking three times in PBS (Lonza) supplemented with 0.01 % Tween 20 for 5 minutes each wash to remove any unbound antibodies. Next, 125 µL of a 2.6 µg/ml goat anti-rabbit secondary antibody labeled with marina blue (Invitrogen - Alexa Fluor 365) was dispensed onto the sample and left for 1 hr at room temperature. The samples were washed with rocking three times in PBS (Lonza) supplemented with 0.01 % Tween 20 for 5 minutes each wash to remove any unbound antibodies. Lastly, the samples were rinsed with DI H_2O to remove any salt residue and dried with nitrogen. Fluorescent images were acquired using an oil immersion Carl Zeiss ApoTome inverted microscope.

Immunofluorescent imaging of the samples provided positive proof that the fibronectin was only adhering to the chemically modified Au posts, as show in Figure 5.6.1. Using a 160X magnification, I was able to image 150 nm fibronectin clusters separated by either 300 nm or 450 nm, just around the resolution of the microscope. To investigate possible rearrangement or desorption of the fibronectin after cell seeding, this procedure was performed 72 hours after cell seeding. No difference was observed between fibronectin not exposed to cell culture conditions and fibronectin exposed to cell

culture conditions for 72 hours. As will be discussed in more detail in Chapter 11, endothelial cells were observed to be able to stretch the fibronectin but not remove it from the posts.

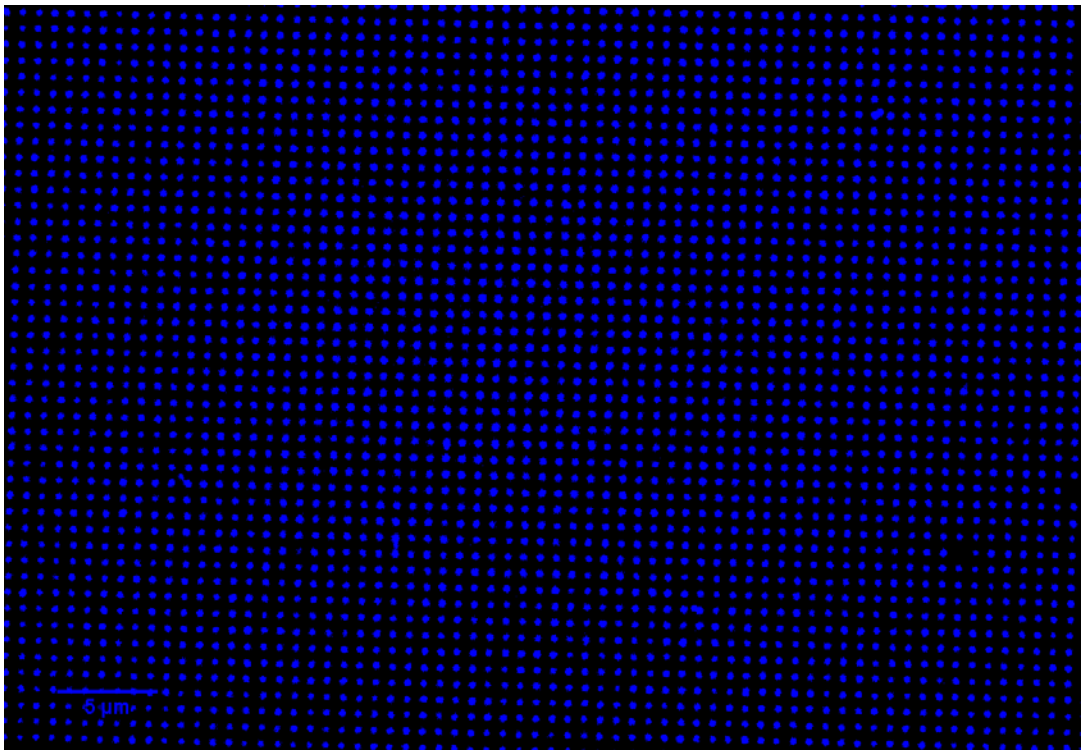

Figure 5.6.1: Adsorbed fibronectin was visualized using immunofluorescence. Using an oil immersion fluorescent microscope at 160X, 200 nm fibronectin clusters spaced 600 nm apart were imaged. Fibronectin was only found on areas with thiolated-Au and no fibronectin was found in areas passivated with PEG-silane. No difference in adsorbed fibronectin was observed between samples exposed or not exposed to cell culture conditions for 72 hours.

Additionally, since a majority of the work in this dissertation was performed on silicon, the transparent nature of the material required that the fibronectin be stained in order to view the samples on conventional microscopy. The reason being is identification marks were placed on the sample in Au to allow the user to navigate through the sample matrix. Since backside illumination was not an option for silicon samples, the user would

have no way of navigating across the sample on a conventional inverted microscope. An easy solution to this problem was to stain the fibronectin, which would then fluoresce the navigation marks, allowing the user to navigate around the sample on a conventional inverted fluorescent microscope. This stain was made routine for all experiments in this dissertation, both for glass and silicon, to provide validation of the surface chemistry for each experiment.

5.7 CELL CULTURE AND VERIFICATION OF FIBRONECTIN BOUNDARIES

Initial cellular adhesion studies were performed to show that the surface functionalization on the nanopatterned surfaces displayed the expected biological functionality. The following procedure was adapted from the documentation supplied with Clonetics Endothelial Cell Systems and a protocol developed by John Slater. Samples were immersed in ETOH (AAPER) for 5 minutes to sterilize the samples before being introduced into a sterile culture hood. Samples were then rinsed 60 seconds, three times in a HEPES buffered saline that was prepared from 11.9 g (HEPES)(Sigma), 5.8 g NaCl (Mallinkckrodt) and 1000 ml DI and adjusted to 7.5 pH with NaOH (Sigma). 125 µL of a 10 µg/ml fibronectin solution (Sigma) in 50 mM HEPES buffered saline was placed on the samples for 20 minutes at room temperature. The samples were then thoroughly rinsed in 50 ml of HEPES buffered saline solution for 60 seconds, 3 times to remove any excess fibronectin. The cells in all the studies were human umbilical vein endothelial cells (HUVECs) (Cambrex) of passage below 8. HUVECs were seeded on the surface at approximately 7 cells/mm^2. The cells were maintained in a serum containing medium (Cambrex), 37˚C and 5% CO_2.

Cells were then seeded on the nanopatterned surfaces and analyzed using a field emission scanning electron microscope (LEO 1530). Samples were prepared for SEM

imaging by washing the cultured cells samples in a HEPES buffered saline solution and then fixing them in a 3.7% solution of formaldehyde (Fischer) in HEPES buffered saline for 5 minutes at 37˚C and rinsing with DI afterwards. A thin layer of Au was sputter coated onto the sample for conductivity. The morphological features of the cells were analyzed along with their ability to respond to the biofunctionalized nanopatterns.

Over the entire sample, surface cells were not located on the unpatterned PEG-functionalized areas surrounding each field of nanopatterns. On the patterned areas, the cells were found to be stably attached. In Figure 5.7.1, an endothelial cell seeded on 150 nm posts clearly aligns to the border between the edge of the nanopattern and the PEG-functionalized background. Even when grown to confluency over the span of 9 days, the endothelial cells still respect the fibronectin border between the patterned area and PEG-silane background (Figure 5.7.2). This also indicates the long term stability of both the fibronectin and PEG-silane background. On lower seeding densities, cells can be seen to extend filopodia to posts on the surface, spanning over the PEG-functionalized areas between the individual nanopatterns (Figure 5.7.3). As validation that the HUVECs were not responding to topographical information, HUVECs were also seeded on samples with poor PEG-silane layers and were found uniformly distributed about the sample surface and did not respect nanopatterned boundaries.

a)

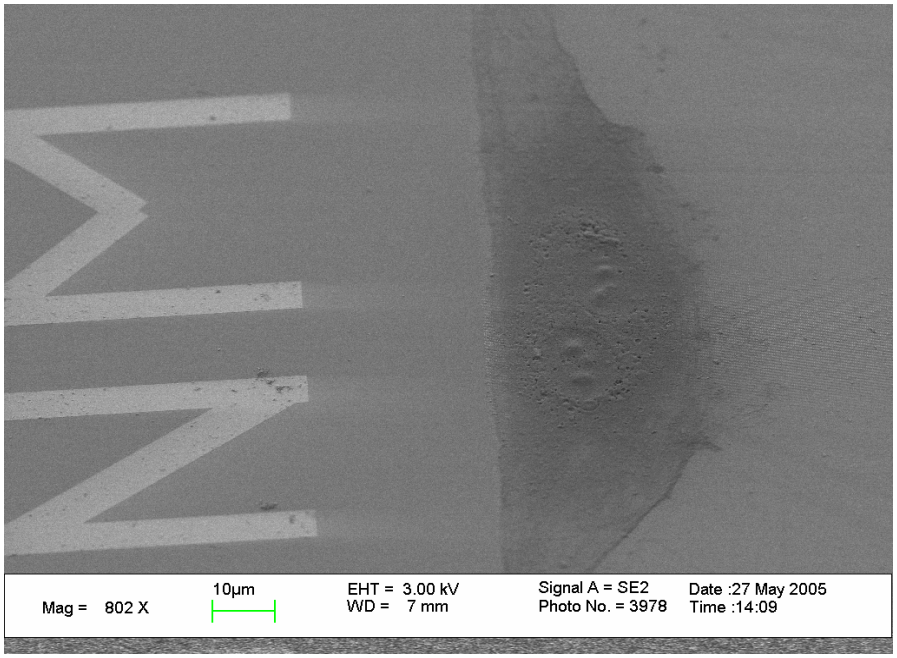

b)

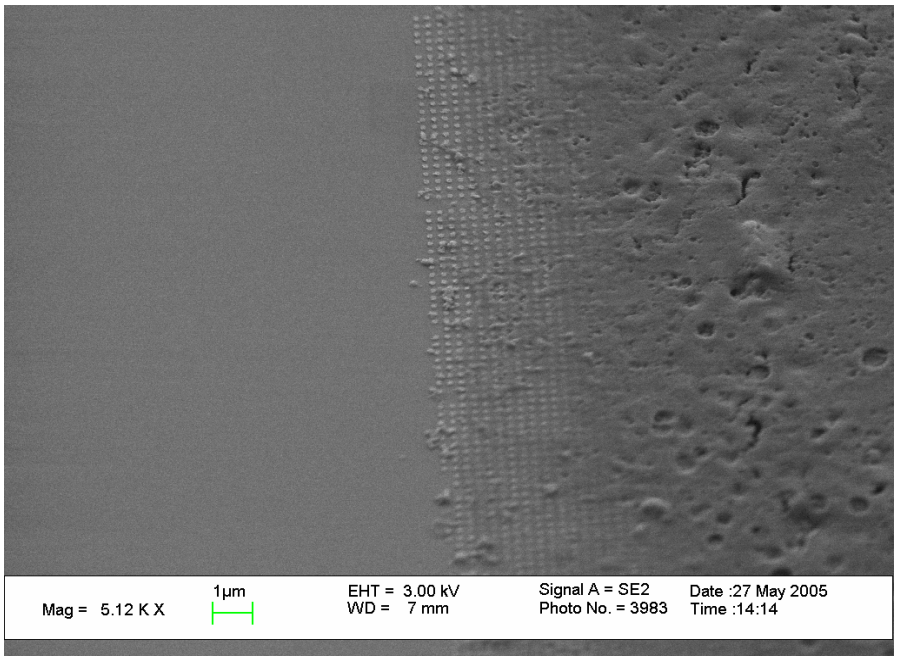

Figure 5.7.1: SEM image of endothelial cell on 150 nm diameter gold adhesion areas with a pitch of 150 nm. (a) An overview of the cell aligning to the border between the edge of the nanopatterned surface and a large PEG surface. (b) Zoom of same cell showing finer detail of the border.

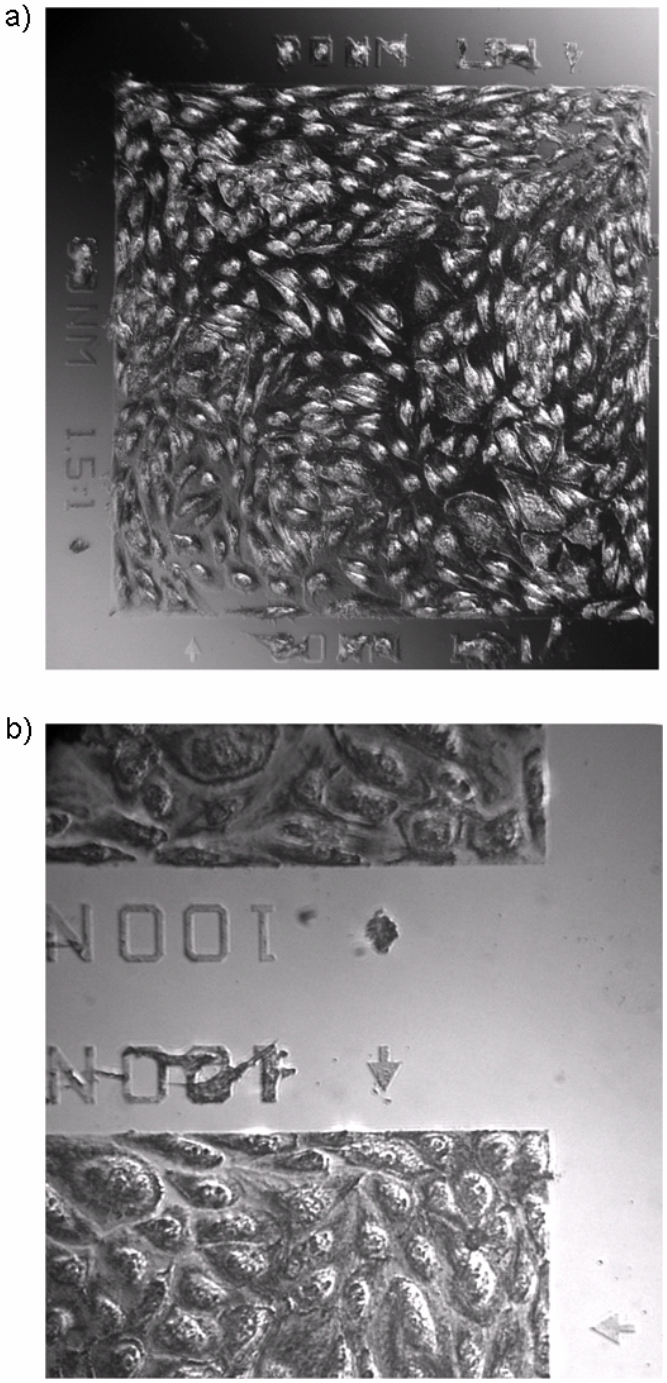

Figure 5.7.2: Differential interference microscopy (DIC) image of confluent HUVECs nine days after seeding. (a) 1 mm x 1 mm nanopatterned area with 120 nm fibronectin clusters showing confluent cells respecting nanopatterned border. (b) Confluent HUVECs crowding at the corner of a nanopattern.

a)

b)

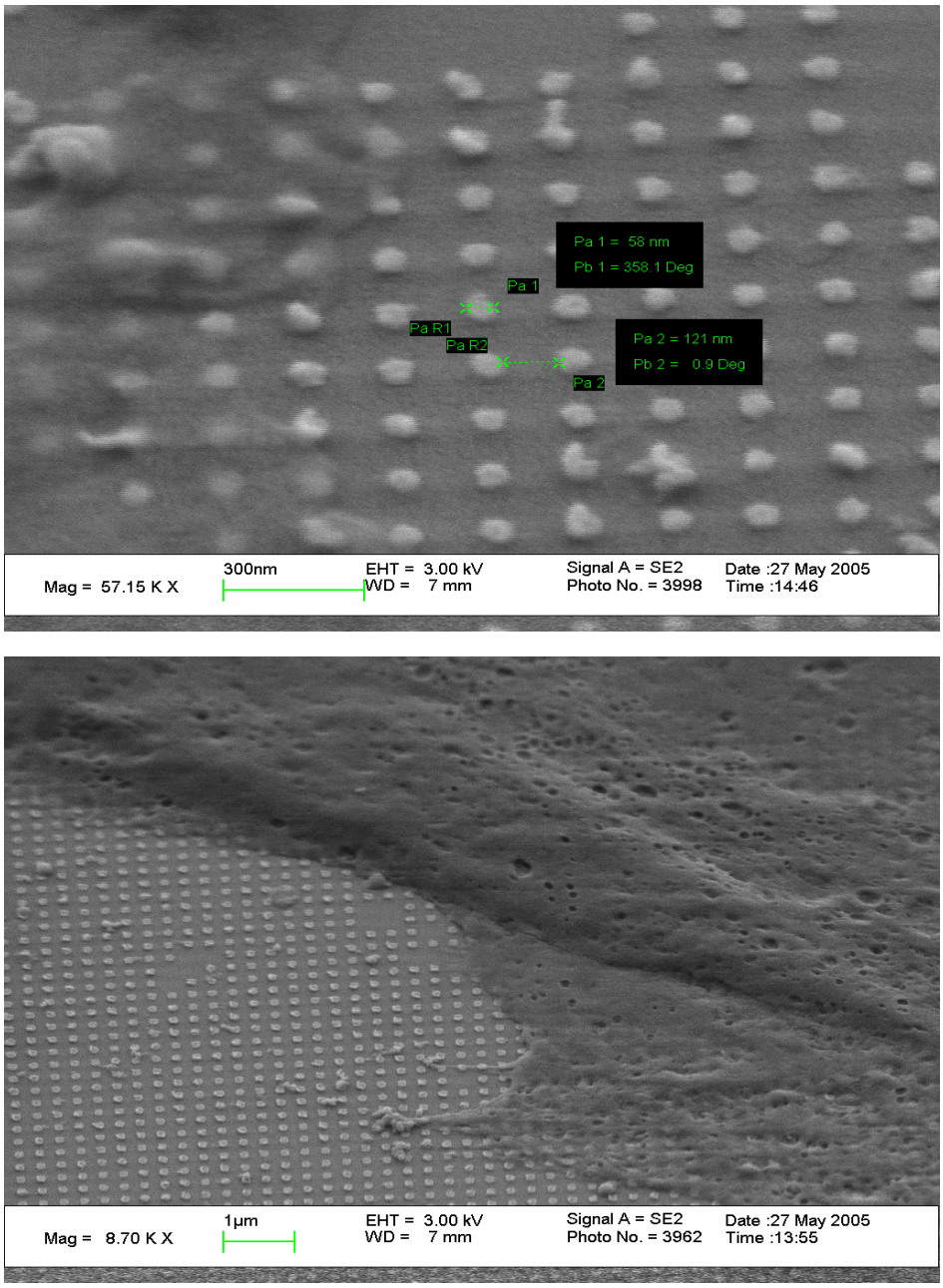

Figure 5.7.3: SEM image of endothelial cells attached to nanostructured surfaces, showing extensions along the posts. (a) 60 nm gold posts spaced 120 nm apart. (b) 150 nm gold posts spaced 150 nm apart.

5.8 CONCLUSIONS

This chapter was concerned with proving that the nanopatterned surfaces could be biologically functionalized in a way to provide a biologically active contrast between nanopatterned areas. It demonstrated using physico-force mapping that the hexadecane-thiol and PEG-silane reacted with only the intended components of the nanopatterned surfaces. Next, it demonstrated that complete fibronectin proteins could be selectively adsorbed to only the Au hexadecane-thiolated regions and this was validated through the use of immunohistochemistry and high-resolution oil immersion fluorescence microscopy. As a final validation of biological activity of the fibronectin, HUVECs were seeded on the surfaces and imaged with SEM, showing that they respected the border between the fibronectin posts and PEG-silane passivated areas. Additionally, in a 9 day experiment, confluent cells also respected the biologically active border, showing the longevity of adsorbed fibronectin and PEG-silinated background.

REFERENCES

Arnold, M., E. A. Cavalcanti-Adam, et al. (2004). "Activation of integrin function by nanopatterned adhesive interfaces." Chemphyschem **5**(3): 383-388.

Hersel, U., C. Dahmen, et al. (2003). "RGD modified polymers: biomaterials for stimulated cell adhesion and beyond." Biomaterials **24**(24): 4385-4415.

Koo, L. Y., D. J. Irvine, et al. (2002). "Co-regulation of cell adhesion by nanoscale RGD organization and mechanical stimulus." Journal of Cell Science **115**(7): 1423-1433.

Okabe, Y., M. Furugori, et al. (2000). "Chemical force microscopy of microcontact-printed self-assembled monolayers by pulsed-force-mode atomic force microscopy." Ultramicroscopy **82**(1-4): 203-212.

Roberts, C., C. S. Chen, et al. (1998). "Using mixed self-assembled monolayers presenting RGD and (EG)(3)OH groups to characterize long-term attachment of bovine capillary endothelial cells to surfaces." Journal of the American Chemical Society **120**(26): 6548-6555.

Slater, J. and W. Frey (2007). "Nanopatterning of Fibronectin and the Influence of Integrin Clustering on Endothelial Cell Spreading and Proliferation." Journal of Biomedical Materials Research Part A.

Vogel, V. and G. Baneyx (2003). "The tissue engineering puzzle: A molecular perspective." Annual Review of Biomedical Engineering **5**: 441-463.

CHAPTER 6: LIMITING ADHESION CLUSTER SIZE

6.1 OVERVIEW

This chapter begins by providing background information on the biological aspects and the fundamental questions that can be answered using the nanopatterned protein cell culture device. Specifically, it discusses cell-surface adhesions and offers perspectives on the scientific research in this area. Following is a section covering the details of the experimental device that explains the various parameters of the device. The section concludes with experimental results that validate basic assumptions of the operation of the device.

6.2 BACKGROUND

Integrin receptors are heterodimeric transmembrane glycoproteins that mediate the adhesion of cells to the extracellular matrix (ECM) by forming links between the ECM and cytoskeleton. Extracellularly, integrins have large domains involved in both acting as a structural link and as a signaling receptor. Intracellularly, they have short cytoplasmic tails that interact with the cytoskeleton signaling network. Integrins are an integral part of regulating many cellular processes including cellular survival, proliferation, motility, differentiation, angiogenesis, wound healing, embryonic morphogenesis and cell-surface signaling (Hynes 1992; Juliano and Haskill 1993; Howe, Aplin et al. 1998; Holly, Larson et al. 2000; Liddington and Ginsberg 2002; Miranti and Brugge 2002; Wilder 2002; Mostafavi-Pour, Askari et al. 2003). Genetic defects in integrins and their adaptor proteins have been shown to cause pathological conditions

such as muscular dystrophy and Glanzmann thrombasthenia (Wehrle-Haller and Imhof 2003).

Although a single integrin can make an attachment to the ECM, it is believed that the clustering of multiple integrins is necessary for the recruitment of regulatory and structural proteins and the machinery required for intracellular signaling (Miyamoto, Akiyama et al. 1995; Miyamoto, Teramoto et al. 1995; Maheshwari, Brown et al. 2000; Coussen, Choquet et al. 2002). Furthermore, it has been shown that the minimum cluster size of three integrin-binding ligands is necessary to link integrins to the cytoskeleton (Coussen, Choquet et al. 2002). The clustered integrins are somewhat of an organization center for the over 30 molecular constituents involved in forming a focal complex, a small heterogeneous plaque of adhesion and signaling proteins (Geiger and Bershadsky 2001). Focal complexes tend to form in the outside perimeter of the filopodia and lamellipodia and their growth is induced by the G-protein Rac (Clark, King et al. 1998). The focal complexes are a transient adhesion and either disassemble or mature into a larger entity known as a focal adhesion (Geiger and Bershadsky 2001; Geiger, Bershadsky et al. 2001; Miriam Cohen 2004; Zaidel-Bar, Cohen et al. 2004). Focal adhesions can then transform into fibrillar adhesions, which are important in fibrillogenesis (Geiger, Bershadsky et al. 2001).

Different types of fibroblasts vary in the amount of force they exert on a substrate and correspondingly have different focal adhesion distributions. However, measurements of cell traction force per unit area of a focal adhesion are relatively consistent. Studies have found that the size of a focal adhesion is directly proportional to the force transmitted through it to its surroundings (Choquet, Felsenfeld et al. 1997; Balaban, Schwarz et al. 2001; Bershadsky, Balaban et al. 2003; Yeung, Georges et al. 2005). Studies using elastic membranes and non-motile fibroblasts found the linear dependence

between the size of a focal adhesion and the force transmitted to be 5.5 nN/μm^2 (Balaban, Schwarz et al. 2001). Similar results were also obtained in micro-post defection experiments where the force to focal adhesion area was proportional with a value of 4.8 nN/μm^2 (Tan, Tien et al. 2003). However adhesions smaller than 1 μm^2, typically found around the peripheral of the cell, seem to show non-proportional force versus size relationship (Tan, Tien et al. 2003).

Studies have also found that cells respond to the stiffness of the substrate to which they are adhered (Pelham and Wang 1997; Discher, Janmey et al. 2005). Cells on a stiff matrix or glass will form stable focal adhesions and well-defined stress fibers. However, on a soft gel matrix, cells will form dynamic adhesions and have a poorly defined cytoskeleton. Given the differing elastic modulus of various tissues in the body, this may not be surprising. The importance of force mediated mechano-transduction is clearly illustrated in the case of stem cell differentiation on elastic substrates; where, under identical chemical conditions, the elasticity of the substrate directed cell differentiation (Engler, Sen et al. 2006).

6.3 NANOSCALE INTERACTIONS

The exact mechanisms of mechano-force transduction are still not well understood. Many of the experiments conducted in this area have used bulk properties, such as elasticity, for investigation. While this has provided validation of the importance of mechanical properties, it still leaves questions about what is happening at the focal adhesion level. The tools developed in this work allow one to investigate these structures at a length scale similar to the ranges found important for an adhesion. For instance, it is known that the maximum distance between integrins needs to be less than 60 nm in order to support cell adhesion, which is about the same distance between fibronectin subunits

and the size of talin. It allows one to ask questions in a way that cannot be answered with experiments that use homogenously coated substrates and that can only provide an average view about how the cell is actually interacting with the surface.

A main theme in the previous section was the relationship between force and mechano-transduction. It was discussed that the force transmitted through a focal adhesion is directly proportional to the area of the adhesion. An interesting question is if the size of a focal adhesion is controlled, how this does this affect the force transmitted through a focal adhesion? Does limiting the size of the adhesion also limit the growth of the actin stress fibers? It is believed that integrin activation is mediated by a system of positive feedback (Iber and Campbell 2006). I hypothesize that the entire process of focal adhesion maturation is governed by a system of positive feedback, which requires the coordination between the recruitment of additional adhesion constituents in order to grow larger stress fibers and transduce greater forces. If it is possible to limit the size of focal adhesions, it may be possible to interrupt this positive feedback system which may shed light into how the feedback system operates and what parameters are important.

Another related point is the effect of integrin clustering in order to achieve a stable focal complex. It has been shown with micelle nanolithography that the spacing between integrins must be less than 60 nm in order to have stable cell adhesion (Arnold, Cavalcanti-Adam et al. 2004). This provides evidence that cells do respond to nanoscale clustering and that there is a distance threshold between integrins which must be achieved in order to form an adhesion. However, this experiment only looked at integrin-to-integrin spacing and not total integrin cluster size. Because the adhesion proteins were homogenously distributed, the cells were not restricted to the size of focal adhesions they could form. Integrin cluster size is known to be important in integrin activation and focal adhesion formation. Knowing that integrin-to-integrin spacing is important, is the size of

the cluster important for focal adhesion maturation? Do restrictions in the integrin cluster sizes cause changes in cellular behavior? There may also be structural requirements for the spacing between the integrin clusters. If clusters are moved farther apart, how does this affect cellular behavior?

Many studies have shown that homogenously ligand coated substrates can produce different cellular behavior depending on the density of surface ligands (Ingber 1990; Maheshwari, Brown et al. 2000). Griffith *et al.* developed a synthetic polymer system to investigate the adhesion strength of fibroblasts (Koo, Irvine et al. 2002). The system allowed the creation of 32 nm clusters that contained on average 1.7, 3.6, or 5.4 RGD peptides. Centrifugal detachment experiments were used to quantify adhesion strength to the clusters. The expected outcome was a linear trend of detachment versus centrifugal force like that found on control surfaces with adsorbed FN, but they found that fibroblasts seeded on these surfaces showed an adhesion reinforcement at low centrifugal forces. These results show that clustering of integrins is important in modulating adhesion strength. However, these polymers can only be controlled by an average density of surface ligand and they are also limited in the size of each cluster, which all influence adhesion strength. This brings up the question to how much is the cell is responding to macroscopic density versus local density at the sites of focal adhesions? For a fixed number of ligands, does the arrangement of ligands on the nanoscale make a difference? Can the cell detect differences in nanoscale arrangements, and if so, how do they react differently?

These are the types of biological questions that can be answered with the use of nanopatterned substrates. Answers to these questions help shed light on structural parameters and thresholds related to the mechano-signaling process. Additionally, they

provide a converse perspective to a body of experimental work on elastic substrates and allow us to ask more specific questions at the nanoscale.

6.4 NANOPATTERNED PROTEIN CELL CULTURE ARRAYS

As shown in previous chapters, the device consists of a large matrix of different nanopatterns with varying sizes and pitch. Given the large number of nanopatterns, a selected number of nanopatterns were chosen for in-depth investigations. These were selected based on preliminary experimental data and information from current literature. Other groups have shown that for cell survival and spreading, the maximum distance between adhesion sites must be 60 nm, which corresponds to a talin length or the RGD repeat on fibronectin (Glass, Moller et al. 2003). A distance of approximately twice this length has not been explored and holds value for determining what occurs once slightly larger clusters are formed. A region of interest on the device was selected that probed a feature set that varied from 150 nm to 1.2 μm. From this region, a further subset of ten patterns was selected based on on-going experimental results. In some cases, data was also collected from two additional patterns that are shown in blue in Figure 6.4.1.

A designation that is used throughout this dissertation is the relationship between fibronectin nanocluster diameter and spacing, known as pitch. The ratios expressed on the top line in Figure 6.4.1 define the pitch of the nanopatterns. The pitch is read as the ratio between fibronectin nanocluster diameter to the edge-to-edge spacing of the cluster. For instance, 200 nm 1:2 is read as a 200 nm diameter fibronectin nanocluster with an edge–to-edge spacing of 400 nm. Another important fact about pitch is it also defines the macroscopic fibronectin density. A pitch of 1:2 has a macroscopic fibronectin density coverage of 8.72% irrespective of the diameter of the fibronectin nanoclusters (Figure 6.4.2).

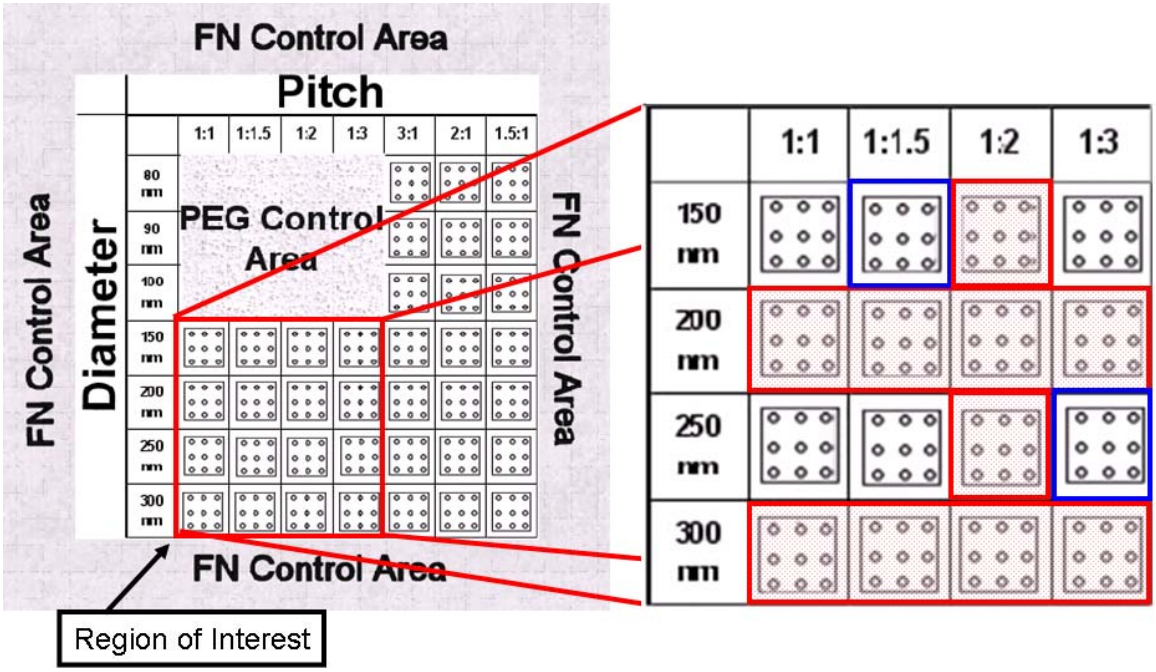

Figure 6.4.1: A region of interest was defined on the device for in-depth investigation. This region was selected based on preliminary experimental results and current literature. A further refined subset of 10 patterns was defined based on experimental results (Red-Shaded). In some cases data was also collected to form two other patterns (Blue-Unshaded)

A unique feature of the nanopatterned array is the ability to hold macroscopic fibronectin density constant while changing the arrangement of fibronectin on the surface. For a given number of fibronectin fibrils per unit area, as shown in part A of Figure 6.4.3, they can be arranged in a number of different configurations. The remaining squares in the figure show a macroscopic representation of the arranged fibronectin. In all three boxes, the total number of ligands stays constant. This allows the system to look at the influence on cellular behavior due to only the nanoscale arrangement of a constant number of fibronectin molecules.

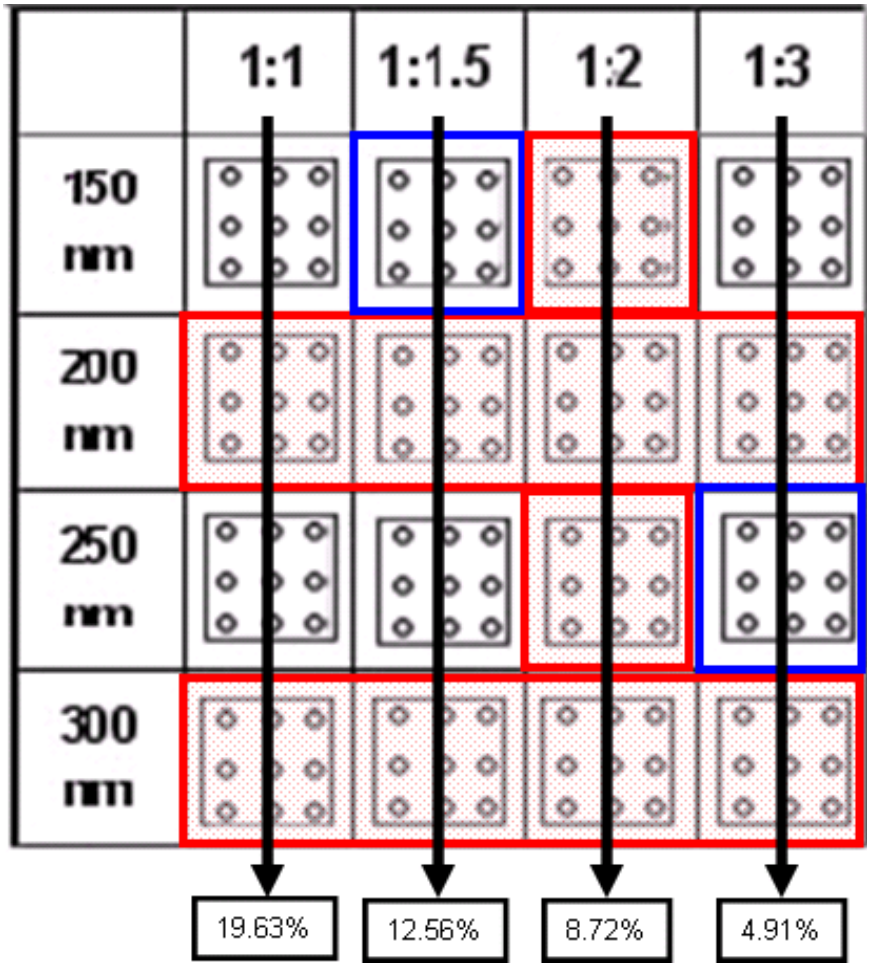

Figure 6.4.2: Pitch is directly related to the macroscopic fibronectin density coverage (Percentages in boxes) and it is not dependent on the size of the fibronectin nanoclusters.

The most common parameters that will be discussed in this dissertation are nanocluster diameter, spacing and pitch. These parameters can also be defined in terms of macroscopic protein density or fibronectin composite, local fibronectin density, number of fibronectins per cluster and cluster area. A chart listing the absolute values of all of these parameters is shown in Table 6.4.3. Additionally, John Slater did a large body of X-ray photoelectron spectroscopy (XPS) work on fibronectin packing densities

on homogenously coated gold surfaces and nanopatterned surfaces (Slater and Frey 2007). He found that fibronectin on homogenous surfaces packed at a density of 2,605 FN/μm^2. Using nanopatterned surfaces, he was able to show that fibronectin still packed at this density even when in nanoscale clusters. Using this data, I was able to estimate the number of fibronectin ligands on each nanoscale cluster, which is also included in Table 6.4.1.

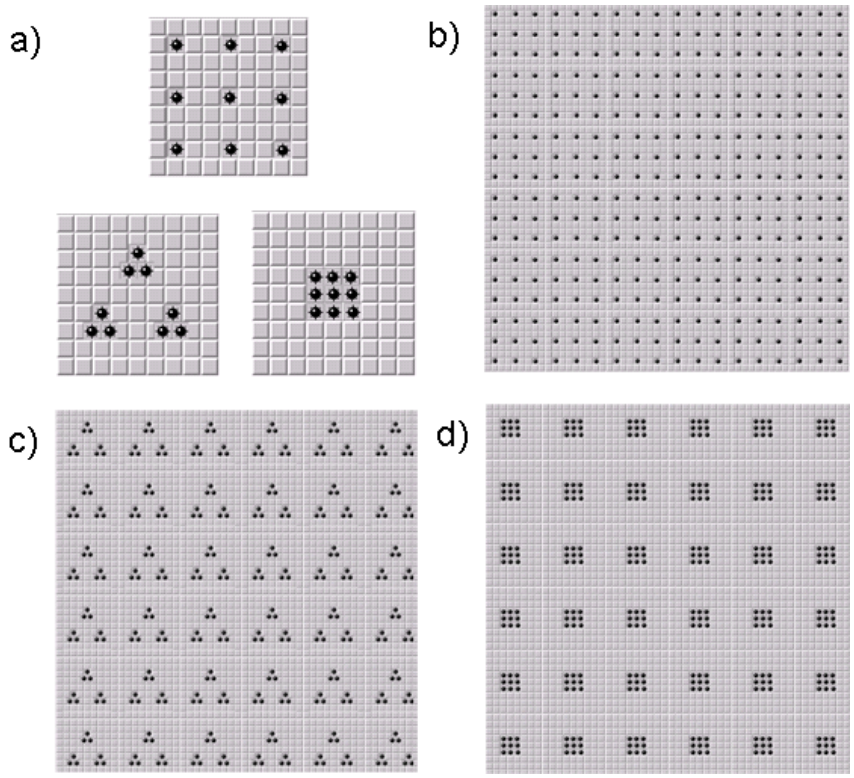

Figure 6.4.2: Cartoon depiction of different nanoscale arrangements of fibronectin. a) Different possible arrangements of 9 nanoscale fibronectin clusters. b-d) Repeats of different nanoscale units that form an identical macroscopic fibronectin density.

Pattern Name	Diameter (nm)	Spacing (nm)	Area (nm2)	Coverage %	FN Composite #/(μm^2)	FN Per Pattern #
300 1:3	300	1,200	70,686	4.91	128	184
300 1:2	300	900	70,686	8.72	227	184
300 1:1.5	300	750	70,686	12.56	327	184
300 1:1	300	600	70,686	19.63	511	184
250 1:3	250	1,000	49,807	4.91	128	130
250 1:2	250	750	49,807	8.72	227	130
250 1:1.5	250	625	49,807	12.56	327	130
250 1:1	250	500	49,807	19.63	511	130
200 1:3	200	800	31,416	4.91	128	82
200 1:2	200	600	31,416	8.72	227	82
200 1:1.5	200	500	31,416	12.56	327	82
200 1:1	200	400	31,416	19.63	511	82
150 1:3	150	600	17,671	4.91	128	46
150 1:2	150	450	17,671	8.72	227	46
150 1:1.5	150	375	17,671	12.56	327	46
150 1:1	150	300	17,671	19.63	511	46

Table 6.4.1: Summary table of the absolute value of the relevant patterns that will be discussed in this dissertation. Pattern name is denoted by a size number and corresponding pitch. Diameter refers to the diameter of the nanocluster. Spacing refers to the edge-to-edge spacing between the clusters. Area is the total area of the nanocluster. Coverage is a function of pitch and describes the percentage of the surface that is covered by fibronectin. FN composite describes the macroscopic protein density. FN per pattern describes the number of fibronectin ligands in a single nanocluster.

6.5 EXPERIMENTAL METHODOLOGY

Silicon samples were prepared and functionalized according to the protocols presented in Chapter 5. Samples were immersed in ETOH (AAPER) for 5 minutes to sterilize the samples before being introduced into a sterile culture hood. Samples were then rinsed 60 seconds, three times in a HEPES buffered saline that was prepared from 11.9 g (HEPES)(Sigma), 5.8 g NaCl (Mallinkckrodt) and 1000 ml DI and adjusted to 7.5 pH with NaOH (Sigma). 125 μL of a 10 μg/ml fibronectin solution (Sigma) in 50 mM HEPES buffered saline was placed on the samples for 20 minutes at room temperature. The samples were then thoroughly rinsed in 50 ml of HEPES buffered saline solution for 60 seconds, 3 times to remove any excess fibronectin. The cells in all the studies were human umbilical vein endothelial cells (HUVECs) (Cambrex, Walkersville, MD) of passage below 4 and cultured according to manufacturer's specifications. They were cultured in T-25 tissue culture flasks coated with 30 μg of human plasma fibronectin (Sigma, Saint Louis, MO) at 37ºC and 5% CO_2 until 80% confluence. During culture and experiment, the HUVECs were bathed in endothelial growth media (Cambrex, Walkersville, MD) supplemented with 2% fetal bovine serum, 0.5 ml human endothelial growth factor, 0.5 ml Hydrocortisome, 0.5 ml GA-1000 (Gentamicin, Amphotericin B). To release cells from flasks for cell seeding, the flasks were first rinsed with 5 ml of HEPES buffered saline at 37ºC. They were then trypsinized using 3 ml of Trypsin/EDTA (Cambrex) for 5 minutes at 37ºC and 5% CO_2. Next, 3 ml of trypsin neutralizing solution (Cambrex) was added to the cell suspension to neutralize the Trypsin/EDTA. The cell suspension was pelleted using a centrifuge set to 240 g for 6 minutes. The cells were then resuspended in 10 ml of endothelial growth media (Cambrex) discussed above. A hemocytometer and trypan blue dye was used to determine the total living cell population

in the resuspension. The HUVECs were then seeded on the sample surface at approximately 7 cells/mm^2. The cells were maintained in 20 ml of endothelial growth media (Cambrex), 37˚C and 5% CO_2 for 24 hours. The cells were fixed by first immersing them in a cold cytoskeleton buffer (0.5% Triton X-100, 100 mM NaCl, 300 mM sucrose, 3 mM MgCl2, 10mM HEPES, pH 6.8) at 4ºC for 1 minute, then immersing them in 5% formaldehyde at 4ºC and then letting the solution warm up by placing in 37ºC water bath for 10 minutes. The surfaces were then rinsed with warm HEPES and covered with 125 µL of a 10% goat serum (Sigma) in PBS (Lonza) for 30 minutes at room temperature to block unspecific binding of antibodies. After rinsing with HEPES, the samples were then dressed with 125 µL PBS solution of 6 µg/ml fibronectin antibody (Abcam) and 1% by volume FITC-conjugated mouse anti-vinculin (Sigma) in 1.0% BSA supplemented with 0.1% Tween-20 for 12 hours at 4ºC. Afterwards, the samples were washed with rocking three times in PBS (Lonza) supplemented with 0.01% Tween-20 for 5 minutes each wash to remove any unbound anti-bodies. Next, 125 µL of a 2.6 µg/ml goat anti-rabbit secondary antibody labeled with marina blue (Invitrogen - Alexa Fluor 365) was dispensed onto the sample and left for 1 hr at room temperature. The samples were washed with rocking three times in PBS (Lonza) supplemented with 0.01% Tween-20 for 5 minutes each wash to remove any unbound anti-bodies. Lastly the samples were rinsed with DI H_2O to remove any salt residue and dried with nitrogen. Coverslips were mounted to the samples using gold antifade reagent (Invitrogen). Fluorescent images were acquired using an oil immersion Carl Zeiss ApoTome inverted microscope.

6.6 VINCULIN IMMUNOFLUORESCENCE – SIZE DEPENDENCE

In Chapter 5, it was shown that fibronectin could be immobilized to form nanoclustered adhesions. As was mentioned in the last section, the ability to artificially

restrict the size of a focal adhesion would be a useful tool in investigating properties of mechano-transduction. In this section, I aim to show that nanoscale clustering of fibronectin can be used to restrict the maximum size of a focal adhesion.

One of the first proteins to be recruited in the formation of a focal complex is vinculin. It plays a role in linking the integrin receptors to the actin cytoskeleton. Because of its early arrival in the formation of adhesions, it is a common marker used in identification of focal complexes and focal adhesions. It was selected as the best protein to analyze for the presence of adhesions and their size.

Dual staining of both fibronectin and vinculin on the nanopatterned surfaces revealed that the focal adhesions were only present on the fibronectin clusters (Figure 6.6.1). The picture on the left shows a vinculin stained cell that is attached to fibronectin clusters 250 nm in diameter that are spaced 750 nm apart. In this picture, only the vinculin, in white, is shown and the fibronectin is not visible. The vinculin can clearly be seen to conform to a digitally distributed matrix of points. This shows that the adhesions are forming in a distribution dictated by the surface patterning. A zoomed in region is shown in the right half of the figure. The top picture in blue shows the fibronectin stain of this area. The fibronectin clusters are clearly distributed in an extremely uniform matrix. The bottom picture in green shows the vinculin stain of this region. An overlay of these two images puts the vinculin adhesions directly on top of the fibronectin clusters, showing a direct match between them. This shows that the orthogonal functionalization with the fibronectin clusters and PEG background was successful in limiting the maximum size of the adhesions and was able to control the spacing between adhesion clusters.

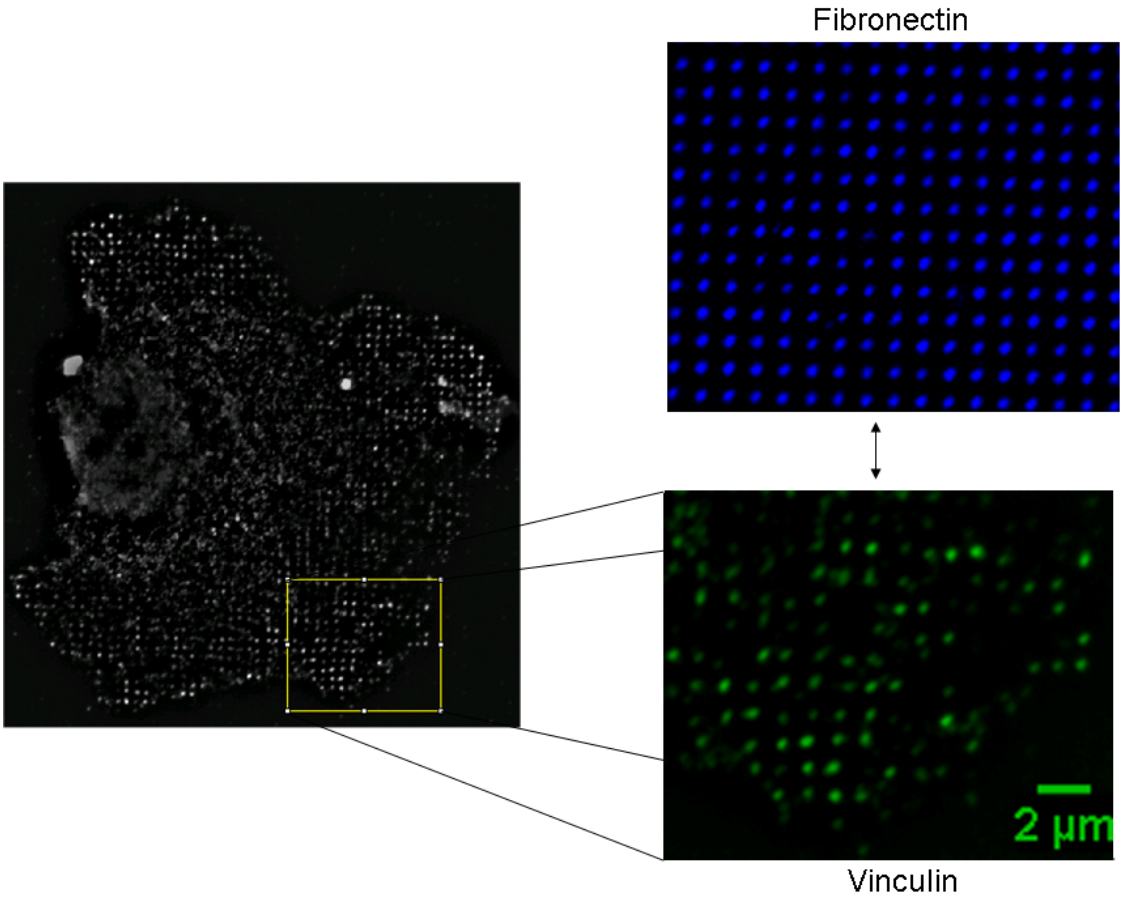

Figure 6.6.1: (Left) Vinculin immunofluorescent image at 64X magnification on a 250 nm 1:3 nanopattern. (Right) Enlarged vinculin area and corresponding fibronectin area. Notice that the vinculin adhesions align with the fibronectin clusters.

Fibronectin in an unstretched state has a compact conformation when immobilized onto a gold surface. However, it is a very elastic molecule and a cell can stretch it up to four times its compacted length (Ohashi, Kiehart et al. 1999). Under normal adhesion conditions, cells engage in a process known as fibrillogenesis which results in the stretching of fibronectin fibrils. This process occurs under mechanical force that is exerted by the cell. Fibrillogenesis is usually thought of as a later stage in focal adhesion formation, when a large enough force has been built up on the surface and a

transformation of a focal adhesion into a fibrillar adhesion occurs. As the fibronectin fibers are stretched out, the adhesions change from a 'dot adhesion', like pictured above, to a 'dash adhesion'. The stretched fibrils have binding sites along the length of the fibril, and adhesions along this length appear as long focal adhesions when labeled with vinculin.

It was shown above that focal complexes or early adhesions clearly were limited by the size of the fibronectin clusters. I was also interested in whether I could restrict later stage dash adhesion that formed over stretched fibrils. In particular, would the cell form elongated adhesions similar to control cells that spanned many fibronectin clusters? Additionally, would the cell stretch the fibronectin in a way to form large round globular adhesions that also spanned several fibronectin clusters?

To investigate formation of fibrillar adhesions, HUVECs were seeded on the pattern diameters 150 nm, 200 nm, 250 nm and 300 nm with a constant pitch of 1:2. Cells on these patterns were also dual stained for vinculin and fibronectin and were imaged at 160X magnification. These images were taken shortly after a trained Ziess technician calibrated the digital measurement feature of the microscope. Verifying correct calibration, digital measurements of the fibronectin clusters agreed with the known pattern sizes. The dot vinculin adhesions on these patterns also directly corresponded to the diameter of the underlying fibronectin cluster.

Although on the nanopatterns, the dot adhesions were always limited by the fibronectin cluster size, fibrillar adhesions were observed that spanned individual fibronectin clusters. Of these fibrillar adhesions, only dash adhesions were observed and no round globular adhesions were present. It was discovered that the width and length of the fibrillar adhesions differed between patterns. On the smaller 150 nm 1:2 pattern, the average fibrillar adhesion was approximately 180 nm wide (Figure 6.6.2). The lengths of

these adhesions were also considerably shorter than those found on the 300 nm 1:2 patterns and controls. As the fibronectin adhesion diameter was increased from 150 nm to 200 nm, the cross sectional width of the fibrillar adhesions also increased to approximately 260 nm. This trend continued through the 300 nm fibronectin cluster diameter, where the cross sectional width of the dash adhesion was approximately 320 nm. On gold control surfaces, dash adhesions appeared as large and very long adhesions in comparison to small focal complexes. They typically had a cross sectional area of 400 nm to 500 nm and lengths on the order of several microns.

The fibronectin stains revealed that an underlying fibronectin fibril was present most of the time for fibrillar adhesions. The measured width of the fibronectin fibrils directly matched the specified pattern diameter. We obtained slightly larger cross sections for the vinculin fibrillar adhesions than the underlying fibronectin fibril. This could be because vinculin is not only limited to where the integrins bind and can accumulate around the border of the fibronectin-integrin adhesion site.

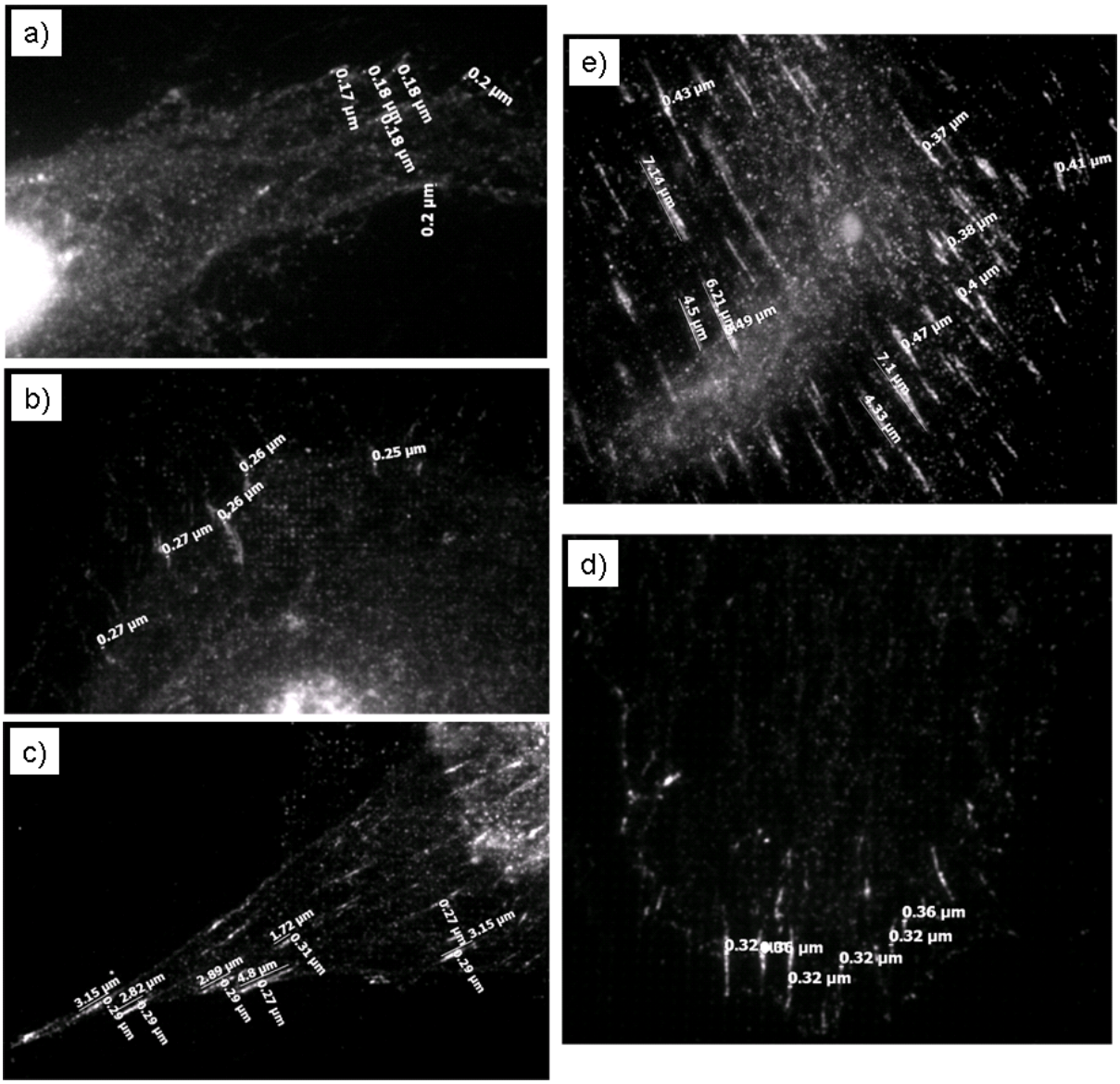

Figure 6.6.2: Vinculin immunofluorescence of endothelial cells imaged at 160X magnification attached to (a) 150 nm fibronectin adhesions spaced 300 nm apart. The cross section width of vinculin cluster is approximately 180 nm. (b) 200 nm fibronectin adhesions spaced 400 nm apart, imaged at 160X. The cross section width of vinculin cluster is approximately 260 nm. (c) 250 nm fibronectin adhesions spaced 500 nm apart, imaged at 160X magnification. The cross section width of vinculin cluster is approximately 290 nm. (d) 300 nm fibronectin adhesions spaced 600 nm apart, imaged at 160X magnification. The cross section width of vinculin cluster is approximately 320 nm. (e) Control surface. The cross section width of vinculin cluster is between 400 nm and 500 nm.

6.4 CONCLUSIONS

This section showed that the maximum size of a focal complex, as probed by vinculin and fibronectin staining, could be controlled by the underlying size of the fibronectin nanocluster. Furthermore, dash adhesions, which had formed due to stretching of the underlying fibronectin, also had a cross sectional width similar to the fibronectin nanocluster. The length of the dash adhesions progressively became smaller as the size of the fibronectin nanoclusters decreased. Additionally, the number of dash adhesions also progressively decreased as the size of the nanoclusters decreased. These results provide an important validation of the experimental system and form a basis for the experimental results that will be presented in subsequent chapters.

REFERENCES

Arnold, M., E. A. Cavalcanti-Adam, et al. (2004). "Activation of integrin function by nanopatterned adhesive interfaces." Chemphyschem **5**(3): 383-388.

Balaban, N. Q., U. S. Schwarz, et al. (2001). "Force and focal adhesion assembly: a close relationship studied using elastic micropatterned substrates." Nature Cell Biology **3**(5): 466-472.

Bershadsky, A. D., N. Q. Balaban, et al. (2003). "Adhesion-dependent cell mechanosensitivity." Annual Review of Cell and Developmental Biology **19**: 677-695.

Choquet, D., D. P. Felsenfeld, et al. (1997). "Extracellular matrix rigidity causes strengthening of integrin-cytoskeleton linkages." Cell **88**(1): 39-48.

Clark, E. A., W. G. King, et al. (1998). "Integrin-mediated signals regulated by members of the Rho family of GTPases." Journal of Cell Biology **142**(2): 573-586.

Coussen, F., D. Choquet, et al. (2002). "Trimers of the fibronectin cell adhesion domain localize to actin filament bundles and undergo rearward translocation." Journal of Cell Science **115**(12): 2581-2590.

Discher, D. E., P. Janmey, et al. (2005). "Tissue cells feel and respond to the stiffness of their substrate." Science **310**(5751): 1139-1143.

Engler, A. J., S. Sen, et al. (2006). "Matrix elasticity directs stem cell lineage specification." Cell **126**(4): 677-689.

Geiger, B. and A. Bershadsky (2001). "Assembly and mechanosensory function of focal contacts." Current Opinion in Cell Biology **13**(5): 584-592.

Geiger, B., A. Bershadsky, et al. (2001). "Transmembrane extracellular matrix-cytoskeleton crosstalk." Nature Reviews Molecular Cell Biology **2**(11): 793-805.

Glass, R., M. Moller, et al. (2003). "Block copolymer micelle nanolithography." Nanotechnology **14**(10): 1153-1160.

Holly, S. P., M. K. Larson, et al. (2000). "Multiple roles of integrins in cell motility." Experimental Cell Research **261**(1): 69-74.

Howe, A., A. E. Aplin, et al. (1998). "Integrin signaling and cell growth control." Current Opinion in Cell Biology **10**(2): 220-231.

Hynes, R. O. (1992). "Integrins - Versatility, Modulation, and Signaling in Cell-Adhesion." Cell **69**(1): 11-25.

Iber, D. and I. D. Campbell (2006). "Integrin activation - the importance of a positive feedback." Bulletin of Mathematical Biology **68**(4): 945-956.

Ingber, D. E. (1990). "Fibronectin Controls Capillary Endothelial-Cell Growth by Modulating Cell-Shape." Proceedings of the National Academy of Sciences of the United States of America **87**(9): 3579-3583.

Juliano, R. L. and S. Haskill (1993). "Signal Transduction from the Extracellular-Matrix." Journal of Cell Biology **120**(3): 577-585.

Koo, L. Y., D. J. Irvine, et al. (2002). "Co-regulation of cell adhesion by nanoscale RGD organization and mechanical stimulus." J Cell Sci **115**(7): 1423-1433.

Liddington, R. C. and M. H. Ginsberg (2002). "Integrin activation takes shape." Journal of Cell Biology **158**(5): 833-839.
Maheshwari, G., G. Brown, et al. (2000). "Cell adhesion and motility depend on nanoscale RGD clustering." J Cell Sci **113**(10): 1677-1686.
Miranti, C. K. and J. S. Brugge (2002). "Sensing the environment: a historical perspective on integrin signal transduction." Nature Cell Biology **4**(4): E83-E90.
Miriam Cohen, D. J. B. G. L. A. (2004). "Spatial and Temporal Sequence of Events in Cell Adhesion: From Molecular Recognition to Focal Adhesion Assembly." ChemBioChem **5**(10): 1393-1399.
Miyamoto, S., S. K. Akiyama, et al. (1995). "Synergistic Roles for Receptor Occupancy and Aggregation in Integrin Transmembrane Function." Science **267**(5199): 883-885.
Miyamoto, S., H. Teramoto, et al. (1995). "Integrin Function - Molecular Hierarchies of Cytoskeletal and Signaling Molecules." Journal of Cell Biology **131**(3): 791-805.
Mostafavi-Pour, Z., J. A. Askari, et al. (2003). "Integrin-specific signaling pathways controlling focal adhesion formation and cell migration." Journal of Cell Biology **161**(1): 155-167.
Pelham, R. J. and Y. L. Wang (1997). "Cell locomotion and focal adhesions are regulated by substrate flexibility." Proceedings of the National Academy of Sciences of the United States of America **94**(25): 13661-13665.
Slater, J. and W. Frey (2007). "Nanopatterning of Fibronectin and the Influence of Integrin Clustering on Endothelial Cell Spreading and Proliferation." Journal of Biomedical Materials Research Part A.
Tan, J. L., J. Tien, et al. (2003). "Cells lying on a bed of microneedles: An approach to isolate mechanical force." Proceedings of the National Academy of Sciences of the United States of America **100**(4): 1484-1489.
Wehrle-Haller, B. and B. A. Imhof (2003). "Integrin-dependent pathologies." Journal of Pathology **200**(4): 481-487.
Wilder, R. L. (2002). "Integrin alpha V beta 3 as a target for treatment of rheumatoid arthritis and related rheumatic diseases." Ann Rheum Dis **61**(90002): 96ii-99.
Yeung, T., P. C. Georges, et al. (2005). "Effects of substrate stiffness on cell morphology, cytoskeletal structure, and adhesion." Cell Motility and the Cytoskeleton **60**(1): 24-34.
Zaidel-Bar, R., M. Cohen, et al. (2004). "Hierarchical assembly of cell-matrix adhesion complexes." Biochemical Society Transactions **32**: 416-420.

CHAPTER 7: CELLULAR MORPHOLOGY

7.1 OVERVIEW

This chapter investigates cellular morphology as a function of several different nanoscale parameters. It aims at elucidating the relationship between adhesion cluster size, spacing and density to observed morphological changes. These changes were quantified using two parameters, cellular spreading area and circularity. These parameters accurately capture the differences in cells by grouping them by size and shape. Many of the observed trends in this chapter will again appear in later chapters, showing the general link between observed morphology and cellular behavior.

7.2 METHODOLOGY

Silicon or glass samples were prepared and functionalized according to the protocols presented in Chapter 5. Samples were immersed in ETOH (AAPER) for 5 minutes to sterilize the samples before being introduced into a sterile culture hood. Samples were then rinsed 60 seconds, three times in a HEPES buffered saline that was prepared from 11.9 g (HEPES)(Sigma), 5.8 g NaCl (Mallinkckrodt) and 1000 ml DI and adjusted to 7.5 pH with NaOH (Sigma). 125 µL of a 10 µg/ml fibronectin solution (Sigma) in 50 mM HEPES buffered saline was placed on the samples for 20 minutes at room temperature. The samples were then thoroughly rinsed in 50 ml of HEPES buffered saline solution for 60 seconds, 3 times to remove any excess fibronectin. The cells in all the studies were human umbilical vein endothelial cells (HUVECs) (Cambrex, Walkersville, MD) of passage below 4 and cultured according to manufacturer's specifications. They were cultured in T-25 tissue culture flasks coated with 30 µg of

human plasma fibronectin (Sigma, Saint Louis, MO) at 37ºC and 5% CO_2 until 80% confluence. During culture and experiment, the HUVECs were bathed in endothelial growth media (Cambrex, Walkersville, MD) supplemented with 2% fetal bovine serum, 0.5 ml human endothelial growth factor, 0.5 ml Hydrocortisome, 0.5 ml GA-1000 (Gentamicin, Amphotericin B). To release cells from flasks for cell seeding, the flasks were first rinsed with 5 ml of HEPES buffered saline at 37ºC. They were then trypsinized using 3 ml of Trypsin/EDTA (Cambrex) for 5 minutes at 37ºC and 5% CO_2. Next, 3 ml of trypsin neutralizing solution (Cambrex) was added to the cell suspension to neutralize the Trypsin/EDTA. The cell suspension was pelleted using a centrifuge set to 240 g for 6 minutes. The cells were then resuspended in 10 ml of endothelial growth media (Cambrex) discussed above. A hemocytometer and trypan blue dye was used to determine the total living cell population in the resuspension. The HUVECs were then seeded on the sample surface at approximately 7 cells/mm^2. The cells were maintained in 20 ml of endothelial growth media (Cambrex), 37˚C and 5% CO_2. The cells were imaged in an incubator box that enclosed our Leica Microscope. Images were captured using a sensicam digital microscope camera and Camware software made by PCO.Imaging at the largest magnification that a cell could fit in the imaging frame. The outline of the cell images was traced by hand using ImageJ (NIH, Bethesda, MD). The digital traces were used to calculate the area and perimeter of the cell. Circularity, a measure of deviation of an arbitrary shape from a perfect circle, was calculated using the following equation:

$$Circularity = 4\pi \frac{Area}{Perimeter^2}$$

All of the collected data was analyzed with a custom Matlab program. Statistical hypothesis testing was performed to quantify the difference in sample means between groups of cells on different patterns assuming unequal variances and unequal sample sizes. The statistical analysis was performed two ways. First, it was assumed that the

spreading area had a lognormal distribution which was found previously in our lab (Truskey and Pirone 1990; Slater and Frey 2007). Secondly, the statistical analysis was performed assuming a normal distribution. Both methods produced similar statistical significance values, with the exception of 300 nm 1:2 not being statistically less than controls for a normal distribution.

7.3.1 CELL SPREADING

When an adherent cell in suspension attaches to a surface, it initially forms adhesions and begins to take on a flattened morphology, a process known as cell spreading. As time progresses, the cell can continue to grow and spread out further. As a quantitative measure, cell spreading is commonly used to classify cell behavior on homogenous surfaces and patterned surfaces. It provides a meaningful and comparable measure of cellular morphology.

7.3.2 CELL SPREADING AS A FUNCTION OF PATTERN SIZE WITH CONSTANT DENSITY

Macroscopic fibronectin density is defined as the number of fibronectin per μm^2. In other words, it is the number of fibronectin available for the cell to bind to for a given unit area. If one assumes that a cell only needs to make a certain number of fibronectin bonds, then the arrangement of fibronectin on a surface should not be a determinant in cellular behavior. Any arbitrary arrangement of fibronectin on the surface should yield identical cellular responses. Many experiments have been conducted having different macroscopic densities of fibronectin on a surface. The observed behavior of the cells might change given extremely high fibronectin densities or extremely low fibronectin densities. Consistent with these types of experiments, our homogenous coated control

surfaces always produced a certain consistent behavior for a given fibronectin surface density. With these results in mind, I was interested in investigating whether at a particular known surface fibronectin density, if simply rearranging the positions of fibronectin on the nanoscale could influence cellular behavior. This is to say, for a given number of fibronectin per μm^2, if these are arranged in different sized circular arrangements, can the cell determine the difference at the nanoscale?

To conduct this experiment, fibronectin clusters were created in the following diameters: 150 nm, 200 nm, 250 nm and 300 nm. These clusters were the arranged so that their total macroscopic fibronectin density was identical. Experiments were conducted at a surface presentation coverage of 4.91%, approximately 148 FN's per μm^2, and 8.72%, approximately 263 FN's per μm^2.

The results from the experiment for the fibronectin surface coverage of 4.91% are presented in Figure 7.3.1. These results show a dramatic increase in cell spreading area as the size of the fibronectin clusters was increased. Keep in mind that the overall fibronectin presentation is 148 FN's per μm^2 irrespective of the size of the cluster. All of the patterns show a statistically significant difference, $p<0.05$, between their adjacent partner. This shows that the cells respond to differences in the size of the fibronectin adhesion clusters independent of macroscopic density. They are also very sensitive to the cluster size, responding to differences as little as 50 nm in diameter.

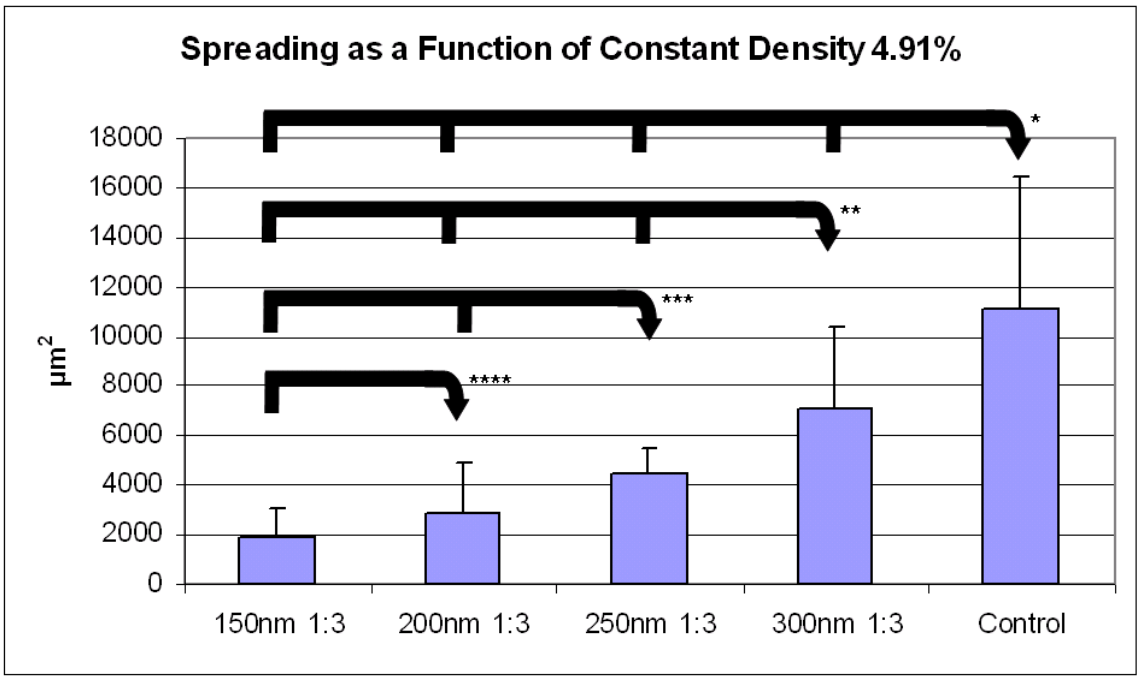

Figure 7.3.1: Keeping the overall macroscopic fibronectin density constant at 4.91%, approximately 148 FN's per μm^2, only the arrangement of the fibronectin was changed. Cluster sizes of 150 nm, 200 nm, 250 nm and 300 nm were created. Cellular spreading was found to increase by simply increasing the size of the cluster. * $p< 0.05$, **$p< 0.05$, *** $p< 0.05$, **** $p< 0.05$ (Control n=36, 300 nm n=9, 250 nm n=5, 200 nm n=22, 150 nm n=10).

To explore the differences due to changes in macroscopic protein density expression, the experiment was also conducted with a macroscopic fibronectin surface coverage of 8.72%. The results from this experiment are presented in Figure 7.3.2. The same general trend was observed at this density. As the size of the fibronectin clusters was increased, the average spreading area also increased. However at this density, statistically significant changes between patterns occurred over changes in diameter of 100 nm. It is possible that with a larger data set a statistically relevant difference could be observed with a smaller diameter change.

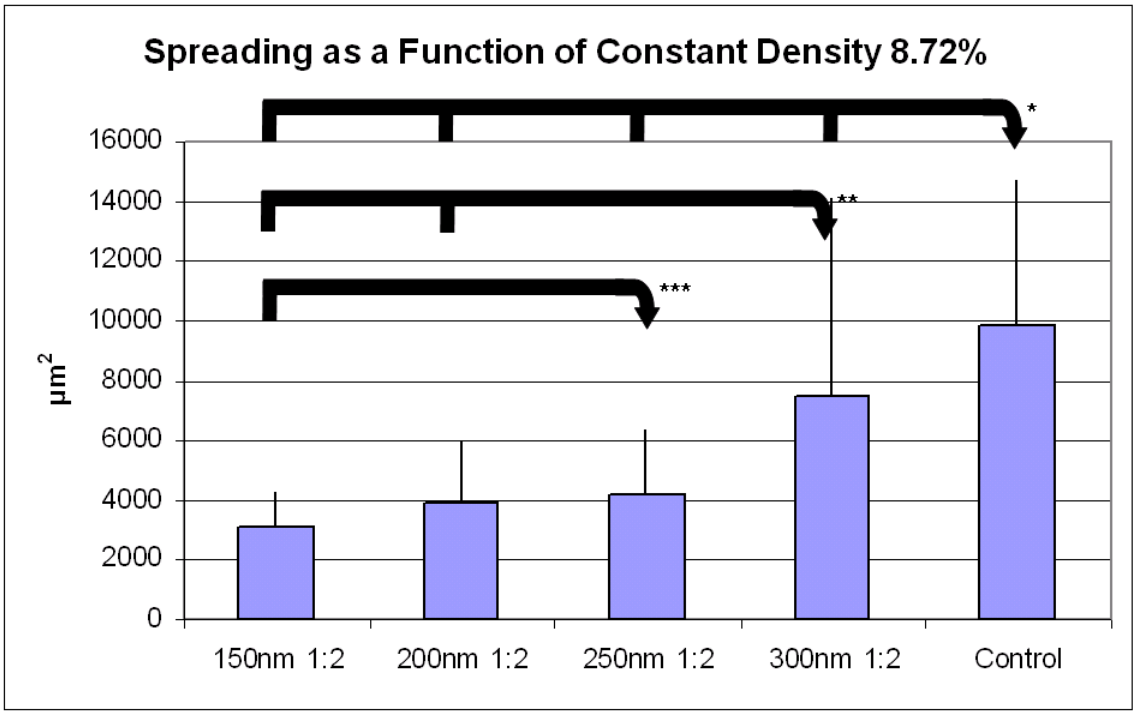

Figure 7.3.2: Keeping the overall macroscopic fibronectin density constant at 8.72%, approximately 263 FN's per μm^2, only the arrangement of the fibronectin was changed. Cluster sizes of 150 nm, 200 nm, 250 nm and 300 nm were created. Cellular spreading was found to increase by simply increasing the size of the cluster. * $p< 0.05$, **$p< 0.05$, *** $p< 0.05$ (Control n=36, 300 nm n=13, 250 nm n=18, 200 nm n=14, 150 nm n=12). Statistical significance between 300 nm and controls was only found when assuming a lognormal distribution for spreading area.

7.3.3 Cell Spreading as a Function of Pattern Size with Constant Spacing

In the last section, it was discovered that cellular behavior on a surface could be influenced by simply changing the arrangement of fibronectin on a surface. In this section, I wish to provide additional evidence that the size of fibronectin clusters directly influences cellular spreading area. In the previous experiments, under constant density, the spacing between the fibronectin clusters had to be varied in order to achieve a constant macroscopic protein density for different adhesion sizes. To show that the

changes observed in these experiments were due to the fibronectin cluster size and not cluster separation distance, the following set of experiments was conducted holding the spacing between the clusters constant. In other words, the cluster sizes were changed like the previous experiment but this time the spacing between clusters was held constant.

The first set of experiments was conducted using a constant separation distance of 300 nm, as shown in Figure 7.3.3. As the size of the fibronectin adhesion cluster was decreased, there was a corresponding decrease in the cell spreading area. This trend also held true for separation distances of 600 nm, as shown in Figure 7.3.4. These results provide additional evidence that independent of adhesion spacing distances, the actual size of the adhesion cluster directly influences the cell spreading area.

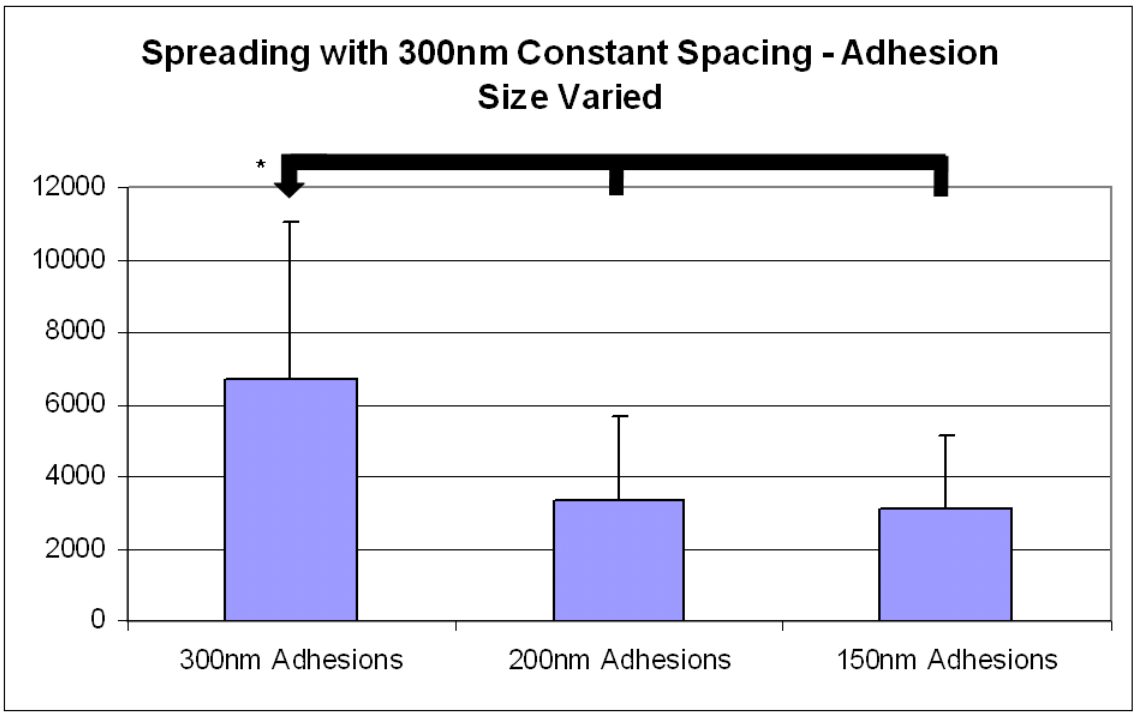

Figure 7.3.3: The distance between fibronectin clusters was kept at a constant distance of 300 nm. As the fibronectin cluster diameter was increased from 150 nm, the average cell spreading area increased. * $p < 0.05$ (300 nm n=11, 200 nm n=12, 150 nm n=12).

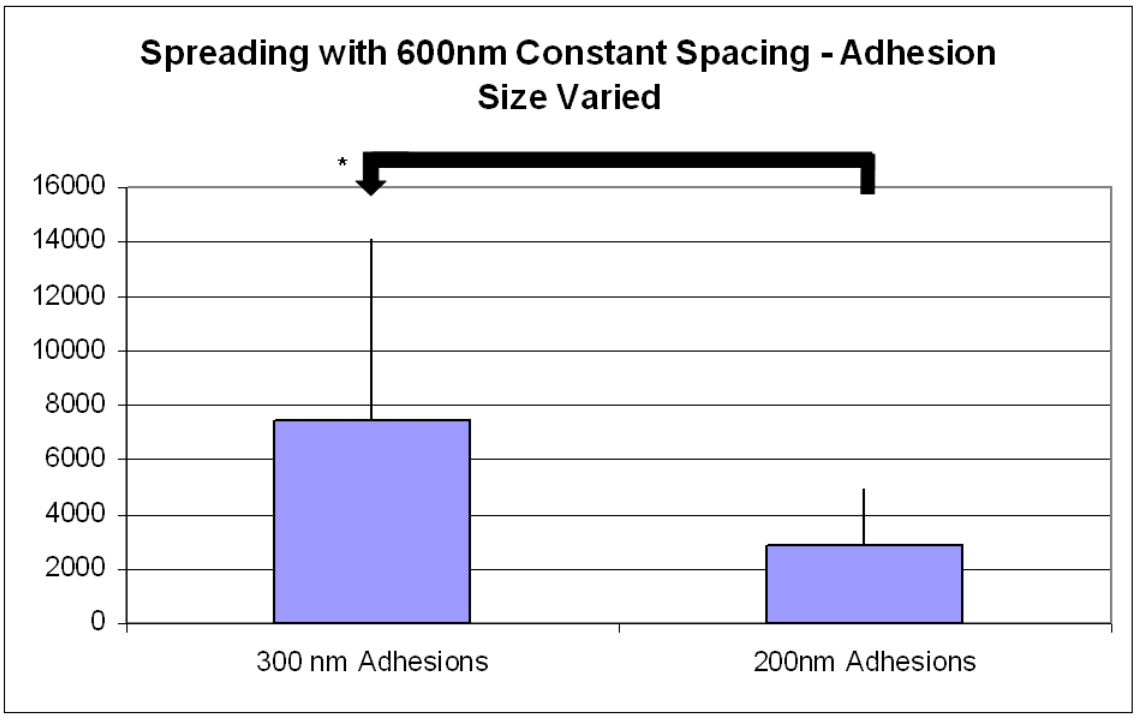

Figure 7.3.4: The distance between fibronectin clusters was kept at a constant distance of 600 nm. As the fibronectin cluster size was increased from 200 nm, the average cell spreading area increased. * $p < 0.05$ (300 nm n=13, 200 nm n=22).

7.4.1 CIRCULARITY

Early on, it was observed that cell shape seemed to vary from pattern to pattern. On some patterns there always seemed to be a greater population of round cells that resembled those on control surfaces, while on other patterns a large portion of the cells would be elongated. A common method of quantifying shape-related changes is using the measure known as circularity (Kawa, Stahlhut et al. 1998). Circularity relates the ratio of area-to-perimeter of an arbitrary shape to the area and perimeter of a perfect circle. As mentioned previously, the equation that describes circularity:

$$Circularity = 4\pi \frac{Area}{Perimeter^2}$$

Conceptually, it is a measure of deviation from a perfect circle for an arbitrary shape. For example, a perfect circle has a circularity of one, whereas an ellipsoid that approaches the shape of an infinite line would have a circularity that approaches zero (Figure 7.4.1).

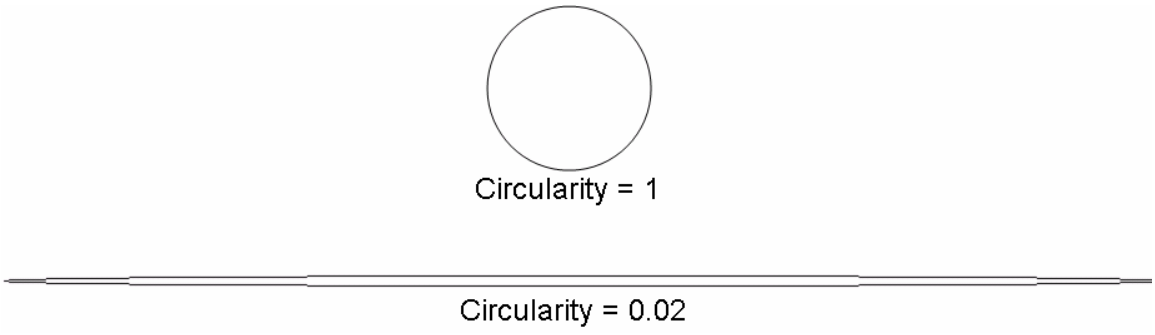

Figure 7.4.1: Cartoon depiction of the differences in circularity between two different shapes. The upper figure shows a perfect circle, which has the circularity of one. The impact on the circularity measure is shown by the ellipsoid (bottom figure), which significantly deviates from a perfect circle.

This measure is widely used and relevant because typically round cells are associated with certain quiescent behavior, whereas elongated shaped cells can be associated such behavior such as increased motility (Figure 7.4.2). It also captures shape changes such as cells with long extensions or the appearance of 'spinyness'.

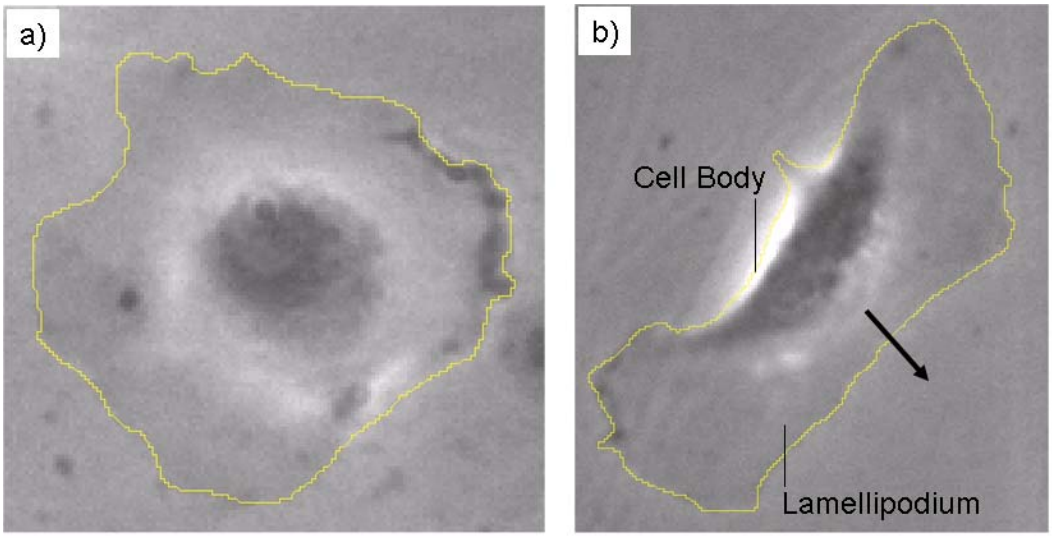

d)

Image	Circularity	Pattern
a	0.73	300nm 1:1
b	0.48	150nm 1:1.5
c	0.23	200nm 1:3

Figure 7.4.2: Circularity is a relevant and widely used measure which captures shape differences. Typically round, well spread cells as shown in Figure (a), are associated with a quiescent state. Keratocyte shaped cells, shown in Figure (b), have a shape known for motile cells. On certain nanopatterns, extremely elongated or spiny cells were observed, as shown in Figure (c). Table (d) summarizes the calculated circularities and what pattern the cell was on.

7.4.2 Circularity as a Function of Pattern Size with Constant Density

Similar to the cell spreading experiments, I was interested in how adhesion size influenced the shape of the HUVECs. Holding macroscopic protein density constant at either 4.91% or 8.72%, adhesion sizes of 150 nm, 200 nm, 250 nm and 300 nm were investigated. The results for the macroscopic protein density of 4.91% are shown in Figure 7.4.3. As adhesion sizes were increased, the circularity of the cells also increased.

Statistically different circularity was observed for diameter changes as small as 50 nm and between 150 nm and 200 nm. Similar to the spreading results, this shows the sensitivity of cells to the fibronectin adhesion size.

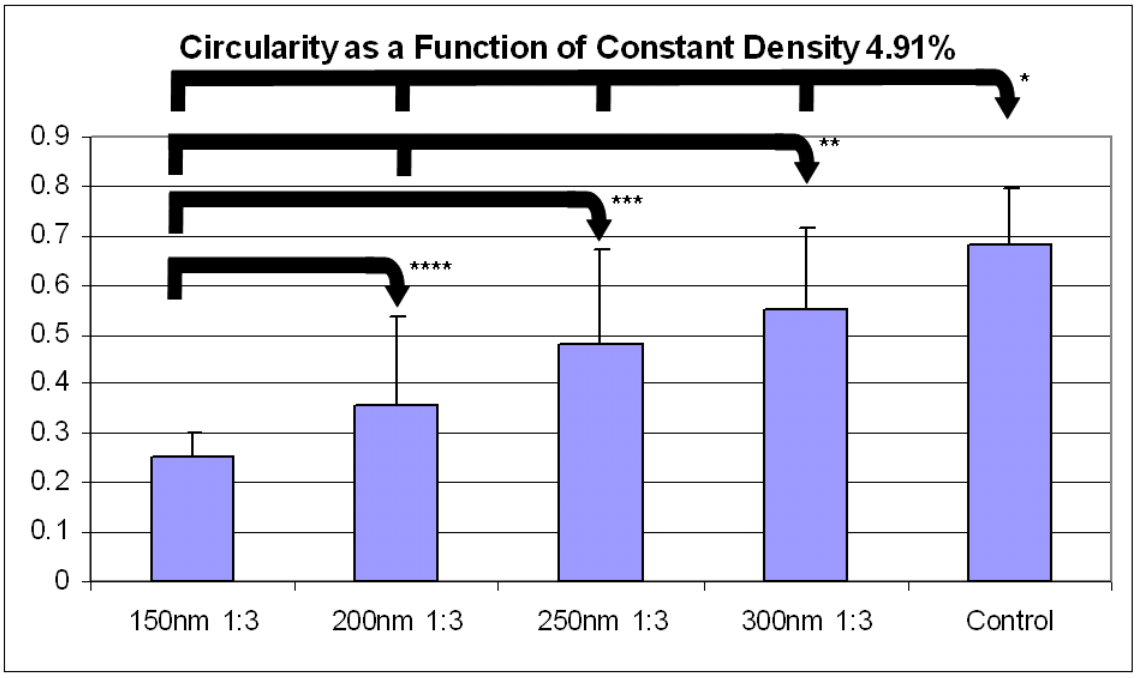

Figure 7.4.3: Keeping the overall presentation of macroscopic protein expression constant at 4.91%, approximately 128 FN's per μm^2, only the arrangement of the fibronectin was changed. Cluster sizes of 150 nm, 200 nm, 250 nm and 300 nm were created. Circularity was found to increase by simply increasing the diameter of the cluster. * $p< 0.05$, **$p< 0.05$, *** $p< 0.05$, **** $p< 0.05$ (Control n=36, 300 nm n=9, 250 nm n=5, 200 nm n=22, 150 nm n=10).

An identical experiment was conducted at a macroscopic protein density of 8.72% (Figure 7.4.4). A similar trend was observed: as the pattern size was increased the circularity correspondingly increased. Every pattern was statistically different, $p<0.05$, from each adjacent pattern. This shows that the cells are consistently sensitive to differences as small as 50 nm in the diameter of fibronectin adhesion clusters.

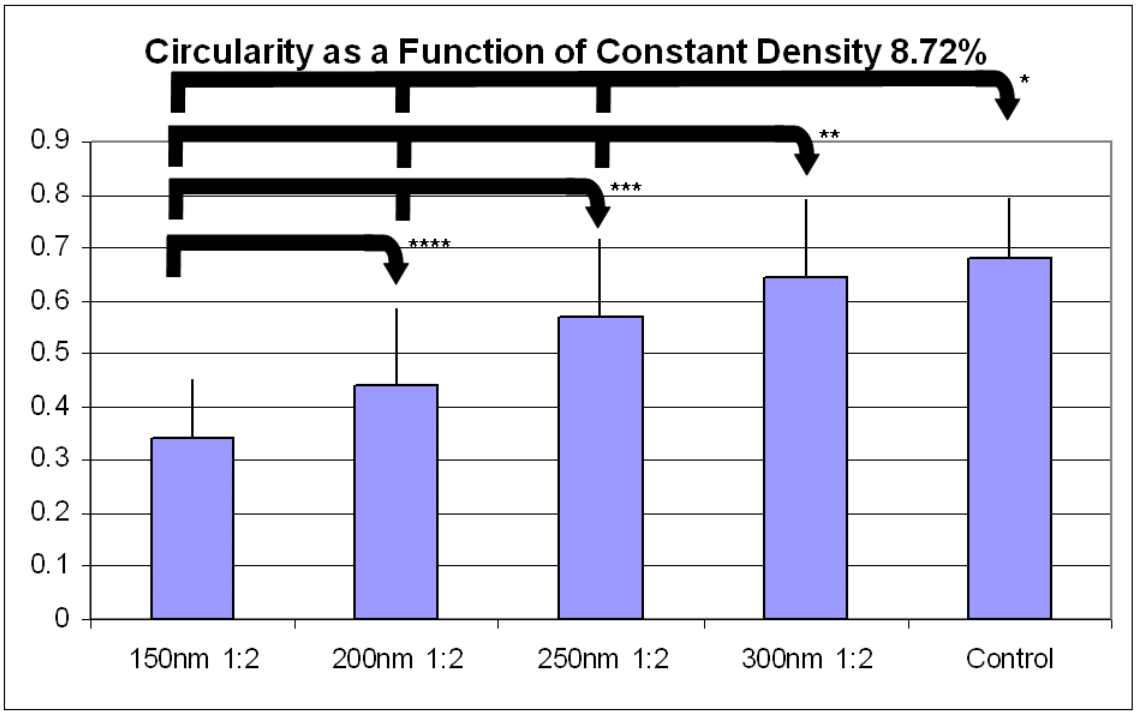

Figure 7.4.4: Keeping the overall presentation of macroscopic protein expression constant at 8.72%, approximately 263 FN's per μm^2, only the arrangement of the fibronectin was changed. Cluster sizes of 150 nm, 200 nm, 250 nm and 300 nm were created. Circularity was found to increase by simply increasing the diamter of the cluster. * $p< 0.05$, **$p< 0.05$, *** $p< 0.05$, **** $p<0.05$ (Control n=36, 300 nm n=13, 250 nm n=18, 200 nm n=14, 150 nm n=12).

7.4.3 CIRCULARITY AS A FUNCTION OF PATTERN SIZE WITH CONSTANT SPACING

To separate the influence due to spacing of adhesion clusters versus the size of the adhesive clusters themselves, experiments were conducted holding the spacing between adhesion cluster sizes constant. In these experiments, adhesion clusters were separated by either 300 nm or 600 nm and the adhesion cluster size was then varied. For the equidistant spacing of 300 nm (Figure 7.4.5), as the pattern size was increased from 150 nm, the circularity correspondingly increased. There was no observed statistical difference between 200 nm and 300 nm at this spacing.

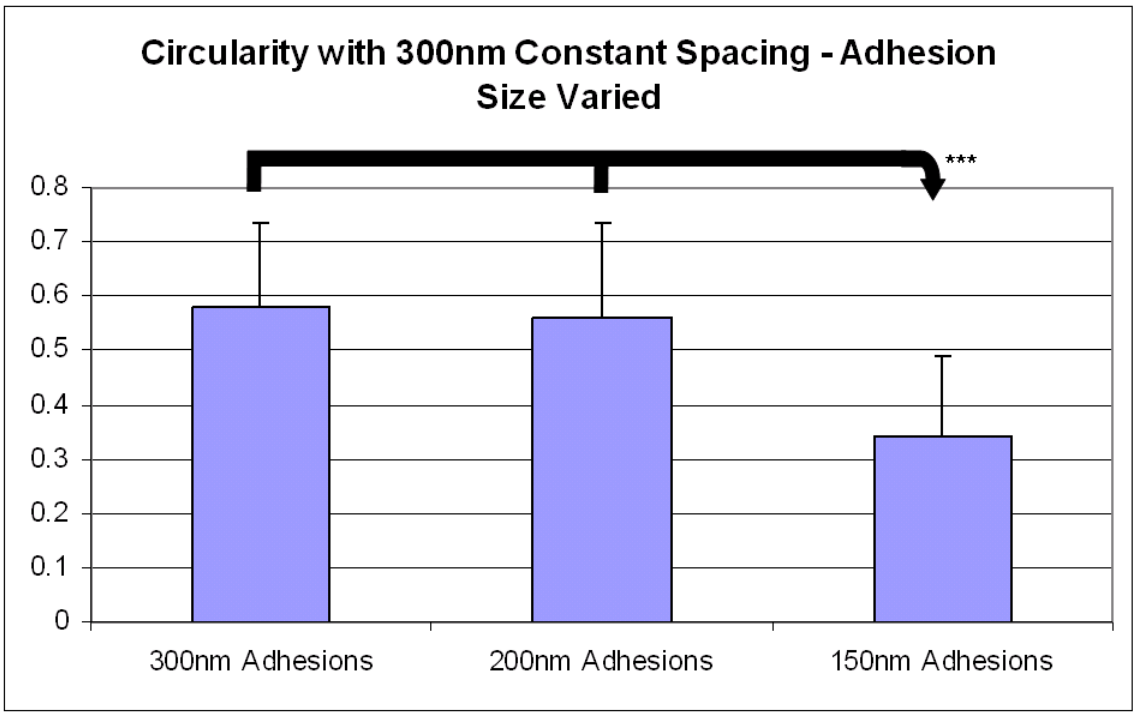

Figure 7.4.5: The distance between fibronectin adhesion clusters was kept at a constant 300 nm distance. As the fibronectin cluster diameter was increased from 150 nm, the average circularity increased. *** $p < 0.05$ (300 nm n=11, 200 nm n=12, 150 nm n=12).

As the spacing was increased to 600nm (Figure 7.4.6), there was a statistically significant change in circularity between the 200 nm adhesions and 300 nm adhesions. These results show that independent of adhesion cluster spacing, the size of the fibronectin adhesions influences cell shape.

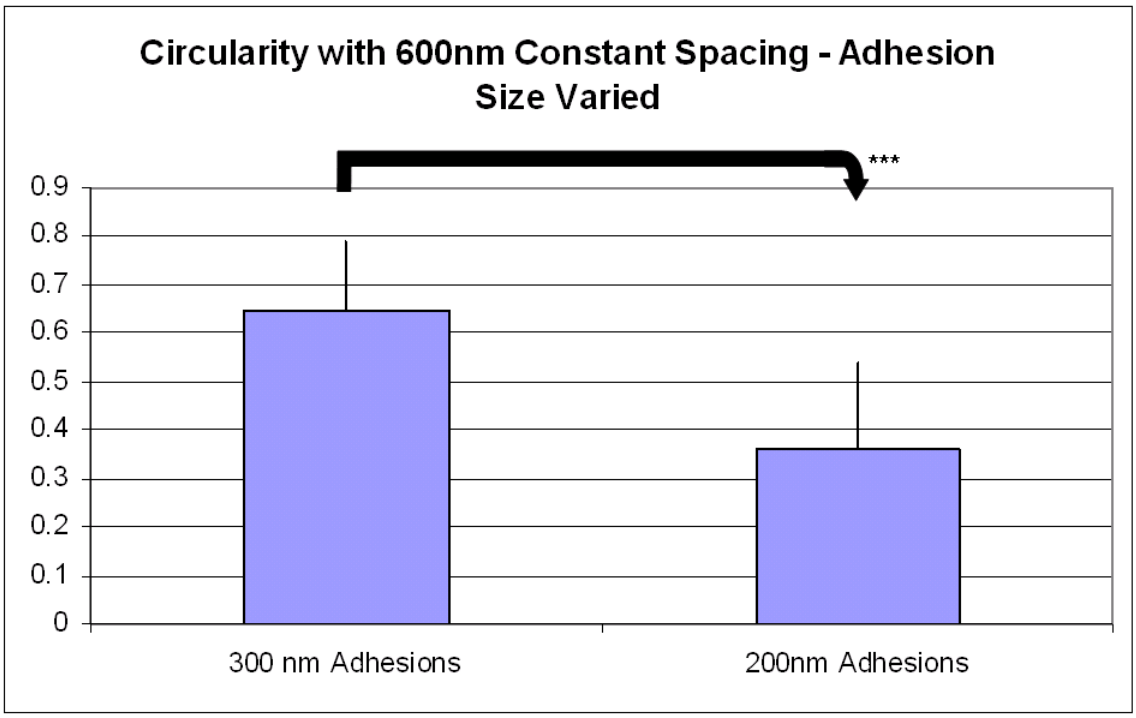

Figure 7.4.6: The distance between fibronectin adhesion clusters was kept at a constant 600 nm distance. As the fibronectin cluster diameter was increased from 200 nm, the average circularity increased. *** $p < 0.05$ (300 nm n=13, 200 nm n=22).

7.5 DISCUSSION

Additional insight can be gained between the relationship of macroscopic protein density, fibronectin cluster diameter and cluster spacing by overlaying the results of both the cell spreading area and circularity (Figure 7.5.1).

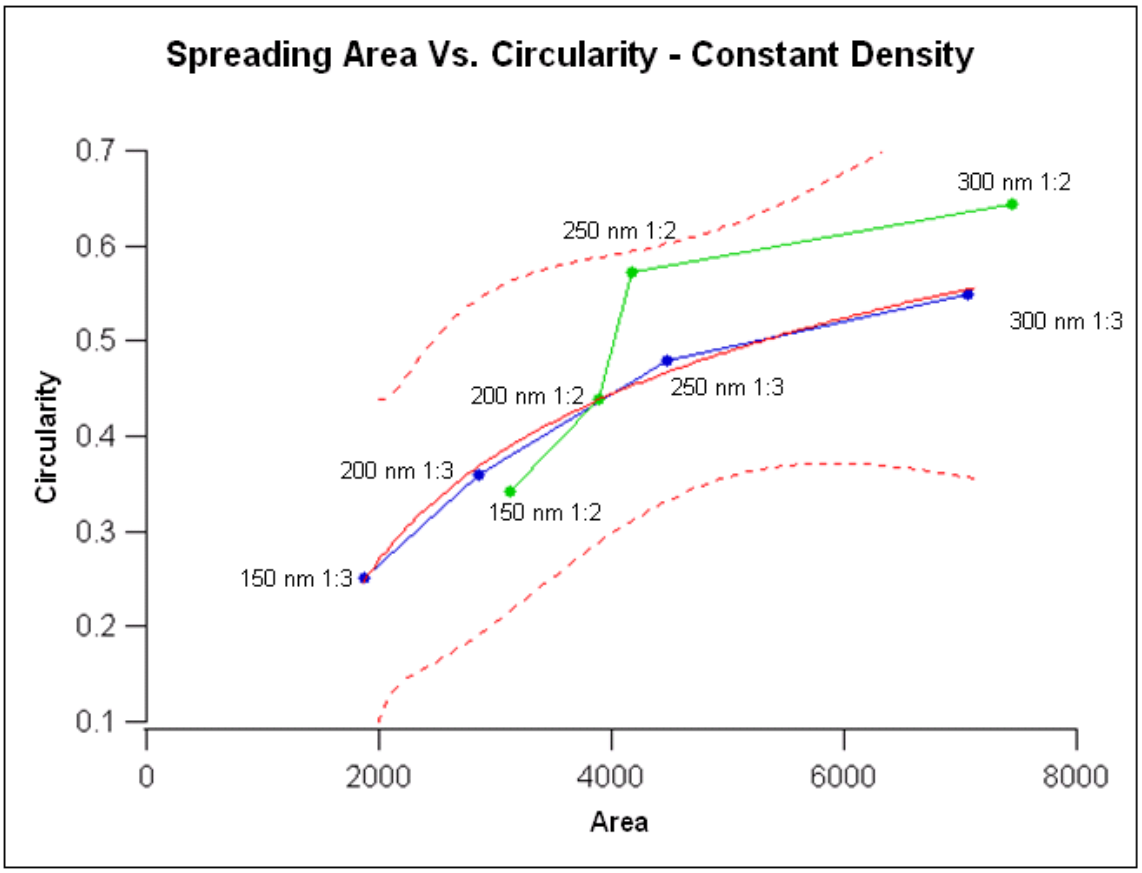

Figure 7.5.1: A plot of cell spreading area versus circularity at a given constant macroscopic surface fibronectin density (Blue 1:3 - 148 FN's per μm^2, Green 1:2 - 263 FN's per μm^2). The red line represents a log fit to the blue curve, with confidence intervals given by the dashed red lines. As the size of the fibronectin adhesions are increased, cell spreading and circularity increase. The transitions between 150 nm and 250 nm have a greater rate of change for circularity. The transition between 250 nm and 300 nm has a greater rate of change for cell spreading area.

Increasing the fibronectin adhesion size while keeping the total macroscopic surface density constant increases both the cell spreading area and cell circularity. From Figure 7.5.1, it is clear that the rate of change in circularity is larger than the spreading area for the smaller adhesion sizes, 150 nm and 200 nm. As the adhesion sizes transition from 250 nm to 300 nm, there is a dramatic increase in spreading area and less of a

change in circularity. As the macroscopic density was increased from approximately 148 FN's per μm^2 to 263 FN's per μm^2, there is a shift of the curve up and to the right. This shift is consistent with experiments that vary homogenous fibronectin density (Ingber 1990). It was also found that that data for the patterns with a pitch of 1:3 could be fit reasonably well with a log or square root function. This would mean that the observed changes in circularity scaled with the radius of the clusters rather than the area. This model may also be applied to the patterns with 1:2 pitch but there is an offset between the two curves. The fit for the patterns with 1:2 pitch is not as good as 1:3 due to a transition between 200 nm and 250 nm. At this time we are unsure about the reason behind this transition but it will consistently appear in experiments in later chapters.

A similar adhesion size versus circularity comparison can be made with the constant spacing data presented in this chapter (Figure 7.5.2). Once again as the size of the adhesion cluster is increased, both circularity and cell spreading increase. This figure also shows the non-linearity that was observed in the previous figure. Between 150 nm and 200 nm, changing the adhesion size greatly affects the circularity but the overall cell spreading area changes very little. However, the transition between 200 nm and 300 nm produces a considerable change in the cell spreading area.

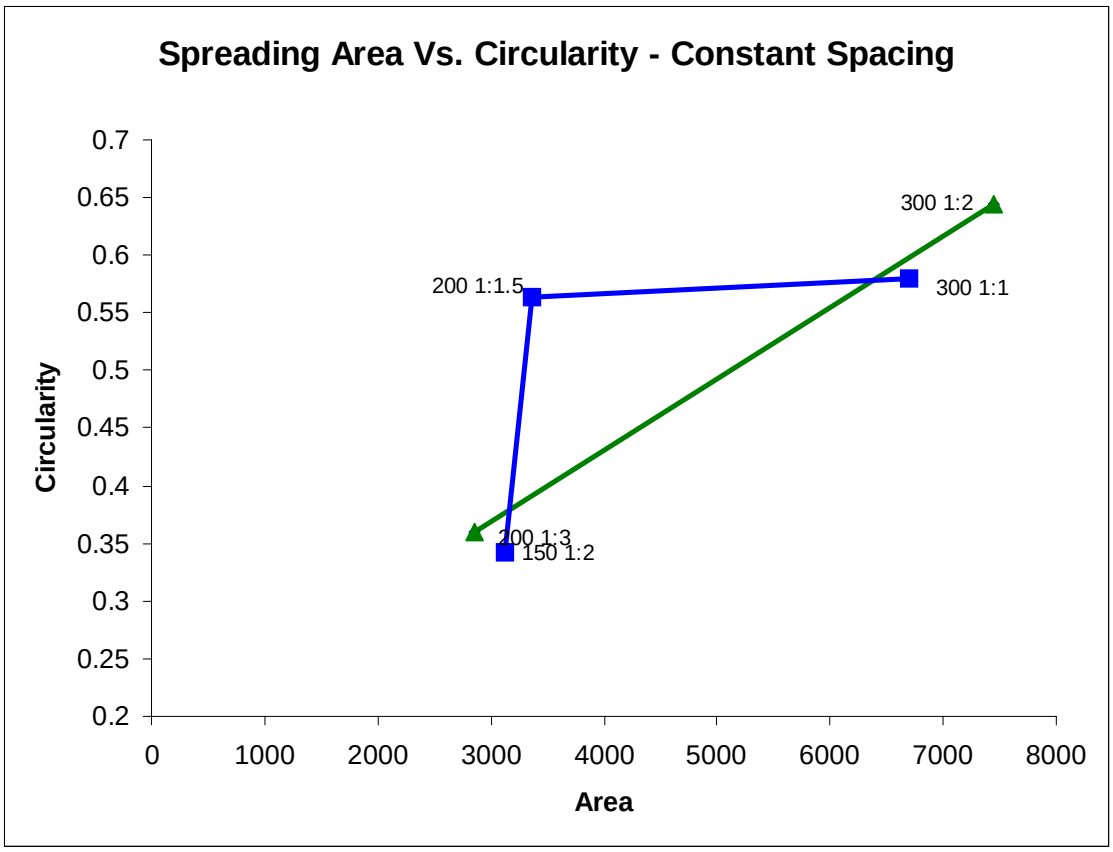

Figure 7.5.2: A scatter plot of cell spreading area versus circularity at a given constant fibronectin adhesion cluster spacing (Squares – 300 nm spacing, Triangles – 600 nm Spacing). As the distance between fibronectin adhesions are increased, cell spreading and circularity increase. This trend is not necessarily linear. The transitions between 150 nm and 200 nm have a greater rate of change for circularity. The transition between 200 nm and 300 nm has a greater rate of change for cell spreading area.

Although it is clear that adhesion size plays a role in influencing both cell spreading area and circularity, there are clues that the spacing between adhesions might also play a role. Comparing cell spreading versus circularity for adhesions of a constant size but varying the spacing is summarized in Figure 7.5.3. As the spacing between the 150nm adhesions is gradually decreased from 450 nm (150 1:3) down to 225 nm (150 1:1.5), there is a corresponding change in circularity and cell spreading. However, the

spacing transition between 225 nm (150 1:1.5) and 150 nm (150 1:1) produces a dramatic shift in cell spreading area. For the adhesion size of 200 nm, the cell spreading area remains nearly constant for a transition from 600 nm (200 1:3) all the way down to 300 nm (200 1:1.5), while the circularity increases by 60%. Then there is a dramatic shift in cell spreading area from a spacing of 300 nm (200 1:1.5) to 200 nm (200 1:1). This dramatic transition is interesting because it shows that there might be an adhesion spacing threshold that, once crossed, the cells begin to spread to a greater extent.

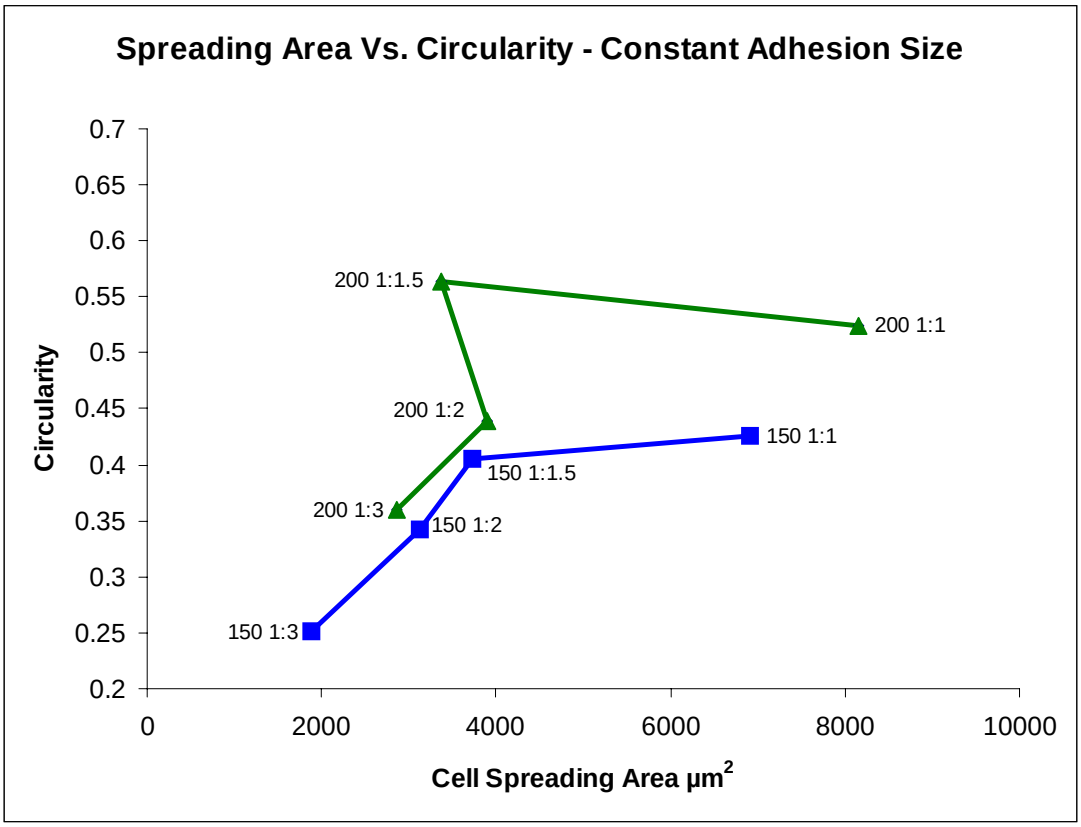

Figure 7.5.3: A scatter plot of cell spreading area versus circularity at a given constant fibronectin adhesion cluster size (Squares – 150 nm adhesion clusters, Triangles – 200 nm adhesion clusters). As the distance between fibronectin adhesions are increased, cell spreading and circularity increase. There is a clear transition for 150 nm adhesion clusters between 225 nm and 150 nm spacings. There is also a clear transition for 200 nm adhesion clusters between 300 nm and 200 nm spacings.

The following 3D plots show the relationship between adhesion size and spacing, Figure 7.5.4 and Figure 7.5.5.

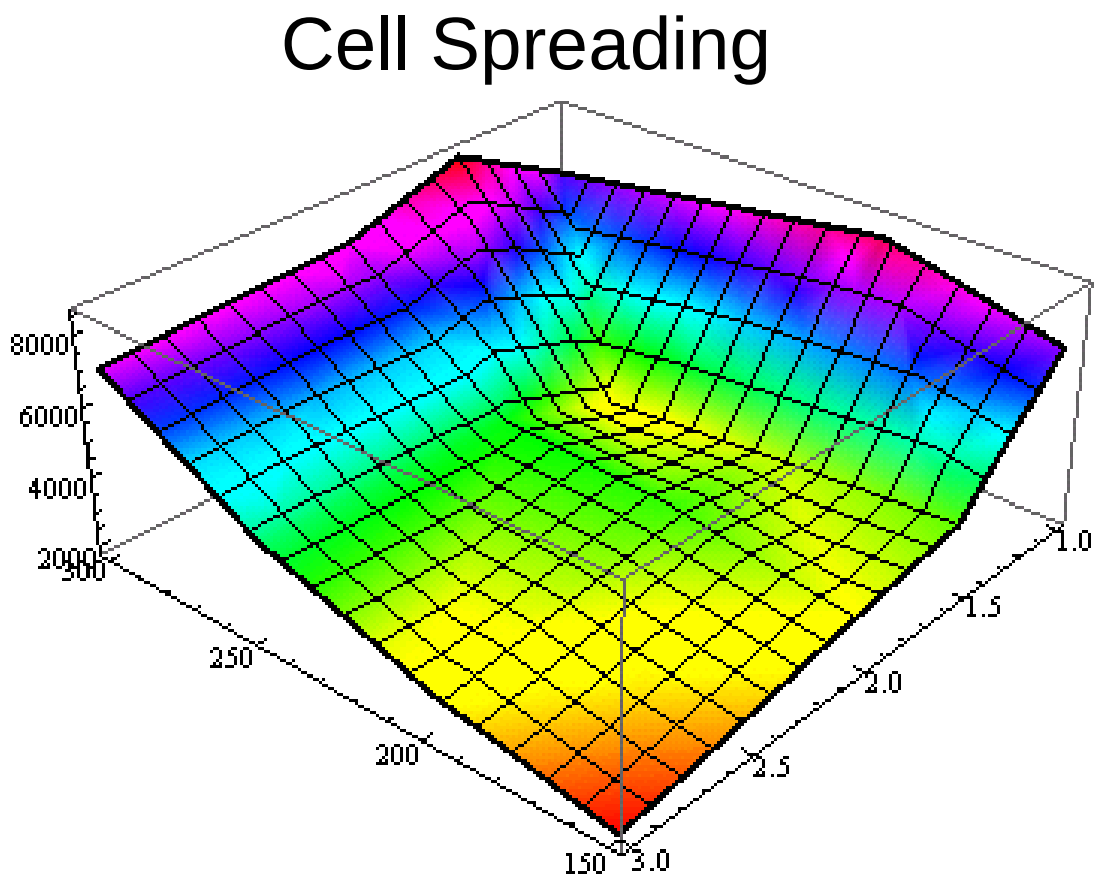

Figure 7.5.4: A three dimensional plot of cellular spreading versus adhesion size and pitch. The z-axis is circularity, the pattern sizes vary from 150 nm – 300 nm and the pitch varies from 1:1 – 1:3.

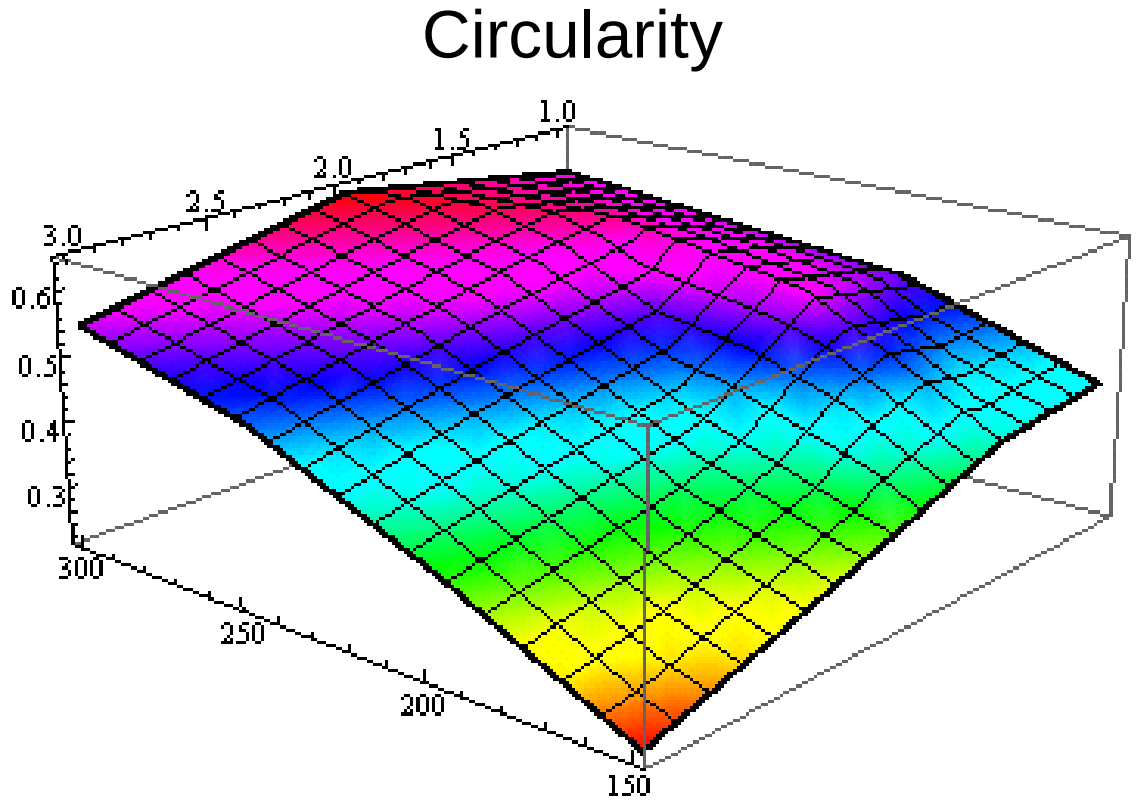

Figure 7.5.5: A three dimensional plot of circularity versus adhesion size and pitch. The z-axis is circularity, the pattern sizes vary from 150 nm – 300 nm and the pitch varies from 1:1 – 1:3.

7.6 CONCLUSIONS

This chapter investigated the relationship between adhesion cluster sizes, spacing and macroscopic density and how they influenced the morphological behavior of cells on nanopatterns. It has been shown previously that cell spreading on homogenous surfaces can be influenced by nanotopography and surface roughness. Fibroblasts (Dalby, Yarwood et al. 2002) and endothelial cells (Dalby, Riehle et al. 2002) were shown to increase cell spreading on polymer demixed topography, and cell spreading was

decreased for fibroblasts 160 nm nanocolumns (Dalby, Riehle et al. 2004). However, these homogenous surfaces only provide an average view on how the cell is actually interacting with the surface. The nanopatterned surfaces presented in this chapter allow us to look at how the cell is actually clustering its integrins to form focal complexes. Restricting the size and spacing of the complexes was shown to influence the morphology of the attached HUVECs.

Studies on polyacrylamide gels have shown that traction forces exerted by cells on the substrate are positively correlated to the degree of cell spreading (Tolic-Norrelykke and Wang 2005). They also found that elongated or cells with small circularity exerted less traction force than wide well-spread cells. Similar results were obtained on micropatterned surfaces, where the cell spreading area was positively correlated to the degree of force exerted on micropatterned elastic posts (Tan, Tien et al. 2003). Additionally, several studies have found that increased force per unit area is positively correlated with the size of focal adhesions (Balaban, Schwarz et al. 2001; Schwarz, Balaban et al. 2003; Tan, Tien et al. 2003). These studies are interesting because the methods used in this chapter allow us to ask the opposite question.

The results presented show that for a given density of fibronectin, the arrangement of the fibronectin on a surface does influence the morphology of attached HUVECs. In particular, the size of the fibronectin cluster diameter influences both the average spreading area of the cells as well as their shape defined by circularity. As was shown in Chapter 6, the diameter of the fibronectin cluster is directly related to the maximum size of a focal adhesion. Given the results of (Balaban, Schwarz et al. 2001; Schwarz, Balaban et al. 2003; Tan, Tien et al. 2003) discussed above, it is possible that limiting the maximum size of the focal adhesion directly limits the force per unit area that can be exerted by the cell. If this is true, then one would expect that larger diameter

fibronectin clusters would result in cells that are able to exert greater force. Smaller diameter clusters, on the other hand, would yield cells that would be restricted in the amount of cell-substrate force they could produce. The work of (Tan, Tien et al. 2003) and (Tolic-Norrelykke and Wang 2005) showed that cell spreading and circularity were positively correlated with the degree of force exerted on the substrate by a cell. If the fibronectin cluster size was directly related to the force that a cell could exert on the substrate, then one would expect the cell spreading area to be positively correlated with the size of the fibronectin clusters. This is exactly the trend that was discovered in this chapter.

REFERENCES

Balaban, N. Q., U. S. Schwarz, et al. (2001). "Force and focal adhesion assembly: a close relationship studied using elastic micropatterned substrates." Nature Cell Biology **3**(5): 466-472.

Dalby, M. J., M. O. Riehle, et al. (2002). "In vitro reaction of endothelial cells to polymer demixed nanotopography." Biomaterials **23**(14): 2945-2954.

Dalby, M. J., M. O. Riehle, et al. (2004). "Changes in fibroblast morphology in response to nano-columns produced by colloidal lithography." Biomaterials **25**(23): 5415-5422.

Dalby, M. J., S. J. Yarwood, et al. (2002). "Increasing fibroblast response to materials using nanotopography: morphological and genetic measurements of cell response to 13-nm-high polymer demixed islands." Experimental Cell Research **276**(1): 1-9.

Ingber, D. E. (1990). "Fibronectin Controls Capillary Endothelial-Cell Growth by Modulating Cell-Shape." Proceedings of the National Academy of Sciences of the United States of America **87**(9): 3579-3583.

Kawa, A., M. Stahlhut, et al. (1998). "A simple procedure for morphometric analysis of processes and growth cones of neurons in culture using parameters derived from the contour and convex hull of the object." Journal of Neuroscience Methods **79**(1): 53-64.

Schwarz, U. S., N. Q. Balaban, et al. (2003). "Measurement of cellular forces at focal adhesions using elastic micro-patterned substrates." Materials Science & Engineering C-Biomimetic and Supramolecular Systems **23**(3): 387-394.

Tan, J. L., J. Tien, et al. (2003). "Cells lying on a bed of microneedles: An approach to isolate mechanical force." Proceedings of the National Academy of Sciences of the United States of America **100**(4): 1484-1489.

Tolic-Norrelykke, I. M. and N. Wang (2005). "Traction in smooth muscle cells varies with cell spreading." Journal of Biomechanics **38**(7): 1405-1412.

CHAPTER 8: ACTIN

8.1 OVERVIEW

Actin stress fibers are a core cytoskeletal component and play an important role in mechanotransduction of force mediated stimulus. This chapter investigates the actin structures of endothelial cells on various nanopatterned surfaces in order to better understand how limiting the maximum adhesion size and spacing affects the way ECs distribute their internal forces. In order to quantify observed changes in the actin cytoskeleton, image processing software was developed to analyze immunofluorescent images and extract information about the cytoskeletal structure. The major results from cytoskeletal analysis studies provide insight into EC behavior on the nanopatterns and how these observed changes relate to the findings presented in previous chapters.

8.2 EXPERIMENTAL METHODOLOGY

Silicon samples were prepared and functionalized according to the protocols presented in Chapter 5. Samples were immersed in ETOH (AAPER) for 5 minutes to sterilize the samples before being introduced into a sterile culture hood. Samples were then rinsed 60 seconds, three times in a HEPES buffered saline that was prepared from 11.9 g (HEPES)(Sigma), 5.8 g NaCl (Mallinkckrodt) and 1000 ml DI and adjusted to 7.5 pH with NaOH (Sigma). 125 μL of a 10 μg/ml fibronectin solution (Sigma) in 50 mM HEPES buffered saline was placed on the samples for 20 minutes at room temperature. The samples were then thoroughly rinsed in 50 ml of HEPES buffered saline solution for 60 seconds, 3 times to remove any excess fibronectin. The cells in all the studies were human umbilical vein endothelial cells (HUVECs) (Cambrex, Walkersville, MD) of

passage below 4 and cultured according to manufacturer's specifications. They were cultured in T-25 tissue culture flasks coated with 30 µg of human plasma fibronectin (Sigma, Saint Louis, MO) at 37ºC and 5% CO_2 until 80% confluence. During culture and experiment, the HUVECs were bathed in endothelial growth media (Cambrex, Walkersville, MD) supplemented with 2% fetal bovine serum, 0.5 ml human endothelial growth factor, 0.5 ml Hydrocortisome, 0.5 ml GA-1000 (Gentamicin, Amphotericin B). To release cells from flasks for cell seeding, the flasks were first rinsed with 5ml of HEPES buffered saline at 37ºC. They were then trypsinized using 3 ml of Trypsin/EDTA (Cambrex) for 5 minutes at 37ºC and 5% CO_2. Next, 3 ml of trypsin neutralizing solution (Cambrex) was added to the cell suspension to neutralize the Trypsin/EDTA. The cell suspension was pelleted using a centrifuge set to 240g for 6 minutes. The cells were then resuspended in 10 ml of endothelial growth media (Cambrex) discussed above. A hemocytometer and trypan blue dye was used to determine the total living cell population in the resuspension. The HUVECs were then seeded on the sample surface at approximately 7 cells/mm^2. The cells were maintained in 20 ml of endothelial growth media (Cambrex), 37˚C and 5% CO_2 for 24 hours. The cells were fixed by first immersing them in a cold cytoskeleton buffer (0.5% Triton X-100, 100 mM NaCl, 300 mM sucrose, 3 mM MgCl2, 10mM HEPES, pH 6.8) at 4ºC for 1 minute, then immersing them in 5% formaldehyde at 4ºC and then letting the solution warm up by placing in 37ºC water bath for 10 minutes. The surfaces were then rinsed with warm HEPES and covered with 125 µL of a 10% goat serum (Sigma) in PBS (Lonza) for 30 minutes at room temperature to block unspecific binding of antibodies. After rinsing with HEPES, the samples were then dressed with 125 µL PBS solution of a 6 µg/ml fibronectin antibody (Abcam) and 0.5 µg/ml TRITC-phalloidin (Sigma) in 1.0% BSA supplemented with 0.1% Tween-20 for 12 hours at 4ºC. Afterwards, the samples were washed with

rocking three times in PBS (Lonza) supplemented with 0.01 % Tween-20 for 5 minutes each wash to remove any unbound anti-bodies. Next, 125 µL of a 2.6 µg/ml goat anti-rabbit secondary antibody labeled with marina blue (Invitrogen - Alexa Fluor 365) was dispensed onto the sample and left for 1 hr at room temperature. The samples were washed with rocking three times in PBS (Lonza) supplemented with 0.01% Tween-20 for 5 minutes each wash to remove any unbound anti-bodies. Lastly, the samples were rinsed with DI H_2O to remove any salt residue and dried with nitrogen. Coverslips were mounted to the samples using gold antifade reagent (Invitrogen). Fluorescent images were acquired using an oil immersion Carl Zeiss ApoTome inverted microscope. Statistical analysis was carried out in MATLAB with a total sample size of 46 cross sections. Statistical hypothesis testing was performed to quantify the difference in sample means which were assumed to have unknown and possibly unequal variances.

8.3.1 PROGRAM AND ALGORITHM

Image pre-processing of the immunofluorescent actin images was performed using ImageJ (NIH, Bethesda, MD). The post-processed images were then analyzed using a custom program written in Matlab. The core of the program includes several intuitive graphical user interfaces (GUIs) that allows the user to perform quantitative analysis on the images, while compensating for different objectives and magnifications (Figure 8.3.1). The key features of the quantitative algorithms are to be able to correctly identify actin fibers in the images of the cell, determine the outside edges of the cell and be able to correctly measure the width of the actin fiber. Identification of these three features allows the program to calculate:

1. Cross sectional length of the cell;
2. Number of fibers per cross sectional length;

3. Density of fibers per unit length;
4. Average fiber diameter in a cross section;
5. Distribution of actin fiber diameters; and
6. Percentage of actin relative to the cross section length.

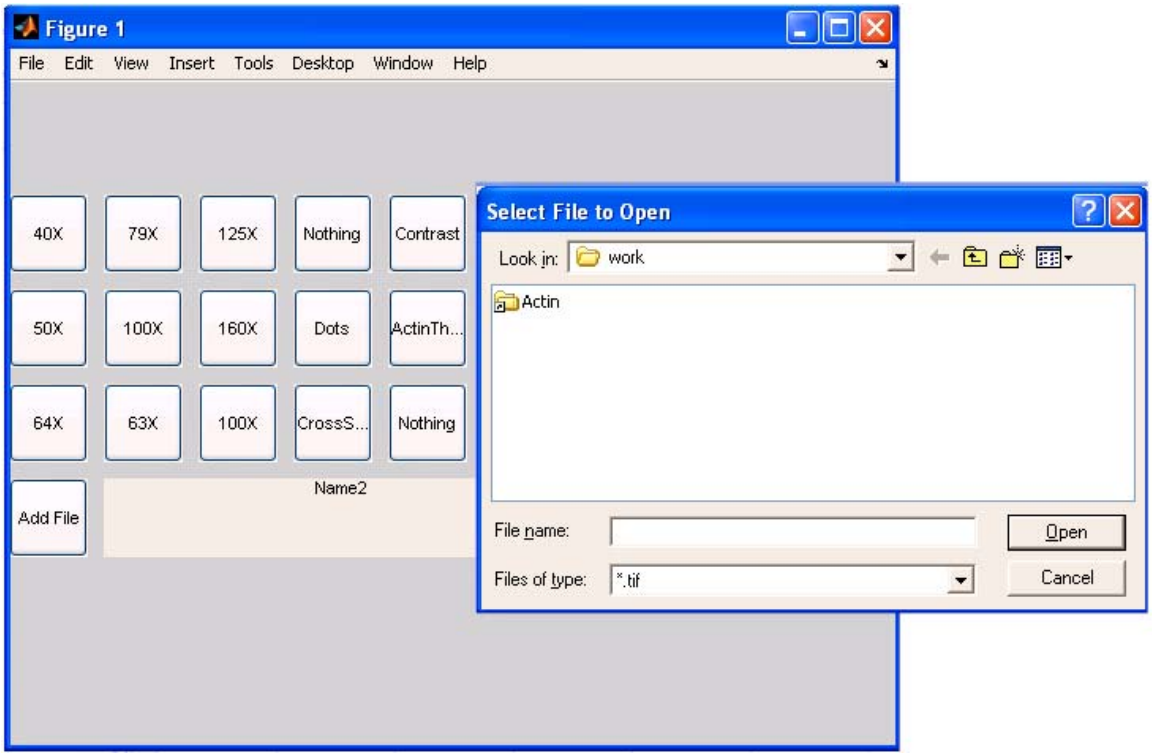

Figure 8.3.1: The main graphical user interface for actin analysis.

Using the graphical interface, a user can easily select an image to be processed through a standard windowed interface. The user can then select a cross section of the cell that is of interest. For the purpose of data analysis in this work, the portion of interest was defined as the portion of the cell with the maximum number of actin fibers. This was selected because it accurately represented a commonality between the entire population of sampled cells (Figure 8.3.2).

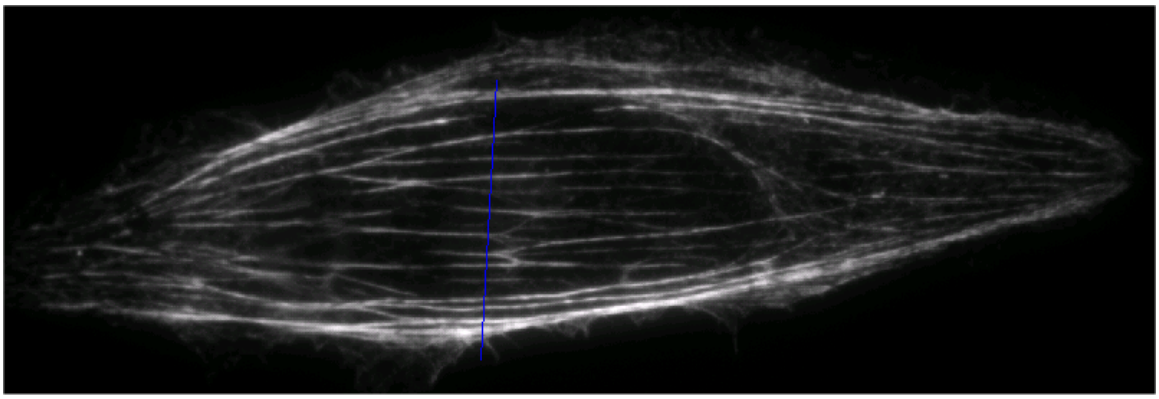

Figure 8.3.2: The user can select a desired cross section of the cell to analyze. The portion of interest in this work was parallel to the area of highest fiber density.

8.3.2 ACTIN FIBER DETECTION ALGORITHM

From the selected cross section, the program generates a matrix that represents the position and intensity value along the portion of the line. This matrix is analyzed using a peak fitting routine, which fits gausians to each of the detected peaks (Figure 8.3.3). The peak fitting routine uses several filters in order to correctly identify between a true fiber and background noise. The first set of filters is the intensity threshold filter. It sets a limit of the minimum height that a peak must be in order to be considered a fiber. To have consistency through all cells analyzed, only well-developed stress fibers that were clearly well above the background noise signal were counted. This prevented introducing errors in the data by excluding any signals that could not clearly be identified as a stress fiber. Next, the algorithm uses a width feature that specifies the minimum width of a detected peak. This sets a lower bound on the fitted peaks to prevent false identification of noise or multipeak assignment to a single fiber. The program also uses a triangular smoothing routine of 2 pixels to remove any roughness in the profiled line. The peak fit

routine returns the positions of the actin fibers along a cross section line (Figure 8.3.3). This allows the program to calculate the edge-to-edge width of the cell, average number of fibers contained in the cross section and the density of fibers per unit length.

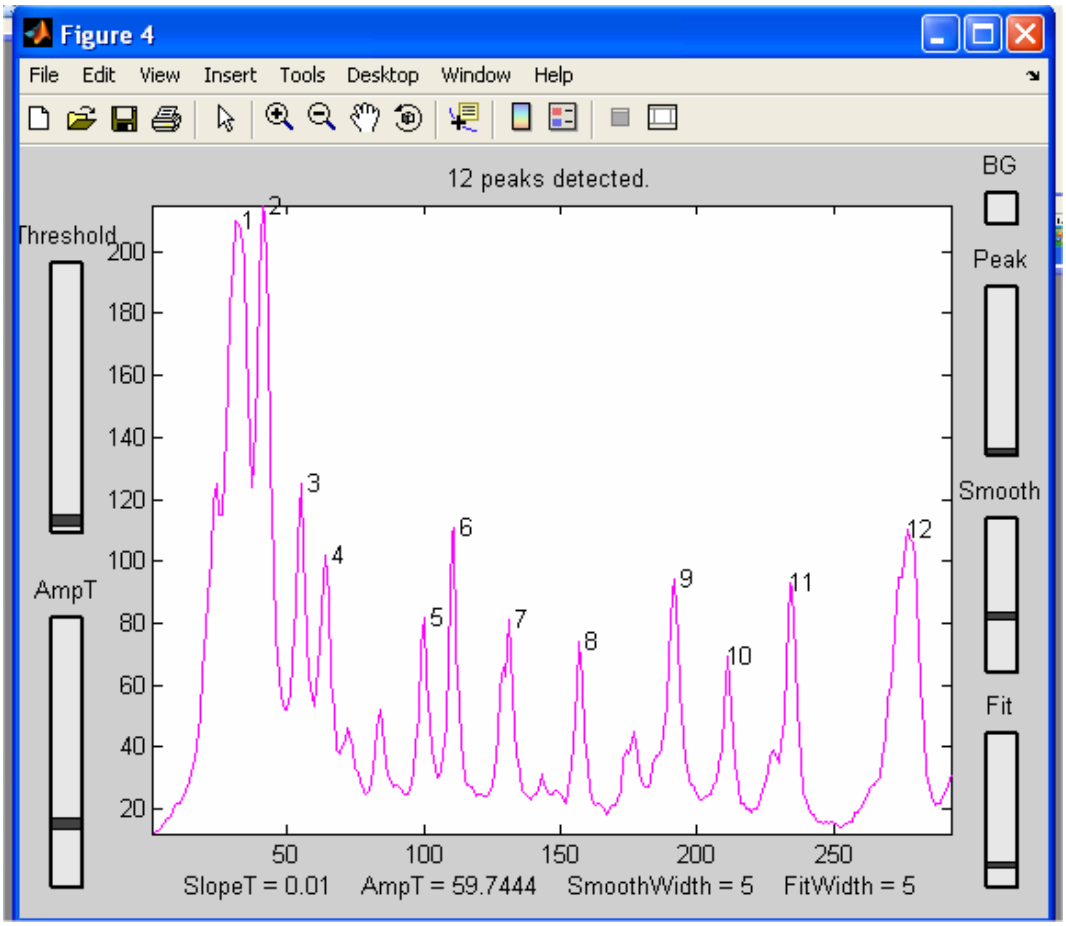

Figure 8.3.2: Interactive actin fiber detection engine. The engine uses a peak fitting algorithm that takes into account peak amplitude and width in detecting position and number of fibers. To have consistency across all cells analyzed, only well-developed stress fibers that were clearly well above the background noise were counted.

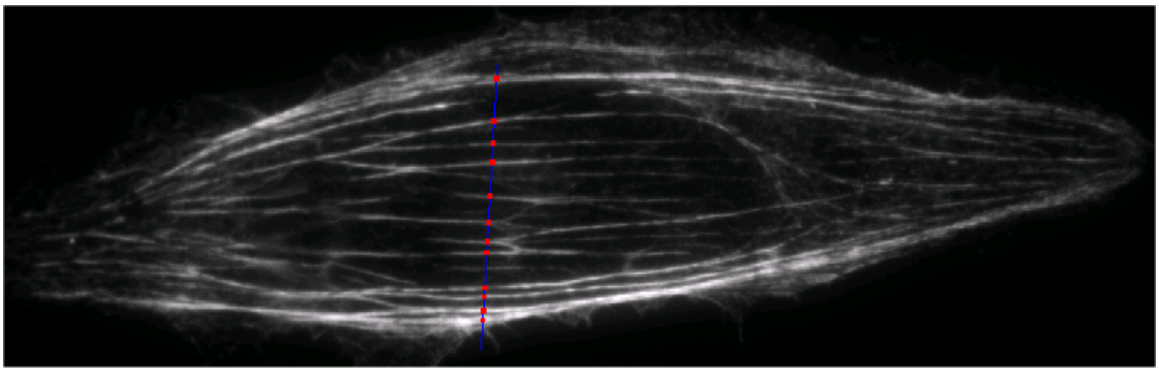

Figure 8.3.3: Graphical output of peak detection algorithm showing the peaks and positions that were detected.

8.3.3 ACTIN THRESHOLD

The second algorithm embedded in the program detects pixels that are actin versus pixels that are background. It uses a threshold on the intensity profile to identify regions along the cross section that are actin pixels (Figure 8.3.4). The intensity threshold is defined as a line that is slightly below the apex of the smallest peak detected in the actin fiber identification algorithm in Section 8.3.2. This information is then referenced with the actin fiber position data to calculate the width of each individual fiber. This allows the program to calculate average fiber diameter, distribution of actin fiber diameters and percentage of actin over the cross sectional length.

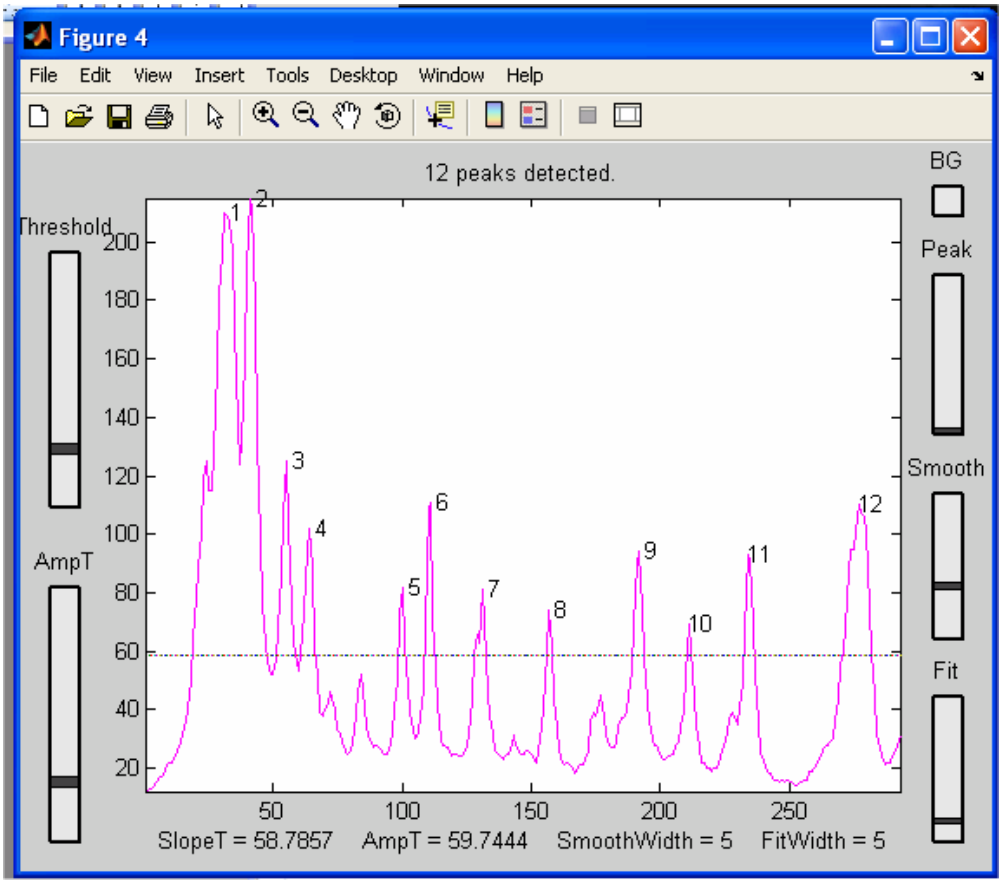

Figure 8.3.4: Interactive actin fiber detection engine. A slider labeled threshold is used as an input to an actin pixel detection algorithm, which determines the pixels that are actin versus the pixels that are background.

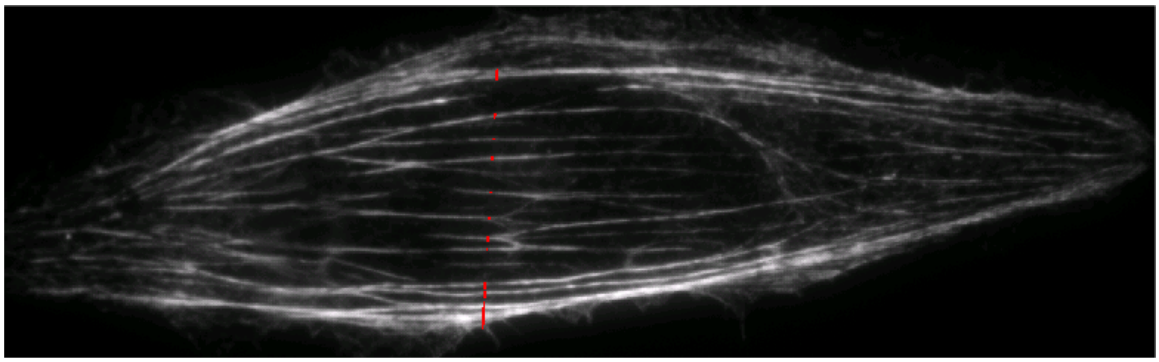

Figure 8.3.5: Graphical output of actin width detection algorithm showing the actin cross sections highlighted.

8.4.1 ACTIN ANALYSIS

In Chapter 6, it was shown that focal adhesion size was directly constrained by the diameter of the underlying fibronectin cluster. It was also noted that focal adhesion size has been directly correlated with the amount of force transduced through the adhesion. This section will investigate the relationship between actin stress fiber formation and the adhesion cluster size, while keeping the total number of ligands available for binding constant for all patterns. In particular, it will investigate the adhesion cluster diameters of 150 nm, 200 nm, 250 nm and 300 nm at a constant macroscopic fibronectin density coverage of 8.7%.

8.4.2 CROSS SECTIONAL ANALYSIS

A cross sectional analysis was performed to determine if there was a correlation between pattern size and the absolute cross sectional distance. Cross sections were selected that were perpendicular to the main axis of actin fiber orientation. From the data in Figure 8.4.1, there is an increasing trend between the average cell cross section distance and pattern size. These results are consistent with the findings from Chapter 7, where it was found that the average cell size was generally larger on patterns with a greater post sizes. Additionally, in Chapter 7, it was also shown that cells on larger post sizes also displayed a greater tendency to have a circular shape. These two combined effects are also seen in the cross section data below.

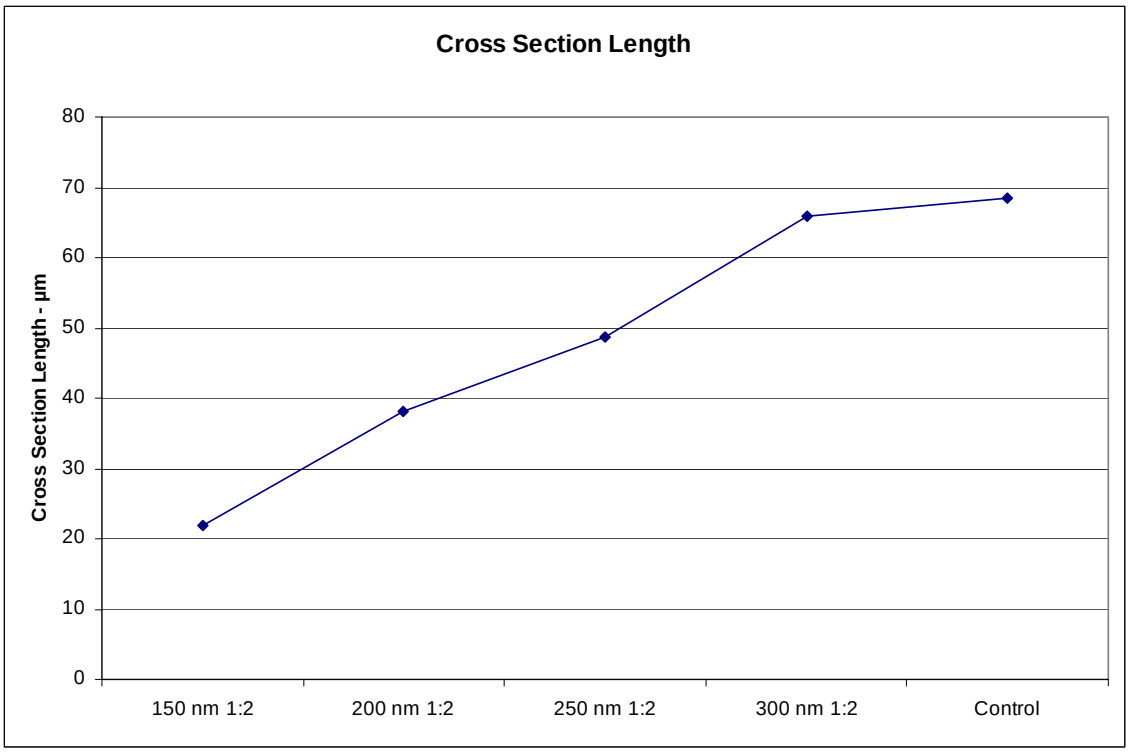

Figure 8.4.1: Under conditions of constant macroscopic protein density, as the maximum adhesion cluster size was increased, the average cross sectional length of the cell increased.

8.4.3 ABSOLUTE NUMBER OF FIBERS

It was observed that cells on all tested nanopatterns on average formed less stress fibers than cells on control patterns. Additionally, it was found that the number of actin stress fibers depended on the size of the adhesive post independent of the macroscopic surface density of fibronectin. This indicates that by limiting the maximum size of the focal adhesions, not the average macroscopic surface density of proteins, the internal stress fiber organization could be dramatically altered. Cells with less stress fibers are generally thought of as exerting less force on their surroundings.

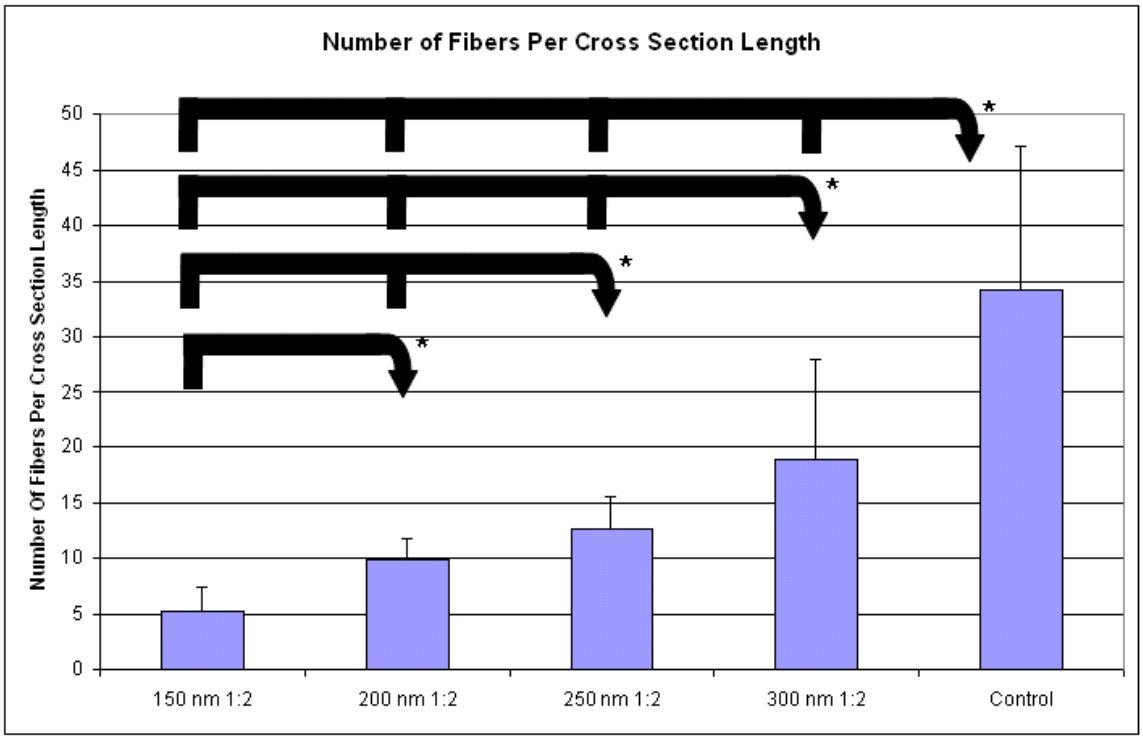

Figure 8.4.2: Under conditions of constant macroscopic protein density, as the maximum adhesion cluster size was increased from 150 nm, the average number of fibers increased. With $p < 0.05$, 150 nm < 200 nm < 250 nm < 300 nm < Control. (150 nm n=11, 200 nm n=9, 250 nm n=6, 300 nm n=10).

8.4.4 Fiber Density as a Function of Pattern Size

Given that the cross sectional areas and number of fibers were lower on smaller patterns, it opened the possibility that the number of fibers was scaling with the cross sectional area. If this was true, one would observe a constant fiber density across all patterns. Fiber density was defined as the cross section length divided by the total number of fibers in that cross section. Figure 8.4.3 shows that cells on the nanopatterned surfaces showed a significant difference in the fiber density as compared to controls. The influence on pattern size was not as strong as the absolute number of fibers presented in

Figure 8.4.2. Absolute fiber density turns out to be a good measure for control cells, which typically have a uniform distribution of actin fibers through the cell. However, for cells on the nanopatterned surfaces, it is a bad measure for several reasons. First, the density equation assumes that all of the actin fibers are uniformly distributed in the cell. Cells on the nanopatterns generally do not have a uniform distribution of fibers. They typically have large peripheral bands with a few neighboring fibers and then a large gap between the peripheral bands which no fibers are located. Secondly, the density equation assumes that all the fibers are of the same size. This was observed to be incorrect for cells on the nanopatterned surfaces. The average fiber diameter appeared to be a function of the pattern size, where larger fibers were typically observed on larger patterns. For these two reasons, the average density measure did not accurately capture the differences of the cells on the nanopatterned surface.

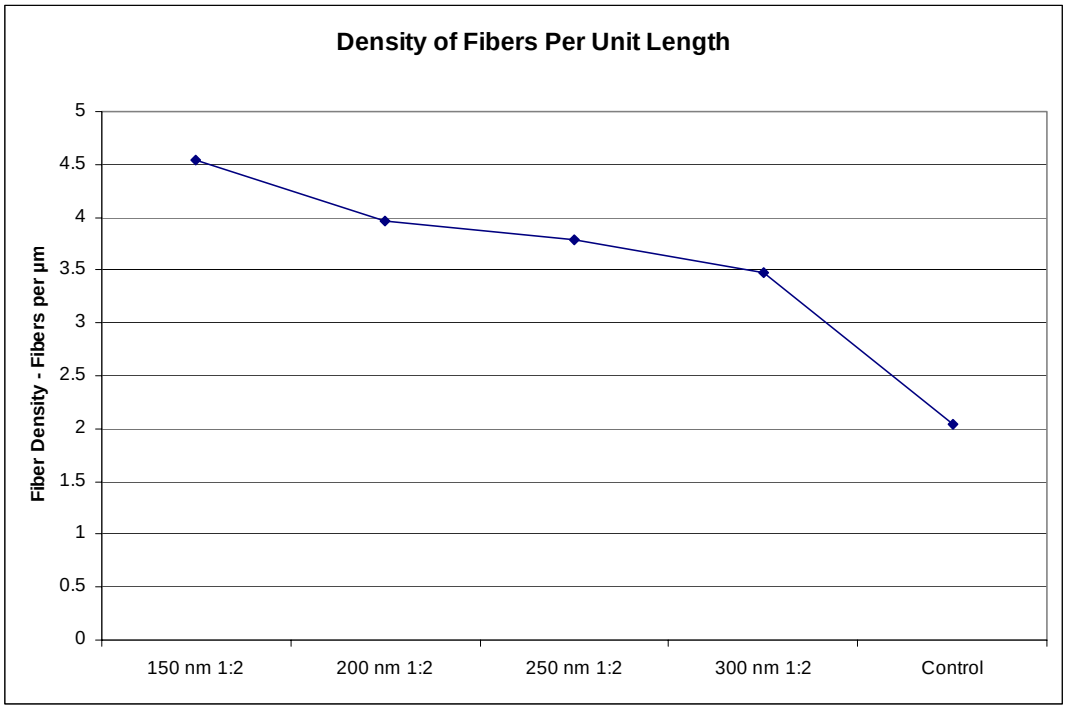

Figure 8.4.3: Under conditions of constant macroscopic protein density, as the maximum adhesion cluster size was increased from 150 nm, the average density of fibers decreased.

8.4.5 PERCENTAGE ACTIN PER CROSS SECTION

As a solution to the average density problems discussed above in Section 8.4.4, a measure that was based on the average percentage of actin per cross section was devised. This measure simply calculated the total number of pixels that were actin and divided that number by the total number of pixels in the cross section. This allowed for a density measure that captured both the differences in actin fiber width and the variance in spatial distribution of the fibers. Figure 8.4.4 shows that the percentage of actin per cross section was dependent on pattern size. Not only did the cells on the smaller patterns form less stress fibers, they also formed smaller fibers in less dense amounts than cells on larger patterns.

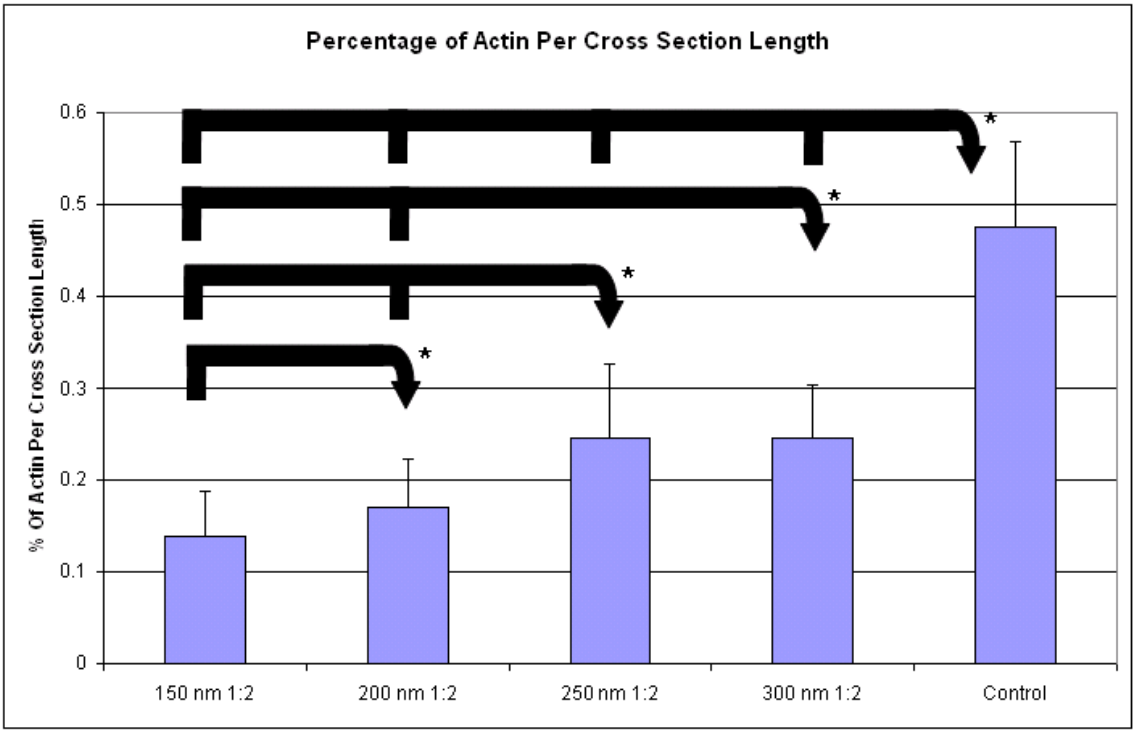

Figure 8.4.4: Under conditions of constant macroscopic protein density, as the maximum adhesion cluster size was increased from 15 0nm, the percentage of actin per cross section increased. All patterns are statistically different, with $p < 0.05$, (150 nm n=11, 200 nm n=9, 250 nm n=6, 300 nm n=10).

8.5 DISCUSSION

Actin stress fibers are an important cytoskeletal component in creating and distributing intracellular forces and are an important mechano-sensing element. Intracellular forces in general have been shown to play an important role in intracellular signal transduction (Shyy and Chien 1997), motility (Pelham and Wang 1997), cytokinesis (Huang and Ingber 1999), apoptosis (Grinnell, Zhu et al. 1999) and ECM remodeling (Harris, Stopak et al. 1981; Zhong, Chrzanowska-Wodnicka et al. 1998). Mechanical force transduced through the actin cytoskeleton has long-range effects and has been shown to propagate to the nucleus and result in conformational changes of a single chromosome (Holth, Chadee et al. 1998). Additionally, the actin cytoskeleton is a dynamic structure which adjusts due mechanical stimulation. This can be seen when endothelial cells remodel their actin cytoskeleton under fluid shear stress conditions to align fibers in the direction of flow, and also on elastic substrates under deformation, they align fibers in the direction of minimal (Wang, Goldschmidt-Clermont et al. 2001; Costa, Hucker et al. 2002; Huen, Park et al. 2002). The actin cytoskeleton of endothelial cells is of clinical interest because its disruption is known to play a role in vascular disease (Lee and Gotlieb 2003).

The ends of actin fibers terminate at focal adhesions, which are known to be a center for mechano-force transduction. The role between actin and the integrins that comprise of a focal adhesion are very co-dependent, and their relationship was succinctly described by Brakebusch and Fassler in the title of their article, “The integrin-actin connection, an eternal love affair” (Brakebusch and Fassler 2003). The results presented in this section directly relate to the way a cell is able to organize its internal and external force. Cytoskeletal reorganization and growth in general depend on signaling from the focal adhesions. Following integrin activation, signaling cascades are activated that

regulate the formation, linkage and disassembly of actin fibers. Pathways of particular importance are those regulated by FAK and SRC-like kinases and the Rho family of GTPases (Schaller 2001; Arthur, Noren et al. 2002).

Because of the importance of focal adhesions in regulating the actin cytoskeleton, an interesting question to ask is whether a minimum size of a focal adhesion must be in order to form a highly fibrous cytoskeleton network as seen on controls. Alternatively, if a population of cells is exposed to an identical number of fibronectin binding sites per unit area on a macro scale, is there a lower limit on fibronectin cluster adhesion size where changes in the cytoskeletal network will occur? The quantitative results in this section indicate that limiting the maximum focal adhesions size while holding the macroscopic density of fibronectin constant does influence cytoskeletal formation. As the maximum focal adhesion size were more restricted, fewer and thinner fibers were formed. The thin fibers could then go on to form thicker structures, such as the peripheral band, so the maximum fiber diameter was not dictated by the focal adhesion size. However, at the smallest cluster sizes, there were very few fibers, and the actin that was present was located mainly in the peripheral band. This is interesting because it has been reported that the size of a focal adhesion is directly proportional to the internal cytoskeletal force applied (Choquet, Felsenfeld et al. 1997; Balaban, Schwarz et al. 2001). The results from this section suggest the converse: restricting the size of adhesion may directly restrict the possible force a cell can exert through an adhesion.

In comparing these results to those found on elastic substrates, it was found that actin stress fibers were not visible for gels softer than 1,600Pa (Yeung, Georges et al. 2005). As the elastic modulus of the gel was increased, the cells began to show a greater number of stress fibers. The elastic modulus has been shown in other experiments to be related to the force that a cell can exert on the substrate (Engler, Bacakova et al. 2004;

Discher, Janmey et al. 2005). For soft materials, the force is less than stiff materials. The results on the smaller adhesion clusters resemble the results on soft gels, and as the adhesion cluster diameters are increased, they resemble the results on stiffer gels. This provides additional evidence that the diameter of adhesive cluster may be influencing the force that can be developed by the cell on the substrate.

The number of actin fibers in a cell directly relates to the force that the cell is exerting on its surroundings. The fact that fewer numbers of stress fibers, which were typically thinner, were observed on smaller patterns indicates that these cells were exerting less force on their surroundings. Another viewpoint is that by limiting the maximum size of the focal adhesion, this limited the size of the terminating actin fiber that could be formed. Additionally, this may have also inhibited the assembly of larger stress fibers that are typically composed of smaller terminating actin fibers. Additionally, it has also been shown that actin fiber formation is also a force dependent process. As the cell increases force on the substrate, it begins to assemble more stress fibers in a process governed by positive feedback. If the maximum force the cell can exert on the substrate is limited, the amount of stress fibers will correspondingly be less. It is a reasonable assumption that the limitation of focal adhesion size is inhibiting a feedback loop or signaling pathway that was preventing the cell from assembling many large stress fibers.

Of the main integrin signaling pathways, FAK is known to play a key role in the regulation of actin cytoskeleton assembly and disassembly. It is possible that the focal adhesion size limitation is inhibiting adhesion maturation and FAK signaling, causing decreased actin cytoskeletal formation. It has been shown previously that cells lacking the FAK-family kinsase activity are not able to arrange their actin fibers into parallel bundles (Ilic, Kovacic et al. 2004). The immunofluorescent images from this study had similar cytoskeletal structure to those found on small nanopatterned surfaces. Future

studies should investigate FAK knockout cells on nanopatterns to explore the influence of FAK.

REFERENCES

Arthur, W. T., N. K. Noren, et al. (2002). "Regulation of Rho family GTPases by cell-cell and cell-matrix adhesion." Biological Research **35**(2): 239-246.

Balaban, N. Q., U. S. Schwarz, et al. (2001). "Force and focal adhesion assembly: a close relationship studied using elastic micropatterned substrates." Nature Cell Biology **3**(5): 466-472.

Brakebusch, C. and R. Fassler (2003). "The integrin-actin connection, an eternal love affair." Embo Journal **22**(10): 2324-2333.

Choquet, D., D. P. Felsenfeld, et al. (1997). "Extracellular matrix rigidity causes strengthening of integrin-cytoskeleton linkages." Cell **88**(1): 39-48.

Costa, K. D., W. J. Hucker, et al. (2002). "Buckling of actin stress fibers: A new wrinkle in the cytoskeletal tapestry." Cell Motility and the Cytoskeleton **52**(4): 266-274.

Discher, D. E., P. Janmey, et al. (2005). "Tissue cells feel and respond to the stiffness of their substrate." Science **310**(5751): 1139-1143.

Engler, A., L. Bacakova, et al. (2004). "Substrate compliance versus ligand density in cell on gel responses." Biophysical Journal **86**(1): 617-628.

Grinnell, F., M. F. Zhu, et al. (1999). "Release of mechanical tension triggers apoptosis of human fibroblasts in a model of regressing granulation tissue." Experimental Cell Research **248**(2): 608-619.

Harris, A. K., D. Stopak, et al. (1981). "Fibroblast Traction as a Mechanism for Collagen Morphogenesis." Nature **290**(5803): 249-251.

Holth, L. T., D. N. Chadee, et al. (1998). "Chromatin, nuclear matrix and the cytoskeleton: Role of cell structure in neoplastic transformation (Review)." International Journal of Oncology **13**(4): 827-837.

Huang, S. and D. E. Ingber (1999). "The structural and mechanical complexity of cell-growth control." Nature Cell Biology **1**(5): E131-E138.

Huen, A. C., J. K. Park, et al. (2002). "Intermediate filament-membrane attachments function synergistically with actin-dependent contacts to regulate intercellular adhesive strength." J. Cell Biol. **159**(6): 1005-1017.

Ilic, D., B. Kovacic, et al. (2004). "FAK promotes organization of fibronectin matrix and fibrillar adhesions." Journal of Cell Science **117**(2): 177-187.

Lee, T. Y. J. and A. I. Gotlieb (2003). "Microfilaments and Microtubules maintain endothelial integrity." Microscopy Research and Technique **60**(1): 115-125.

Pelham, R. J. and Y. L. Wang (1997). "Cell locomotion and focal adhesions are regulated by substrate flexibility." Proceedings of the National Academy of Sciences of the United States of America **94**(25): 13661-13665.

Schaller, M. D. (2001). "Biochemical signals and biological responses elicited by the focal adhesion kinase." Biochimica Et Biophysica Acta-Molecular Cell Research **1540**(1): 1-21.

Shyy, J. Y. J. and S. Chien (1997). "Role of integrins in cellular responses to mechanical stress and adhesion." Current Opinion in Cell Biology **9**(5): 707-713.

Wang, J. H. C., P. Goldschmidt-Clermont, et al. (2001). "Specificity of endothelial cell reorientation in response to cyclic mechanical stretching." Journal of Biomechanics **34**(12): 1563-1572.

Yeung, T., P. C. Georges, et al. (2005). "Effects of substrate stiffness on cell morphology, cytoskeletal structure, and adhesion." Cell Motility and the Cytoskeleton **60**(1): 24-34.

Zhong, C. L., M. Chrzanowska-Wodnicka, et al. (1998). "Rho-mediated contractility exposes a cryptic site in fibronectin and induces fibronectin matrix assembly." Journal of Cell Biology **141**(2): 539-551.

CHAPTER 9: PROLIFERATION

9.1 OVERVIEW

Proliferation is a tightly regulated process that receives inputs from environmental factors, such as growth factors, cell-to-cell contacts and adhesions to the ECM. Focal adhesions are thought to be involved in translating mechanical stress into proliferative signals in conjunction with growth factors. This section investigates the role of focal adhesion size and spacing on proliferation.

9.2 METHODOLOGY

Silicon samples were prepared and functionalized according to the protocols presented in Chapter 5. Samples were immersed in ETOH (AAPER) for 5 minutes to sterilize the samples before being introduced into a sterile culture hood. Samples were then rinsed 60 seconds, three times in a HEPES buffered saline that was prepared from 11.9 g (HEPES)(Sigma), 5.8 g NaCl (Mallinkckrodt) and 1000 ml DI and adjusted to 7.5 pH with NaOH (Sigma). The nanopatterns were coated with 125 μL of a 10 μg/ml fibronectin solution (Sigma) in 50 mM HEPES buffered saline for 20 minutes at room temperature. Controls were coated with either a 2 μg/ml, 10 μg/ml, or 25 μg/ml fibronectin solution (Sigma) in 50 mM HEPES buffered saline for 20 minutes at room temperature. The controls were then blocked with 1.0 % BSA solution in HEPES buffered saline for 20 minutes to minimize serum proteins from adsorbing to the gold surface. The samples were then thoroughly rinsed in 50 ml of HEPES buffered saline solution for 60 seconds, 3 times to remove any excess fibronectin. The cells in all the studies were human umbilical vein endothelial cells (HUVECs) (Cambrex, Walkersville,

MD) of passage below 4 and cultured according to manufacturer's specifications. They were cultured in T-25 tissue culture flasks coated with 30 μg of human plasma fibronectin (Sigma, Saint Louis, MO) at 37ºC and 5% CO_2 until 80% confluence. During culture and experiment, the HUVECs were bathed in endothelial growth media (Cambrex, Walkersville, MD) supplemented with 2% fetal bovine serum, 0.5 ml human endothelial growth factor, 0.5 ml Hydrocortisome, 0.5 ml GA-1000 (Gentamicin, Amphotericin B). To release cells from flasks for cell seeding, the flasks were first rinsed with 5 ml of HEPES buffered saline at 37 ºC. They were then trypsinized using 3 ml of Trypsin/EDTA (Cambrex) for 5 minutes at 37 ºC and 5% CO_2. Next, 3 ml of trypsin neutralizing solution (Cambrex) was added to the cell suspension to neutralize the Trypsin/EDTA. The cell suspension was pelleted using a centrifuge set to 240 g for 6 minutes. The cells were then resuspended in 10 ml of endothelial growth media (Cambrex) discussed above. A hemocytometer and trypan blue dye was used to determine the total living cell population in the resuspension. The HUVECs were then seeded on the sample surface at approximately 7 cells/mm^2. The cells were maintained in 20 ml of endothelial growth media (Cambrex), 37 ˚C and 5% CO_2 and the media was exchanged after 24 hours. Cell counts were taken using a manual hand counter at 4 hrs, 24 hrs, 48 hrs and 72 hrs after seeding. For the purpose of graphing the raw data, the cell populations were normalized to a starting density of ten by dividing each time point by the density recorded at 4 hrs then multiplying by ten.

9.3 ALGORITHM DESIGN

A unique feature of the design of the nanopatterned surface is that it corrals cells for a particular pattern into a 1 mm x 1 mm box. Each box is uniquely marked for identification so that one can easily photograph the same population of cells over an

extended period of time. This results in more accurate measurements, as population changes can be directly tracked without introducing errors from average population behavior. It was assumed that a population of cells grew exponentially and they could be expressed by a doubling rate, as shown in Equation 9.3.1, where the time to double is described by the variable t_d.

$$population(t) = population_{t=0} \cdot 2^{t/t_d}$$

Equation 9.3.1: Population doubling growth rate equation. Time in hours is denoted by t and the doubling rate by t_d.

It was desired to have a population growth rate for each experiment. One possible way to do this would be using a ratio measurement that takes the ratio between two observations, for instance, 24 hours and 48 hours. This provides a linear approximation of the exponential growth rate, and assuming that the interval between observations is small enough, it provides a reasonable approximation. However, it is very sensitive to any deviations in the datapoints that may not exactly lay on the true but unknown curve. It also neglects information in the experiment contained at 0 hours and 72 hours. However to overcome this, the ratios between 0 hrs – 24 hrs, 24 hrs – 48 hrs and 48hrs – 72 hrs could be averaged to obtain an average growth rate value. Another method is to approximate the growth rate for a single experiment by minimizing the sum of the squares for all of the data points using an exponential equation. This would provide an average over all of the points for a single experiment and minimize the impact of an outlier. Since the cells are known to grow in an exponential fashion, a value for t_d was obtained by minimizing the sum of the squares for Equation 9.3.1. This method provides an average growth rate that is a better approximation to the true but unknown curve than a ratio based approximation. Hypothesis testing was used for both methods to determine the probability that the average growth values between patterns are different. Both

methods will have some variances associated with the measurements due to the fact that the cell cycles are not synchronized.

A Matlab program was written that would compute t_d by minimizing the sum of squares of the data for a given experiment. Hypothesis testing was performed using a two-sample t-test, where the mean of a given set of growth rates was assumed to be greater than the mean of another set of growth rates. Probabilities, or p-values, that were less than 0.05 were assumed to be statistically significant. Both the exponential fit method and ratio method produced identical conclusions in regards to statistical significance.

9.4 GOLD FIBRONECTIN CONTROL

Data for the controls was obtained in collaboration with John Slater from the Frey Lab. Glass slides were uniformly coated with Au and prepared identically to the nanopatterned surfaces. To investigate density dependence on proliferation, fibronectin was applied in quantities of 5 μg/ml, 10 μg/ml, 25 μg/ml and 50 μg/ml, prepared as described in (Slater and Frey 2007). The population data were fit according to Equation 9.3.1, and the fit lines are displayed in Figure 9.4.1. The populations were normalized to a value of 10 cells per mm^2 at time 0 hrs, which reflects the seeding density as given by a hemocytometer at the time of seeding. The average growth rate that was observed between the three concentrations was 0.9888 doublings per day. There was no statistical significant difference between any of the control patterns at this range of protein density concentrations. However, John Slater has shown that at very low concentrations, 2 μg/ml, proliferation is nearly eliminated (Slater and Frey 2007).

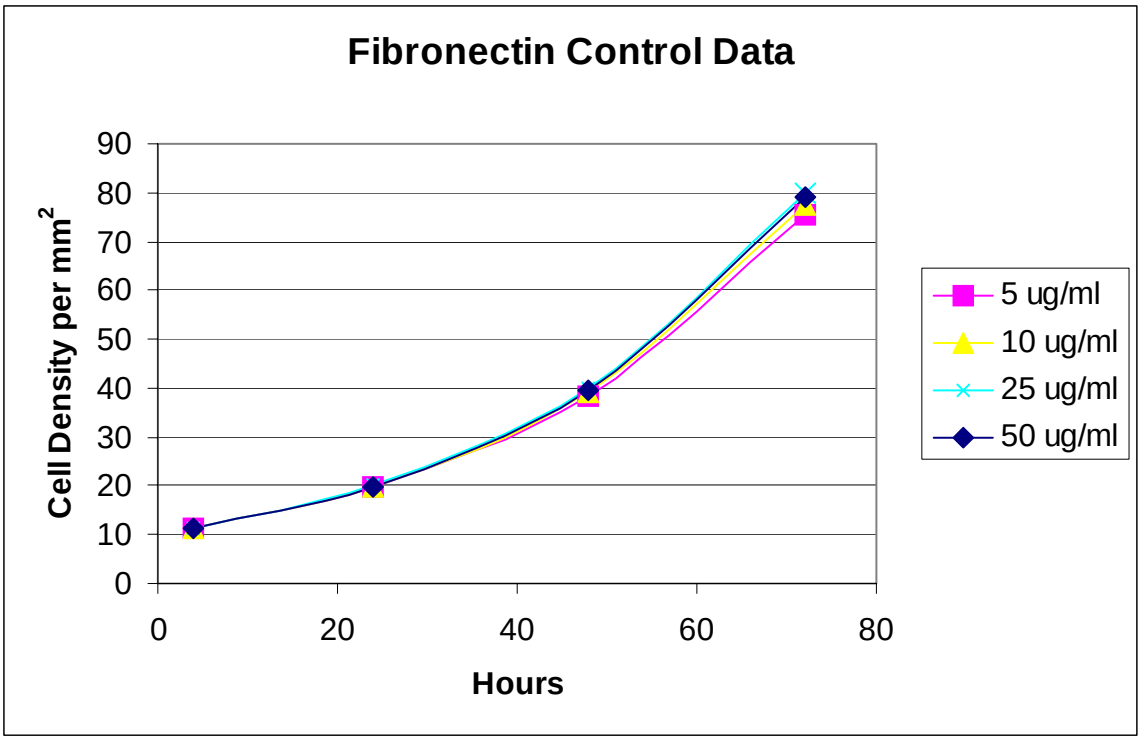

Figure 9.4.1: Fit lines for the population data for the four different fibronectin concentrations fit according to Equation 9.3.1. The populations were normalized to a value of 10 cells per mm^2 at time 0 hrs, which reflects the seeding density as given by a hemocytometer at the time of seeding. The points on the graph indicate the fit points corresponding to the observation times. The average growth rate that was observed between the three concentrations was 0.9888 doublings per day. No systematic differences were found at this range of concentrations. n=80 observations for each fibronectin concentration.

9.5 Serum Starved Cells

As part of an investigation to reduce the proliferation rate of cultured HUVECs for other experiments where low populations of cells were needed for 72 hours, cells were cultured on standard glass slides with modifications to the media. Fibronectin was uniformly applied to glass slides in the concentration of 10 ug/ml and the cells were

seeded according to the protocol outlined above. It must be noted that this experiment was performed on glass slides without gold and was not subjected to the standard surface chemistry process. Although this experiment was not intended to provide control data for this chapter, and should be treated as such, it does provide insight into the influence of soluble factors on proliferation. The three media constituents that were adjusted were human endothelial growth factor (hEGF), bovine brain extract (BBE) and fetal bovine serum (FBS). They were removed in different percentages according to Table 9.5.1.

	hEGF	*BBE*	*FBS*
Control	100%	100%	100%
Sample 1	50%	100%	100%
Sample 2	0%	100%	100%
Sample 3	50%	50%	50%
Sample 4	0%	50%	50%
Sample 5	25%	25%	25%
Sample 6	50%	50%	25%

Table 9.5.1: Six media concentrations were prepared using various percentages of human endothelial growth factor, bovine brain extract and fetal bovine serum.

After seeding, the cells were counted at 4 hrs, 12 hrs, 24 hrs, 36 hrs, 48 hrs, 60 hrs, 72 hrs and fitted to Equation 9.3.1. The results of the analysis are presented below in Figure 9.5.1.

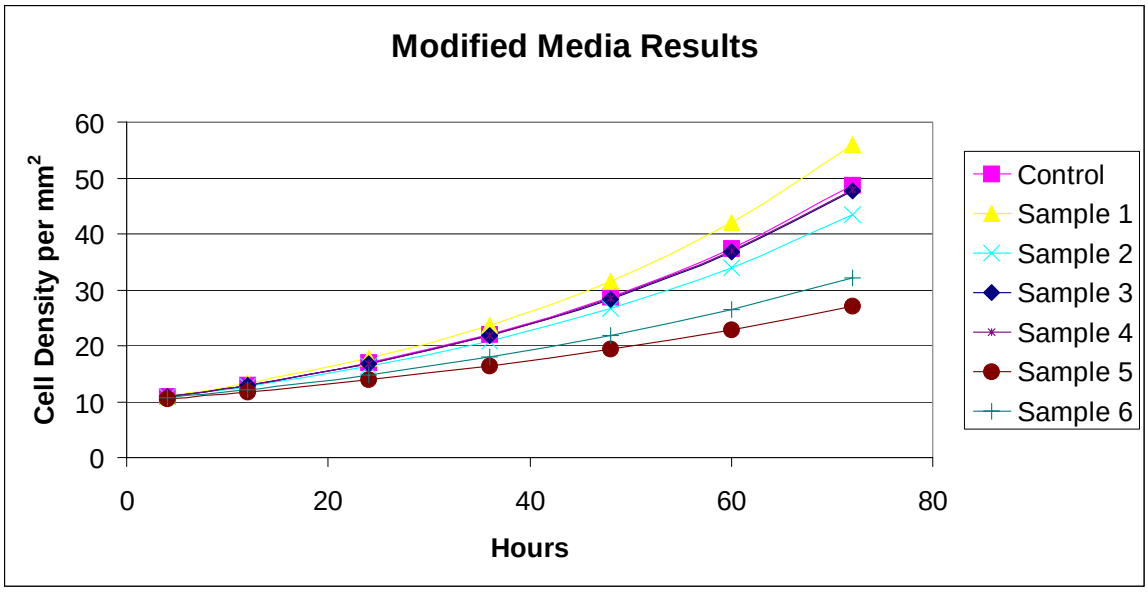

Figure 9.5.1: Results from removing various constituents from media and observing the changes in proliferation. The figure shows fit lines for each of the samples, that were fit according to Equation 9.3.1, with fitted points representing the times of the observations. The populations were normalized to a value of 10 cells per mm^2 at time 0 hrs, which reflects the seeding density as given by a hemocytometer at the time of seeding. Fetal bovine serum was found to have the most impact on proliferation rates followed by bovine brain extract. n=140 observations for each sample.

The results from this study indicate that the percentage of fetal bovine serum concentration had the largest impact on proliferation followed by bovine brain extract. Decreasing the fetal bovine serum concentration by 75% of the original concentration resulted in a decrease in the proliferation rate by approximately 30%.

9.6.1 NANOPATTERNED RESULTS

The following section will review the impact on proliferation rates by varying the diameter of the adhesion clusters, the spacing between adhesion clusters and the overall macroscopic density. In particular, adhesion cluster size will be probed independently of

adhesion cluster spacing and macroscopic density to isolate the influence due to the clustering of integrins.

9.6.2 PROLIFERATION AS A FUNCTION OF PATTERN SIZE WITH CONSTANT MACROSCOPIC DENSITY

As was demonstrated in Chapter 8, actin cytoskeletal changes were observed by simply changing the diameter of adhesive clusters while holding the macroscopic protein density constant at 8.72%. Additionally, constant macroscopic density experiments in Chapter 7 found that the spreading area and circularity increased as the diameter of the fibronectin clusters were increased from 150 nm to 300 nm. A similar experiment was conducted to investigate the effects on cellular proliferation using the same set of patterns. We were interested if proliferation also showed changes when the macroscopic density of the fibronectin clusters was held constant but the diameter of the fibronectin clusters was varied. Cells were seeded and observed at 0 hrs, 24 hrs, 48 hrs and 72 hrs according to the protocol outlined in Section 9.2. The results from this experiment indicated that with a constant macroscopic density of 8.72%, that restricting the size of the focal adhesion did affect the proliferation rates of HUVECs (Figure 9.6.1). The growth rates for the diameters of 300 nm, 250 nm and 200 nm were statistically lower than the growth rates observed on the control patterns. However, the growth rates for cells seeded on the 150 nm diameter patterns had a growth rate similar to that of controls (Table 9.6.1). There is also an observable trend across the different diameters of fibronectin clusters. As the diameter of the fibronectin clusters were increased, the proliferation rates on the nanopatterned surfaces decreased. This is particularly interesting because it leaves a large difference between the 300 nm diameter fibronectin cluster and the control. It seems reasonable to believe that if the cluster diameter was

increased larger than 300 nm, proliferation, at some point, would begin to increase to match controls. Thus, there may be a transition region that is associated with limiting the size of a focal adhesion. Another interesting point about the data is the seeming transition in proliferation between 250 nm and 200 nm. The p-value of this step was marginally statistically significant with a p-value of 0.068. However, the growth rates between the 300 nm and 250 nm diameter clusters are very similar in comparison to growth rate of the 200 nm cluster. This same type of transition was observed in Chapter 8 for the actin cytoskeleton. Cells on the 300 nm and 250 nm diameter clusters had a greater percentage of actin relative to the cross section length than cells on the 200 nm diameter clusters. This transition will also be visible in the next chapter on motility. Given the common trend in the results presented so far, cell shape, cytoskeleton and proliferation all appear to be influenced by the diameter of the fibronectin clusters with the macroscopic protein density held constant at 8.72%.

	Ratio Method	*Exponential Fit Method*			
	Average Doublings Per Day	*Average Doublings Per Day*	t_d	*Average* R^2	*Standard Deviation* t_d
150 nm 1:2	1.80X	1.71X	0.0322	0.96	0.0079
200 nm 1:2	1.70X	1.46X	0.0227	0.87	0.0100
250 nm 1:2	1.20X	1.15X	0.0084	0.75	0.0086
300 nm 1:2	1.13X	1.09X	0.0054	0.79	0.0063
Control	1.95X	1.98X	0.0412	0.90	0.0005

Table 9.6.1: Average doublings per day calculations using a ratio based method and an exponential fit method. Experiments over a 3-month period produced consistent growth rates over the range of patterns investigated. The lower R^2 values for 250 nm and 300 nm are due to the slow rate of growth of the cells versus the observation time of 72 hours. Increasing the observation time will better capture the exponential behavior of the growth rate and an increase the R^2 value.

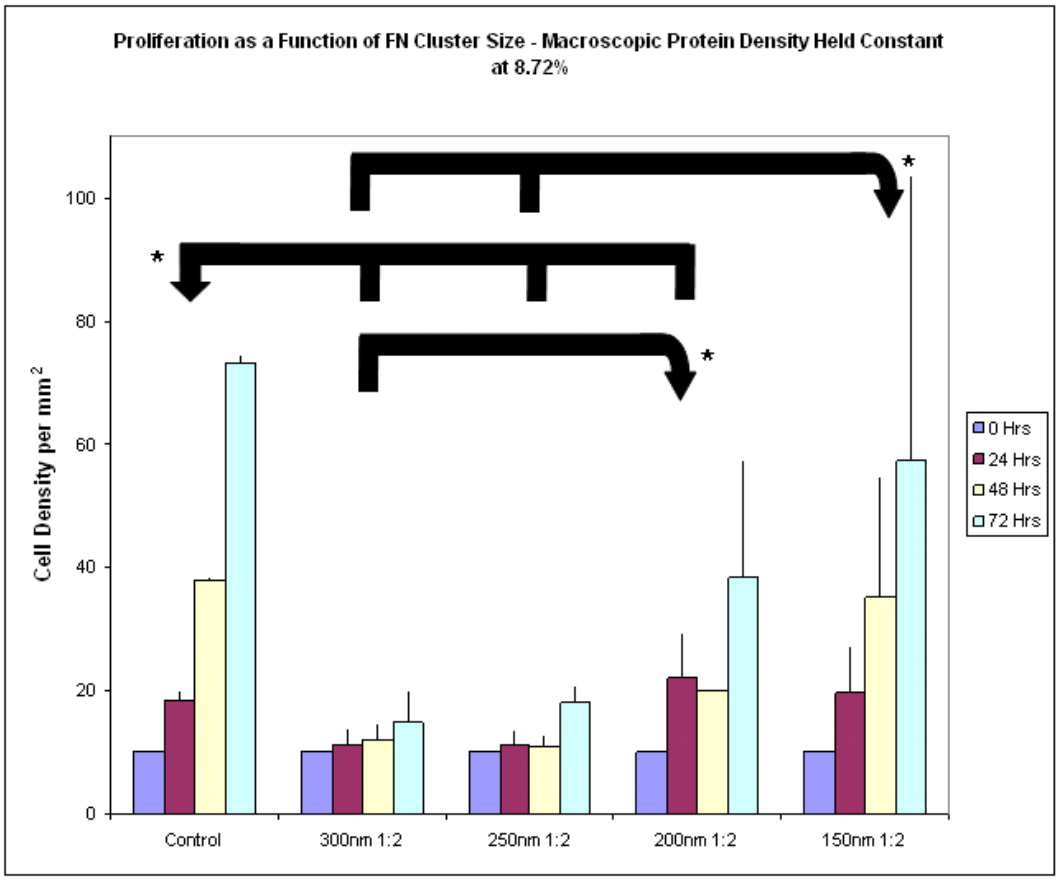

Figure 9.6.1: This data shows proliferation as a function of fibronectin cluster diameter while holding the macroscopic protein density constant at 8.72%. All of the cell populations have been normalized to a starting value of 10 cells per mm^2, which represents the seeding density calibrated with a hemocytometer. As the fibronectin cluster diameter is decreased from 300 nm to 150 nm, the proliferation growth rate increases. * $p < 0.05$. (300 nm n=4 experiments, 250 nm n=3 experiments, 200 nm n=3 experiments, 150 nm n= 4 experiments).

9.6.4 PROLIFERATION AS A FUNCTION OF PATTERN SIZE - LUMPED

As shown in Section 9.6.2, pattern size was a statistically significant driver of proliferation rate with the macroscopic protein density held constant at 8.72%. In analyzing the data, cells on the 200 nm diameter fibronectin clusters appear to have higher proliferation rates than the cells on the 300 nm diameter clusters across the

macroscopic densities of 4.91% to 12.56%. To investigate this, data from the three macroscopic densities, 4.91%, 8.72% and 12.56% were lumped together for the diameters of 200 nm and 300 nm (Figure 9.6.2). The results indicate that there is a statistical difference between the diameters of 200 nm and 300 nm for this range of macroscopic densities. Interestingly, cells on the 300 nm diameter patterns displayed low proliferation across all ranges of macroscopic protein density explored, 4.91% - 19.63%. This suggests that there is something significant about the adhesion cluster size of 300 nm. It inhibits proliferation in comparison to controls and smaller sized adhesion clusters.

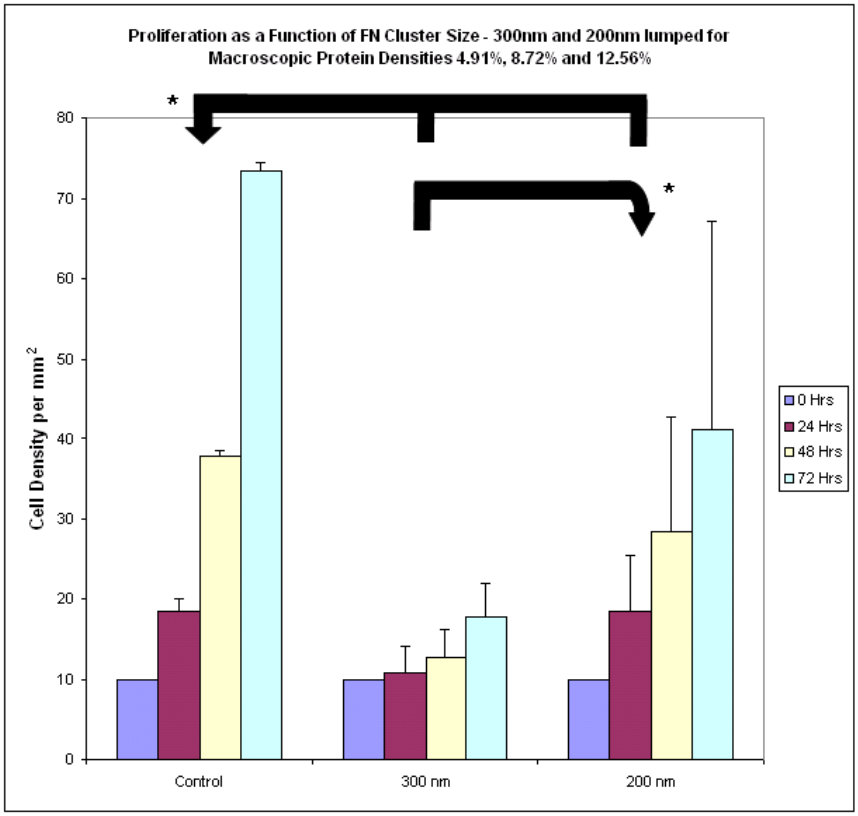

Figure 9.6.2: This data shows proliferation as a function of fibronectin cluster diameter that was grouped for the macroscopic protein densities of 4.91%, 8.72% and 12.56%. All of the cell populations have been normalized to a starting value of 10 cells per mm^2, which represents the seeding density calibrated with a hemocytometer. * $p < 0.05$. (300 nm n=8 experiments, 200 nm n=12 experiments).

9.6.5 PROLIFERATION AS A FUNCTION OF ADHESION SIZE WITH CONSTANT SPACING

In the previous section, macroscopic protein density was held constant at 8.72% while the diameter of the adhesion was varied. In order for the macroscopic density to be held constant, the spacing between the adhesions had to be adjusted. To separate the effects due to the different spacing versus the effects due to the adhesion cluster diameter, a set of experiments was conducted that held the distance between clusters constant but varied their diameter. As shown in Figure 9.6.3, adhesion clusters were spaced a constant 300 nm apart, while the diameter of the clusters were varied from 300 nm to 150 nm. The results indicate that decreasing the adhesion cluster size resulted in increased proliferation.

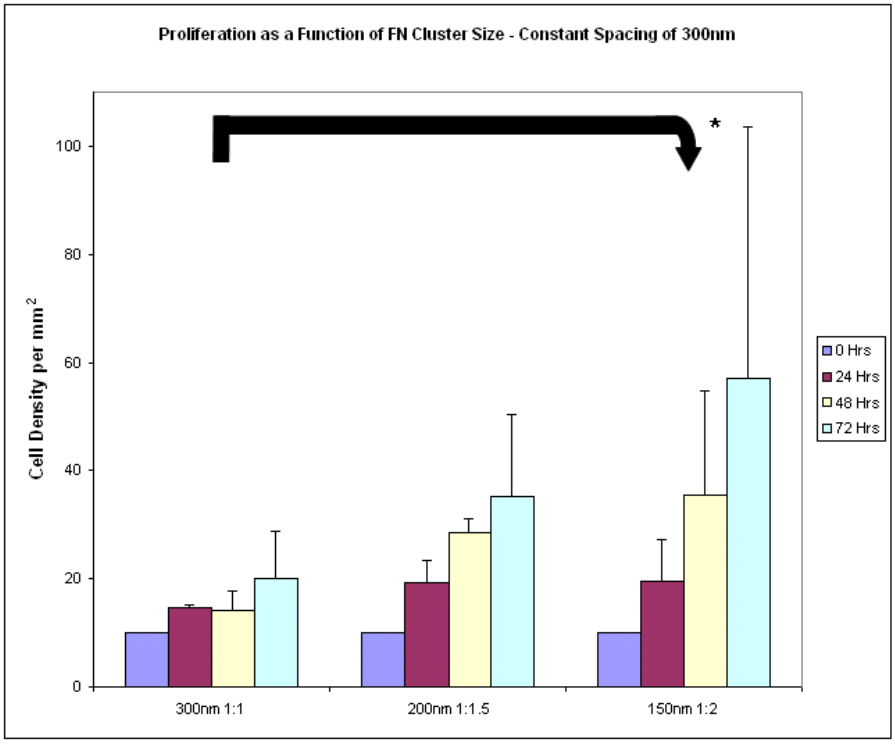

Figure 9.6.3: Proliferation as a function of maximum adhesion size with the spacing between adhesions held constant at 300 nm. The trend above shows that as the maximum adhesion size is decreased from 300 nm proliferation increases. * $p < 0.05$. (300 nm n=3, 200 nm n=3, 150nm n=4).

The analysis was also carried out for adhesion clusters spaced 600 nm apart (Figure 9.6.4). As the diameter of the cluster was decreased from 300 nm to 200 nm, the proliferation rate of the cells increased. These results provide a final validation of the trend that adhesion cluster diameter is a key determinant influencing proliferation on the nanopatterned surfaces.

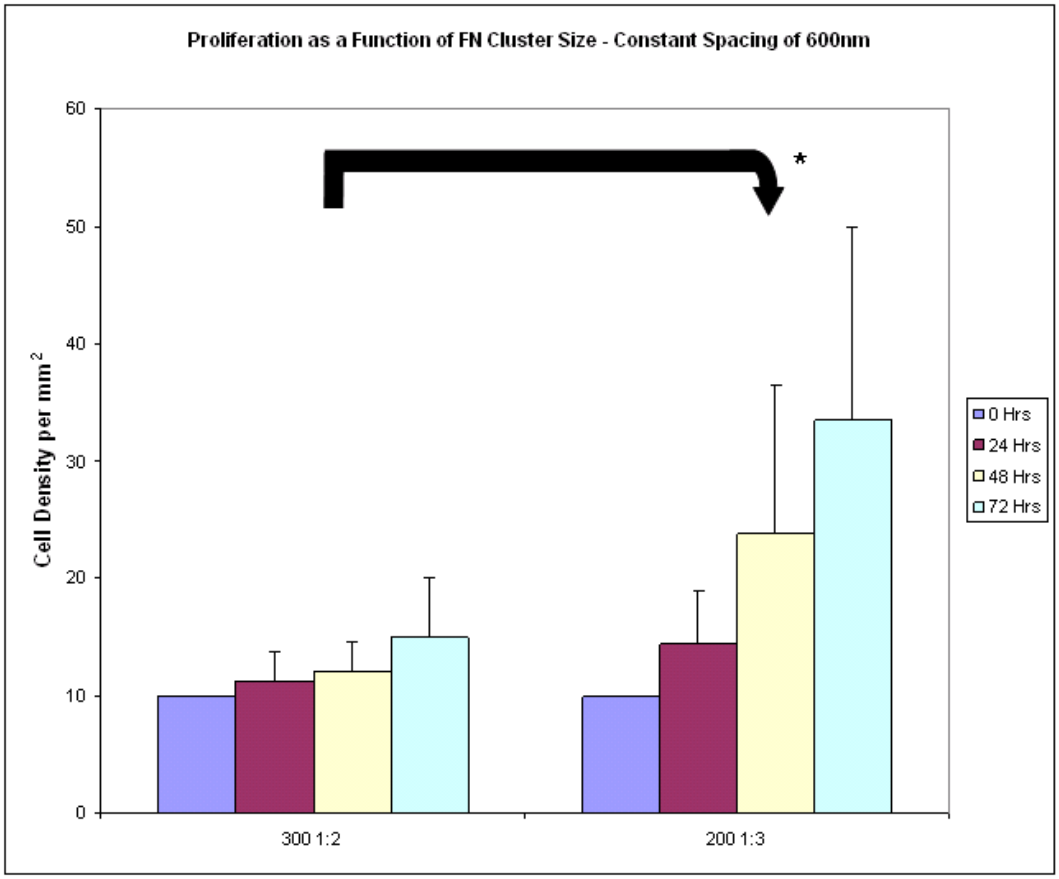

Figure 9.6.4: Proliferation as a function of maximum adhesion size with the spacing between adhesions held constant at 600 nm. The trend above shows that as the maximum adhesion size is decreased from 300 nm, proliferation increases. * $p < 0.05$. (300 nm n=4 experiments, 200 nm n=5 experiments).

The trends that have been discussed can also be visualized as a three dimensional plot shown in Figure 9.6.5. One aspect that the plot captures is the interplay between adhesion diameter and spacing. As the adhesion clusters become smaller and farther apart, the proliferation rate increases. The opposite is true; as the adhesions become larger and spaced closer, together proliferation decreases. The 300 nm diameter adhesions consistently had lower proliferation than other adhesion diameters, even for very large separation distances. There is also some apparent influence from spacing, as can be seen for the 200 nm diameter adhesions. Adhesion cluster diameter appears to play a larger role in impacting the proliferation rate for lower macroscopic protein densities.

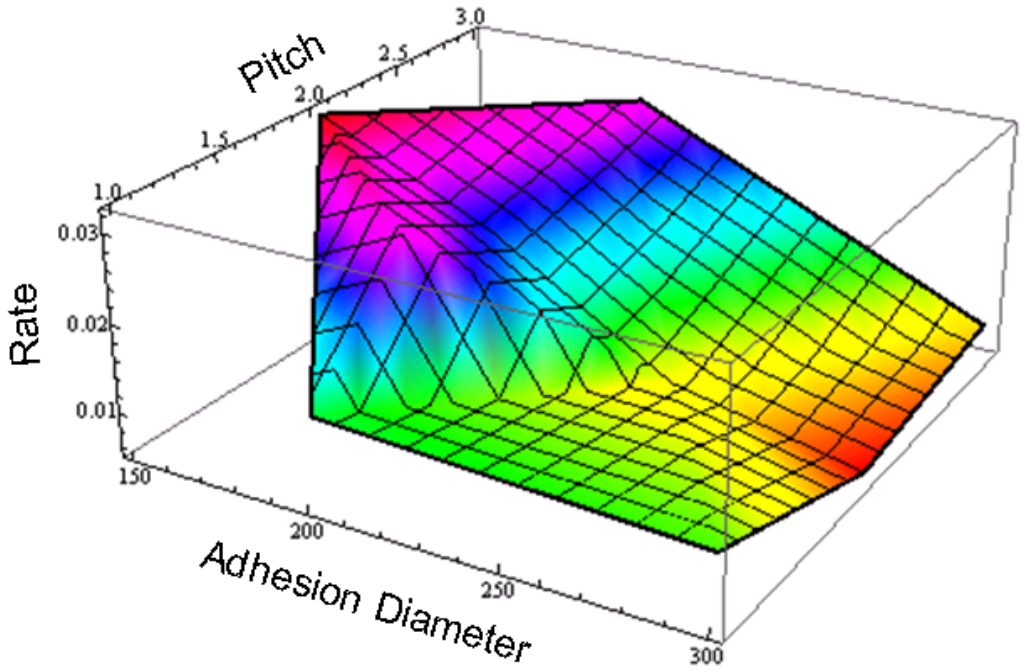

Figure 9.6.5: Three dimensional proliferation map showing the relationship between adhesion cluster diameter and macroscopic density versus proliferation growth rate.

9.7 DISCUSSION

In comparing these results to those obtained on elastic substrates, it has been shown that slightly lower proliferation rates are found on softer materials (Yeung, Georges et al. 2005). However, the difference in proliferation is slight across a large range of elasticities, and there is no evidence that proliferation is greatly affected by substrate elasticity. This also indicates that cell-surface tension may not play a major role in determining proliferation rates. In Janmey's studies, he found that endothelial cells on extremely soft gels proliferate at nearly the same rate as controls even though the cells did not spread and presented a balled-up morphology (Yeung, Georges et al. 2005). Additionally, he found that the balled-up cells did not have well-defined stress fibers, which provides additional evidence that cell-substrate force is less of a determining factor.

Macroscopic fibronectin density was determined to be an influential factor in cell growth rates in studies with capillary endothelial cells on plastic well plates (Ingber 1990). Cells did not proliferate and actually underwent apoptosis for macroscopic surface densities of 235 fibronectin molecules per μm^2. For macroscopic surface densities larger than 547 fibronectin molecules per μm^2, growth rates increased and were found to be positively dependent on surface concentration. These results indicate that endothelial cell growth rates are influenced by receptor-FN interactions.

The results from this chapter focused on the influence of adhesion cluster size on proliferation with either the macroscopic density held constant or the spacing between adhesions held constant. It was important to have these two views because there is some interplay between adhesion cluster sizes, macroscopic density, and adhesion spacing as

shown in the three dimensional plot in Figure 9.6.5. Holding one parameter constant allowed for a view of the influence of the cluster size independent of that parameter.

The first set of results investigated cluster size with macroscopic protein density held constant at 8.72% and included the patterns 150 nm 1:2, 200 nm 1:2, 250 nm 1:2, 300 nm 1:2. This set of four patterns was also used in experiments in other chapters investigating the influence of cluster size with constant macroscopic density. In Chapter 7, it was discovered that as the diameter of the cluster size was increased from 150 nm to 300 nm, there was an increase in the spreading area of the cell, and the cells had a more rounded morphology. In Chapter 8, the absolute number of fibers and the percentage of actin relative to the cross section length increased as the cluster size was increased. The proliferation studies in this chapter found that increasing the size of the fibronectin cluster resulted in decreased proliferation rates. This is interesting because the cells on the smaller clusters proliferated faster, were typically smaller, and had less developed stress fibers than those on larger clusters.

Experiments were also conducted holding the spacing between clusters constant while varying the diameter of the clusters. This gave a view of cluster size dependence, independent of any influence that the cluster spacing may have on proliferation. A similar trend was discovered in comparison to the constant macroscopic density experiments. As the diameters of the clusters were increased, the proliferation rate decreased. This was true for both a constant cluster spacing of 300 nm and 600 nm. Thus, adhesion cluster size plays a role in influencing proliferation independent of adhesion cluster spacing and macroscopic density.

It was also observed that the cells on the 300 nm patterns had lower proliferation rates for all ranges of macroscopic density. Interestingly, a similar trend was observed in Chapter 7, where the cells on the 300 nm patterns consistently had a large spreading area

and rounded morphology for all ranges of macroscopic density. These two quantitative results correspond with the qualitative observation that the 300 nm patterns typically had large well spread cells that did not divide often.

The general trend that can be extrapolated from the three dimensional plot in Figure 9.6.5 is that as the fibronectin clusters become smaller, further apart and less dense, the rate of proliferation increases. The opposite is true if the fibronectin clusters are larger, closer together and denser, the rate of proliferation decreases. This trend is particularly interesting because it has been reported when macroscopic fibronectin density is decreased, that proliferation also decreases (Ingber 1990; Slater and Frey 2007). Thus, there seems to be a transition region between the nanopatterned surfaces and what would be expected on control surfaces. This general relationship is shown in the following diagram:

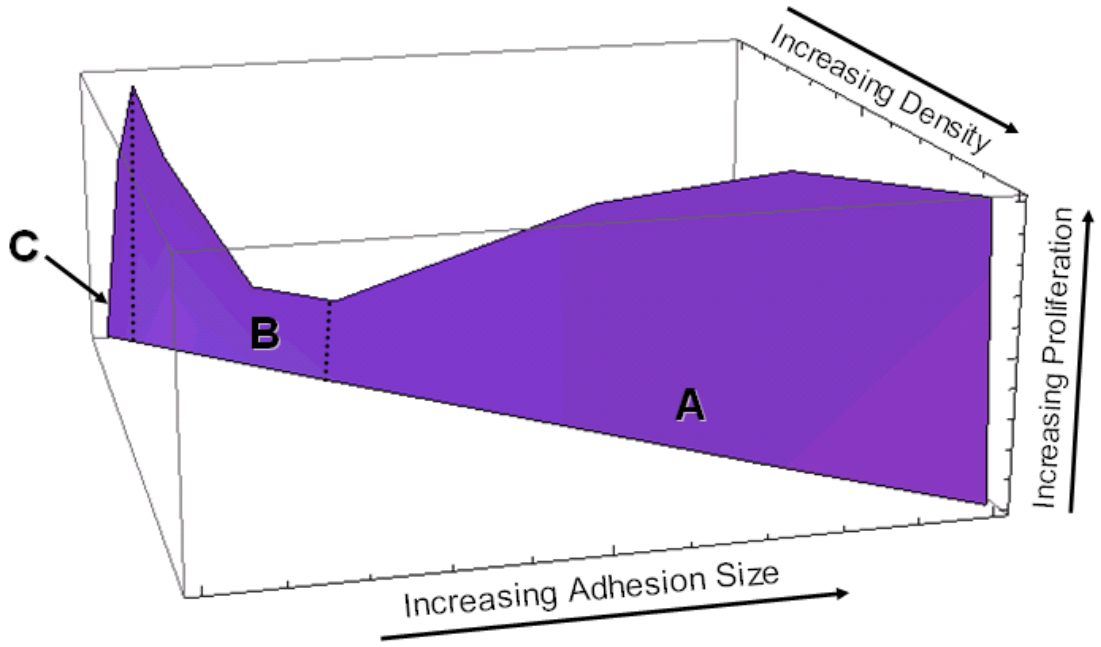

Figure 9.7.1: Hypothetical proliferation map. (A) Generalized trends found for cells seeded on various macroscopic densities of fibronectin. (B) Generalized trend found in the data presented in this chapter. (C) Hypothetical decline in proliferation when the surface no longer supports cell attachment.

The section B in Figure 9.7.1 corresponds to the nanopatterned data presented in this chapter. This same trend can be extracted from looking at Figure 9.6.5 and taking a diagonal cut across the plane. Section A of this figure represents the general trend observed for cells seeded on different densities of fibronectin. For the sake of discussion, it will be assumed that a patterned surface will begin to behave similarly to a control surface when the pattern size becomes larger than 300 nm and the pitch of the patterns is less than 1:1. On the diagram, this behavior would occur somewhere around the dotted line between B and A. The section C is a drop in proliferation that must occur as the pattern size and spacing can no longer support cell adhesion. Previous work from our group showed that proliferation growth rates on gold coated surfaces were relatively constant for fibronectin densities from 1,199 FN/μm^2 to 2,605 FN/μm^2. However, for surfaces coated with a density of 537 FN/μm^2, the cells had a very low proliferation rate that was similar to the 300 nm 1:1 adhesion clusters. The 300 nm 1:1 adhesion clusters happen to have a macroscopic protein density of 511 FN/μm^2 which is nearly identical to the 537 FN/μm^2 on the control surface. It is likely a reasonable assumption that patterns larger than 300 nm with a pitch less than 1:1 behave close to control surfaces. Based on the results from homogenous coated gold control surfaces, it would be expected that the cells would cease to proliferate at densities lower than 537 FN/μm^2. However, on the nanopatterned surfaces, the opposite happens and there is increased proliferation. The cells begin to show increased proliferation at macroscopic densities far below what is expected to support cell proliferation.

Section C in the figure is also interesting because it represents a point where the nanoclusters become so small and spaced so far apart that they cease to support cell adhesion. This size regime has actually been probed by others using block-copolymer micelle nanolithography (Glass, Moller et al. 2003; Arnold, Cavalcanti-Adam et al.

2004). In their work, they patterned RGD peptides onto adhesive gold nanodots with diameters 8 nm and smaller. This allowed the binding of one integrin per gold dot as the diameter of an integrin is approximately 10 nm. They find that for dots spaced 28 nm and 58 nm apart, cells adhere and spread on the surface. However, for dots spaced 73 nm, cells did not spread or adhere well. Their results suggest that gold dots spaced 28 nm or 58 nm could support cell growth whereas gold dots spaced 73 nm could not. Given that an integrin diameter is approximately 10 nm, a spacing distance of 28 nm corresponds to a pitch of approximately 1:2 (edge-to-edge), 58 nm corresponds to 1:5 (edge-to-edge) and 73 nm corresponds to 1:6 (edge-to-edge). The pitch of 1:5 and 1:6 are much greater than the maximum pitch of 1:3 explored in this work and the adhesion sizes for all three are much smaller. In relating this to section C of Figure 9.7.1, their results on the 28 nm patterns overlap in macroscopic density near the transition region between C and B. The results for the spacing of 58 nm are represented on the higher proliferation rate part of section C, while the 73 nm results are represented in the bottom portion.

Additional evidence for the section C has been shown by our group using nanosphere lithography (Slater and Frey 2007). Nanosphere lithography is a self-assembly technique that can be used to create nanopatterned surfaces, and an overview is provided in Section 2.5 of this dissertation. Nanopatterned surfaces that were created with a bilayer of 300 nanometer spheres produced patterns with a cluster area equivalent to a 60 nm diameter cluster with a pitch of 1:3.6. On these surfaces, the proliferation rate of the cells was much greater than observed on the control surface coated with 537 FN/μm^2 but slightly less than the surfaces coated with densities from 1,199 FN/μm^2 to 2,605 FN/μm^2. The same was true for surfaces created with a monolayer of 300 nm spheres which produce a cluster area equivalent to 80 nm diameter clusters with a pitch of 1:1. Combining these results with those using block-copolymer provides validation

for region C and provides evidence for the continuous transition from section C to section B.

The transition illustrated by section B in Figure 9.7.1 has not been distinguished in any other literature. However, the transition between B and A seems to correspond well with previously reported results on homogenous coated surfaces, and the transition between B and C fit nicely with the work using micelle nanolithography and nanosphere lithography. This transition we have discovered may correspond to a region between two signaling pathways that are possibly inhibited or stimulated by restricting the size and spacing of the adhesion clusters.

It is well known that proliferation is a highly regulated process that depends on a number of feedback loops and signaling inputs. FAK is a major signaling component in focal adhesions, which plays both a stimulator and inhibitory role in proliferation (Pirone, Liu et al. 2006). It has been shown that on rigid substrates, where adhesion forces are high, FAK will be upregulated and will play a stimulatory role. However, on micropatterned substrates, where adhesions are measured to be much lower than rigid substrates, FAK plays an inhibitory role. In Chapter 8, it was noted that cells on the 300 nm adhesion clusters had half as many actin stress fibers, and the percentage of actin relative to the cross section length was less than cells on controls. Although a direct adhesion measurement could not be taken, the difference in cytoskeletal structure suggests that adhesion strength is reduced on nanopatterned surfaces versus cells with well-developed stress fibers on rigid controls. In this case, the results on the 300 nm diameter clusters would be consistent with the view of FAK; decreased adhesion resulted in FAK playing an inhibitory role in proliferation. However, this does not explain the upward proliferation rates as the adhesion clusters get progressively smaller. In FAK knockout experiments, it was discovered that cells in a low adhesion context increased

proliferation (Pirone, Liu et al. 2006). In this case, FAK was not present to inhibit proliferation and proliferation but was found to proceed under a RhoA process. In light of this result, it might be possible that on the smaller adhesion islands, FAK is not active or at least not in high enough quantities to inhibit proliferation, which is similar to the FAK knockouts. This would explain why proliferation is observed to increase on diameters smaller than 300 nm.

At this time, positive determining experiments have not been completed to identify the exact molecular mechanisms behind the observed transition in the nanopatterns. There is evidence that there are multiple surface related signals that are driving the overall growth rates of the cells. The results from these experiments provide a quantitative measurement of where the transition region occurs with respect to fibronectin cluster diameter, spacing and macroscopic density. Clearly, the next experimental steps would be to utilize knockout cells, such as a FAK knockout, or fluorescently labeled cells to see if there is a correlation with certain proteins.

REFERENCES

Arnold, M., E. A. Cavalcanti-Adam, et al. (2004). "Activation of integrin function by nanopatterned adhesive interfaces." Chemphyschem **5**(3): 383-388.

Glass, R., M. Moller, et al. (2003). "Block copolymer micelle nanolithography." Nanotechnology **14**(10): 1153-1160.

Ingber, D. E. (1990). "Fibronectin Controls Capillary Endothelial-Cell Growth by Modulating Cell-Shape." Proceedings of the National Academy of Sciences of the United States of America **87**(9): 3579-3583.

Pirone, D. M., W. F. Liu, et al. (2006). "An inhibitory role for FAK in regulating proliferation: a link between limited adhesion and RhoA-ROCK signaling." Journal of Cell Biology **174**(2): 277-288.

Slater, J. and W. Frey (2007). "Nanopatterning of Fibronectin and the Influence of Integrin Clustering on Endothelial Cell Spreading and Proliferation." Journal of Biomedical Materials Research Part A.

Yeung, T., P. C. Georges, et al. (2005). "Effects of substrate stiffness on cell morphology, cytoskeletal structure, and adhesion." Cell Motility and the Cytoskeleton **60**(1): 24-34.

CHAPTER 10: MOTILITY

10.1 OVERVIEW

Cellular motility is a complex process involving the remodeling of the cytoskeleton and changes in cellular anchoring points. It involves forming cytoskeletal protrusions at the leading edge of the cell, new stable adhesions that occupy these protrusions, contraction of the cytoskeleton and release of adhesions in the rear. Due to the importance of adhesions and force transduction in motility, studying the movement of cells on the nanopatterned cell culture system offers an interesting perspective of how nanoscale adhesion parameters influence cell motility.

10.2 METHODOLOGY

Silicon samples were prepared and functionalized according to the protocols presented in Chapter 5. Controls were prepared by coating glass slides with 5 nm of Chromium and 15 nm of Gold and functionalizing them in an identical manner to nanopatterned samples. Samples were immersed in ETOH (AAPER) for 5 minutes to sterilize the samples before being introduced into a sterile culture hood. Samples were then rinsed 60 seconds, three times in a HEPES buffered saline that was prepared from 11.9 g (HEPES)(Sigma), 5.8 g NaCl (Mallinkckrodt) and 1000 ml DI and adjusted to 7.5 pH with NaOH (Sigma). The nanopatterns were coated with 125 µL of a 10 µg/ml fibronectin solution (Sigma) in 50 mM HEPES buffered saline for 20 minutes at room temperature. Controls were coated with either a 2 µg/ml, 10 µg/ml, or 25 µg/ml fibronectin solution (Sigma) in 50 mM HEPES buffered saline for 20 minutes at room temperature. The controls were then blocked with 1.0 % BSA solution in HEPES

buffered saline for 20 minutes to minimize serum proteins from adsorbing to the gold surface. The samples were then thoroughly rinsed in 50 ml of HEPES buffered saline solution for 60 seconds, 3 times to remove any excess fibronectin. The cells in all the studies were human umbilical vein endothelial cells (HUVECs) (Cambrex, Walkersville, MD) of passage below 4 and cultured according to manufacturer's specifications. They were cultured in T-25 tissue culture flasks coated with 30 μg of human plasma fibronectin (Sigma, Saint Louis, MO) at 37ºC and 5% CO_2 until 80% confluence. During culture and experiment, the HUVECs were bathed in endothelial growth media (Cambrex, Walkersville, MD) supplemented with 2% fetal bovine serum, 0.5 ml human endothelial growth factor, 0.5 ml Hydrocortisome, 0.5 ml GA-1000 (Gentamicin, Amphotericin B). To release cells from flasks for cell seeding, the flasks were first rinsed with 5 ml of HEPES buffered saline at 37 ºC. They were then trypsinized using 3ml of Trypsin/EDTA (Cambrex) for 5 minutes at 37 ºC and 5% CO_2. Next, 3 ml of trypsin neutralizing solution (Cambrex) was added to the cell suspension to neutralize the Trypsin/EDTA. The cell suspension was pelleted using a centrifuge set to 240 g for 6 minutes. The cells were then resuspended in 10 ml of endothelial growth media (Cambrex) discussed above. A hemocytometer and trypan blue dye was used to determine the total living cell population in the resuspension. The HUVECs were then seeded on the sample surface at approximately 7 cells/mm^2. The cells were maintained in 20 ml of endothelial growth media (Cambrex), 37˚C and 5% CO_2 and the media was exchanged after 24 hours. The cells were filmed in a special incubator box that enclosed our Leica Microscope. During filming, the cells were maintained at 37˚C and 5% CO_2. Images were captured at 15X magnification at 60 seconds intervals using a sensicam digital microscope camera and Camware software made by PCO.Imaging. A minimum of 120 frames or 2 hours of video were captured per pattern filming session. Imaging

sessions were conducted at 24, 48 and 72 hours for each of the selected nanopatterns, with three to four filming sessions being performed on a single experimental day. Tracking of the cells was performed manually to generate a list of X and Y coordinates of cell movement using a simple particle tracking plug-in developed for ImageJ (NIH, Bethesda, MD) by Fabrice Cordelieres, Institut Curie, Orsay (France). The coordinates were then processed using a custom algorithm to calculate velocities and distance traveled. The algorithm also corrected for sub-pixel errors, noise reduction and compensated for sample drift. Information from the different patterns in the matrix on the cell culture array was used to create a map linking cluster size and spacing to average motility velocity. Hypothesis testing was performed in Matlab using a two-sample t-test, where a set of motility velocities was assumed to be greater than another set of motility velocities. P-values that were less than 0.05 were assumed to be statistically significant.

10.3.1 SOFTWARE DESIGN AND ALGORITHM

Special analysis software was developed to compensate for a number of non-idealities encountered during the experimental process. One such occurrence during filming was a slight sample drift in the range of 10 μm. Sample drift is defined as a directed movement in one direction where the entire sample would uniformly drift in that direction. Although special sample holders were made to drastically reduce the presence of drift, it was never entirely eliminated. Drift was caused by a number of factors including the microscope table being bumped during or settling of the sample. A second occurrence was vibration noise that could have been caused by laboratory equipment or other disturbances to the microscope table. Vibration noise showed up as clearly cyclical oscillations across the sample surface. To compensate for these two non-idealities, three points on the sample were tracked to create a sample vibration and drift map. These two

maps were used to adjust the sampled cell data to remove any movements that were not associated with the cells movements. The second type of non-ideality was sub-pixel errors due to the discretization of the cell movement. Sub-pixel errors were removed by using a 3 pixel averaging routine that produced a path more realistic to the actual path the cell traversed.

The algorithm discussed above was implemented in a Microsoft Excel workbook. The input to the algorithm is a two column list of X and Y coordinates that were manually obtained for each cell using a particle tracking plug-in developed for ImageJ (NIH, Bethesda, MD) by Fabrice Cordelieres, Institut Curie, Orsay (France). The plug-in produced a simple X and Y list of coordinates, which were then pasted into Microsoft Excel. The algorithm required three control points to calculate sample drift and vibration noise. Afterwards, measured cells could be pasted one-by-one into their own worksheets which would then automatically be processed through the algorithm. The output included cell velocities and graphs of the paths traveled.

10.4.1 MOTILITY RESULTS

Data for the motility experiments was collected over the time periods of 24, 48 and 72 hours. During this time, the paths and velocities of the HUVECS for a specific pattern were tracked for a minimum of 2 hours. An overview of all of the data collected is presented in Figure 10.4.1. A general feature of the data is a biomodal distribution of velocities across different patterns, especially at 24 hours. At 24 hours, there are certain patterns that display particularly high velocities in the range of 0.9 – 1.2 μm/min and another group of patterns that display velocities closer to controls in the range of 0.6 – 0.35 μm/min. The average velocities were between 0.359 - 0.368 μm/min on different homogenous gold controls. For patterns where high motility was observed at 24 hours, as

time progressed, the velocities of the cells on these patterns gradually decreased. This was true for all but one pattern 150nm 1:2. For greater clarity, a 3D surface map was created with the data points available for 24hrs (Figure 10.4.2).

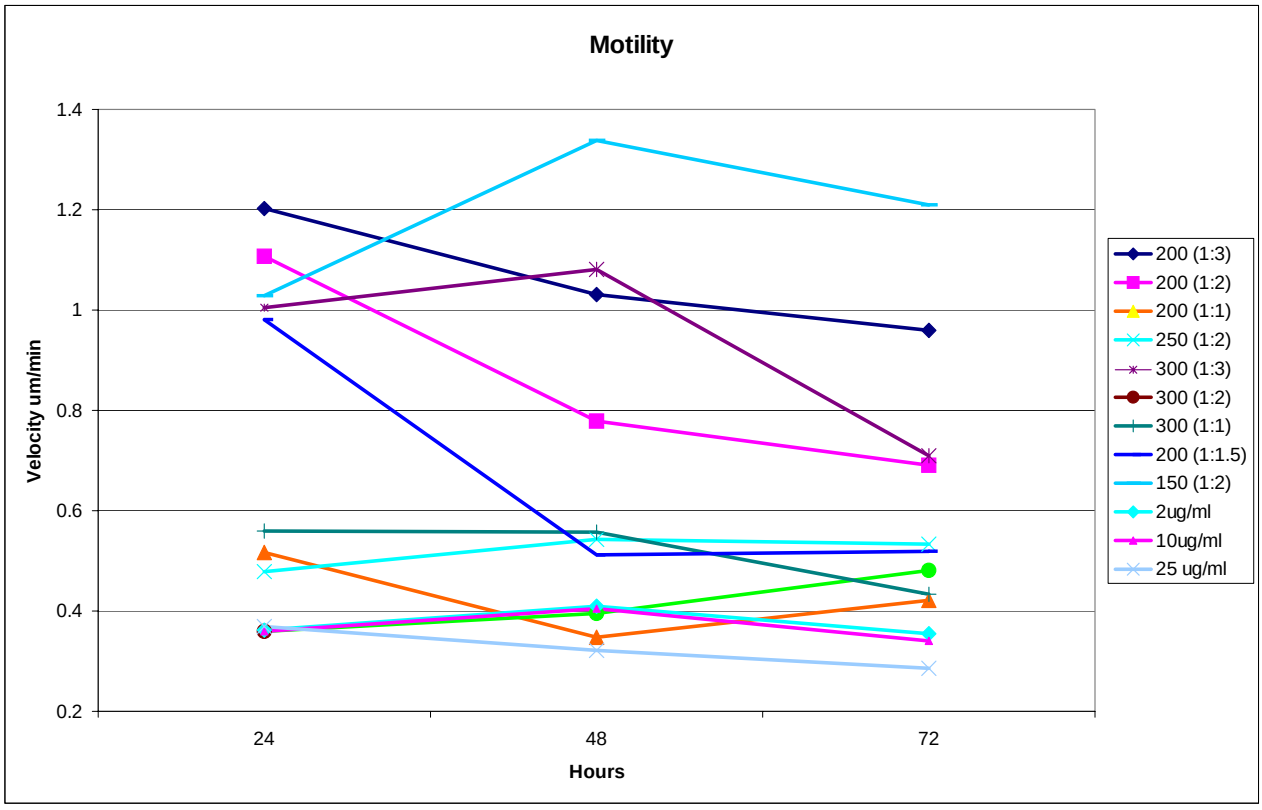

Figure 10.4.1: Overview of all data points collected. The control data is located at the bottom potion of the graph, showing low motility velocity. Certain nanopatterns induced higher motilities, which are seen at the top of the graph. As a general trend, cells that exhibited high velocities on certain patterns at 24 hours gradually began to slow down towards 72 hours.

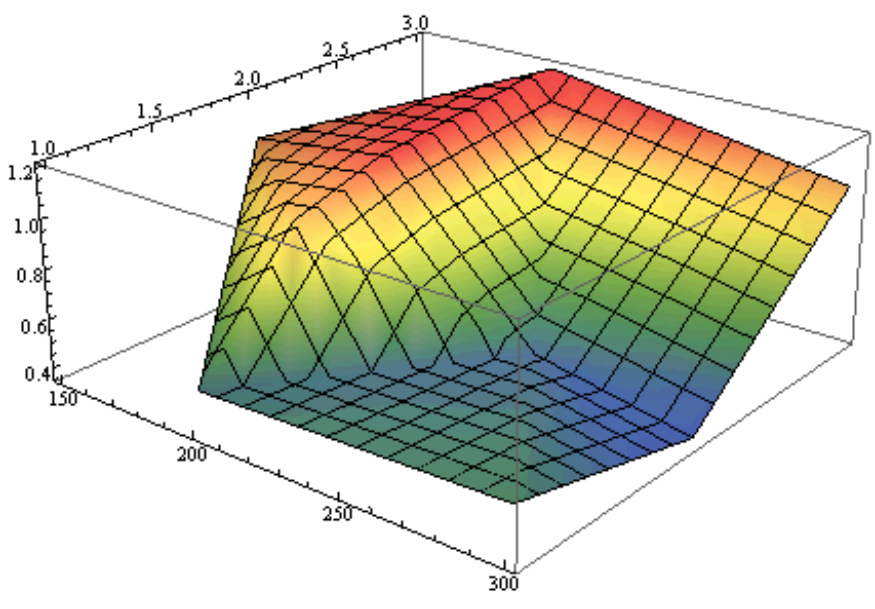

Figure 10.4.2: 3D surface plot consisting of the 24 hour data presented in Figure 10.4.1. A transition in the motility is seen in the pattern size range of 200-250 nm and at large distances between adhesions.

10.4.2 MOTILITY ON GOLD CONTROL SURFACES

Similar to other control experiments performed for this dissertation, glass slides were uniformly coated with Au and prepared identically to the nanopatterned surfaces. To investigate homogenous density dependence on motility, fibronectin was applied in quantities of 2 μg/ml, 10 μg/ml and 25 μg/ml functionalized gold coated glass slides. The results from these experiments are presented in Figure 10.4.1. It has been shown previously that motility has a biphasic dependence on average density concentration (Dimilla, Stone et al. 1993; Huttenlocher, Sandborg et al. 1995). However, no significant difference in motility was observed between the fibronectin concentrations that were tested. The average cell velocities were similar to those reported for endothelial cells on glass substrates (Kouvroukoglou, Dee et al. 2000). It is believed that there should be

some lower limit of the concentration of homogenous fibronectin density where the cells will cease to move. However, this concentration may occur below the density needed for cells to attach and spread.

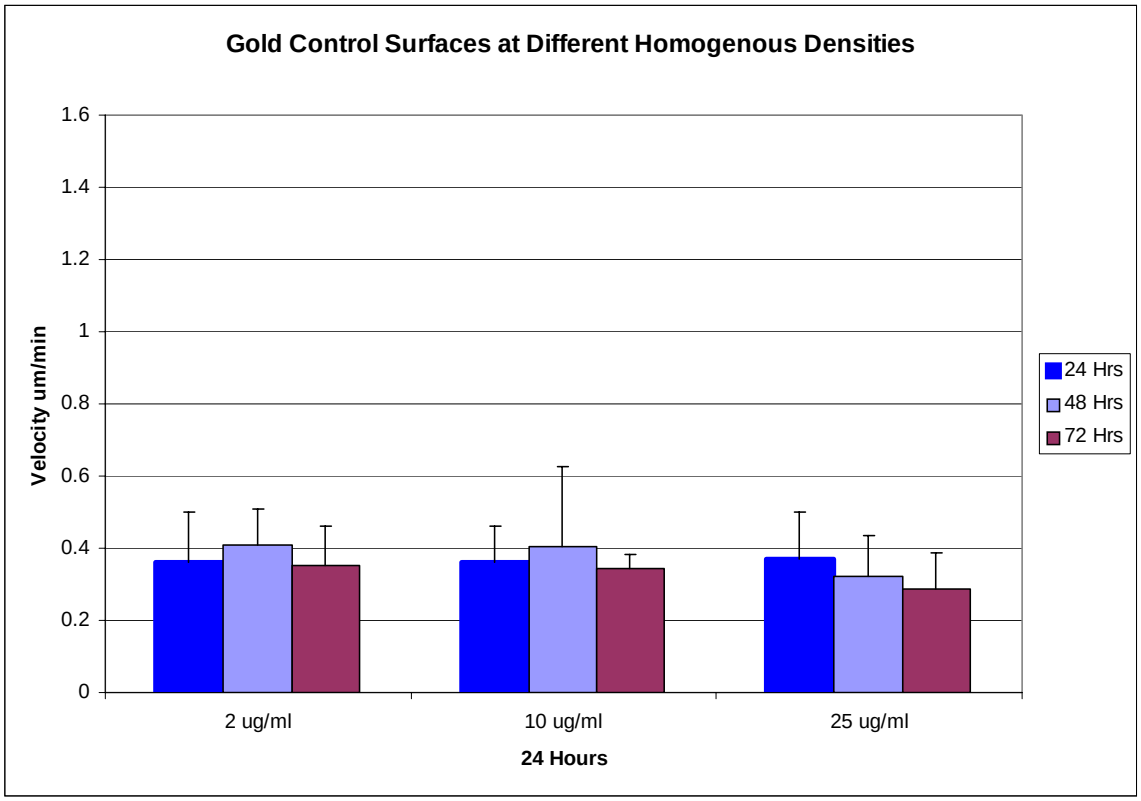

Figure 10.4.1: Motility on Au control surfaces with homogenous fibronectin at either 2 µg/ml, 10 µg/ml and 25 µg/ml. No significant difference was observed between any of the three fibronectin concentrations. n=62.

10.4.3 Motility as a Function of Maximum Adhesion Size with Constant Density

Motility as a function of maximum adhesion size with a constant macroscopic fibronectin density coverage of 8.7% was investigated for the nanopatterns of diameter

150 nm, 200 nm, 250 nm and 300 nm. This density was selected because of the need to have a uniform and comparable dataset across all experiments, a known noticeable change in cellular behavior at this density and that it is a similar density to data we have on NSL surfaces. Motility was investigated at 24 hours, 48 hours and 72 hours. The compilation of the data is presented in Figure 10.4.2. As the average adhesion diameter was decreased from 300 nm to 150 nm, the velocity of the cells increased. There is a sharp transition that can be seen in the graph between 250 nm and 200 nm. This transition is similar to the transition observed in Chapter 9 in Figure 9.6.1, where an increase in proliferation was observed between 250 nm and 200 nm. Thus, it seems that the adhesion cluster diameter is influencing a signaling switch for both motility and proliferation at similar cluster sizes. Interestingly, it also demonstrates the sensitivity of the cells to a change as small as 50 nm in the diameter of the adhesion cluster. The movement of the cells was also tracked to determine if the overall displacement was more directed than controls (Figure 10.4.3). As can be seen in the figure, the cells on the smaller adhesions clusters reached distances much farther than the larger clusters.

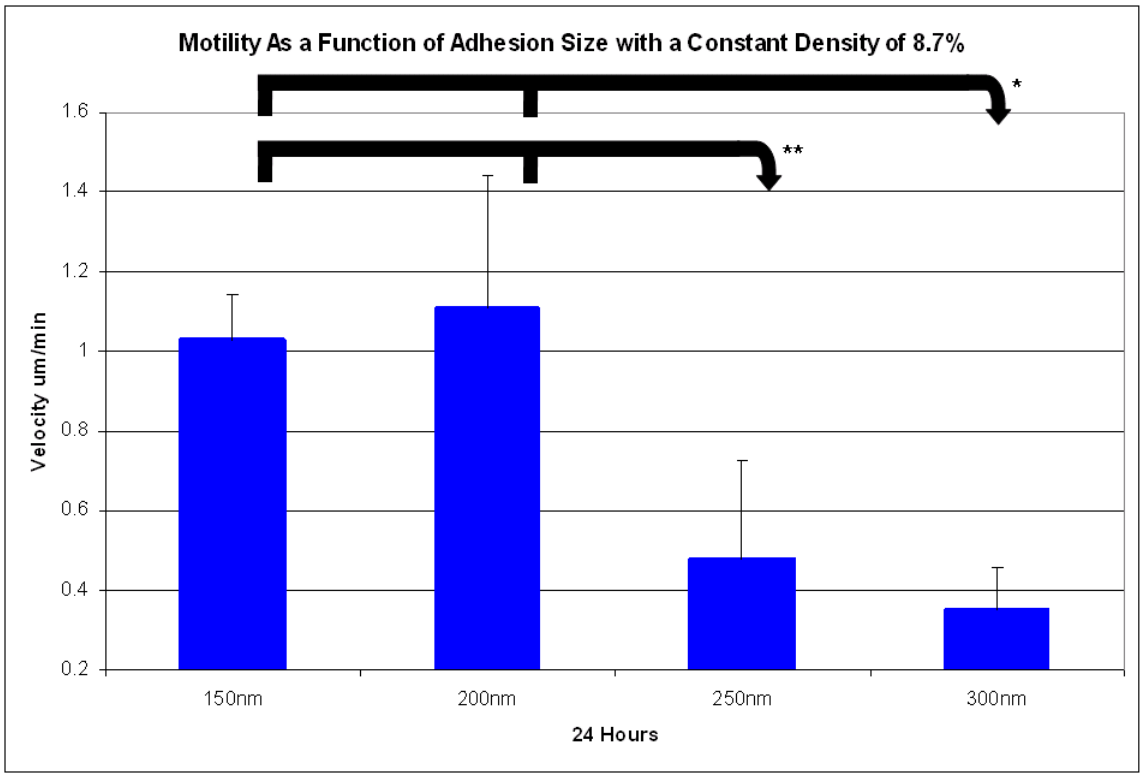

Figure 10.4.2: Motility on nanopatterned surfaces with a constant macroscopic fibronectin density coverage of 8.7%. The nanopattern adhesion sizes were varied between 150 nm, 200 nm, 250 nm and 300 nm. As the maximum size of the adhesion was decreased, motility increased. There was also a noticeable transition in velocity between 250 nm and 200 nm. * $p < 0.05$. (150 nm n=6, 200 nm n=7, 250 nm n=8, 300 nm n=9).

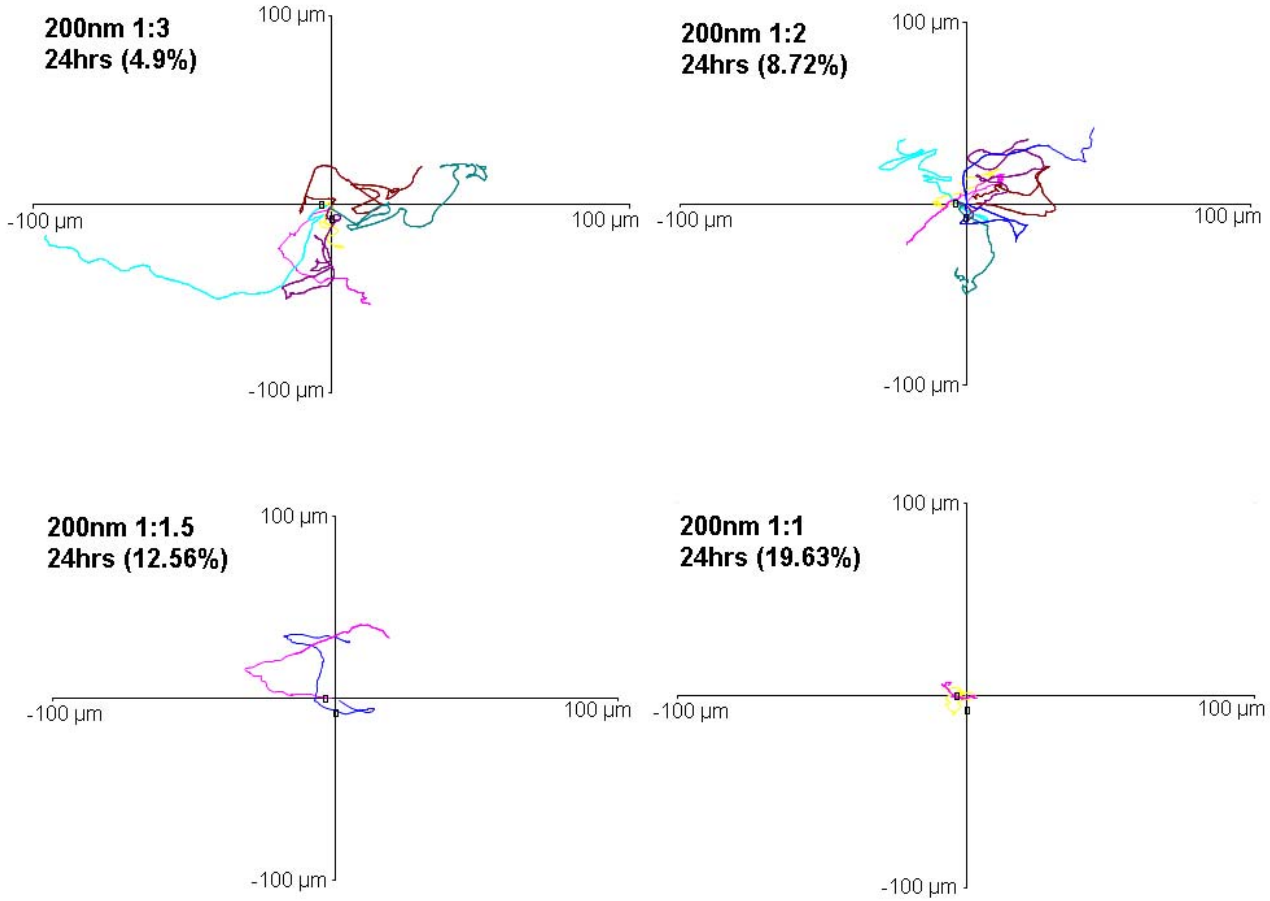

Figure 10.4.3: Cell movement map on nanopatterned surfaces with a constant macroscopic fibronectin density coverage of 8.7%. As the maximum size of the adhesion increased, the distance traveled by the cell also increased. Cells behaved in a more persistent manner on smaller nanopatterns as opposed to a random walk.

10.4.4 MOTILITY AS A FUNCTION OF ADHESION SPACING WITH CONSTANT MAXIMUM ADHESION SIZE

From the previous section, we learned that motility, resembling the decrease in proliferation observed on larger fibronectin adhesion clusters, also decreased when the diameter of the fibronectin cluster was increased. This section investigates the influence on motility of the spacing distance between fibronectin clusters. For this experiment, the adhesion cluster diameter was kept at a constant diameter but the distance between the clusters was varied from 200 nm to 600 nm. As the spacing between the adhesions was increased, the average velocity on the pattern increased (Figure 10.4.4). There is a noticeable decrease in motility between the spacing of 300 nm and 200 nm. A similar transition was also seen in cell spreading in Figure 7.5.4, where cells spaced 200 nm apart had a much greater spreading area than cells spaced 300 nm apart. This could indicate that the cell has greater adhesion to the substrate as the adhesions are brought closer together, but may also mirror the size transition seen for pattern size between 200 and 250 nm. The increased adhesion strength would result in decreased motility and greater cell spreading. A cell movement map was also created for this dataset to show the paths of the tracked cells (Figure 10.4.5). As the spacing between the adhesions was increased, the distance traveled by the cells increased and the movement was more persistent as opposed to a random walk.

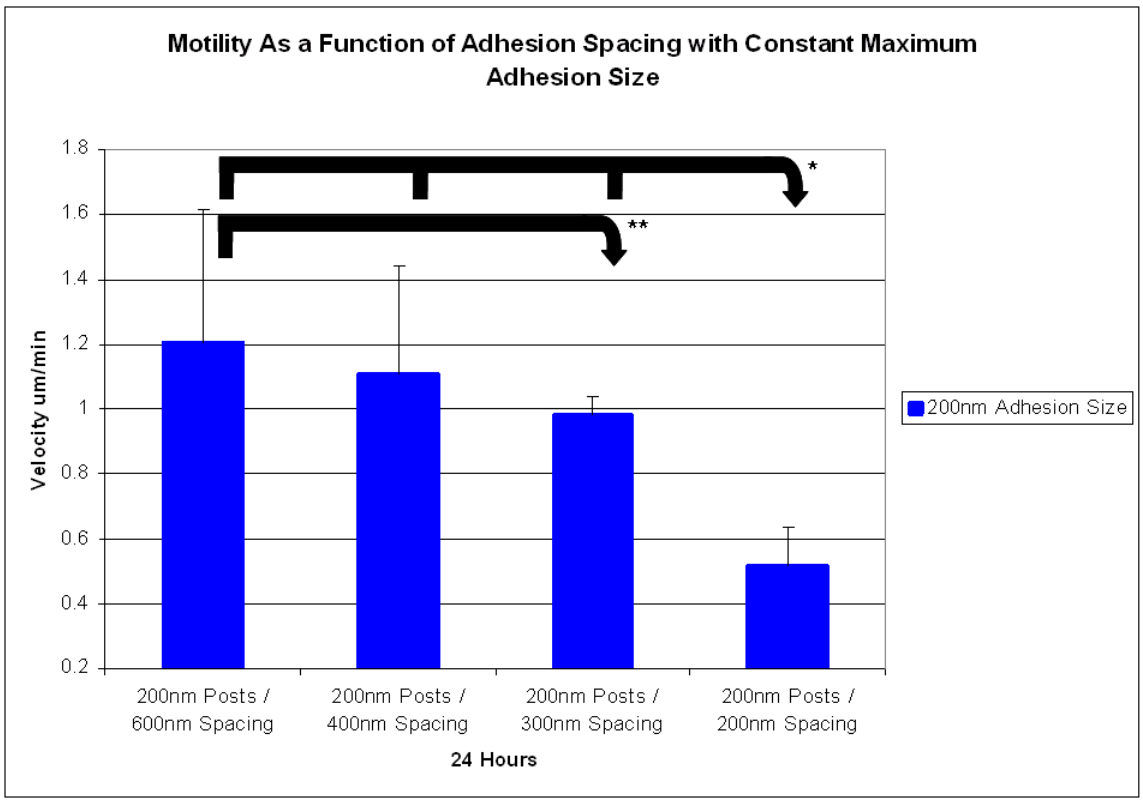

Figure 10.4.4: Motility on nanopatterned surfaces with a constant adhesion size of 200 nm. The spacing of the posts was varied from 600 nm to 200 nm, and a decreasing trend was observed by decreasing spacing with a large decrease between 300 nm and 200 nm. * $p<0.05$ with n= 17. ** $p< 0.05$ (600 nm spacing n=6, 400 nm spacing n=7, 300 nm spacing n=2, 200 nm spacing n=2).

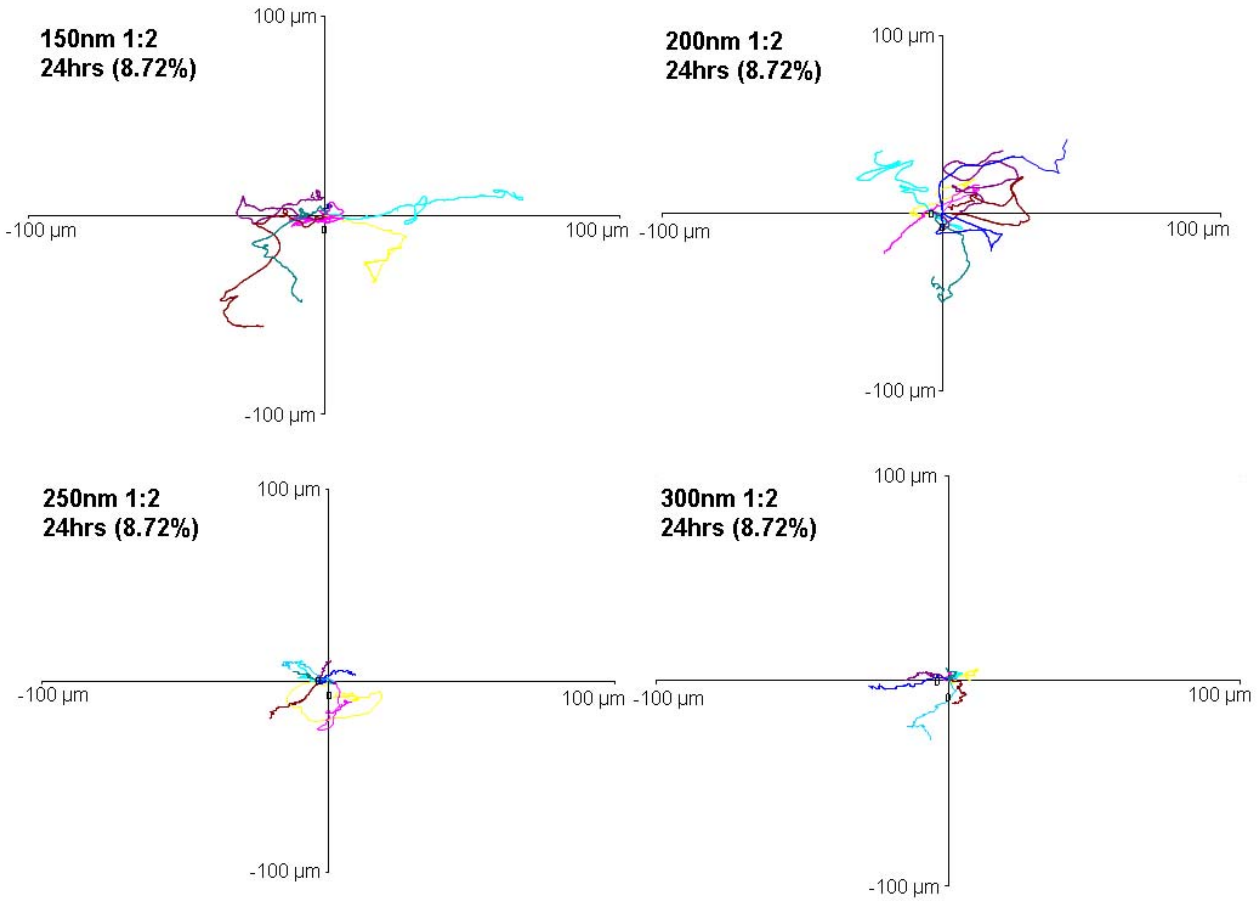

Figure 10.4.5: Cell movement map on nanopatterned surfaces with a constant adhesion size of 200 nm. As the distance between the adhesions was decreased, the distance traveled by the cell also decreased. Cells moved in a more persistent manner on the more closely spaced fibronectin adhesion clusters.

10.4.5 MOTILITY AS A FUNCTION OF MAXIMUM ADHESION SIZE WITH CONSTANT ADHESION SPACING

To separate the influence due to the spacing of adhesion clusters and the size of the adhesive clusters themselves, motility experiments were conducted holding the spacing distance between adhesion clusters constant. In this set of experiments, adhesion clusters were separated by either 300 nm or 600 nm, and the adhesion cluster diameter was then varied. For the equidistant spacing of 600 nm, as shown in Figure 10.4.6, there is a clear velocity dependence on adhesion cluster diameter. For a 200 nm adhesion cluster diameter, the average measured velocity was 1.2 μm/min in comparison to 0.36 μm/min for the 300 nm diameter cluster. In Chapter 7, it was observed that for a constant spacing distance of 600 nm, the cell spreading for the 300 nm diameter adhesions was far greater than the 200 nm diameter adhesions. A greater circularity factor was also obtained for the 300 nm diameter adhesion than the 200 nm diameter adhesions. Similar to the previous section, this could indicate that as the adhesion cluster diameters are increased from 200 nm to 300 nm, the cell might be forming stronger adhesions. In a stronger adhesion context, there would be greater spreading and a morphology and motility similar to controls. Interestingly, in Chapter 9, it was also discovered that increasing the adhesion cluster size from 200 nm to 300 nm resulted in increased proliferation. Thus, there also seems to be a link between the increased motility and increased proliferation by simply changing the adhesion diameter by 100 nm.

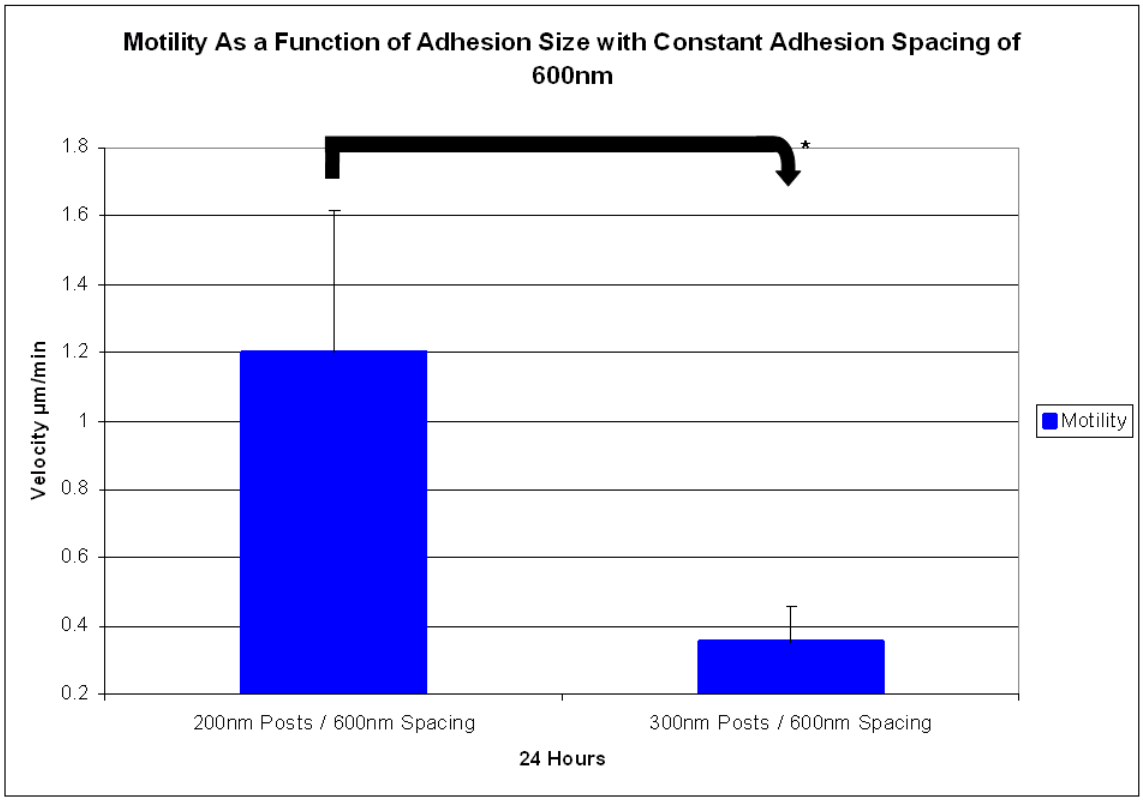

Figure 10.4.6: Motility on nanopatterned surfaces with a constant spacing distance of 600 nm. The size of the posts was varied from 200 nm to 300 nm, and a considerable difference in the motility of the cells was observed. The difference between the motilities is statistically significant with a $p<0.05$. (200 nm n=6, 300 nm n=9).

A similar trend was observed when the distance between adhesion clusters was separated by 300 nm, as shown in Figure 10.4.7. In this case, both 150 nm and 200 nm diameter adhesion clusters showed an increase in motility in comparison to the 300 nm adhesion cluster. It was also demonstrated in Chapter 7 that for a constant cluster separation distance of 300 nm, increasing the diameter of the adhesion cluster from 150 nm to 300 nm resulted in a corresponding increase in cell spreading area and circularity. There was also a downward trend in proliferation, in Chapter 9, as the diameter of the adhesion cluster was decreased from 150 nm to 300 nm. It is interesting

to note the consistent trends among motility, proliferation, cell spreading and circularity that are all dependent on the diameter of the adhesion cluster. They also seem to hold in the case of constant spacing between adhesions for both 300 nm and 600 nm.

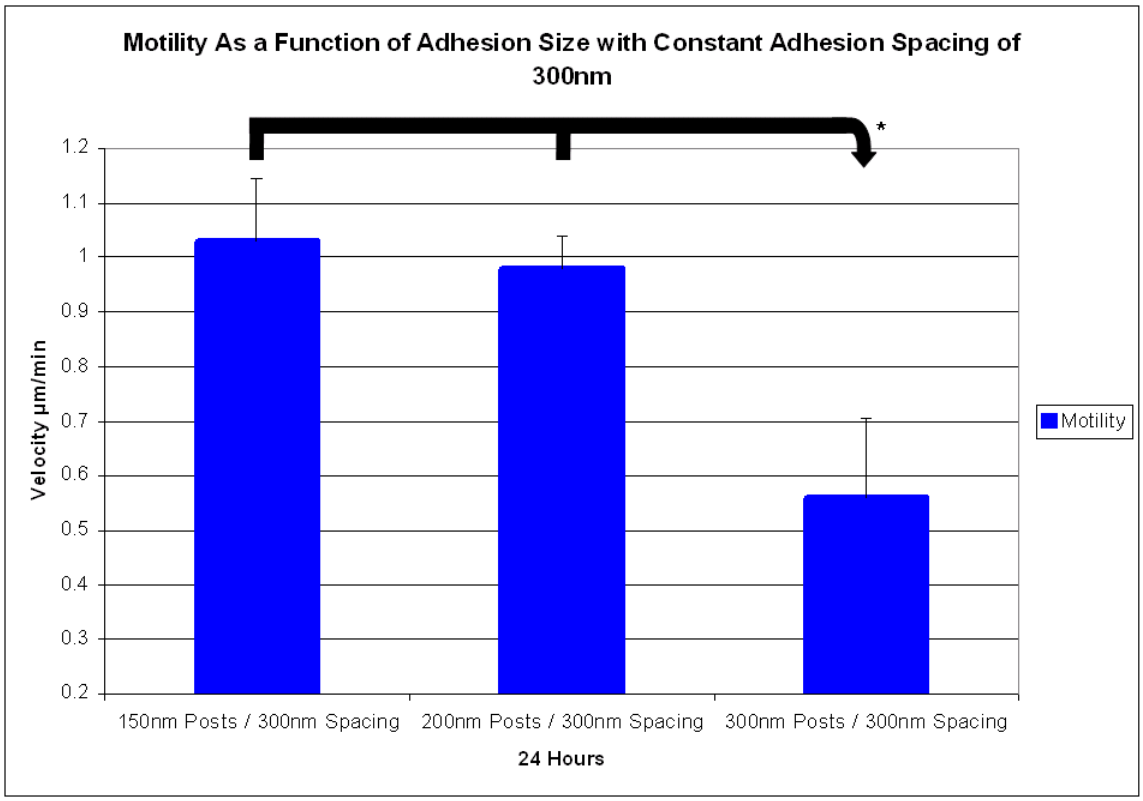

Figure 10.4.7: Motility on nanopatterned surfaces with a constant spacing distance of 300 nm. The size of the posts was varied from 150 nm to 300 nm, and a considerable difference in the motility of the cells was observed. The difference between 150 nm and 200 nm versus 300 nm is statistically significant with a $p<0.05$. (150 nm n=6, 200 nm n=2, 300 nm n=5).

10.5 DISCUSSION

Cellular motility depends on microenvironment cues that are derived from cell-cell signaling, soluble factors and cell-ECM contacts. These signals direct the cell into either a quiescent, non-motile state or motile state. Cell movement is achieved through a

complicated set of cellular processes and regulatory loops that coordinate the structural components of the cell. At the leading edge of the cell, the polymerization of actin produces protrusion which take the form of fillopodia or lamellipodia (Ballestrem, Hinz et al. 2001; Small, Stradal et al. 2002; Wehrle-Haller and Imhof 2003). Contained within these extended portions are focal complexes that connect the actin cytoskeleton to the extracellular matrix. These short lived adhesions are either disassembled or are reinforced to form mature focal contacts or fibrilliar adhesions in order to drive the cell body forward.

It has been shown that the density of ECM proteins, as well as the elasticity of the substrate, influences cellular motility. It is believed that these two factors directly influence the rate of migration by modulating adhesion strength. In experiments using various average densities of ECM ligands, it has been found that motility has a biphasic dependence on the surface concentration (Dimilla, Stone et al. 1993; Huttenlocher, Sandborg et al. 1995). The maximum migration rate is achieved at an intermediate concentration of surface ligands. It has also been shown that integrin expression and integrin-ligand affinity are also correlated with migration speed (Palecek, Loftus et al. 1997). Vinculin stains revealed that the more motile cells had many transient adhesions that did not mature into stable focal adhesions, as seen on stiffer substrates and controls. This finding is consistent with other findings showing that increasing the ECM stiffness strengthens the linkages between integrins and the actin cytoskeleton (Choquet, Felsenfeld et al. 1997). At the interface between a soft and stiff material, cells will demonstrate durotaxis, where they will preferentially move to the stiffer material (Lo, Wang et al. 2000). An explanation for this behavior is that the leading edge of the cell on the stiffer material can form stronger adhesions that allow more force to be transmitted through the substrate causing a pulling effect on the body of the cell (Katz, Zamir et al.

2000). The trailing edge on the soft substrate has weaker adhesions and can detach from the material easier (Sheetz, Felsenfeld et al. 1998). This balance between adhesion forces has been shown on elastic substrates where it has been found that the motility of cells depended on the stiffness of the substrate. For instance, fibroblasts on flexible substrates demonstrated decreased spreading and increased motility velocities in comparison to rigid substrates (Pelham and Wang 1997). Other groups have reported a biphasic dependence, where at very low elasticities and very high elasticities relatively slow motilities are observed, in comparison to the high motility observed on intermediate range elasticities (Discher, Janmey et al. 2005; Peyton and Putnam 2005).

It has been recently shown that adhesion and cytoskeleton protrusion are highly interrelated processes with cellular motility (Gupton and Waterman-Storer 2006). This finding builds upon the biphasic model proposed by Lauffenburger and Horwitz (Lauffenburger and Horwitz 1996). The biphasic model suggests that under low adhesive contexts the cell can not generate traction force, but under high adhesive contexts, the release of adhesions is inhibited. As discussed above, there is an optimal balance of adhesive force. The new finding from Gupton and Waterman-Storer states that actin assembly and disassembly is mediated by fibronectin density and, correspondingly, adhesion strength. On low fibronectin densities, cells have high rates of adhesion assembly and disassembly. The opposite is true for cells on high fibronectin densities. They found that by modulating myosin contractility, they could shift the peak of the biphasic curve which shows the importance of contractile force in relation to motility velocity.

The results from Section 10.4.3 showed that by holding the macroscopic protein density constant at 8.7%, the cells motility was dependent on the diameter of the adhesive cluster. As the diameter of the adhesion was increased, the average velocity of the cells

correspondingly decreased. However, this trend did not appear to be linear. There was a noticeable transition in motile velocity between the adhesive diameters 250 nm and 200 nm at 24 hours. A transition between these two diameters was also observed for the actin cytoskeleton in Figure 8.4.4, where there was a noticeable increase in the percentage of actin in the cell, as measured in a cross section. Additionally, it is present in the proliferation data presented in Figure 9.6.1, where the average growth rate decreases. Thus, there is size threshold between cluster diameters of 200 nm and 250 nm that appears to trigger changes in motility, actin cytoskeletal structure and proliferation. This threshold appears to result in stronger adhesions to the surface, as evidenced by the increased cytoskeletal formation. The stronger adhesions may result in hindering of the trailing edge detachment of the cell causing a decrease in the velocity of the cell. The exact relationship between these two and proliferation is not known, but all three have FAK as a signaling constituent. It is possible that the size threshold between 250 nm and 200 nm might be related to the way FAK is activated in the adhesion.

Since the spacing between the fibronectin clusters in the constant density experiments was adjusted to maintain a constant macroscopic protein density, it was also desirable to conduct experiments holding the spacing distance constant while varying the adhesion size. The results from this study indicated that independent of cluster distance, the diameter of the adhesion cluster was a determining factor in motility. As the diameter of the cluster was decreased, the motility increased. Additionally, it was also noted that in previous experiments cell spreading and circularity decreased and proliferation increased for increased motility when holding the spacing between clusters constant. These results are then consistent to those found in the constant density experiments.

In contrasting these results with those on elastic substrates, one expects cells on softer substrates to have higher average velocities. It is also expected that the force

transduced through the adhesions on softer substrates will be less than that on rigid substrates. The experiments in this chapter found that smaller clusters resulted in higher motile velocities. From the actin experiments, it was shown that cells on smaller cluster sizes had fewer stress fibers and generally had a less developed actin cytoskeletons. These results suggest that the total stress developed by the cell is less on surfaces where the adhesion clusters are smaller. The higher motility observed on these patterns would then be consistent with the findings on soft substrates. Restricting the size of the integrin clusters results in weaker ECM to actin linkage and less developed cytoskeletons. This causes smaller, dynamic adhesions to form that are easily detached from the surface during migration. The overall cell is less anchored to the surface, which results in higher motilities on smaller patterns similar to soft substrates.

REFERENCES

Ballestrem, C., B. Hinz, et al. (2001). "Marching at the front and dragging behind: differential alpha-V beta 3-integrin turnover regulates focal adhesion behavior." Journal of Cell Biology **155**(7): 1319-1332.

Choquet, D., D. P. Felsenfeld, et al. (1997). "Extracellular matrix rigidity causes strengthening of integrin-cytoskeleton linkages." Cell **88**(1): 39-48.

Dimilla, P. A., J. A. Stone, et al. (1993). "Maximal Migration of Human Smooth-Muscle Cells on Fibronectin and Type-Iv Collagen Occurs at an Intermediate Attachment Strength." Journal of Cell Biology **122**(3): 729-737.

Discher, D. E., P. Janmey, et al. (2005). "Tissue cells feel and respond to the stiffness of their substrate." Science **310**(5751): 1139-1143.

Gupton, S. L. and C. M. Waterman-Storer (2006). "Spatiotemporal feedback between actomyosin and focal-adhesion systems optimizes rapid cell migration." Cell **125**(7): 1361-1374.

Huttenlocher, A., R. R. Sandborg, et al. (1995). "Adhesion in Cell-Migration." Current Opinion in Cell Biology **7**(5): 697-706.

Katz, B. Z., E. Zamir, et al. (2000). "Physical state of the extracellular matrix regulates the structure and molecular composition of cell-matrix adhesions." Molecular Biology of the Cell **11**(3): 1047-1060.

Kouvroukoglou, S., K. C. Dee, et al. (2000). "Endothelial cell migration on surfaces modified with immobilized adhesive peptides." Biomaterials **21**(17): 1725-1733.

Lauffenburger, D. A. and A. F. Horwitz (1996). "Cell migration: A physically integrated molecular process." Cell **84**(3): 359-369.

Lo, C. M., H. B. Wang, et al. (2000). "Cell movement is guided by the rigidity of the substrate." Biophysical Journal **79**(1): 144-152.

Palecek, S. P., J. C. Loftus, et al. (1997). "Integrin-ligand binding properties govern cell migration speed through cell-substratum adhesiveness." Nature **385**(6616): 537-540.

Pelham, R. J. and Y. L. Wang (1997). "Cell locomotion and focal adhesions are regulated by substrate flexibility." Proceedings of the National Academy of Sciences of the United States of America **94**(25): 13661-13665.

Peyton, S. R. and A. J. Putnam (2005). "Extracellular matrix rigidity governs smooth muscle cell motility in a biphasic fashion." Journal of Cellular Physiology **204**(1): 198-209.

Sheetz, M. P., D. P. Felsenfeld, et al. (1998). "Cell migration: Regulation of force on extracellular-matrix-integrin complexes." Trends in Cell Biology **8**(2): 51-54.

Small, J. V., T. Stradal, et al. (2002). "The lamellipodium: where motility begins." Trends in Cell Biology **12**(3): 112-120.

Wehrle-Haller, B. and B. A. Imhof (2003). "Actin, microtubules and focal adhesion dynamics during cell migration." International Journal of Biochemistry & Cell Biology **35**(1): 39-50.

CHAPTER 11: FIBRILLOGENESIS

11.1 OVERVIEW

Fibrillogenesis is an important part of the cellular interaction with the ECM. This chapter will investigate fibronectin reorganization and fibrillar formation on the nanopatterned surfaces. The nanoclustered fibronectin patterns are an interesting platform to study this phenomenon because of the level of control over the size and spacing of fibronectin. This provides a view of fibril formation that cannot be obtained in other systems.

11.2 METHODOLOGY

Silicon samples were prepared and functionalized according to the protocols presented in Chapter 5. Samples were immersed in ETOH (AAPER) for 5 minutes to sterilize the samples before being introduced into a sterile culture hood. Samples were then rinsed 60 seconds, three times in a HEPES buffered saline that was prepared from 11.9 g (HEPES)(Sigma), 5.8 g NaCl (Mallinkckrodt) and 1000 ml DI and adjusted to 7.5 pH with NaOH (Sigma). 125 μL of a 10 μg/ml fibronectin solution (Sigma) in 50 mM HEPES buffered saline was placed on the samples for 20 minutes at room temperature. The samples were then thoroughly rinsed in 50ml of HEPES buffered saline solution for 60 seconds 3 times to remove any excess fibronectin. The cells in all the studies were human umbilical vein endothelial cells (HUVECs) (Cambrex, Walkersville, MD) of passage below 4 and cultured according to manufactures specifications. They were cultured in T-25 tissue culture flasks coated with 30 μg of human plasma fibronectin (Sigma, Saint Louis, MO) at 37 ºC and 5% CO_2 until 80% confluence. During culture and experiment, the HUVECs were bathed in endothelial growth media

(Cambrex, Walkersville, MD) supplemented with 2% fetal bovine serum, 0.5 ml human endothelial growth factor, 0.5 ml Hydrocortisome, 0.5 ml GA-1000 (Gentamicin, Amphotericin B). To release cells from flasks for cell seeding, the flasks were first rinsed with 5 ml of HEPES buffered saline at 37 ºC. They were then trypsinized using 3ml of Trypsin/EDTA (Cambrex) for 5mins at 37 ºC and 5% CO_2. Next, 3 ml of trypsin neutralizing solution (Cambrex) was added to the cell suspension to neutralize the Trypsin/EDTA. The cell suspension was pelleted using a centrifuge set to 240 g for 6 minutes. The cells were then resuspended in 10ml of endothelial growth media (Cambrex) discussed above. A hemocytometer and trypan blue dye was used to determine the total living cell population in the resuspension. The HUVECs were then seeded on the sample surface at approximately 7 cells/mm^2. The cells were maintained in 20 ml of endothelial growth media (Cambrex), 37 ˚C and 5% CO_2 for 24 hours. The cells were fixed by first immersing them in a cold cytoskeleton buffer (0.5% Triton X-100, 100 mM NaCl, 300 mM sucrose, 3 mM MgCl2, 10 mM HEPES, pH 6.8) at 4 ºC for 1 minute, and then immersing them in 5% formaldehyde at 4 ºC and then letting the solution warm up by placing in 37 ºC water bath for 10 minutes. The surfaces were then rinsed with warm HEPES and covered with 125 µL of a 10% goat serum (Sigma) in PBS (Lonza) for 30 min at room temperature to block unspecific binding of antibodies. After rinsing with HEPES, the samples were then dressed with 125 µL PBS solution of 6 µg/ml fibronectin antibody (Abcam) and 1% by volume FITC-conjugated mouse anti-vinculin (Sigma) in 1.0% BSA supplemented with 0.1% Tween-20 for 12 hours at 4 ºC. Afterwards, the samples were washed with rocking three times in PBS (Lonza) supplemented with 0.01% Tween-20 for 5 minutes each wash to remove any unbound anti-bodies. Next, 125 µL of a 2.6 µg/ml goat anti-rabbit secondary antibody labeled with marina blue (Invitrogen - Alexa Fluor 365) was dispensed onto the sample and left

for 1 hr at room temperature. The samples were washed with rocking three times in PBS (Lonza) supplemented with 0.01% Tween-20 for 5 minutes each wash to remove any unbound anti-bodies. Lastly, the samples were rinsed with DI H_2O to remove any salt residue and dried with nitrogen. Coverslips were mounted to the samples using gold antifade reagent (Invitrogen). Fluorescent images were acquired using an oil immersion Carl Zeiss ApoTome inverted microscope.

11.3 BACKGROUND

Fibrillogenesis describes the process by which a cell assembles fibronectin into fibrils and is important part of building the ECM. As was discussed in Chapter 6, upon initial engagement of integrins to a fibronectin cluster, a transient adhesion is formed named a focal complex, which either disassembles or matures into a larger entity known as a focal adhesion (Geiger and Bershadsky 2001; Geiger, Bershadsky et al. 2001; Miriam Cohen 2004; Zaidel-Bar, Cohen et al. 2004). A focal adhesion can then transform into fibrillar adhesion, which is important for the formation of fibronectin fibrils (Geiger, Bershadsky et al. 2001). This chapter will be investigating the formation of fibronectin fibrils and fibronectin reorganization in relation to nanocluster size.

The fibronectin molecule is described in terms of thee subunits named FN-I, FN-II and FN-III. The main cellular binding site on fibronectin is located on the FN-III-10 subunit and consists of the well known RGD attachment sequence and an adjacent synergy site located on the FN-III-9 subunit (Wierzbicka-Patynowski and Schwarzbauer 2003). Fibrillogenesis is mainly mediated by α5β1 integrins on the cell surface that bind to the RGD sequence (Mao and Schwarzbauer 2005). In addition to the cellular binding site, the molecule also has additional FN-FN binding domains along the molecule (Homandberg and Erickson 1986; Aguirre, McCormick et al. 1994; Bultmann, Santas et

al. 1998). These sites are hidden along the molecule when it is in a compact form on the surface. As the fiber is stretched, its conformation changes and this exposes the hidden FN-FN binding domains. As previously stated, fibronectin is a particularly elastic molecule, which can be stretched by cells up to four times its compacted length (Ohashi, Kiehart et al. 1999). It also can be deformed, for instance during cell motility, and the molecule does not rupture.

Fibronectin fibril assembly depends on the mechanical contractility of the cytoskeleton to stretch the fibrils. It has been shown that an α5β1 integrin ligated to a fibronectin molecule will translocate from a stationary focal adhesion along an actin fiber while pulling on the fibronectin molecule (Pankov, Cukierman et al. 2000). This process forms fibrillar adhesions and allows the ligated integrins to transduce actin-myosin generated force to the fibronectin molecules. Once stretched, the fibronectin molecules can interact with one another through FN-FN binding domains to form a fibril.

11.4 FIBER DIAMETER DEPENDS ON PATTERN SIZE

A theme through this dissertation has been the influence of cellular behavior by nanoscale clustering of fibronectin. Through the static and dynamic cell experiments, it has been concluded that nanoscale clustering of integrins does have an affect on cellular behavior. Fibronectin experiments were conducted to try to understand if there are any differences in the way a cell stretched or reorganized the fibronectin that could provide additional information about what was driving the observed changes.

In Chapter 6, it was demonstrated that that nanoscale clustering of fibronectin limited the maximum size of focal adhesion formation. If focal adhesion formation was restricted, then there was the possibility that fibril diameter may also be restricted. However, since it is the maturation of focal adhesions into fibrillar adhesions that is

responsible for the formation of fibronectin fibrils, it could also be possible that the cells would stretch multiple fibers into one large bundle. This would be similar to the actin results, where many small fibers were bundled together to form the peripheral band of the cell.

The fibronectin experiments were conducted at a constant macroscopic fibronectin density of 8.72%, and the diameters of the fibronectin clusters were varied from 150 nm to 300 nm. It was desired to use a constant macroscopic density so that all of the cells had access to the same number of fibronectin, 227 FN per μm^2, to assemble fibers. If different densities would have been used, then cells on a higher density would have more accessible fibronectin than cells on lower densities. Cells were seeded onto the surfaces and incubated for 24 hours before being fixed and stained for fibronectin and vinculin. The results from these experiments are shown below in Figure 11.4.1.

On control surfaces, the cells built elaborate fibrillar matrixes with the width of the fibrils in the range of 600 nm to 740 nm. The fibrillar networks on controls were denser than those on the nanopatterned surfaces. On the nanopatterned surfaces, fibronectin fibrils could be seen that originated on one cluster and terminated on another. The diameters of the fibrils were on the order of the diameter of the patterned fibronectin cluster. In overlaying a vinculin stain, it was noted that all of the vinculin clusters aligned with fibronectin clusters and 'dash' adhesions aligned with fibrils. However, fibrils were present were there were no vinculin clusters. This is due to two reasons. After a fibril has been stretched, it will persist in a stretched form for a duration of time even though a cell is no longer attached to the fibril. Thus, the fibronectin stains also provide historical information about what the cell was previously doing. Secondly, in well developed fibrillar adhesions vinculin is in a much lower concentration than in focal

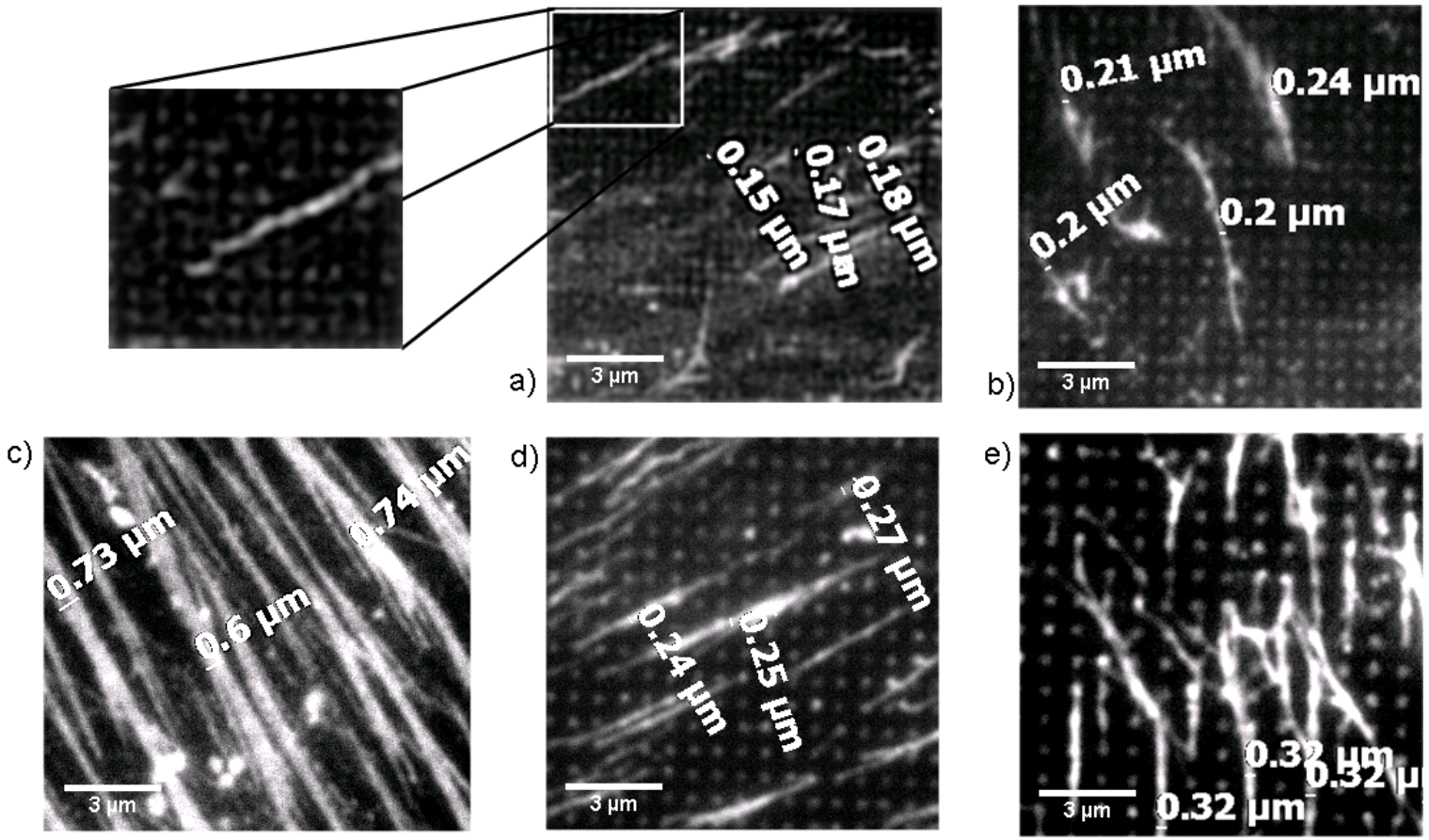

Figure 11.4.1: Immunofluorescent labeling of fibronectin fibrils 24 hours after cell seeding. Measurement labels are fiber widths. c) Control surfaces have a well developed fibronectin fibrillar matrix and the diameters of the fibrils are in the range of 600 nm to 750 nm. a) 150 nm adhesions with a sparse distribution of thin fibrils that are on the order of pattern diameter b) 200 nm adhesions with fibril diameters approximately the width of the clusters d) 250 nm adhesions e) 300 nm adhesions with a denser fibril network.

adhesions. On the 150 nm pattern, the fibrils were very sparse and thin compared to other patterns (Figure 11.4.1). The labels correspond to the measured widths of fibrils that had corresponding dash adhesions. The fibril diameter on the 150 nm pattern had widths between 150 nm and 180 nm. In the magnified portion of the figure, a fibril can be clearly seen that stretches across a number of fibronectin clusters, but its width is on the range of the underlying cluster. On the 200 nm pattern, the fibril formation was similarly sparse but the diameters of the fibrils were larger. On the 250 nm clusters, the fibers were directionally aligned, were greater in number and the widths were approximately 250 nm. Lastly, on the 300 nm patterns, it can clearly be seen that cells are pulling fibers in alignment to the pattern, and the width of these fibers are directly proportional to the underlying 300 nm diameter fibronectin clusters.

11.5 FOOTPRINTS IN THE SAND

It was discovered that fibronectin fibrils persisted on the surface for a duration of time even after the cell was no longer attached to them. Thus, fibronectin stains provided historical information about how the cell remodeled the fibronectin on the substrate surface. Dual stains with vinculin and fibronectin, allowed us to separate the historical information from information at the time of fixing because the vinculin stain identified how the cell was attached to the substrate when the cell was fixed. This was particularly interesting in the case of cell motility where there was a well defined leading and trailing edge.

As discussed in the last chapter, cell motility is achieved through a set of cellular processes and regulatory loops that coordinate the structural components of the cell. At the leading edge of the cell, the polymerization of actin produces protrusions which take the form of fillopodia or lamellipodia (Ballestrem, Hinz et al. 2001; Small, Stradal et al.

2002; Wehrle-Haller and Imhof 2003). Contained within these extended portions are focal complexes that connect the actin cytoskeleton to the extracellular matrix. These short lived adhesions are either disassembled or are reinforced to form mature focal contacts or fibrilliar adhesions in order to drive the cell body forward. In the process of driving the cell body forward, the actin generated pulling force is transduced through the integrins to the underlying fibronectin matrix (Katz, Zamir et al. 2000). In the case of fibrillogenesis, the force transmitted through an α5β1 integrin ligated to a fibronectin causes the fibronectin molecule to extend, exposing FN-FN binding domains that can then bind with other fibronectin molecules to form a fibril. At the trailing edge of the cell, adhesions must release from the stressed ECM in order for the trailing edge to retract.

The nanopatterned surfaces provide a unique way to look at this process because the initial focal complexes and focal adhesions are limited by the size of the nanopatterned cluster diameter. Additionally, the fibrils are also restricted in width to the cluster which they are stretched from, which makes it easy to identify which direction the cell was applying force. For this experiment, cells were seeded on a 300 nm 1:3 pattern and dual stained for fibronectin and vinculin. This particular pattern was chosen because the pattern is easily viewable at lower magnifications, 40X and 50X, allowing the entire cell plus the surrounding area to be captured in a single frame. This allows a macroscopic view of the fibronectin reorganization by the cell.

Figure 11.4.2 shows a HUVEC migrating along the border of the 300 nm 1:3 pattern, with the bottom black portion being a homogenous layer of PEG. The vinculin stain is shown in green, which shows the adhesions, nucleus and outline of the cell. The fibronectin stain is shown in blue and the underlying nanopatterned clusters are clearly visible in addition to fibronectin fibril formations. The direction of the cell was

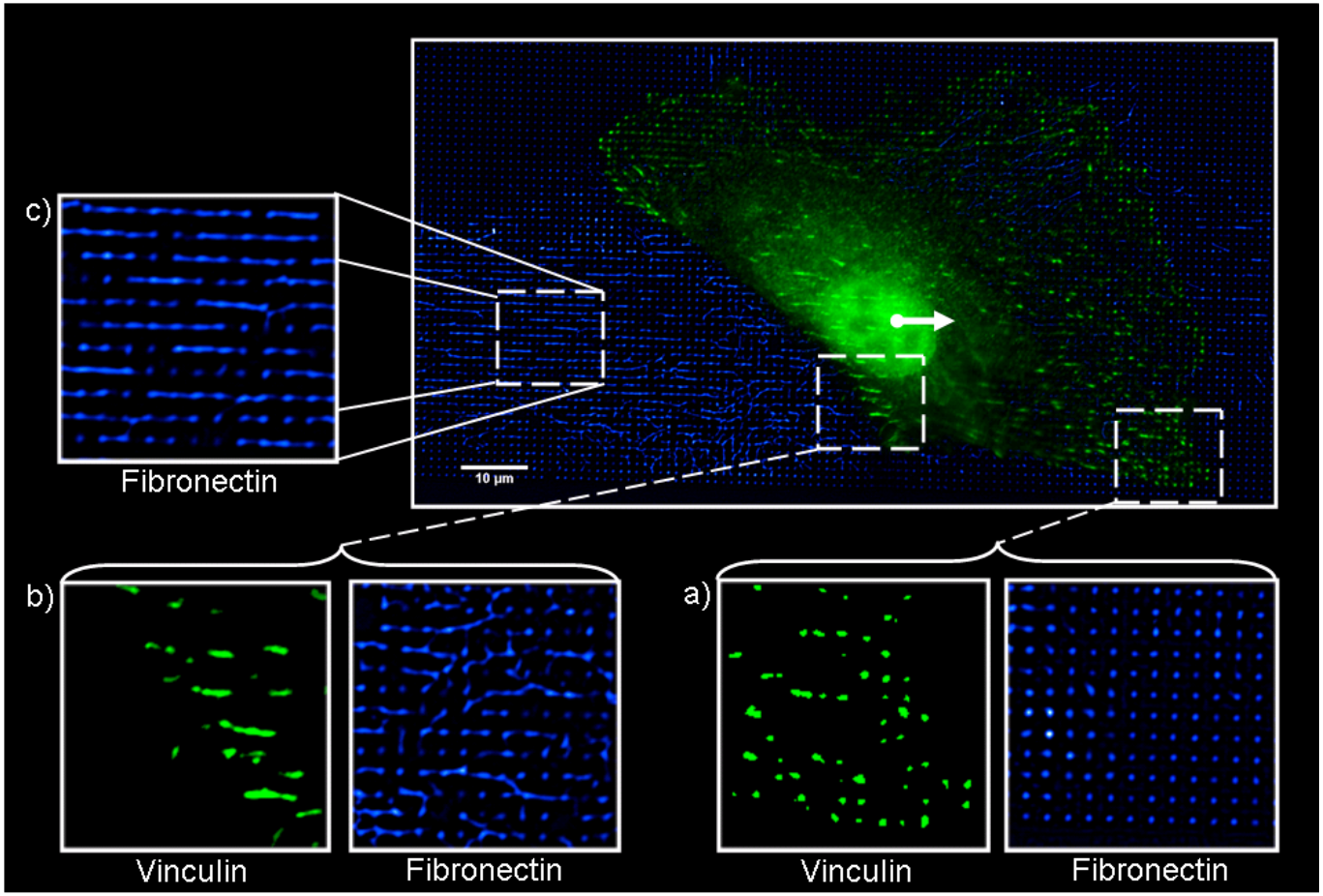

Figure 11.4.2: Immunofluorescent labeling of fibronectin (blue) and vinculin (green) 24 hours after cell seeding on a 300 nm 1:3 nanopattern. The leading edge of this motile cell can be seen extending to the right. The trailing ledge is to the left and marked by the presence of stretched fibronectin. a) The leading edge is composed of focal complexes and focal adhesions. The underlying fibronectin has not been stretched into fibrils. b) Dash adhesions can be seen in the trailing edge and are localized with fibronectin fibrils. c) The cell leaves 'tracks' in the fibronectin. Fibrils are oriented in the direction of cell travel.

determined by the morphology of the cell, adhesion distribution, historical information contained in the fibronectin and the bordering effect of the PEG. The morphology of the cell is typical of a motile cell, where there is a clear leading and trailing edge. The adhesion distribution on the leading edge consists of a dense distribution of focal adhesions and focal complexes. Notice in part (a) of the figure how the adhesions are uniformly distributed across the nanopatterned surface. These early adhesions are limited in size by the diameter of the underlying fibronectin clusters. Additionally, the minimum separation distance between the adhesions is also controlled by the spacing of the fibronectin clusters. An overlay of the vinculin image and the fibronectin image show that the vinculin is located directly on the fibronectin clusters. The right hand image shows the orderly arrayed fibronectin clusters that have not been stretched into fibrils. The leading edge of the cell mainly extends to the right half, but the top portion of the cell also shows early adhesions and unstretched fibronectin. Directionality of the cell can also be determined from the historical information contained in the fibronectin. Fibronectin to the right and to the top of the cell have not been remodeled indicating that the cell has not been in these areas. The left part of the cell clearly shows remodeled fibronectin indicating the cell has been in that area. Furthermore, the portion below the cell is the non-adhesive PEG border which prevents the cell from moving south. Part (b) of the figure shows a magnified region of the trailing edge of the cell. In this area dash adhesions can be seen which were only observed in the trailing edge and did not appear in other regions of the cell. Underlying the dash adhesions were stretched fibronectin fibrils. The widths of the fibrils were on the order of the fibronectin cluster diameters. The individual fibers begin on one fibronectin cluster and then are stretched to adjacent clusters. The stretching from one cluster to the next forms the basis of a fibronectin fibril. In the overlay, it is clear that there are stretched fibrils that are not bound to the

cell as investigated by vinculin. It should also be noted that the vinculin clusters appear slightly enlarged over their true size. Due to the low magnification at which the images were captured and the high background fluorescence, it was difficult to threshold the vinculin without some enlargement of the clusters. Images that are taken at a higher magnification, such as 160X, show that the vinculin cluster size is smaller and on the range of the fibronectin clusters, as shown in Section 6.6. In part (c), stretched fibronectin can be seen aligned in the direction of the cell movement. This area provides a historical perspective on the approximate direction of force that was applied to the fibril by the cytoskeleton. As a macroscopic generalization, the majority of the fibrils left behind the cell are oriented in the direction of cellular movement. This shows that the cell is applying force on the fibrils in the direction that it is traveling.

11.6 FOOTPRINTS DON'T LAST FOREVER

The fibronectin fibrils formed by the cell are transient structures that dissolve or relax back to their clustered state. This behavior can be captured by looking at 'tracks' that the cell leaves on the surface as it migrates. In the case of the cell investigated in the previous section, a low magnification image of the track is shown in Figure 11.4.3. Two different lengths were labeled on this image. The 70 μm length corresponds to the distance that a majority of fibrils could be observed including randomly oriented fibrils. After 70 μm, there is a gap of approximately 50 μm, where little if any stretched fibrils are visible. Between 120 μm and 160 μm, several long fibronectin fibrils are visible that are oriented in the direction of the cell movement. However, no randomly oriented fibrils are visible. This may indicate that fibrils that are oriented in the direction of cell movement or where the cell was exerting a directional force to propel itself are more stable than fibers not associated with forces in the direction of cellular movement.

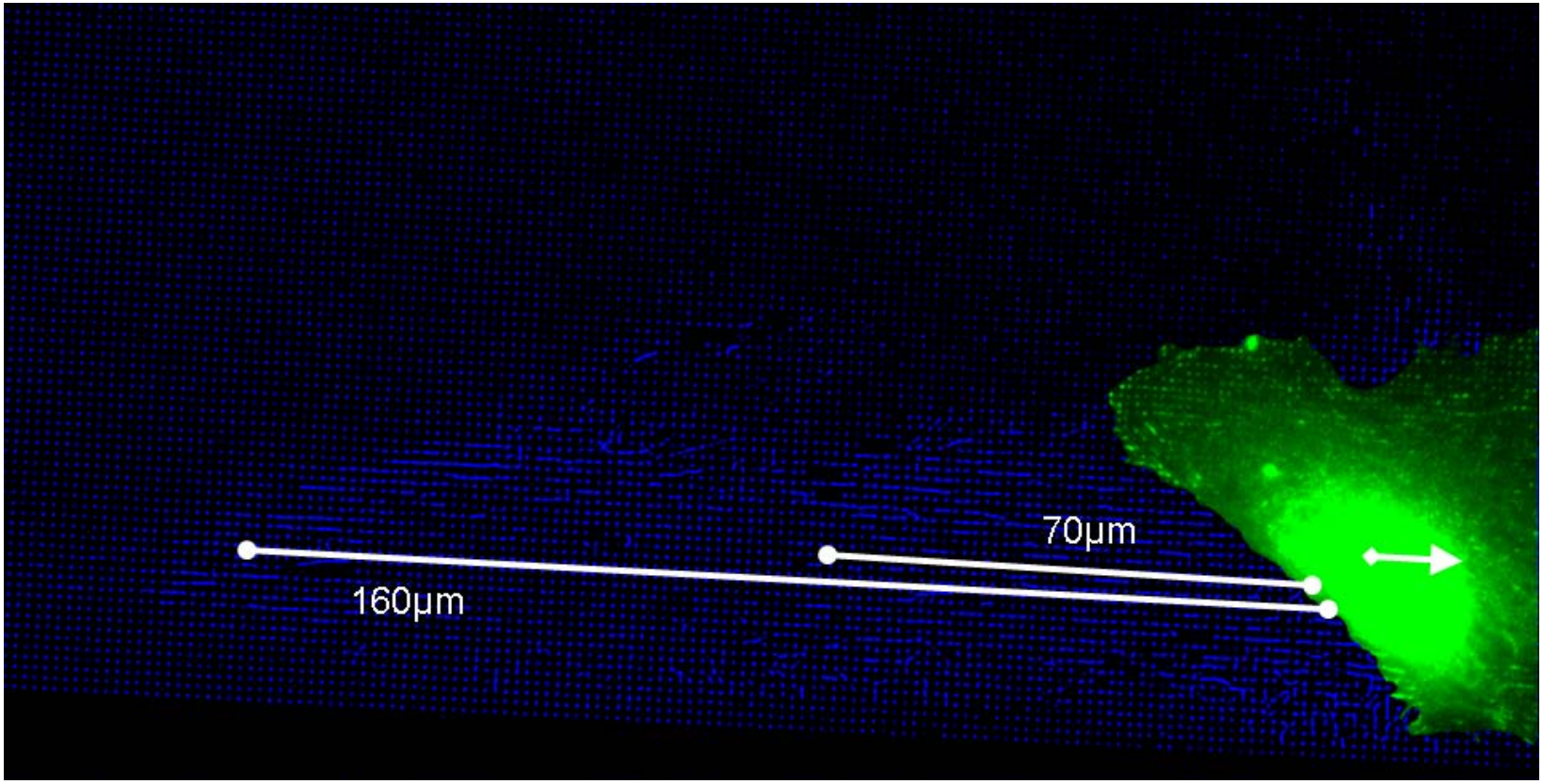

Figure 11.4.3: Immunofluorescent labeling of fibronectin (blue) and vinculin (green) 24 hours after cell seeding on a 300 nm 1:3 nanopattern. This image shows a trail of aligned fibronectin behind a motile cell. The majority of the fibrils are within 70 µm of the trailing edge of the cell. There is then a 50 µm gap with few fibrils followed by an area 120 µm to 160 µm where some aligned fibrils are visible again. Randomly oriented fibrils only appear in the area 70 µm behind the cell.

In the motility experiments covered in Chapter 10, it was discovered that the average cell velocity for a HUVEC on a 300 nm 1:3 pattern was 1.0 μm/min. Using this data, a rough figure can be calculated about the lifetime of the fibrils on the nanopattern surface. The bulk portion of the trail left by the cell is encompassed in the 70 μm region, which would put the lifetime fibril duration at a little over an hour for most fibrils. However, the presence of fibrils in the region between 120 μm and 160 μm shows that they may persist on the surface at least 2 to 2.5 hours.

11.6 DISCUSSION

The nanopatterned surfaces provide an interesting way to look at fibrillogenesis and fibronectin reorganization. The diameter of the fibronectin cluster was shown to restrict both the size of the focal adhesions as well as the width of the fibrils that could be formed. Stained fibronectin clearly revealed that fibrils start at one adhesion cluster and terminate at another, often spanning more than one cluster. This provided an interesting way to look at fibril formation at the length scales of an average focal adhesion complex and also provided a way to visualize the directionality of forces applied by the cell. An example of this was provided in the analysis of a cell on a 300 nm 1:3 pattern, which captured a number of factors regarding cellular motility on nanopatterned surfaces. The leading edge of the cell was found to be populated with focal adhesions and focal complexes which were limited in size by the diameter of the underlying fibronectin cluster. In general the leading edge of the cell did not appear to form fibronectin fibrils. In contrast, the trailing edge of the cell was marked by long dash adhesions which were aligned with the underlying fibrils. Tracks left in the fibronectin by the cell showed fibrils that were aligned in the direction of the cell movement. However, the fibronectin

fibrils had a finite lifetime and were only found to extend a finite distance from the rear of the cell.

REFERENCES

Aguirre, K. M., R. J. McCormick, et al. (1994). "Fibronectin Self-Association Is Mediated by Complementary Sites within the Amino-Terminal One-Third of the Molecule." Journal of Biological Chemistry **269**(45): 27863-27868.

Ballestrem, C., B. Hinz, et al. (2001). "Marching at the front and dragging behind: differential alpha-V beta 3-integrin turnover regulates focal adhesion behavior." Journal of Cell Biology **155**(7): 1319-1332.

Bultmann, H., A. J. Santas, et al. (1998). "Fibronectin fibrillogenesis involves the heparin II binding domain of fibronectin." Journal of Biological Chemistry **273**(5): 2601-2609.

Geiger, B. and A. Bershadsky (2001). "Assembly and mechanosensory function of focal contacts." Current Opinion in Cell Biology **13**(5): 584-592.

Geiger, B., A. Bershadsky, et al. (2001). "Transmembrane extracellular matrix-cytoskeleton crosstalk." Nature Reviews Molecular Cell Biology **2**(11): 793-805.

Homandberg, G. A. and J. W. Erickson (1986). "Model of Fibronectin Tertiary Structure Based on Studies of Interactions between Fragments." Biochemistry **25**(22): 6917-6925.

Katz, B. Z., E. Zamir, et al. (2000). "Physical state of the extracellular matrix regulates the structure and molecular composition of cell-matrix adhesions." Molecular Biology of the Cell **11**(3): 1047-1060.

Mao, Y. and J. E. Schwarzbauer (2005). "Fibronectin fibrillogenesis, a cell-mediated matrix assembly process." Matrix Biology **24**(6): 389-399.

Miriam Cohen, D. J. B. G. L. A. (2004). "Spatial and Temporal Sequence of Events in Cell Adhesion: From Molecular Recognition to Focal Adhesion Assembly." ChemBioChem **5**(10): 1393-1399.

Ohashi, T., D. P. Kiehart, et al. (1999). "Dynamics and elasticity of the fibronectin matrix in living cell culture visualized by fibronectin-green fluorescent protein." Proceedings of the National Academy of Sciences of the United States of America **96**(5): 2153-2158.

Pankov, R., E. Cukierman, et al. (2000). "Integrin dynamics and matrix assembly: Tensin-dependent translocation of alpha(5)beta(1) integrins promotes early fibronectin fibrillogenesis." Journal of Cell Biology **148**(5): 1075-1090.

Small, J. V., T. Stradal, et al. (2002). "The lamellipodium: where motility begins." Trends in Cell Biology **12**(3): 112-120.

Wehrle-Haller, B. and B. A. Imhof (2003). "Actin, microtubules and focal adhesion dynamics during cell migration." International Journal of Biochemistry & Cell Biology **35**(1): 39-50.

Wierzbicka-Patynowski, I. and J. E. Schwarzbauer (2003). "The ins and outs of fibronectin matrix assembly." Journal of Cell Science **116**(16): 3269-3276.

Zaidel-Bar, R., M. Cohen, et al. (2004). "Hierarchical assembly of cell-matrix adhesion complexes." Biochemical Society Transactions **32**: 416-420.

CHAPTER 12: CONCLUSIONS AND FUTURE WORK

12.1 CONCLUSIONS

The nanopatterned cell culture system developed in this work can potentially play a similar role for bioengineering and biotechnological applications on the nanometer scale as soft-lithography plays on the micron scale. Large samples of complex nanopatterns of variable pattern density can be fabricated inexpensively and quickly to achieve patterns of two materials that can be converted into well-defined biofunctionality patterns by surface conjugation chemistry. Although gold and SiO_2 were used to demonstrate orthogonal surface functionalization, materials other than gold could be used with this technique as well. Surfaces created with NOBIL are not limited to nanopatterned cell culture substrates but are also applicable to creating biosensors with nanometer-sized elements. For instance, nanosensors could be fabricated with functionalized gold as the sensing unit. The development of a highly ordered nanopatterned cell culture system opens up many opportunities for studying nanoscale surface interactions.

To show applicability of this technique, it was used to create disposable large scale arrays of nanopatterned cell adhesion proteins for cell culture for the purpose of investigating the influence of nanoscale geometrical parameters on cell-surface interactions. These cell culture arrays were used to systematically vary the size, spacing and density of fibronectin adhesion clusters, which were expected to modulate the signaling induced by the cell adhesion, the clustering of adhesion molecules and the force generated in the cytoskeleton. Using the orthogonal biofunctionalization procedure developed in NOBIL, fibronectin was nanopatterned onto a substrate with a desired size

and distribution. Areas surrounding the fibronectin were passivated with a layer of PEG. This produced well defined adhesion clusters and prevented cellular binding outside of a defined area. The design of the disposable cell culture system allowed for various cluster arrangements and sizes to be investigated on a single experimental chip.

To verify that adhesion size could be controlled by the nanopatterned surfaces, dual fibronectin and vinculin immunofluorescence labeling was used. The results from these experiments showed that early focal complexes were indeed restricted by the size of the nanoscale fibronectin clusters. As the adhesions matured and began to exert a significant contractile force in the cytoskeleton and stretching force on the fibronectin clusters, the fibronectin developed fibrils bridged across several patterns while the diameter of the fibrils stayed constant with the diameter of the patterned fibronectin cluster. Consequently, the associated dash focal adhesions also had a cross section similar to the diameter of the fibrils. As the size of the nanoclusters was decreased, the number of dash adhesions also progressively decreased. The conclusion for these studies indicated that focal complexes and adhesions could be controlled on the nanoscale and that their maximum size was restricted by the size of the underlying fibronectin cluster. Furthermore, the spacing between cellular adhesions could also be controlled as adhesions were only formed were fibronectin was present.

It was observed that the morphology of HUVECs on the nanopatterns could be influenced by the underlying fibronectin cluster diameter and spacing. For the macroscopic protein coverage of 4.91% and 8.72%, as the size of the protein cluster was increased the level of cell spreading increased. An identical trend was also observed for the shape or circularity of the cells. As the protein clusters were increased in size, the cells assumed a more rounded shape. If rather than density, the spacing between patterns was held constant, the cells displayed identical behavior when the size of the clusters

were increased. This is an interesting finding because studies have found that the size of a focal adhesion is directly proportional to the force transmitted through it to its surroundings (Choquet, Felsenfeld et al. 1997; Balaban, Schwarz et al. 2001; Bershadsky, Balaban et al. 2003; Yeung, Georges et al. 2005). Additionally, studies on polyacrylamide gels have shown that traction forces exerted by cells on the substrate are positively correlated to the degree of cell spreading (Tolic-Norrelykke and Wang 2005). The study also found that elongated cells or cells with small circularity exerted less traction force than well-spread cells. The work of (Tan, Tien et al. 2003) and (Tolic-Norrelykke and Wang 2005) showed that cell spreading and circularity were positively correlated with the degree of force exerted on the substrate by a cell (What is the difference to the sentence before. If the fibronectin cluster size was directly related to the force that a cell could exert on the substrate, then one would expect the cell spreading area to be positively correlated with the size of the fibronectin clusters. This is exactly the trend that was discovered on the nanopatterned surfaces.

The analysis of actin stress fibers supports the correlation of force and adhesion size. The absolute number of stress fibers per cell is directly related to the size of the fibronectin nanocluster, independent of macroscopic protein density, and the density or percentage of actin in a cell cross section of the cell was significantly less for smaller fibronectin nanoclusters. These results correlate with results found on elastic substrates, with gels softer than 1,600Pa having no visible actin stress fibers (Yeung, Georges et al. 2005). As the elastic modulus of the gel was increased, the cells began to show a greater number of stress fibers. The elastic modulus has been shown in other experiments to be related to the force that a cell can exert on the substrate (Engler, Bacakova et al. 2004; Discher, Janmey et al. 2005). The fiber distribution of the actin stress fiber arrangement can be used as a rough measure for cell-surface forces. Given the noticeable decrease in

stress fiber number, distribution and a decrease in the total percentage of actin in a cell, it is reasonable to conclude that the total force exerted by a cell on the substrate was less on smaller clustered patterns. This result is consistent with the idea that smaller adhesions are associated with less transmitted force (Choquet, Felsenfeld et al. 1997; Balaban, Schwarz et al. 2001), and that the nanoscale ligand clustering and restricting the size of the focal adhesions is limiting the development of cytoskeletal tension.

Proliferation on nanoclustered fibronectin is influenced in a biphasic size dependence. At constant macroscopic protein density, increasing adhesions size resulted in decreased proliferation. The same was true if clusters were spaced at a constant distance and the diameter of the cluster was varied. At first these results appear to be counter intuitive because studies using homogenous fibronectin density have shown that decreasing the surface density of fibronectin decreases the proliferation rate. However, there appears to be a transition between the results on homogenous surfaces and when integrins are restricted to nanoscale clusters, Figure 9.7.1. The transition we have discovered may correspond to a region between two signaling pathways that are possibly inhibited or stimulated by restricting the size and spacing of the adhesion clusters, possibly involving FAK signaling.

The motility studies produced a similar biphasic trend: Motility incresed as the size of the adhesion clusters was reduced at constant macroscopic density This was also true when the spacing between the adhesions was held at a constant distance but their sizes varied. Comparing these results to the cytoskeletal results, it can be concluded that increased motility on the nanopatterns is associated with decreased actin stress fiber formation and decreased motility is associated with increased stress fiber formation. It has been shown previously that cellular motility on elastic surfaces display a biphasic behavior and the differences in motility are due to the strength of adhesion (Schwartz and

Horwitz 2006). If the increased stress fiber formation is related to increased adhesion strength, then these stronger adhesions may result in hindering the detachment of the trailing edge of the cell causing a decrease in the velocity of the cell. Interestingly, a large transition in cell velocity was found between the adhesive diameters 250 nm and 200 nm at 24 hours. A similar transition was also observed for the actin cytoskeleton, where there was a noticeable increase in the percentage of actin in the cell as measured in a cross section. Additionally, the transition is present in the proliferation data where the average growth rate decreases at this size range. The exact relationship between motility, proliferation and actin cytoskeletal formation is not known, but all three have FAK as a signaling constituent. It is possible that the size threshold between 250 nm and 200 nm might be related to the way FAK is activated in the adhesion.

12.2.1 FUTURE WORK

The results from the studies indicate that the cell can sense differences in nanoscale arrangement of fibronectin on a surface. These appear to be related to the way that a cell clusters its integrins in forming focal adhesions, and how the adhesion mediates signals downstream. It was shown that cell spreading, proliferation, cytoskeletal formation, motility, focal adhesion size and fibrillogenesis were all influenced by fibronectin cluster size independent of macroscopic density. All of these observed behaviors showed similar transition regimes, in particular the difference between adhesions 200 nm in diameter and 250 nm in diameter. Additionally, the results indicated that there was possibly competing signaling switches that were dependent on integrin cluster size.

Having such a consistent size dependent transition point for so many behaviors is suggestive of a signaling ‘switch’ that occurs far upstream in the signaling cascades. One

possible such mediator is FAK, which is a key signaling component in focal adhesions. FAK is known to regulate many cellular processes including cell motility, proliferation, matrix assembly, cell fate and cytoskeletal tension, Figure 12.2.1 (Romer, Birukov et al. 2006).

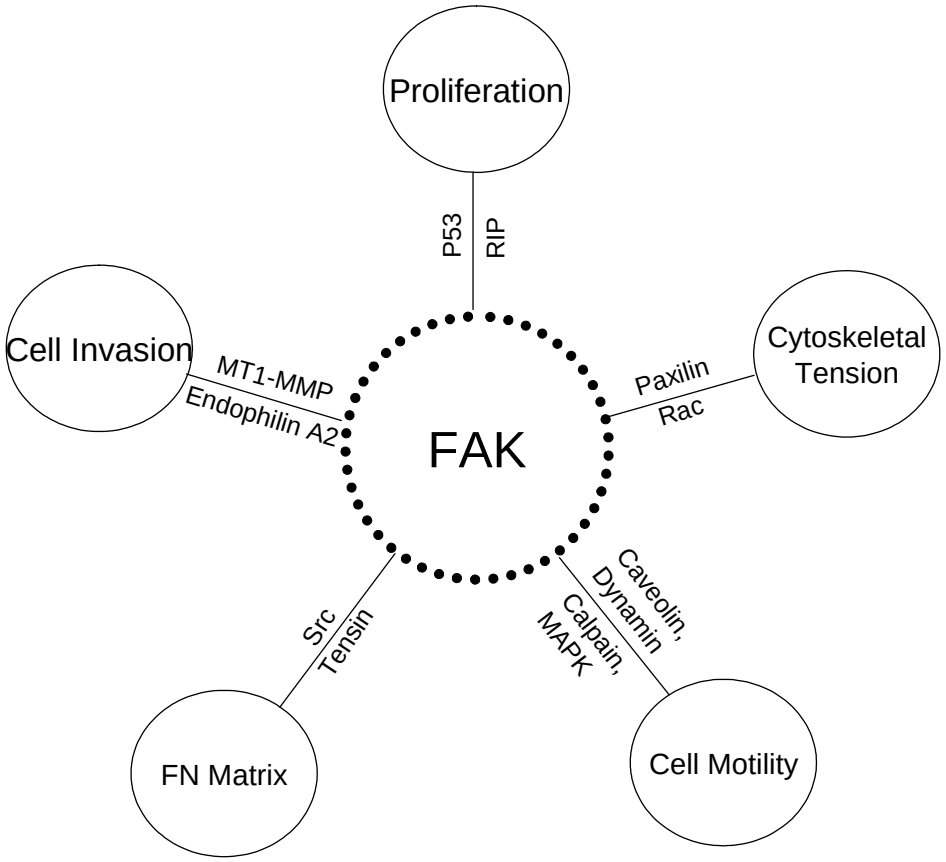

Figure 12.2.1: FAK is a key signaling component in focal adhesions that mediates the signaling of proliferation, cytoskeletal tension, cell motility, fibronectin matrix assembly and cell invasion. Adapted from (Pirone, Liu et al. 2006).

Interestingly, studies using FAK knockouts have shown that FAK deficient cells have similar stress fiber organizations as those on smaller nanopattern clusters (Ilic, Kovacic et al. 2004). They also do not form a well-defined FN matrix, and the FN fibrils present are thin and sparse similar to cells on the 150 nm clusters. Proliferation is increased for

FAK knockouts compared to controls where the cells did not proliferate (Pirone, Liu et al. 2006). The observed switching transition in these studies is similar to the switching behavior of cells on 200 nm versus 300 nm patterns in the studies presented here. The consistency of the results found on the nanopatterns with reported literature using FAK knockouts provides evidence for an integrin cluster size dependence of the activation of regulatory pathways mediated by FAK. Further experiments should explore the role of FAK and the behavior of cells on the nanopatterns. Such experiments may shed light on the exact mechnism of the transition between 200 nm and 250 nm that dictates such different behavior in the cells.

The results from the experiments in this dissertation also suggest the relationship between force and adhesion size. Previous experiments have linked the force transduced through an adhesion to the size of the adhesion. However, looking at the question in the opposite direction, does limiting the size of the adhesion limit the force that can be transduced. The results from this work suggest that the force is modulated by limiting the integrin cluster size. However, it would be helpful to have a quantitative measure of the forces exerted by the cell at the adhesions. One possible way to accomplish this would be growing elastic linkers on the nanopatterns that had a defined elastic modulus. These could be used as a nanosized force sensor to determine the cellular forces in relation to integrin cluster size.

REFERENCES

Balaban, N. Q., U. S. Schwarz, et al. (2001). "Force and focal adhesion assembly: a close relationship studied using elastic micropatterned substrates." Nature Cell Biology **3**(5): 466-472.

Bershadsky, A. D., N. Q. Balaban, et al. (2003). "Adhesion-dependent cell mechanosensitivity." Annual Review of Cell and Developmental Biology **19**: 677-695.

Choquet, D., D. P. Felsenfeld, et al. (1997). "Extracellular matrix rigidity causes strengthening of integrin-cytoskeleton linkages." Cell **88**(1): 39-48.

Discher, D. E., P. Janmey, et al. (2005). "Tissue cells feel and respond to the stiffness of their substrate." Science **310**(5751): 1139-1143.

Engler, A., L. Bacakova, et al. (2004). "Substrate compliance versus ligand density in cell on gel responses." Biophysical Journal **86**(1): 617-628.

Ilic, D., B. Kovacic, et al. (2004). "FAK promotes organization of fibronectin matrix and fibrillar adhesions." Journal of Cell Science **117**(2): 177-187.

Pirone, D. M., W. F. Liu, et al. (2006). "An inhibitory role for FAK in regulating proliferation: a link between limited adhesion and RhoA-ROCK signaling." Journal of Cell Biology **174**(2): 277-288.

Romer, L. H., K. G. Birukov, et al. (2006). "Focal adhesions - Paradigm for a signaling nexus." Circulation Research **98**(5): 606-616.

Schwartz, M. A. and A. R. Horwitz (2006). "Integrating adhesion, protrusion, and contraction during cell migration." Cell **125**(7): 1223-1225.

Tan, J. L., J. Tien, et al. (2003). "Cells lying on a bed of microneedles: An approach to isolate mechanical force." Proceedings of the National Academy of Sciences of the United States of America **100**(4): 1484-1489.

Tolic-Norrelykke, I. M. and N. Wang (2005). "Traction in smooth muscle cells varies with cell spreading." Journal of Biomechanics **38**(7): 1405-1412.

Yeung, T., P. C. Georges, et al. (2005). "Effects of substrate stiffness on cell morphology, cytoskeletal structure, and adhesion." Cell Motility and the Cytoskeleton **60**(1): 24-34.

BIBLIOGRAPHY

Abbott, N. L., J. P. Folkers, et al. (1992). "Manipulation of the Wettability of Surfaces on the 0.1-Micrometer to 1-Micrometer Scale through Micromachining and Molecular Self-Assembly." Science **257**(5075): 1380-1382.

Abbott, N. L., A. Kumar, et al. (1994). "Using Micromachining, Molecular Self-Assembly, and Wet Etching to Fabricate 0.1-1-Mu-M-Scale Structures of Gold and Silicon." Chemistry of Materials **6**(5): 596-602.

Abbott, W. M., J. Megerman, et al. (1987). "Effect of Compliance Mismatch on Vascular Graft Patency." Journal of Vascular Surgery **5**(2): 376-382.

Aguirre, K. M., R. J. McCormick, et al. (1994). "Fibronectin Self-Association Is Mediated by Complementary Sites within the Amino-Terminal One-Third of the Molecule." Journal of Biological Chemistry **269**(45): 27863-27868.

Anderson, J. M. and J. J. Langone (1999). "Issues and perspectives on the biocompatibility and immunotoxicity evaluation of implanted controlled release systems." Journal of Controlled Release **57**(2): 107-113.

Angelini, G. D. (1992). "Saphenous-Vein Graft Failure - Etiologic Considerations and Strategies for Prevention." Current Opinion in Cardiology **7**(6): 939-944.

Ao, P. Y., W. J. Hawthorne, et al. (2000). "Development of intimal hyperplasia in six different vascular prostheses." European Journal of Vascular and Endovascular Surgery **20**(3): 241-249.

Arnold, M., E. A. Cavalcanti-Adam, et al. (2004). "Activation of integrin function by nanopatterned adhesive interfaces." Chemphyschem **5**(3): 383-388.

Arthur, W. T., N. K. Noren, et al. (2002). "Regulation of Rho family GTPases by cell-cell and cell-matrix adhesion." Biological Research **35**(2): 239-246.

Aumailley, M., M. Gerl, et al. (1990). "Identification of the Arg-Gly-Asp Sequence in Laminin-a Chain as a Latent Cell-Binding Site Being Exposed in Fragment P1." Febs Letters **262**(1): 82-86.

Autio, I., U. Maloranta, et al. (1989). "Cultured Bovine Aortic Endothelial-Cells Secrete Factor(S) Chemotactic for Aortic Smooth-Muscle Cells." Artery **16**(2): 72-83.

Babensee, J. E., J. M. Anderson, et al. (1998). "Host response to tissue engineered devices." Advanced Drug Delivery Reviews **33**(1-2): 111-139.

Bailey, T., B. J. Choi, et al. (2000). "Step and flash imprint lithography: Template surface treatment and defect analysis." Journal of Vacuum Science & Technology B **18**(6): 3572-3577.

Bailey, T., B. Smith, et al. (2001). "Step and flash imprint lithography: Defect analysis." Journal of Vacuum Science & Technology B **19**(6): 2806-2810.

Bailey, T. C., S. C. Johnson, et al. (2002). "Step and flash imprint lithography: An efficient nanoscale printing technology." Journal of Photopolymer Science and Technology **15**(3): 481-486.

Balaban, N. Q., U. S. Schwarz, et al. (2001). "Force and focal adhesion assembly: a close relationship studied using elastic micropatterned substrates." Nature Cell Biology **3**(5): 466-472.
Ballestrem, C., B. Hinz, et al. (2001). "Marching at the front and dragging behind: differential alpha-V beta 3-integrin turnover regulates focal adhesion behavior." Journal of Cell Biology **155**(7): 1319-1332.
Bershadsky, A. D., N. Q. Balaban, et al. (2003). "Adhesion-dependent cell mechanosensitivity." Annual Review of Cell and Developmental Biology **19**: 677-695.
Blau, H. M. and D. Baltimore (1991). "Differentiation Requires Continuous Regulation." Journal of Cell Biology **112**(5): 781-783.
Boontheekul, T. and D. J. Mooney (2003). "Protein-based signaling systems in tissue engineering." Current Opinion in Biotechnology **14**(5): 559-565.
Brakebusch, C. and R. Fassler (2003). "The integrin-actin connection, an eternal love affair." Embo Journal **22**(10): 2324-2333.
Bultmann, H., A. J. Santas, et al. (1998). "Fibronectin fibrillogenesis involves the heparin II binding domain of fibronectin." Journal of Biological Chemistry **273**(5): 2601-2609.
Byrne, J., R. C. Darling, et al. (1999). "Infrainguinal arterial reconstruction for claudication: Is it worth the risk? An analysis of 409 procedures." Journal of Vascular Surgery **29**(2): 259-267.
Caes, F. L. and G. J. Vannooten (1994). "Use of Internal Mammary Artery for Emergency Grafting after Failed Coronary Angioplasty." Annals of Thoracic Surgery **57**(5): 1295-1299.
Canfield, A. E., R. P. Boothandford, et al. (1990). "Thrombospondin Gene-Expression by Endothelial-Cells in Culture Is Modulated by Cell-Proliferation, Cell-Shape and the Substratum." Biochemical Journal **268**(1): 225-230.
Chen, C. S., X. Y. Jiang, et al. (2005). "Microengineering the environment of mammalian cells in culture." Mrs Bulletin **30**(3): 194-201.
Chen, C. S., M. Mrksich, et al. (1997). "Geometric control of cell life and death." Science **276**(5317): 1425-1428.
Choi, B. J., M. Meissl, et al. (2001). Layer-to-layer alignment for step and flash imprint lithography, USA, SPIE-Int. Soc. Opt. Eng
SPIE.
Choquet, D., D. P. Felsenfeld, et al. (1997). "Extracellular matrix rigidity causes strengthening of integrin-cytoskeleton linkages." Cell **88**(1): 39-48.
Clark, E. A., W. G. King, et al. (1998). "Integrin-mediated signals regulated by members of the Rho family of GTPases." Journal of Cell Biology **142**(2): 573-586.
Colburn, M., T. Bailey, et al. (2001). "Development and advantages of step-and-flash lithography." Solid State Technology **44**(7): 67-+.
Colburn, M., A. Grot, et al. (2000). Step and flash imprint lithography for sub-100 nm patterning, USA, SPIE-Int. Soc. Opt. Eng
SPIE.

Colburn, M., A. Grot, et al. (2001). "Patterning nonflat substrates with a low pressure, room temperature, imprint lithography process." Journal of Vacuum Science & Technology B **19**(6): 2162-2172.
Colburn, M., S. Johnson, et al. (1999). "Step and flash imprint lithography: a new approach to high-resolution patterning." Proc. SPIE, Emerging Lithographic Technologies III, Yuli Vladimirsky; Ed **3676**: 379-389.
Colburn, M., I. Suez, et al. (2001). "Characterization and modeling of volumetric and mechanical properties for step and flash imprint lithography photopolymers." Journal of Vacuum Science & Technology B **19**(6): 2685-2689.
Costa, K. D., W. J. Hucker, et al. (2002). "Buckling of actin stress fibers: A new wrinkle in the cytoskeletal tapestry." Cell Motility and the Cytoskeleton **52**(4): 266-274.
Coussen, F., D. Choquet, et al. (2002). "Trimers of the fibronectin cell adhesion domain localize to actin filament bundles and undergo rearward translocation." Journal of Cell Science **115**(12): 2581-2590.
Cybulsky, M. I. and M. A. Gimbrone (1991). "Endothelial Expression of a Mononuclear Leukocyte Adhesion Molecule During Atherogenesis." Science **251**(4995): 788-791.
Dalby, M. J., M. O. Riehle, et al. (2002). "In vitro reaction of endothelial cells to polymer demixed nanotopography." Biomaterials **23**(14): 2945-2954.
Dalby, M. J., M. O. Riehle, et al. (2004). "Changes in fibroblast morphology in response to nano-columns produced by colloidal lithography." Biomaterials **25**(23): 5415-5422.
Dalby, M. J., S. J. Yarwood, et al. (2002). "Increasing fibroblast response to materials using nanotopography: morphological and genetic measurements of cell response to 13-nm-high polymer demixed islands." Experimental Cell Research **276**(1): 1-9.
Dauksher, W. J., K. J. Nordquist, et al. (2002). "Characterization of and imprint results using indium tin oxide-based step and flash imprint lithography templates." Journal of Vacuum Science & Technology B **20**(6): 2857-2861.
Davies, P. F., A. Robotewskyj, et al. (1994). "Quantitative Studies of Endothelial-Cell Adhesion - Directional Remodeling of Focal Adhesion Sites in Response to Flow Forces." Journal of Clinical Investigation **93**(5): 2031-2038.
Davies, P. F. and S. C. Tripathi (1993). "Mechanical-Stress Mechanisms and the Cell - an Endothelial Paradigm." Circulation Research **72**(2): 239-245.
Dertinger, S. K. W., X. Y. Jiang, et al. (2002). "Gradients of substrate-bound laminin orient axonal specification of neurons." Proceedings of the National Academy of Sciences of the United States of America **99**(20): 12542-12547.
Dimilla, P. A., J. A. Stone, et al. (1993). "Maximal Migration of Human Smooth-Muscle Cells on Fibronectin and Type-Iv Collagen Occurs at an Intermediate Attachment Strength." Journal of Cell Biology **122**(3): 729-737.
Discher, D. E., P. Janmey, et al. (2005). "Tissue cells feel and respond to the stiffness of their substrate." Science **310**(5751): 1139-1143.
Duffy, D. C., R. J. Jackman, et al. (1999). "Patterning electroluminescent materials with feature sizes as small as 5 mu m using elastomeric membranes as masks for dry lift-off." Advanced Materials **11**(7): 546-+.

Edelman, E. R. (1999). "Vascular tissue engineering - Designer arteries." Circulation Research **85**(12): 1115-1117.
Engler, A., L. Bacakova, et al. (2004). "Substrate compliance versus ligand density in cell on gel responses." Biophysical Journal **86**(1): 617-628.
Engler, A. J., S. Sen, et al. (2006). "Matrix elasticity directs stem cell lineage specification." Cell **126**(4): 677-689.
Folch, A., B. H. Jo, et al. (2000). "Microfabricated elastomeric stencils for micropatterning cell cultures." Journal of Biomedical Materials Research **52**(2): 346-353.
Frey, W., C. K. Woods, et al. (2000). "Ultraflat nanosphere lithography: A new method to fabricate flat nanostructures." Advanced Materials **12**(20): 1515-1519.
Furchgott, R. F. and J. V. Zawadzki (1980). "The Obligatory Role of Endothelial-Cells in the Relaxation of Arterial Smooth-Muscle by Acetylcholine." Nature **288**(5789): 373-376.
Gates, B. D., Q. B. Xu, et al. (2005). "New approaches to nanofabrication: Molding, printing, and other techniques." Chemical Reviews **105**(4): 1171-1196.
Geiger, B. and A. Bershadsky (2001). "Assembly and mechanosensory function of focal contacts." Current Opinion in Cell Biology **13**(5): 584-592.
Geiger, B., A. Bershadsky, et al. (2001). "Transmembrane extracellular matrix-cytoskeleton crosstalk." Nature Reviews Molecular Cell Biology **2**(11): 793-805.
Glass, R., M. Moller, et al. (2003). "Block copolymer micelle nanolithography." Nanotechnology **14**(10): 1153-1160.
Griffith, L. G. (2002). Emerging design principles in Biomaterials and scaffolds for tissue engineering. Reparative Medicine: Growing Tissues and Organs. **961:** 83-95.
Grinnell, F., M. F. Zhu, et al. (1999). "Release of mechanical tension triggers apoptosis of human fibroblasts in a model of regressing granulation tissue." Experimental Cell Research **248**(2): 608-619.
Gupton, S. L. and C. M. Waterman-Storer (2006). "Spatiotemporal feedback between actomyosin and focal-adhesion systems optimizes rapid cell migration." Cell **125**(7): 1361-1374.
Harris, A. K., D. Stopak, et al. (1981). "Fibroblast Traction as a Mechanism for Collagen Morphogenesis." Nature **290**(5803): 249-251.
Healy, K. E. (1999). "Molecular engineering of materials for bioreactivity." Current Opinion in Solid State & Materials Science **4**(4): 381-387.
Herring, M., A. Gardner, et al. (1978). "Single-Staged Technique for Seeding Vascular Grafts with Autogenous Endothelium." Surgery **84**(4): 498-504.
Hersel, U., C. Dahmen, et al. (2003). "RGD modified polymers: biomaterials for stimulated cell adhesion and beyond." Biomaterials **24**(24): 4385-4415.
Holland, N. B., Y. X. Qiu, et al. (1998). "Biomimetic engineering of non-adhesive glycocalyx-like surfaces using oligosaccharide surfactant polymers." Nature **392**(6678): 799-801.
Holly, S. P., M. K. Larson, et al. (2000). "Multiple roles of integrins in cell motility." Experimental Cell Research **261**(1): 69-74.

Holth, L. T., D. N. Chadee, et al. (1998). "Chromatin, nuclear matrix and the cytoskeleton: Role of cell structure in neoplastic transformation (Review)." International Journal of Oncology **13**(4): 827-837.
Homandberg, G. A. and J. W. Erickson (1986). "Model of Fibronectin Tertiary Structure Based on Studies of Interactions between Fragments." Biochemistry **25**(22): 6917-6925.
Howe, A., A. E. Aplin, et al. (1998). "Integrin signaling and cell growth control." Current Opinion in Cell Biology **10**(2): 220-231.
Huang, S., C. S. Chen, et al. (1998). "Control of cyclin D1, p27(Kip1), and cell cycle progression in human capillary endothelial cells by cell shape and cytoskeletal tension." Molecular Biology of the Cell **9**(11): 3179-3193.
Huang, S. and D. E. Ingber (1999). "The structural and mechanical complexity of cell-growth control." Nature Cell Biology **1**(5): E131-E138.
Hubbell, J. A. (1999). "Bioactive biomaterials." Current Opinion in Biotechnology **10**(2): 123-129.
Huen, A. C., J. K. Park, et al. (2002). "Intermediate filament-membrane attachments function synergistically with actin-dependent contacts to regulate intercellular adhesive strength." J. Cell Biol. **159**(6): 1005-1017.
Hulteen, J. C. and R. P. Vanduyne (1995). "Nanosphere Lithography - a Materials General Fabrication Process for Periodic Particle Array Surfaces." Journal of Vacuum Science & Technology a-Vacuum Surfaces and Films **13**(3): 1553-1558.
Huttenlocher, A., R. R. Sandborg, et al. (1995). "Adhesion in Cell-Migration." Current Opinion in Cell Biology **7**(5): 697-706.
Hynes, R. O. (1992). "Integrins - Versatility, Modulation, and Signaling in Cell-Adhesion." Cell **69**(1): 11-25.
Iber, D. and I. D. Campbell (2006). "Integrin activation - the importance of a positive feedback." Bulletin of Mathematical Biology **68**(4): 945-956.
Ilic, D., B. Kovacic, et al. (2004). "FAK promotes organization of fibronectin matrix and fibrillar adhesions." Journal of Cell Science **117**(2): 177-187.
Ingber, D. E. (1990). "Fibronectin Controls Capillary Endothelial-Cell Growth by Modulating Cell-Shape." Proceedings of the National Academy of Sciences of the United States of America **87**(9): 3579-3583.
Ip, J. H., V. Fuster, et al. (1991). "The Role of Platelets, Thrombin and Hyperplasia in Restenosis after Coronary Angioplasty." Journal of the American College of Cardiology **17**(6): B77-B88.
Ishihara, K., N. P. Ziats, et al. (1991). "Protein Adsorption from Human Plasma Is Reduced on Phospholipid Polymers." Journal of Biomedical Materials Research **25**(11): 1397-1407.
Jackman, R. J., D. C. Duffy, et al. (1999). "Using elastomeric membranes as dry resists and for dry lift-off." Langmuir **15**(8): 2973-2984.
Johnson, S., D. J. Resnick, et al. (2003). "Fabrication of multi-tiered structures on step and flash imprint lithography templates." Microelectronic Engineering **67-8**: 221-228.
Juliano, R. L. and S. Haskill (1993). "Signal Transduction from the Extracellular-Matrix." Journal of Cell Biology **120**(3): 577-585.

Katz, B. Z., E. Zamir, et al. (2000). "Physical state of the extracellular matrix regulates the structure and molecular composition of cell-matrix adhesions." Molecular Biology of the Cell **11**(3): 1047-1060.
Kawa, A., M. Stahlhut, et al. (1998). "A simple procedure for morphometric analysis of processes and growth cones of neurons in culture using parameters derived from the contour and convex hull of the object." Journal of Neuroscience Methods **79**(1): 53-64.
Kenis, P. J. A., R. F. Ismagilov, et al. (1999). "Microfabrication inside capillaries using multiphase laminar flow patterning." Science **285**(5424): 83-85.
Kingshott, P. and H. J. Griesser (1999). "Surfaces that resist bioadhesion." Current Opinion in Solid State & Materials Science **4**(4): 403-412.
Koo, L. Y., D. J. Irvine, et al. (2002). "Co-regulation of cell adhesion by nanoscale RGD organization and mechanical stimulus." Journal of Cell Science **115**(7): 1423-1433.
Koo, L. Y., D. J. Irvine, et al. (2002). "Co-regulation of cell adhesion by nanoscale RGD organization and mechanical stimulus." J Cell Sci **115**(7): 1423-1433.
Kouvroukoglou, S., K. C. Dee, et al. (2000). "Endothelial cell migration on surfaces modified with immobilized adhesive peptides." Biomaterials **21**(17): 1725-1733.
Kumar, A., H. A. Biebuyck, et al. (1992). "The Use of Self-Assembled Monolayers and a Selective Etch to Generate Patterned Gold Features." Journal of the American Chemical Society **114**(23): 9188-9189.
Kumar, A. and G. M. Whitesides (1993). "Features of Gold Having Micrometer to Centimeter Dimensions Can Be Formed through a Combination of Stamping with an Elastomeric Stamp and an Alkanethiol Ink Followed by Chemical Etching." Applied Physics Letters **63**(14): 2002-2004.
Lauffenburger, D. A. and A. F. Horwitz (1996). "Cell migration: A physically integrated molecular process." Cell **84**(3): 359-369.
Lauffenburger, D. A. and A. Wells (2001). "Getting a grip: new insights for cell adhesion and traction." Nature Cell Biology **3**(5): E110-E112.
Lee, T. Y. J. and A. I. Gotlieb (2003). "Microfilaments and Microtubules maintain endothelial integrity." Microscopy Research and Technique **60**(1): 115-125.
Liddington, R. C. and M. H. Ginsberg (2002). "Integrin activation takes shape." Journal of Cell Biology **158**(5): 833-839.
Lo, C. M., H. B. Wang, et al. (2000). "Cell movement is guided by the rigidity of the substrate." Biophysical Journal **79**(1): 144-152.
Lutolf, M. P. and J. A. Hubbell (2005). "Synthetic biomaterials as instructive extracellular microenvironments for morphogenesis in tissue engineering." Nature Biotechnology **23**(1): 47-55.
Madou, M. J. (2002). Fundamentals of microfabrication : the science of miniaturization. Boca Raton, CRC Press.
Magometschnigg, H., M. Kadletz, et al. (1992). "Prospective Clinical-Study with Invitro Endothelial-Cell Lining of Expanded Polytetrafluoroethylene Grafts in Crural Repeat Reconstruction." Journal of Vascular Surgery **15**(3): 527-535.
Maheshwari, G., G. Brown, et al. (2000). "Cell adhesion and motility depend on nanoscale RGD clustering." J Cell Sci **113**(10): 1677-1686.

Mao, Y. and J. E. Schwarzbauer (2005). "Fibronectin fibrillogenesis, a cell-mediated matrix assembly process." Matrix Biology **24**(6): 389-399.
Mathur, A. B., G. A. Truskey, et al. (2000). "Atomic force and total internal reflection fluorescence microscopy for the study of force transmission in endothelial cells." Biophysical Journal **78**(4): 1725-1735.
Mathur, A. B., G. A. Truskey, et al. (2000). "Total internal reflection microscopy and atomic force microscopy (TIRFM-AFM) to study stress transduction mechanisms in endothelial cells." Critical Reviews in Biomedical Engineering **28**(1-2): 197-202.
Matsushita, S. I., T. Miwa, et al. (2001). "Stable two-dimensional fine-particle arrays in solution." Langmuir **17**(4): 988-992.
Matsushita, S. I., Y. Yagi, et al. (2000). "Light propagation in composite two-dimensional arrays of polystyrene spherical particles." Langmuir **16**(2): 636-642.
McBeath, R., D. M. Pirone, et al. (2004). "Cell shape, cytoskeletal tension, and RhoA regulate stem cell lineage commitment." Developmental Cell **6**(4): 483-495.
Miranti, C. K. and J. S. Brugge (2002). "Sensing the environment: a historical perspective on integrin signal transduction." Nature Cell Biology **4**(4): E83-E90.
Miriam Cohen, D. J. B. G. L. A. (2004). "Spatial and Temporal Sequence of Events in Cell Adhesion: From Molecular Recognition to Focal Adhesion Assembly." ChemBioChem **5**(10): 1393-1399.
Mirkin, C. A. (2001). "Dip-pen nanolithography: Automated fabrication of custom multicomponent, sub-100-nanometer surface architectures." Mrs Bulletin **26**(7): 535-538.
Miyamoto, S., S. K. Akiyama, et al. (1995). "Synergistic Roles for Receptor Occupancy and Aggregation in Integrin Transmembrane Function." Science **267**(5199): 883-885.
Miyamoto, S., H. Teramoto, et al. (1995). "Integrin Function - Molecular Hierarchies of Cytoskeletal and Signaling Molecules." Journal of Cell Biology **131**(3): 791-805.
Mogab, C. J., A. C. Adams, et al. (1978). "Plasma Etching of Si and Sio2 - Effect of Oxygen Additions to Cf4 Plasmas." Journal of Applied Physics **49**(7): 3796-3803.
Mostafavi-Pour, Z., J. A. Askari, et al. (2003). "Integrin-specific signaling pathways controlling focal adhesion formation and cell migration." Journal of Cell Biology **161**(1): 155-167.
Motwani, J. G. and E. J. Topol (1998). "Aortocoronary saphenous vein graft disease - Pathogenesis, predisposition, and prevention." Circulation **97**(9): 916-931.
Nelson, C. M. and C. S. Chen (2002). "Cell-cell signaling by direct contact increases cell proliferation via a PI3K-dependent signal." Febs Letters **514**(2-3): 238-242.
Ohashi, T., D. P. Kiehart, et al. (1999). "Dynamics and elasticity of the fibronectin matrix in living cell culture visualized by fibronectin-green fluorescent protein." Proceedings of the National Academy of Sciences of the United States of America **96**(5): 2153-2158.
Okabe, Y., M. Furugori, et al. (2000). "Chemical force microscopy of microcontact-printed self-assembled monolayers by pulsed-force-mode atomic force microscopy." Ultramicroscopy **82**(1-4): 203-212.

Olivier, L. A., J. Yen, et al. (1999). "Short-term cell/substrate contact dynamics of subconfluent endothelial cells following exposure to laminar flow." Biotechnology Progress **15**(1): 33-42.
Ostuni, E., R. Kane, et al. (2000). "Patterning mammalian cells using elastomeric membranes." Langmuir **16**(20): 7811-7819.
Palecek, S. P., J. C. Loftus, et al. (1997). "Integrin-ligand binding properties govern cell migration speed through cell-substratum adhesiveness." Nature **385**(6616): 537-540.
Pankov, R., E. Cukierman, et al. (2000). "Integrin dynamics and matrix assembly: Tensin-dependent translocation of alpha(5)beta(1) integrins promotes early fibronectin fibrillogenesis." Journal of Cell Biology **148**(5): 1075-1090.
Parikh, S. A. and E. R. Edelman (2000). "Endothelial cell delivery for cardiovascular therapy." Advanced Drug Delivery Reviews **42**(1-2): 139-161.
Pelham, R. J. and Y. L. Wang (1997). "Cell locomotion and focal adhesions are regulated by substrate flexibility." Proceedings of the National Academy of Sciences of the United States of America **94**(25): 13661-13665.
Petit, V. and J. P. Thiery (2000). "Focal adhesions: structure and dynamics." Biology of the Cell **92**(7): 477-494.
Peyton, S. R. and A. J. Putnam (2005). "Extracellular matrix rigidity governs smooth muscle cell motility in a biphasic fashion." Journal of Cellular Physiology **204**(1): 198-209.
Pierschbacher, M. D. and E. Ruoslahti (1984). "Cell Attachment Activity of Fibronectin Can Be Duplicated by Small Synthetic Fragments of the Molecule." Nature **309**(5963): 30-33.
Pirone, D. M., W. F. Liu, et al. (2006). "An inhibitory role for FAK in regulating proliferation: a link between limited adhesion and RhoA-ROCK signaling." Journal of Cell Biology **174**(2): 277-288.
Pomposelli, F. B., S. Arora, et al. (1998). "Lower extremity arterial reconstruction in the very elderly: Successful outcome preserves not only the limb but also residential status and ambulatory function." Journal of Vascular Surgery **28**(2): 215-223.
Ratner, B. D. and S. J. Bryant (2004). "Biomaterials: Where we have been and where we are going." Annual Review of Biomedical Engineering **6**: 41-75.
Resnick, D. J., W. J. Dauksher, et al. (2003). "Imprint lithography for integrated circuit fabrication." Journal of Vacuum Science & Technology B **21**(6): 2624-2631.
Resnick, D. J., D. Mancini, et al. (2003). "Improved step and flash imprint lithography templates for nanofabrication." Microelectronic Engineering **69**(2-4): 412-419.
Risau, W. (1995). "Differentiation of Endothelium." Faseb Journal **9**(10): 926-933.
Roberts, C., C. S. Chen, et al. (1998). "Using mixed self-assembled monolayers presenting RGD and (EG)(3)OH groups to characterize long-term attachment of bovine capillary endothelial cells to surfaces." Journal of the American Chemical Society **120**(26): 6548-6555.
Romer, L. H., K. G. Birukov, et al. (2006). "Focal adhesions - Paradigm for a signaling nexus." Circulation Research **98**(5): 606-616.
Ruchhoeft, P., M. Colburn, et al. (1999). "Patterning curved surfaces: Template generation by ion beam proximity lithography and relief transfer by step and flash

imprint lithography." Journal of Vacuum Science & Technology B **17**(6): 2965-2969.
Ruegg, C. and A. Mariotti (2003). "Vascular integrins: pleiotropic adhesion and signaling molecules in vascular homeostasis and angiogenesis." Cellular and Molecular Life Sciences **60**(6): 1135-1157.
Salacinski, H. J., A. Tiwari, et al. (2001). "Cellular engineering of vascular bypass grafts: role of chemical coatings for enhancing endothelial cell attachments." Medical & Biological Engineering & Computing **39**(6): 609-618.
Schaller, M. D. (2001). "Biochemical signals and biological responses elicited by the focal adhesion kinase." Biochimica Et Biophysica Acta-Molecular Cell Research **1540**(1): 1-21.
Schmid, H. and B. Michel (2000). "Siloxane polymers for high-resolution, high-accuracy soft lithography." Macromolecules **33**(8): 3042-3049.
Schwartz, M. A. and A. R. Horwitz (2006). "Integrating adhesion, protrusion, and contraction during cell migration." Cell **125**(7): 1223-1225.
Schwarz, U. S., N. Q. Balaban, et al. (2003). "Measurement of cellular forces at focal adhesions using elastic micro-patterned substrates." Materials Science & Engineering C-Biomimetic and Supramolecular Systems **23**(3): 387-394.
Sheetz, M. P., D. P. Felsenfeld, et al. (1998). "Cell migration: Regulation of force on extracellular-matrix-integrin complexes." Trends in Cell Biology **8**(2): 51-54.
Shen, M. C., L. Martinson, et al. (2002). "PEO-like plasma polymerized tetraglyme surface interactions with leukocytes and proteins: in vitro and in vivo studies." Journal of Biomaterials Science-Polymer Edition **13**(4): 367-390.
Shin, H., S. Jo, et al. (2003). "Biomimetic materials for tissue engineering." Biomaterials **24**(24): 4353-4364.
Shyy, J. Y. J. and S. Chien (1997). "Role of integrins in cellular responses to mechanical stress and adhesion." Current Opinion in Cell Biology **9**(5): 707-713.
Slater, J. and W. Frey (2007). "Nanopatterning of Fibronectin and the Influence of Integrin Clustering on Endothelial Cell Spreading and Proliferation." Journal of Biomedical Materials Research Part A.
Small, J. V., T. Stradal, et al. (2002). "The lamellipodium: where motility begins." Trends in Cell Biology **12**(3): 112-120.
Smith, J. W. and D. A. Cheresh (1988). "The Arg-Gly-Asp Binding Domain of the Vitronectin Receptor - Photoaffinity Cross-Linking Implicates Amino-Acid Residues-61-203 of the Beta-Subunit." Journal of Biological Chemistry **263**(35): 18726-18731.
Smith, K. H., J. R. Wasson, et al. (2001). "Cr absorber etch process for extreme ultraviolet lithography mask fabrication." Journal of Vacuum Science & Technology B **19**(6): 2906-2910.
Staatz, W. D., K. F. Fok, et al. (1991). "Identification of a Tetrapeptide Recognition Sequence for the Alpha-2-Beta-1-Integrin in Collagen." Journal of Biological Chemistry **266**(12): 7363-7367.
Stamatas, G. N. and L. V. McIntire (2001). "Rapid flow-induced responses in endothelial cells." Biotechnology Progress **17**(3): 383-402.

Stewart, M. D., S. C. Johnson, et al. (2005). "Nanofabrication with step and flash imprint lithography." Journal of Microlithography Microfabrication and Microsystems **4**(1).
Takayama, S., E. Ostuni, et al. (2001). "Topographical micropatterning of poly(dimethylsiloxane) using laminar flows of liquids in capillaries." Advanced Materials **13**(8): 570-+.
Tan, J. L., J. Tien, et al. (2003). "Cells lying on a bed of microneedles: An approach to isolate mechanical force." Proceedings of the National Academy of Sciences of the United States of America **100**(4): 1484-1489.
Tarry, W. C., D. B. Walsh, et al. (1998). "Fate of the contralateral leg after infrainguinal bypass." Journal of Vascular Surgery **27**(6): 1039-1047.
Tassiopoulos, A. K. and H. P. Greisler (2000). "Angiogenic mechanisms of endothelialization of cardiovascular implants: a review of recent investigative strategies." Journal of Biomaterials Science-Polymer Edition **11**(11): 1275-1284.
Thompson, L. F., C. G. Willson, et al. (1994). Introduction to microlithography. Washington, DC, American Chemical Society.
Tiwari, A., H. J. Salacinski, et al. (2001). "Tissue engineering of vascular bypass grafts: Role of endothelial cell extraction." European Journal of Vascular and Endovascular Surgery **21**(3): 193-201.
Tolic-Norrelykke, I. M. and N. Wang (2005). "Traction in smooth muscle cells varies with cell spreading." Journal of Biomechanics **38**(7): 1405-1412.
Topper, J. N. and M. A. Gimbrone (1999). "Blood flow and vascular gene expression: fluid shear stress as a modulator of endothelial phenotype." Molecular Medicine Today **5**(1): 40-46.
Truskey, G. A. and J. S. Pirone (1990). "The Effect of Fluid Shear-Stress Upon Cell-Adhesion to Fibronectin-Treated Surfaces." Journal of Biomedical Materials Research Part A **24**(10): 1333-1353.
Vogel, V. and G. Baneyx (2003). "The tissue engineering puzzle: A molecular perspective." Annual Review of Biomedical Engineering **5**: 441-463.
Wang, D., T. Rafferty, et al. (2005). "Advanced prototyping using step-and-flash imprint." Solid State Technology **48**(12): 60-62.
Wang, J. H. C., P. Goldschmidt-Clermont, et al. (2001). "Specificity of endothelial cell reorientation in response to cyclic mechanical stretching." Journal of Biomechanics **34**(12): 1563-1572.
Wehrle-Haller, B. and B. A. Imhof (2003). "Actin, microtubules and focal adhesion dynamics during cell migration." International Journal of Biochemistry & Cell Biology **35**(1): 39-50.
Wehrle-Haller, B. and B. A. Imhof (2003). "Integrin-dependent pathologies." Journal of Pathology **200**(4): 481-487.
Whitesides, G. M., E. Ostuni, et al. (2001). "Soft lithography in biology and biochemistry." Annual Review of Biomedical Engineering **3**: 335-373.
Wierzbicka-Patynowski, I. and J. E. Schwarzbauer (2003). "The ins and outs of fibronectin matrix assembly." Journal of Cell Science **116**(16): 3269-3276.
Wilder, R. L. (2002). "Integrin alpha V beta 3 as a target for treatment of rheumatoid arthritis and related rheumatic diseases." Ann Rheum Dis **61**(90002): 96ii-99.

Xia, Y. N., E. Kim, et al. (1996). "Complex optical surfaces formed by replica molding against elastomeric masters." Science **273**(5273): 347-349.
Xia, Y. N., J. J. McClelland, et al. (1997). "Replica molding using polymeric materials: A practical step toward nanomanufacturing." Advanced Materials **9**(2): 147-149.
Xia, Y. N., J. A. Rogers, et al. (1999). "Unconventional methods for fabricating and patterning nanostructures." Chemical Reviews **99**(7): 1823-1848.
Yeung, T., P. C. Georges, et al. (2005). "Effects of substrate stiffness on cell morphology, cytoskeletal structure, and adhesion." Cell Motility and the Cytoskeleton **60**(1): 24-34.
Zaidel-Bar, R., M. Cohen, et al. (2004). "Hierarchical assembly of cell-matrix adhesion complexes." Biochemical Society Transactions **32**: 416-420.
Zamir, E. and B. Geiger (2001). "Components of cell-matrix adhesions." Journal of Cell Science **114**(20): 3577-3579.
Zhang, H., S. W. Chung, et al. (2003). "Fabrication of sub-50-nm solid-state nanostructures on the basis of dip-pen nanolithography." Nano Letters **3**(1): 43-45.
Zhao, X. M., Y. N. Xia, et al. (1996). "Fabrication of three-dimensional micro-structures: Microtransfer molding." Advanced Materials **8**(10): 837-&.
Zhong, C. L., M. Chrzanowska-Wodnicka, et al. (1998). "Rho-mediated contractility exposes a cryptic site in fibronectin and induces fibronectin matrix assembly." Journal of Cell Biology **141**(2): 539-551.

VITA

Harold Edward Gaubert III was born in April 1979 in Lafayette Louisiana, the son of Harold and Ginger Gaubert. After graduating from Clements High School in Sugarland, Texas in 1998, he enrolled in the University of Texas at Austin, earning a Bachelors of Science in Electrical Engineering. He entered the department of Biomedical Engineering in 2003 and completed his Masters of Science in Biomedical Engineering in May 2006.

Permanent address: 2002-A Guadalupe St. #273, Austin, Texas 78705

This dissertation was typed by the author.